Spring 2020

Observer-based event-triggered and set-theoretic neuro-adaptive controls for constrained uncertain systems

Abdul Ghafoor

Department: Mechanical and Aerospace Engineering

OBSERVER-BASED EVENT-TRIGGERED AND SET-THEORETIC NEURO-ADAPTIVE CONTROLS FOR CONSTRAINED UNCERTAIN SYSTEMS

by

ABDUL GHAFOOR

A DISSERTATION

Presented to the Graduate Faculty of the

MISSOURI UNIVERSITY OF SCIENCE AND TECHNOLOGY

In Partial Fulfillment of the Requirements for the Degree

DOCTOR OF PHILOSOPHY

in

MECHANICAL ENGINEERING

2020

Approved by:

S. N. Balakrishnan, Advisor
Jagannathan Sarangapani
Henry Pernicka
K. Krishnamurthy
Tansel Yucelen

PUBLICATION DISSERTATION OPTION

This dissertation consists of the following three articles, formatted in the style used by the Missouri University of Sciences and Technology:

Paper I, found on pages 6–48, has been submitted to *Journal of Franklin Institute*.

Paper II, found on pages 49–95, is intended for submission to *Journal of Acta Astronautica*.

Paper III, found on pages 96–132, has been submitted to *IEEE transactions on Control System Technology*.

ABSTRACT

In this study, several new observer-based event-triggered and set-theoretic control schemes are presented to advance the state of the art in neuro-adaptive controls. In the first part, six new event-triggered neuro-adaptive control (ETNAC) schemes are presented for uncertain linear systems. These comprehensive designs offer flexibility to choose a design depending upon system performance requirements. Stability proofs for each scheme are presented and their performance is analyzed using benchmark examples. In the second part, the scope of the ETNAC is extended to uncertain nonlinear systems. It is applied to a case of precision formation flight of the microsatellites at the Sun-Earth/Moon L1 libration point. This dynamic system is selected to evaluate the performance of the ETNAC techniques in a setting that is highly nonlinear and chaotic in nature. Moreover, factors like restricted controls, response to uncertainties and jittering makes the controller design even trickier for maintaining a tight formation precision. Lyapunov function-based stability analysis and numerical results are presented. Note that most real-world systems involve constraints due to hardware limitations, disturbances, uncertainties, nonlinearities, and cannot always be efficiently controlled by using linearized models. To address all these issues simultaneously, a barrier Lyapunov function-based control architecture called the segregated prescribed performance guaranteeing neuro-adaptive control is developed and tested for the constrained uncertain nonlinear systems, in the third part. It guarantees strict performance that can be independently prescribed for each individual state and/or error signal of the given system. Furthermore, the proposed technique can identify unknown dynamics/uncertainties online and provides a way to regulate the control input.

ACKNOWLEDGEMENTS

I'd like to express my gratitude to my advisor, Dr. S. N. Balakrishnan who provided me with the opportunity to be part of this project. This work would have not been possible without his helpful insight and guidance throughout. I would also like to thank all members of my advisory committee, Dr. J. Sarangapani, Dr. H. Pernicka, Dr. K. Krishnamurthy, and Dr. T. Yucelen, for their patient discussions and valuable suggestions.

Special gratitude goes to my beloved wife, Katie L. Gondal, to my family, and to new addition during this period, my firstborn, Elias W. Gondal. Their smiles and support got me through this period in a positive way. My special thanks to my precious parents, Hafiz. M. Ramzan and Halima Bi, and to all my lovely brothers and sister.

I also appreciate the continuous help from my friends, colleagues, faculty of Missouri University of Sciences and Technology in my courses/research. I met wonderful people in Rolla, I am thankful to all of them for their support and help, especially to Pakistani Student Association, my colleagues, my first American family from Tower house (all of my roommates), Muslim community of Rolla, all other of my local and international crazy friends, with whom I worked and partied. I am sad that I cannot put their names here due to limited space. I am also thankful to this wonderful country, the United State of America, for giving me the opportunity to study and work here, and to learn a great deal from it. I would also like to thank National Aeronautics and Space Administration, for their Grants NNX15AM51A and NNX15AN04A, to partially support this research.

Finally, I am grateful and thankful to Almighty ALLAH for the faith, guidance and strength he has provided me through all this time and forever.

TABLE OF CONTENTS

Page

LIST OF ILLUSTRATIONS

Page

PAPER I

LIST OF TABLES

Page

PAPER II

NOMENCLATURE

Symbol	Description
e_r	Tracking Error
e_a	Estimation Error
μ	Gravitational Parameter
m_1	Mass of the Sun
m_2	Mass of the Earth
ψ_{sun}	Solar Constant
R_i	Distance of Spacecraft from i_{th}body
$A_\odot$	Exposed Surface Area of Spacecraft to Sun
$r_{sat\odot}$	Spacecraft to Sun Vector
c_r	Coefficient of Reflectivity
X	State of the System
f(.)	Generic Functions
X_d	Desired State
e_{evt}	Event Sampling Error
cg	Center of Gravity
G	Generator Gody
α	Angle of Attack
CFC	Regression Based Polynomial Curve Fitting Coefficients

1. INTRODUCTION

1.1. BACKGROUND

Adaptive control systems have started to play an important role in shaping human life and technology. These control systems are enabling technology in almost every field such as autopilot design in aerospace, precision flights in rockets and satellites, autonomy in automobiles, intelligence in robots, and automation in industrial plants. Design architecture of these controllers comprises of sensing and measurements, observers, and neural networks/machine learning algorithms. Modern control systems can handle many challenges which classical controllers were not able to address before. Modern controls are adaptive, intelligent and do not need perfect knowledge of the system model and can handle multivariable systems. These controllers, especially adaptive controllers can learn and improve their performance, cater to system and parameter uncertainties and are tuned to the actual need of the system. At the same time, in the system engineering side, factors like recent advancement in hardware technology, economical deployment, and design/operational flexibility have given rise to networked/swarm systems. Though these developments (modern controls and flexible networked system) came handy with traditional problems of not having operational flexibility or not being adaptable as per uncertainty, they led to new challenges, such as handling and processing of a lot of data, needed higher data communication, and higher processing power. This created the need for a controller which not only makes use of classical/modern control theory but also reduces communication and computational cost. This is where proposed controller designs, named as an event-triggered neuro-adaptive controller (ETNAC) come into play. ETNAC design

includes a neural network (NN) and machine learning (regression) based modified state observer (MSO), which makes it adaptive and intelligent so it can estimate the unknown system model or external disturbances. It has an event-triggering mechanism (ETM), which helps to reduce communication and computations cost and to utilize resources in an optimal way. In Paper I, six different ETNAC schemes are presented for uncertain linear systems, offering flexibility to choose between them depending on the need of a given system. While in Paper II, ETNAC scope is extended to uncertain nonlinear systems, where its performance is tested for a very challenging problem of providing formation precision flying control and reduced jittering for microsatellites used in deep space missions. In paper III, a controller design for constrained uncertain nonlinear systems is considered. Many practical applications involve hardware limitations that put constraints on the system states. Most of the real-world systems are inherently nonlinear and cannot be controlled or stabilized in an efficient manner by using linearized models. At the same time, the presence of disturbances and uncertainties cannot be avoided. In addition, some priori prescribed tracking/stability performance is needed to be ensured all the time. This need comes from practical design requirements to avoid undesired operations. To address all these problems simultaneously, a barrier Lyapunov function (BLF)-based control architecture called the segregated prescribed performance guaranteeing neuro-adaptive control (SPPGNAC) is proposed in proposed in Paper III.

1.2. CONTRIBUTIONS

The contributions of the first paper include the derivation and implementation of six different ETNAC schemes. This paper is comprehensive in the way that it contains one-

way and two-way data exchange methods; it also gives the flexibility to choose between static or dynamic triggering. Triggering conditions have been developed to make the control design and execution efficient. Each scheme of the proposed ETNAC architecture is capable of closely approximating the uncertainty including during the inter-event time when actual measurements are not available and can identify the system behavior quite accurately. Event-triggering conditions are designed on the basis of real performance parameters as compared to extended time sampling which is commonly seen in existing Event-Triggered Control (ETC) papers. In the two-way data exchange methods, state information transmission depends on the state estimation error, and control transmission depends on estimator tracking error and on control sampling error. On the other hand, in the one-way method, both state and control transmission depend on tracking error. The potential of these new techniques in terms of data communication bandwidth and computational cost-effectiveness with control performance is evaluated in this paper. So, the contributions of the first study can be summarized as (i) a comprehensive design is proposed that incorporates different ETC architectures while offering the flexibility to choose between them depending on the need of a given system. (ii) System performance parameters based novel event-triggering architectures are designed to reduce the data communication bandwidth and to update the control based on actual system events. (iii) Using artificial neural network (ANN) and machine learning (polynomial regression), novel MSO designs are proposed to approximate uncertainty/unmolded dynamics in the system, including during the inter-event time.

In the second paper, ETNAC design applicability is expanded to the control restricted uncertain nonlinear systems. The feasibility of the ETNAC providing precision

formation flying control and extended period of silence for microsatellites used in deep space missions is examined. A single microsatellite at the Sun-Earth/Moon L1 libration point is considered as a follower spacecraft in a formation with a single leader spacecraft. A halo orbit is generated as a reference trajectory for the leader spacecraft and modelled as a virtual node defined along the reference trajectory about which the follower spacecraft maintains its relative position. For such "smallsats," limited capabilities of the platform, including restricted controls and actuation, and sensitive responses to uncertainties and jittering make the controller design challenging task for tight formation precisions. To address such challenges, two ETNAC schemes are derived and numerically simulations are performed. Lyapunov analysis is used to prove stability and derive the event-triggering conditions. Simulation results show that ETNAC can be an excellent solution for such highly nonlinear, sensitive, and resource-constrained problems.

In the third paper, a BLF-based neuro-adaptive controller design is proposed that guarantees strict performance for the constrained uncertain nonlinear system. This performance can be independently prescribed for each individual/segregated state and/or error signal of the given system. Main features of the proposed design are (i) guaranteed priori user-defined tracking performance at all times (transient and steady-state) that can satisfy constraints on the state signals, (ii) flexibility to have different constraints on separate state and error signals, and not just on the norm of errors or states, (iii) flexibility to have symmetric/asymmetric constraints/bounds, (iv) change in control can be regulated in proportion to proximity of threshold which helps to avoid excessive input force, which is generally observed in BLF-based controls, (v) it can estimate uncertainties and can

identify unmodeled dynamics by using NN-based MSO. Benchmark numerical examples are used to show the effectiveness of the proposed technique.

1.3. ORGANIZATION

Organization of this dissertation is as follows. After this introductory section, Paper I presents the design and analysis of the ETNAC schemes for the uncertain linear systems. Paper II extends the ETNAC to uncertain nonlinear systems. Paper III presents a segregated prescribed performance guaranteeing neuro-adaptive control (SPPGNAC) for constrained uncertain nonlinear systems. Finally, overall conclusions from this study are summarized in Section 2, followed by Appendices where all proofs are given, Bibliography, and Vita.

PAPER

I. DESIGN AND ANALYSIS OF EVENT-TRIGGERED NEURO-ADAPTIVE CONTROLLER (ETNAC) FOR UNCERTAIN SYSTEMS

Abdul Ghafoor* and S. N. Balakrishnan

Department of Mechanical and Aerospace Engineering, Missouri University of Science and Technology, Rolla, MO 65409

ABSTRACT

In this paper, six new event-triggered neuro-adaptive control (ETNAC) schemes are presented for uncertain linear systems. Novelty of this paper lies in (i) the construction of the proposed ETNAC schemes, (ii) the design of event-triggering conditions, and (iii) the design of an observer called the modified state observer (MSO). In the proposed schemes, the MSO, the controller, and the event-triggering mechanisms are constructed and organized in a way such that they provide the control system designer with flexibility to choose between the one-way or two-way data exchange and also between the dynamic or static triggering conditions. The event-triggering conditions are designed on the basis of real performance parameters, such as the estimation/tracking errors that render control updates more on actual system events instead of the often-used extended time sampling. Another unique feature of ETNAC is its online uncertainty approximation capability even during inter-event times, which makes the controller robust and efficient. This part is developed with the help of an artificial neural network (ANN) and a polynomial regression-based MSO. The MSO formulations have two tuneable gains, which allow fast uncertainty

estimation without inducing high frequency oscillations, even while the system is in a transient state. Lyapunov analysis is used to show the stability of the system as well as to develop the event-triggering conditions. Effectiveness of the proposed controllers is demonstrated using benchmark numerical examples.

1. INTRODUCTION

Recent advancements in technology have resulted in systems where small chips have become an integral part of numerous applications. At the same time, economical deployment and increased flexibility have led to networked systems where different components, including actuators, controllers, and sensors, are distributed over networks. Microcontrollers and microprocessors are essential components for these networked systems, and they carry out data monitoring, transmission of information packets over the channels, dealing with unknown disturbances and uncertainties, and processing all information related to control calculations. This situation becomes even more complex when data needs to be transmitted continuously/periodically, which in general is the case. In order to cope with such challenges, six ETNAC designs are proposed in this paper. Depending upon the nature of the given problem, the most suitable architecture can be picked.

In the ETNAC framework, state information transmission from physical systems to the controller and updated control transmission and execution are carried out only when certain triggering conditions come into play. This specific event-based aperiodic transmission/update is more practical than conventional periodic updates. ETNAC is not

only advantageous in reducing the frequency of communication, computations, and control execution, but at the same time allows for approximating uncertainties while guaranteeing stability and satisfactory closed loop performance.

Gupta first came up with different techniques in 0 as to how to sample state efficiently, which led to the development of ETC strategies. Later, Tabuada provided a strong mathematical basis to ensure stability with event-triggered control in [2] . In [3], Heemel et al. presented event-triggered control for linear systems and proved input to state stability (ISS).

Presence of uncertainties/disturbances is unavoidable in a system's dynamics. Therefore, it is important for the controller to be adaptive and robust to counter uncertainties and disturbances. After McCulloch [4], the first to introduce the ANN, more and more researchers have been attracted by the power of neural networks (NN) and started using them to design adaptive controllers. In [5], Narendra considered the application of the neural network controller for nonlinear systems. Amongst other developments, Sanner et al. in [6] and Lewis in [7] used a different radial basis and a multilayer ANN in controls to approximate uncertainties. G. Zhang et al. in [8], presented a dynamical virtual ship (DVS) guidance principle and a robust controller design for underactuated marine vessels while in [10], the same authors modified DVS principle resulting in a guidance law to generate the real-time attitude reference capable to avoid multi-obstacles. They also presented an adaptive algorithm in [9] to investigate dynamic positioning vessel when input amplitude and rate are saturated. Some other recent contributions involve [11], [12], and [13], where authors used ANN and AI-based models for the uncertainty and function approximation.

Adaptive event-triggered control is a relatively recent topic in control theory. On this topic, Lunze and Lehmann [14] considered ETC for linear systems, assuming boundedness on disturbances. Liu and Jiang in [15] and Postoyan et al. in [16] came up with different novel ETC designs to address the nonlinear uncertainty while considering the input to state stability (ISS). In [17], Garcia and Antaklis proposed a model-based scheme for adaptive ETC. Wang et al. in [21]-[22] considered two-way data exchange, but this approach requires knowledge of the upper bound on the unknown gains from their parametrization of the uncertainty. On the other hand, Ali et al. [24]-[25] presented a scheme that allows two-way data communication without any such assumption. Furthermore, Sahoo et al. [19]-[20] proposed a dynamic event-triggering condition for one-way data exchange. The concept of MSO was originally proposed by Padhi, Unnikrishnan, and Balakrishnan in [26] to estimate the unknown/un-modeled dynamics in a system. In [28], Abdul et al. presented an MSO-based decentralized control for large scale interconnected uncertain systems, while in [28] the scope of MSO was extended to event-triggered control for affine nonlinear uncertain systems. In [30], an MSO-based event-triggered control was developed for linear systems in which the observer has access to only sampled states. While in [31], an MSO-based dynamically triggered two-way ETNAC was presented and in [32], it was extended to enable formation flight of the microsatellies at libration points. Some other recent researches on uncertain event-triggered control systems include [33], where Dong et al. proposed a delay system model-based event-triggered H_∞ controller for the networked control systems. In [34], Tian et al. developed finite horizon H_∞ control architecture for the time varying systems to satisfy the prespecified H_∞ disturbance attenuation and to ensure certain chance constraints on the output vector. Zhan

and Sun in [35] proposed an event-triggered control for uncertain linear systems. In their paper, parametric uncertainty was considered with some bounds, stability was investigated, and observer-related calculations were performed on the plant side. On the other hand Qi et al. [36], examined an uncertain switched linear system containing parametric uncertainties. They provide an upper bound on cost due to uncertainties. In [37], Tripathy et al. designed an event-trigger-based control to make linear discrete systems ISS. In [38], Riccati-based designs were proposed by Borgers et al. for dynamic and static triggering, but it is not shown how the disturbance is handled. Other examples include [39] and [42], where event-based robust controllers were devised for uncertain linear systems.

Contributions of this paper include: the derivation and implementation of MSO-based adaptive event-triggered controls. Now we will explain the differences between our own earlier conference papers and the current paper. This paper is comprehensive and contains one-way and two-way data exchange methods, it also gives the flexibility to choose between static or dynamic triggering. Triggering conditions have been developed to make the controller design and execution efficient. Each scheme of the proposed ETNAC architecture is capable of closely approximating the uncertainty, even during inter-event time, and can identify the system behavior quite accurately. Event-triggering conditions are designed on the basis of real performance parameters as compared to extended time sampling which is common in existing ETC papers. In two-way data exchange methods, state information transmission depends on state estimation error and control transmission depends on estimator tracking error and control sampling error. On the other hand, in the one-way method both state and control transmission depend on tracking error. The potential of these new techniques in terms of data communication

bandwidth and computational cost effectiveness with control performance is evaluated in this paper. So, the contributions of this study can be summarized as:

- A comprehensive design is proposed that incorporates different ETC architectures while offering the flexibility to choose between them depending on the need of a given system
- System performance parameters-based novel event-triggering architectures are designed to reduce the data communication bandwidth and to update the control based on actual system events
- Using ANN and machine learning (polynomial regression), novel MSO designs are proposed to approximate uncertainty/unmolded dynamics in the system, including during inter-event time

The rest of the paper is organized such that Section 2 provides problem formulation while in Section 3, proposed ETNAC designs are given. Sections 4 presents numerical examples, including results and discussion. Finally, Section 5 presents the conclusions from this paper followed by acknowledgement, references, and appendices.

2. PROBLEM FORMULATION

In this paper, $\mathbb{R}$ stands for the real numbers, $\mathbb{N}_+$ for the set of positive integers, $\mathbb{R}^n$ for the set of $n \times 1$ real column vectors, $\mathbb{R}^{n\times m}$ for the set of $n \times m$ real matrices, $\mathbb{R}_+$ for the set of positive real numbers, $\mathbb{D}^{n\times n}$ for the $n \times n$ diagonal matrices, t_i is sampling time instant for the control update, t_i^s stands for the state sampling time instant to transmit to the feedback loop and observer, $\phi(.)$ for the basis functions used in uncertainty

approximations, $\lambda_{max}(Q)$ and $\lambda_{min}(Q)$) respectively for the maximum and minimum eigenvalues of matrix Q, and $\|.\|$ represents the Euclidean norm.

The dynamics of an uncertain linear system can be represented as

$$\dot{x}(t) = A\,x(t) + B(\,u(t_i) + f\big(x(t)\big)\,) \qquad t_i \le t < t_{i+1} \tag{1}$$

where $x(t) \in \mathbb{R}^n$ is the state of the system, $A \in \mathbb{R}^{n\times n}$ and $B \in \mathbb{R}^{n\times m}$ are known matrices such that (s.t.) $\{A, B\}$ is controllable, $f\big(x(t)\big)$: $\bar{\mathbb{R}}_+ \times \mathbb{R}^n \to \mathbb{R}^m$ is the unknown uncertainty in the system dynamics, and $u(t_i) \in \mathbb{R}^m$ is the sampled control input.

The objective here is to design an event-triggered neuro-adaptive controller for the system in (1) to make it follow the response of the reference system given by:

$$\dot{x}_r(t) = A_m x_r(t) + B_m r(t) \tag{2}$$

where $x_r \in \mathbb{R}^n$ is the reference state, $A_m \in \mathbb{R}^{n\times n}$ is Hurwitz, $B_m \in \mathbb{R}^{n\times q}$ $(q \le m)$, and $r(t) \in \mathbb{R}^q$ is the bounded piecewise continuous reference input.

3. PROPOSED SOLUTION: ETNAC SCHEMES WITH TRIGGERING CONDITIONS

Proposed ETNAC schemes and event-triggering conditions are described in this section.

3.1. TWO-WAY ETNAC

3.1.1. Dynamically Triggered Two-Way ETNAC. Before developing the controller design, some background and basic assumptions that are made for this study are given first. Unlike continuous data transmission, in the two-way ETNAC framework, signals from the physical system to the controller and signals from the controller to the

physical system are transmitted only at specific sampling instants. These instants for state transmission are determined when an event/interruption occurs, known as the event-triggering condition Trg_{1a}^{s}, and is denoted as $\{t_i^s\}_{i=1}^{\infty}$. Similarly, the control sampling instants are determined by other event-triggering conditions, Trg_{1a}^{u} & Trg_{1b}^{u}, and are denoted as $\{t_i\}_{i=1}^{\infty}$. Both satisfy the inequalities $t_{i+1} > t_i$, $t_{i+1}^s > t_i^s \quad \forall i = 1,2,\ldots$ where $t = 0$ is the initial sampling instant for the two-way updates. At each state sampling event, the sampled state $x(t_i^s)$ is sent to the controller, overwriting the previous sampled state $x\,(t_{i-1}^s)$ and held by using a Zero-Order-Hold (ZOH) at the controller until the next state is received. Similarly, the control values are sent and held by ZOHs until the next control update event occurs. Since the updates are event-based and aperiodic, errors are introduced, which are called state sampling error (e_{evt}) and control sampling errors (u_{evt}), given as

$$e_{evt} \triangleq x(t) - x(t_i^s) \qquad t_i^s \le t < t_{i+1}^s \tag{3}$$

$$u_{evt} \triangleq u(t) - u(t_i) \qquad t_i \le t < t_{i+1}. \quad \forall i = 1,2,\ldots \tag{4}$$

Some standard assumptions are made in the development of the control schemes.

Assumption 1: The system uncertainty can be linearly parametrized. From the universal function approximation property of NN, a real valued function $f\big(x(t)\big)$ can be estimated with an accuracy of ϵ, such that:

$$f\big(x(t)\big) = W^T \phi(x(t)) + \epsilon(t,x) \tag{5}$$

where $W \in \mathbb{R}^{s\times m}$ ($s \in \mathbb{N}_+$) is the unknown ideal weight matrix. It is assumed that for a compact set Ω, $W \in \Omega$, $x \in D_x$ for sufficiently large compact set D_x, $\phi(x(t)) \colon \mathbb{R}^n \to \mathbb{R}^s$, user-defined basis function is bounded s.t. $\|\phi(x)\| \le \phi^*$ and $\epsilon(t,x)$ is the residual error satisfying $|\epsilon(t,x)| \le \epsilon^*$. Also, it is assumed that all states are available for measurement.

Assumption 2: The basis functions $\phi(.)$ are locally Lipschitz continuous (LLC).

$$\|\phi(x) - \phi(y)\| \leq L \|x - y\| \tag{6}$$

where $x, y \in D_x$, $\phi(.) \in \mathbb{R}$ and $L \in \mathbb{R}_+$. In ETNAC design, an intermediate step is to formulate an appropriate MSO. Even though all states are assumed measurable here, the MSO notion is used because its inclusion in uncertainty estimation has been shown to avoid large oscillations during the system's transient motion, which is a characteristic that is usually observed with a typical model reference adaptive controller. Note that the development and design of the MSO in this study is *different* in order to cater to the asymmetric data transfer to the feedback network. The relevant MSO equations are:

$$\text{MSO Model 1:} \quad \dot{\hat{x}}(t) = A\,\hat{x}(t) + B\big(u(t) + \hat{f}(x(t_i^s))\big) \qquad t_i^s < t < t_{i+1}^s \tag{7a}$$

$$\text{MSO Model 2:} \quad \dot{\hat{x}}(t) = A\,\bar{x}(t) + B\big(u(t) + \widehat{W}^T\phi\big(\bar{x}(t)\big)\big) - K_2(\bar{x}(t) - \hat{x}(t)) \qquad t_i^s \leq t \leq t_{i+1}^s \tag{7b}$$

where approximation $\hat{f}\big(\bar{x}(t)\big) \triangleq \widehat{W}^T\phi\big(\bar{x}(t)\big)$ represents the estimation of $f\big(x(t)\big)$, $\widehat{W}$ is the estimate of W, K_2 is a user-defined Hurwitz gain matrix, and $\bar{x}$ is the interpolated state, given as

$$\bar{x}(t) \triangleq \begin{cases} x(t) & t = t_i^s \\ C_1 t^n + C_2 t^{n-1} \ldots + C_n t + C_{n+1} & t_i^s \leq t < t_{i+1}^s \end{cases} \tag{8}$$

where $C_i \;\; i = 1,2, \ldots n$ are the polynomial curve fitting coefficients (PCFCs) computed by using machine learning (polynomial regression). These coefficients are determined in the system state measurement history in the inter-event time period. After the coefficients are determined, they are transmitted along with state information whenever an event is

triggered. Note that both MSO models have access to the state information only when the triggering switch is closed, and the latest state and PCFCs are transmitted.

Equations (7a/7b) may appear ambiguous, so we have added some explanation here. The MSO model 1 in Equation (7a) is used during the inter-event time to find the triggering instant t_i^s when the state triggering condition Trg_{1a}^s**,** defined in (21) later, becomes active. Note that the MSO model 1 is simulated *without* any weight update but uses the $\hat{f}(x(t_i^s))$ value obtained from the last sampling instant. However, once event $Trg_{1\,a/b}^u$, defined in (22-23) happens, the MSO model 2 in equation (7b) is used to reset and update the observer. Though MSO model 2 is updated only at each sampling instant, it is basically simulated between the current and the past sampling time instants. The true state is interpolated using the PCFCs between the past and the current event time instants for use with the MSO model 2 and also for computing the error terms in the weight estimates. Before the next Trg_{1a}^s, the observer is simulated again using MSO model 1, starting with current values from MSO model 2. For example, let us suppose that the first event Trg_{1a}^s occurred at t_1^s, so we store the measured state at $x(t_1^s)$, use it as the initial state for the MSO model 1, and propagate it and use it to update the controller and to check the triggering condition for the next event Trg_{1a}^s which will occur at t_2^s. Whenever Trg_{1a}^s occurs again at time instant t_2^s and state $x(t_2^s)$ and PCFCs are received, then the MSO model 2 takes over and simulates $\hat{x}$ between t_1^s and the current time instant t_2^s by making use of actual states $x(t_1^s)$ and $x(t_2^s)$ and its PCFCs for the time in between the events. In this way, the updated $\hat{x}(t_2^s)$ and NN weights $\widehat{W}(t_2^s)$ at t_2^s are used in the controller and as initial states for MSO model 1 to simulate the observer with $\hat{x}(t_2^s)$ until the next (third) event Trg_{1a}^s at t_3^s . This pattern continues.

Now to get the interpolated state-based uncertainty approximation, $W^T\phi(x(t_i^s))$ is added and subtracted in (5),

$$f\big(x(t)\big) = W^T\phi\big(x(t)\big) + W^T\phi\big(\bar{x}(t_i^s)\big) - W^T\phi(\bar{x}(t_i^s)) + \epsilon(t,x)$$

$$= W^T\phi\big(\bar{x}(t_i^s)\big) + \check{\epsilon}(x,t,\bar{x}) \tag{9}$$

where $\check{\epsilon} \triangleq W^T[\phi\big(x(t)\big) - \phi\big(\bar{x}(t_i^s)\big)] + \epsilon(x,t)$. By substituting (9) into (1), we get

$$\dot{x}(t) = A\,x(t) + B(\,u(t_i) + W^T\phi\big(\bar{x}(t_i^s)\big) + \check{\epsilon}(x,t,\bar{x})). \tag{10}$$

The feedback controller is generated as

$$u(t) = u_n(t) + u_a(t_i^s) \tag{11}$$

where $u_n \in \mathbb{R}^m$ is the nominal feedback control input given by

$$u_n(t) = -K_1 x(t_i^s) + K_3 r(t) \tag{12}$$

where $K_1 \in \mathbb{R}^{m\times n}$ is the nominal feedback gain , $K_3 \in \mathbb{R}^{m\times q}$ is the feedforward gain such that $A_m \triangleq A - BK_1$ and $B_m \triangleq BK_3$ [25], [44], and $u_a \in \mathbb{R}^m$ is the adaptive control input

$$u_a = -\hat{f}\big(\bar{x}(t_i^s)\big) = -\widehat{W}^T\phi\big(\bar{x}(t_i^s)\big) \tag{13}$$

where $\widehat{W}$ is the estimate of W. Event-triggering condition Trg_{1a}^s , triggers the current state transmission and event-triggering conditions $Trg_{1\,a/b}^u$ trigger the updated control transmission. In most of ETC literature, the state sampling condition (here denoted as Trg_{1a}^s) is based on extended time or state sampling error [2],[14], but in the proposed method, we came with the idea to relate the Trg_{1a}^s to the state estimation error. Similarly, relating $Trg_{1\,a/b}^u$(for control transmission) to the control sampling error and the estimator tracking error makes more sense, as event-triggering conditions will be directly related in this way to the desired objectives of tracking and estimation.

The tracking error is defined as

$$e_r(t) \triangleq x(t) - x_r(t). \tag{14}$$

Its dynamics are found by using (2) and (10). After some algebra, it is simplified as

$$\dot{e}_r(t) = A_m e_r(t) + B\widetilde{W}^T \phi\big(x(t_i^s)\big) + B\check{\epsilon} + BK_1 e_{evt}. \tag{15}$$

Similarly, the estimation error is defined as

$$e_a(t) \triangleq x(t) - \hat{x}(t). \tag{16}$$

Based on (7a) and (7b), the error dynamics are also found in two ways, given in Equations (17a/17b)

$$\begin{aligned}\dot{e}_a(t) = A_m e_a(t) + B_m\big(r(t) - r(t_i^s)\big) + BK_1 e_{evt} + BW^T\phi\big(x(t)\big) \\ - B\widehat{W}^T\phi\big(\hat{x}(t_i^s)\big)\end{aligned} \tag{17a}$$

$$\dot{e}_a(t) = K_2 e_a(t) + Bu_{evt} + B\widetilde{W}^T\phi\big(\bar{x}(t_i^s)\big) + B\check{\epsilon} + (A - K_2)e_{int} \tag{17b}$$

where $e_{int} \triangleq x(t) - \bar{x}(t)$ is the interpolation error from polynomial regression. In (15) and (17), the terms e_{int} and e_{evt} appear due to evet-triggered-based aperiodic sampling. These need to be bounded for the actual errors to be bounded.

The neural network weights (NNWs) update rule for $\widehat{W}$ is given as:

$$\dot{\widehat{W}} = \gamma\, Proj_m(\widehat{W}, \phi\big(\bar{x}(t)\big)\, \bar{e}_a{}^T PB) \tag{18}$$

where

$$\bar{e}_a \triangleq \begin{cases} x(t_i^s) - \hat{x}(t_i^s) & t = t_i^s \\ \bar{x}(t) - \hat{x}(t) & t_i^s < t < t_{i+1}^s \end{cases} \tag{19}$$

where $\gamma \in \mathbb{R}_+$ is the adaptation rate for the update rule of $\widehat{W}$, and $Proj_m(.,.)$ denotes a smooth projection operator [44]. Note that the projection operator guarantees that $\widehat{W} \in \Omega$, and there exists $W^* \in \Omega$ s.t. $\|\widehat{W}\| \leq W^*$. Matrix P is the solution for the Lyapunov equation:

$$0 = K_2{}^T P + P K_2 + Q \tag{20}$$

where $Q > 0$ and $K_2 < 0$. We use three triggering conditions for this scheme. They are

$$Trg_{1a}^{s}: \quad \|e_{evt}\|^2 \leq \propto_a \beta_a \|e_a\|^2 \tag{21}$$

$$Trg_{1a}^{u}: \quad \|u_{evt}\|^2 \leq \beta_u \tag{22}$$

$$Trg_{1b}^{u}: \quad \|\hat{e}_r\|^2 \leq \beta_{\hat{e}_r} \tag{23}$$

where $\beta_a \triangleq \frac{(\|PBK_1\|^2 + L^2)}{\sigma}, \sigma \in \mathbb{R}_+, 0 < \propto_a \leq 1,$ and $\hat{e}_r(t) \triangleq x_r(t) - \hat{x}(t)$. Parameter $\propto_a$ helps to tune Trg_{1a}^{s} to adjust the inter-event time duration for state events. On the other hand, β_u and $\beta_{\hat{e}_r}$ are user-defined thresholds for the control sampling error (u_{evt}) and the estimator tracking error ($\hat{e}_r$) respectively. Values for Lipschitz constant (L) are picked based on the chosen basis functions for a given problem. In this case it is taken from [19]. Note that the eigenvalues of K_2 should be about equal or farther in the left half plane as compared to that of A_m. Figure 1 shows the overall block diagram of the proposed scheme.

Theorem 1: Consider the system in (1) with the observer models in (7a/7b) and the desired system described by (2). Let assumptions 1 and 2 hold. Consider the NN approximation with the control generated by (11-13) and the weight update law in (18). Let the sampled state signal be transmitted from the plant to the controller at each event sampling instant when (21) is violated (the dynamic state event-triggering condition $Trg_{1\,a}^{s}$), and let the control signal be transmitted to the plant when (22-23) are violated (the control event-triggering $Trg_{1\,a/b}^{u}$). Then the state estimation error and tracking error are uniformly ultimately bounded (UUB).

a. Proof: Proof of Theorem 1 is given in Appendix A.

b. *ISS Stability:* An interesting point to note is that this formulation with theorem 1 exhibits ISS characteristics as shown below whereas it is an assumption in [2] and [16]. From (66), $L(e_r)$ is continuously differentiable, and since $\lambda_{min}(P)\|e_r\|^2 + \|\gamma^{-1}\|\|\widetilde{W}\| \leq \|L(e_r)\| \leq \lambda_{max}(P)\|e_r\|^2 + \|\gamma^{-1}\|\|\widetilde{W}\|$, so $\|L(e_r)\|$ is upper and lower bounded by K_∞ functions. Also, (70) and (76) show that e_r will stay bounded and $\dot{L}(.)$ is less than or equal to a negative definite function. Then by definition in [46], system $\dot{e_r} = f(e_r(t), e_{evt})$ is ISS.

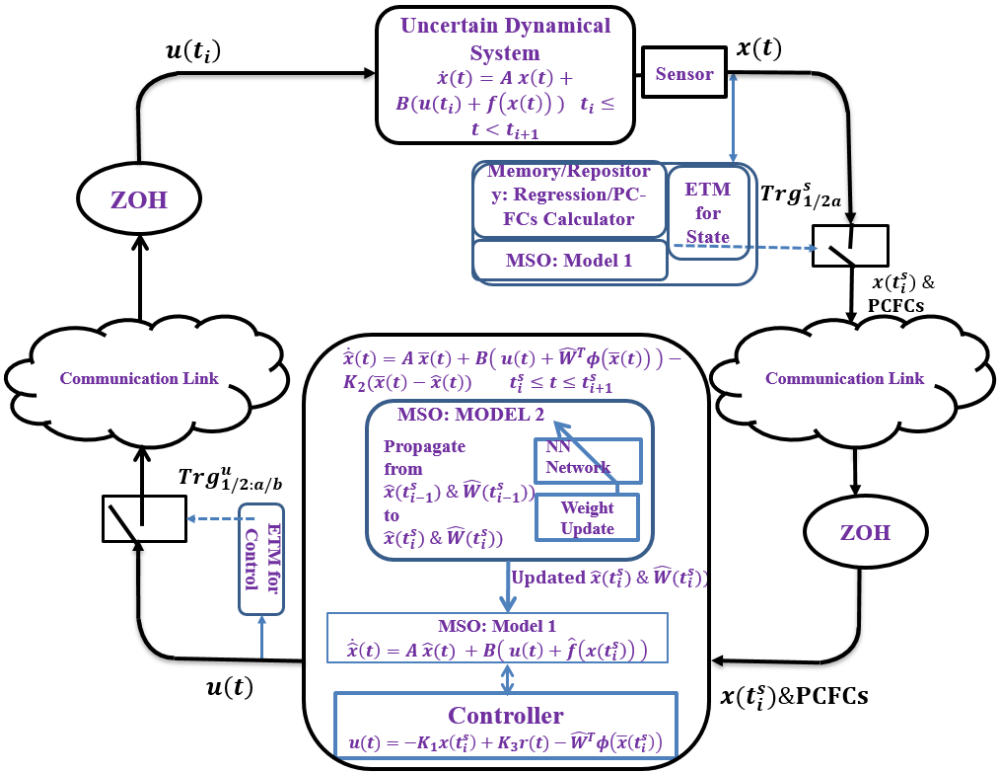

Figure 1. Block diagram for Two-Way ETNAC.

c. *Corollary 1: Ultimate Upper Bound on Tracking Error:* From (70) and (76) it follows that $\dot{L}(.) \leq 0$ outside the compact set D_s:

$$D_s \triangleq \{e_a, \hat{e}_r : \|e_a\| \leq \psi_1\} \cap \{e_a, \hat{e}_r : \|\hat{e}_r\| \leq \varepsilon\}.$$

Since L cannot grow outside D_s, it is lower and upper bounded as

$$\lambda_{min}(P)\| e_r\|^2 \leq \|L\| \leq \lambda_{max}(P)\| e_r\|^2. \tag{24}$$

As we know, $\|e_r\| = \|e_a\| + \|\hat{e}_r\| \leq \psi_1 + \varepsilon$, so

$$\lambda_{min}(P)\| e_r\|^2 \leq \|L\| \leq \lambda_{max}(P)\psi_1 + \lambda_{max}(P)\varepsilon$$

$$\lambda_{min}(P)\| e_r\|^2 \leq \vartheta_1$$

$$\|e_r\| \leq \sqrt{\vartheta_1/\lambda_{min}(P)} \tag{25}$$

where ϑ_1 is $\vartheta_1 \triangleq \lambda_{max}(P)\psi_1 + \lambda_{max}(P)\varepsilon$.

3.1.2. ETNAC-2: Statically Triggered Two-Way ETNAC. In the static event-triggering, user-defined constant threshold are used as triggers. Static even-triggering conditions for ETNAC-2 are:

$$Trg_{2a}^{s}: \qquad \|e_a\| \leq \beta_{2ea} \tag{26}$$

$$Trg_{2a}^{u}: \qquad \|u_{evt}\| \leq \beta_{2u} \tag{27}$$

$$Trg_{2b}^{u}: \qquad \|e_r\| \leq \beta_{2\hat{e}r} \tag{28}$$

where β_{2ea}, β_{2u}, and $\beta_{2\hat{e}r}$ are the user-defined constant-valued thresholds for the estimation error, the control sampling error, and the estimator tracking error respectively. Note that these thresholds are quite different from the static-triggering condition-based ETCs already exist in literature [21]-[25] which depend on state sampling error, control sampling error or state thresholds. The values of the thresholds for event-triggering conditions can be chosen depending upon performance requirements. The rest of the scheme is the same as ETNAC-1 and shown in Figure 1.

Theorem 2: Consider the system in (1) with the observer models in (7a/7b) and the desired system described by (2). Let assumptions 1 and 2 hold. Consider the NN

approximation with the control generated by (11-13) and the weight update law in (18). Let the sampled state signal be transmitted from the plant to the controller at each event sampling instant when (26) is violated (the static triggering condition for state update Trg_{2a}^{s}*) and let the control signal be transmitted to the plant when (27-28) are violated (the static triggering condition for control update* $Trg_{2a/b}^{u}$*). Then the state estimation error and tracking error are UUB.*

Proof: Proof of theorem 2 can be derived by following the same approach as used in proving theorem 1.

3.2. ONE-WAY ETNAC WITH THE MSO IN THE CONTROLLER MODULE

3.2.1. ETNAC-3: Dynamically Triggered One-Way ETNAC with the MSO in the Controller.

This proposed design is called one-way ETNAC because only one event-triggering condition is used to transmit both data exchanges: the states and the PCFCs transmission to the control system and the updated control to the physical system. The sampling instant for the state transmission and the control update is represented as t_i. The MSO equation for this scheme is

$$\dot{\hat{x}}(t) = A\,\bar{x}(t) + B\big(\,u(t_i) + \widehat{W}^T\phi\big(\bar{x}(t)\big)\,\big) - K_2(\bar{x}(t) - \hat{x}(t)) \tag{29}$$

where $\widehat{W}^T\phi\big(\bar{x}(t)\big)$ is the estimate of $f\big(x(t)\big)$, ϕ is the basis function vector, and $\bar{x}$ is the interpolated state between two sampling instants. Assumptions 1 and 2 are still valid. The controller expression is given by

$$u(t) = -K_1 x(t_i) + K_3 r - \widehat{W}^T\phi\big(\bar{x}(t)\big). \tag{30}$$

Although the control expression is similar as in (11-13), note that the triggering mechanism and the way to update control are different now. The tracking error dynamics for this design is given by

$$\dot{e}_r(t) = A_m e_r(t) + B\widetilde{W}^T\phi\big(x(t_i)\big) + B\check{\epsilon} + BK_1 e_{evt} \tag{31}$$

and the estimation error dynamics is described by

$$\dot{e}_a(t) = K_2 e_a(t) + B\widetilde{W}^T\phi\big(\bar{x}(t)\big) + B\check{\epsilon} + (A - K_2)e_{int}. \tag{32}$$

NNWs update rule and the Lyapunov equation expression remain the same as in (18) and (20), respectively. Dynamic event-triggering condition becomes active when (33) is violated:

$$Trg_{3r}^{s} \qquad \|e_{evt}\|^2 \leq \propto_r \beta_r \|e_r\|^2 \tag{33}$$

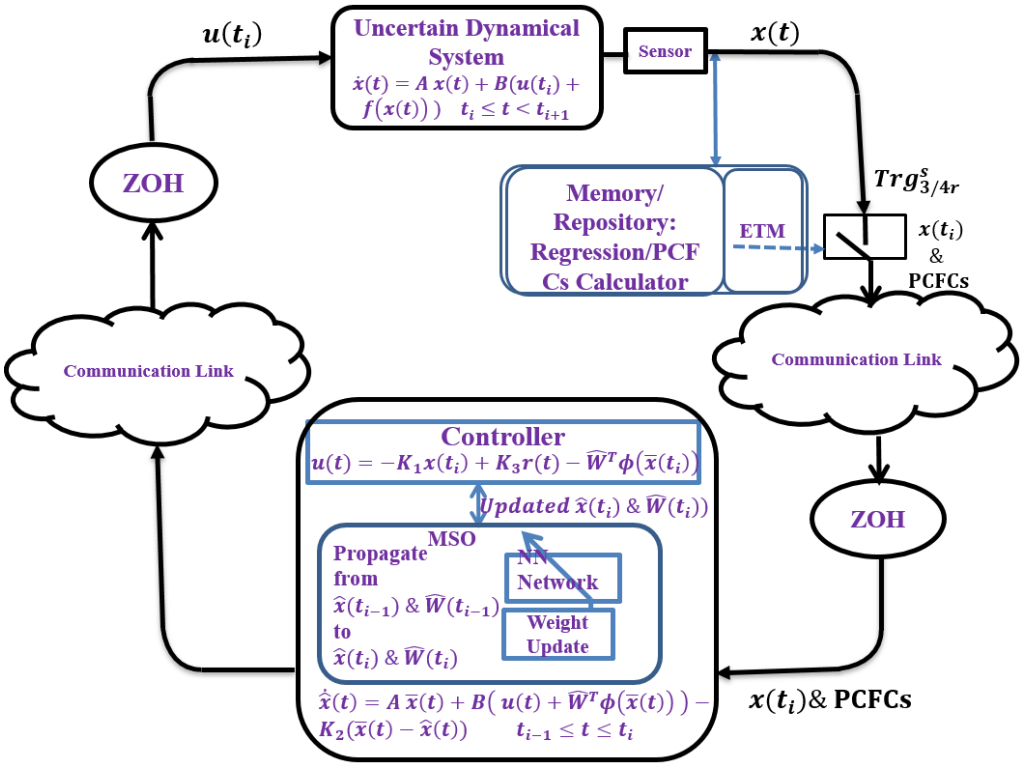

Figure. 2. Block diagram for One-Way ETNAC with MSO in the controller module.

where $\beta_r = \sigma/(1 + (L\|PB\|)^2)$. As can be seen from (33), the sampling condition in this case is directly related to the tracking error and the state sampling error. A pictorial representation of the ETNAC-3 is shown in Figure 2:

Theorem 3: Consider the system in (1) with the observer in (29) and the reference system described by (2). Let assumptions 1 and 2 hold. Consider the NN approximation with control generated by (30) and the weight update law in (18). Let the control be updated at the event sampling instants when (33) is violated (the dynamic triggering condition). Then the tracking error and the state estimation error are UUB.

Proof: Proof of theorem 3 is given in Appendix A. ISS properties and the upper bound on tracking error for ETNAC-3 can also be found by following the same approach used for ETNAC-1.

3.2.2. ETNAC-4: Statically Triggered One-Way ETNAC with the MSO in the Controller Module. In this scheme, a constant threshold on tracking error is set as trigger for the sampling and transmission.

$$Trg_{4r}^{s} \qquad \|e_r\| \leq \beta_4. \tag{34}$$

This scheme follows the same discussion as in subsection 3.2.1. Corollary 3.1 can now be given as*:*

Corollary 3.1: Consider the system in (1) with the observer in (29) and the reference system described by (2). Let assumptions 1 and 2 hold. Consider the NN approximation with control generated by (30) and the weight update law in (18). Let the control values be updated at the event sampling instants when (34) is violated (the static triggering condition). Then the tracking error and the state estimation error are UUB.

Proof: Its proof can be derived by following same approach as used for the theorem 3.

3.3. ONE-WAY ETNAC WITH MSO IN THE SENSOR SUBSYSTEM

3.3.1. ETNAC-5: Dynamically Triggered One-Way ETNAC with MSO in the Sensor Subsystem.

The next scheme presented is the one-way ETNAC, in which the MSO stays at the top level where calculations related to the physical system are carried out, as shown in Figure 3. In this scheme, the MSO has access to the actual states. At each event, the current state values and updated NNWs are transmitted to the controller. At the same time, updated control is transmitted to the physical system. The MSO equation for this scheme is given as

$$\dot{\hat{x}}(t) = A\,x(t) + B\big(\,u(t_i) + \widehat{W}^T\phi\big(x(t)\big)\,\big) - K_2(x(t) - \hat{x}(t)) \tag{35}$$

where $\widehat{W}^T\phi\big(x(t)\big)$ represents the estimation of the uncertainty $f\big(x(t)\big)$. Since the MSO is in the sensor subsystem, it has access to the measurements as they are received. The control is computed as

$$u(t_i) = -K_1x(t_i) + K_3r\ - \widehat{W}^T\phi\big(x(t_i)\big). \tag{36}$$

Here, the updated NNWs are already available and are transmitted along with state data at each sampling instant. Consequently, no regression is needed. The tracking error dynamics can be written as

$$\dot{e}_r(t) = A_me_r(t) + B\widetilde{W}^T\phi\big(x(t_i)\big) + B\check{\epsilon} + BK_1e_{evt} \tag{37}$$

and the estimation error dynamics as

$$\dot{e}_a(t) = K_2e_a(t) + B\widetilde{W}^T\phi\big(x(t)\big) + B\,\epsilon(t,x). \tag{38}$$

The NNW update law is given now as

$$\dot{\widehat{W}} = \gamma\,Proj_m(\widehat{W}, \phi\big(x(t)\big)\,\mathrm{e}_a{}^TPB) \tag{39}$$

The Lyapunov equation expression remains the same as in (20). Again, the dynamic triggering condition is related to the tracking error and the state sampling error as given in (40).

$$Trg_{5r}^{s} \qquad \|e_{evt}\|^2 \leq \propto_{5r} \beta_{5r} \|e_r\|^2 \tag{40}$$

where $\beta_{5r} = \sigma/(1 + (L\|PB\|)^2)$.

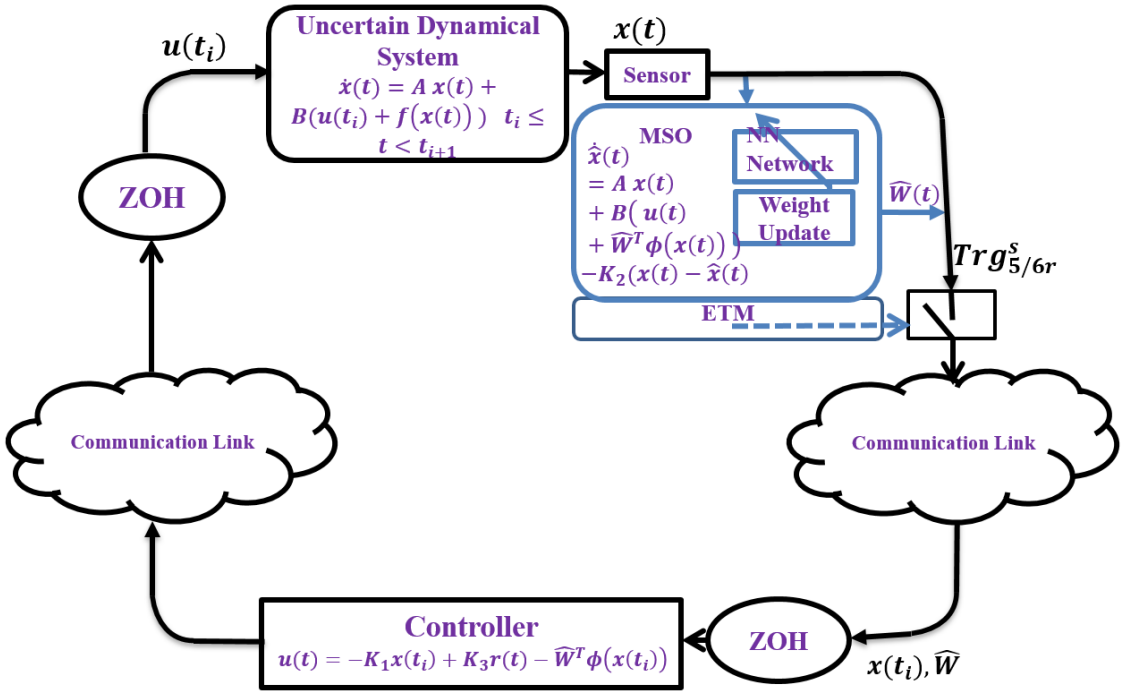

Figure 3. Block diagram for One-Way ETNAC with MSO in the sensor subsystem.

Theorem 4: Consider the system in (1) with the observer in (35) and the reference system described by (2). Let assumptions 1 and 2 hold. Consider the NN approximation with control generated by (36) and the weight update law in (39). Let the control be updated at the event sampling instant when (40) is violated (the dynamic triggering

condition). Then the state estimation error is asymptotically stable (AS), and the tracking error is uniformly ultimately bounded (UUB).

Proof: Proof is given in Appendix A. ISS properties, the upper bound on tracking error, and the lower bound for inter-event time for ETNAC-5 can be found by following the same approach as used for ETNAC-1.

3.3.2. ETNAC-6: Statically Triggered One-Way ETNAC with MSO in the Sensor Subsystem. The tracking error-based static event-triggering condition used for ETNAC-6 is given in (41). It is true when (41) is violated.

$$Trg_{6r}^{s} \qquad \|e_r\| \leq \beta_6. \tag{41}$$

This scheme will save more on communication frequency since the observer with access to all measurements is likely to be more accurate and yield better uncertainty estimates. The following corollary can be stated as:

Corollary 4.1: Consider the system in (1) with the observer in (35) and the reference system described by (2). Let assumptions 1 and 2 hold. Consider the NN approximation with control generated by (36) and the weight update law in (39). Let the control be updated at each event sampling instant when (41) is violated (the static triggering condition). Then the state estimation error is asymptotically stable (AS), and the tracking error is uniformly ultimately bounded (UUB).

Proof: Proof for Corollary can be derived by following the same lines as used for proving theorem 4.

4. NUMERICAL IMPLEMENTATION: RESULTS, DISCUSSION AND ANALYSIS

To show the efficacy of the proposed schemes, we have considered two benchmark examples in this study. Simulation results, analysis, and comparison are given for each example.

4.1. EXAMPLE 1: F-16 SHORT PERIOD DYNAMICS

The short period dynamics of F-16 in a high angle of attack flight, neglecting the influence of thrust and gravity, can be given as

$$\dot{\alpha} = -\frac{L_\alpha}{V}\alpha + q - \frac{L_{\delta_e}(\alpha_0)}{V}\delta_e \tag{42}$$

$$\dot{q} = M_0(\alpha) + M_q(\alpha)q + M_{\delta_e}(\alpha, \delta_e)\delta_e \tag{43}$$

where α is the angle of attack (AoA), q is the pitch rate, δ_e denotes the elevator deflection, V is the trimmed air speed, M_0, M_q, M_{δ_e} represent pitch, damping and moment components respectively, L_α represent lift curve slope, and L_{δ_e} represents the lift effectiveness. These equations of motion can be rewritten as

$$\dot{\alpha} = -\frac{L_\alpha}{V}\alpha + q \tag{44}$$

$$\dot{q} = M_\alpha(\alpha_0)\alpha + M_q(\alpha_0)q + M_{\delta_e}(\alpha_0)\delta_e + \underbrace{M_{\delta_e}((\Delta M_0(\alpha) + \Delta M_{\delta_e}(\alpha, \delta_e))}_{f(\alpha, \delta_e)} \tag{45}$$

where $f(\alpha, \delta_e)$ represents matched nonlinear uncertainties. This unknown nonlinear function is estimated in [47] and is given as

$$f(\alpha, \delta_e) = ((1 - C_0)e\frac{(\alpha - \alpha_0)^2}{2\sigma_c^2} + C_0)(\tanh(\delta_e + h) + (\tanh(\delta_e - h) + 0.01\delta_e) \quad (46)$$

where C_0, h, and σ_c are the constant. So, system's state space model augmented with integral of AoA (α_i), can be written as

$$\begin{bmatrix} \dot{\alpha}_i \\ \dot{\alpha} \\ \dot{q} \end{bmatrix} = \begin{bmatrix} 0 & 1 & 0 \\ 0 & -\frac{L_\alpha}{V} & 1 \\ 0 & M_\alpha & M_q \end{bmatrix} \begin{bmatrix} \alpha_i \\ \alpha \\ q \end{bmatrix} + \begin{bmatrix} 0 \\ 0 \\ M_{\delta_e} \end{bmatrix} (\delta_e + f(\alpha, \delta_e)) + \begin{bmatrix} -1 \\ 0 \\ 0 \end{bmatrix} r. \quad (47)$$

For simulation, F-16 data from [27] and [43] at the trim condition of $V = 502\ ft/s$ and trim AoA is α_0 = 2.11 deg are used. The reference model is developed with the help of a linear quadratic regulator (LQR) using nominal model with a control weight $R = 3$,the state weight $Q = diag(25, 5, 0)$, the system matrices $A = \begin{bmatrix} 0 & 1 & 0 \\ 0 & -1.019 & 1 \\ 0 & 0.822 & -1.077 \end{bmatrix}$, $B = \begin{bmatrix} 0 \\ 0 \\ -0.176 \end{bmatrix}$, and the nominal gains used are$[-2.89 - 4.62 - 3.37]$**.** The reference command is generated as

$$r(t) = 0.25\left(\frac{1}{1 + e^{t-8}} - \frac{0.5}{1 + e^{t-8}} + \frac{1}{1 + e^{t-20}} - e^{-0.2t} - 0.5\right). \quad (48)$$

This input $r(t)$ has a fast-varying part with a steep slope, a slow varying part and also a constant value part, which provides a good test to analyse the controller performance. Values of parameters used in this study are $C_0 = 0.1$, $h = 0.14$, $\sigma_c = 0.25$, $L = 1$, $\gamma = 40$, $\sigma = 3$, $Q = 50I$, and $K_2 = -7I$. Values for K_1 and K_3 are calculated using (12), A_m, and B_m. The sampling time is set at $\Delta t = 0.01$. All simulations are run using Matlab 2014a on a computer with Intel(R) Core(TM) i7-3770 CPU@3.40GHz with 8 GB RAM. Proposed

schemes are compared with three methods: (i) continuously updated adaptive controller, (ii) ETC from paper [2], called ETC-2, and (iii) ETC from [19], called ETC-1.

Basic control gains and MSO parameters for the simulations are kept same for all methods to do a meaningful comparison.

4.1.1. Example 1 Results with Each ETNAC Scheme. Now results are given for each scheme for the example 1.

4.1.2. Results with Two-Way ETNAC.

4.1.2.1. ETNAC-1. For ETNAC-1, the values used are $\propto_a = 0.18$ and β_a is calculated as per (23). The control values are computed using (11), (12), and (13). Figure 4a shows the time histories of the desired AoA α_r (blue) and output AoA α from continuous control calculations (yellow), ETNAC-1(red), ETC-1 (green), and from ETC-2 (magenta). Figure 4b shows the errors (difference between the corresponding output AoA to the desired reference AoA). Similarly, Figures 5a and 5b contain the time evolution for the pitch rate (q) and the corresponding errors. As can be seen from these figures, the tracking performance is good with all the schemes. The error plots in Figure 4b/5b show a better comparison. As expected, the system that gets continuous updates (yellow) provides the best results. Errors with ETC-2 from [2] are comparatively higher as its event-triggering is based on the state sampling error only, and there is no mechanism for adaptation or learning. Results from the proposed technique ETNAC-1 and ETC-1 are somewhat comparable, but note that when systems converge, error magnitudes are relatively smaller with ETNAC-1. Similar trends are observed in the pitch rate plots, as shown in Figures 5a and 5b. Note that the proposed ETNAC-1 scheme is achieves this performance with the least sampling instants when compared to both ETC-1 and ETC-2.

As shown in Figure 6a and 6b, ETNAC-1 outperforms all given techniques in terms of sampling instants. Only 587 (88.26% less) state updates and 269 (94.620% less) control updates are observed as compared to the continuous case where updates are 5000 for each, the state and the control. On the other hand, 1381 updates for each (state and control) are needed by the ETC-1 and 2241 for each by the ETC-2. *An additional distinct feature of the ETNAC is its uncertainty approximation including inter-event time, even when actual state information is not available. It can be seen from Figure 7a that the uncertainty is closely approximated even with 88.8% less sampling instants.* Though the actual updates are done only at the sampling instants, the true state (measurement) is interpolated using polynomial regression between the sampling instants, and this interpolated state is used in the NNWs updates. In this way, the NN provides a good approximation of the uncertainty. In this study, we used and analysed linear to fourth-order regression models. The third-order polynomial regression was found to yield the best results. Figure 7b represents the control histories.

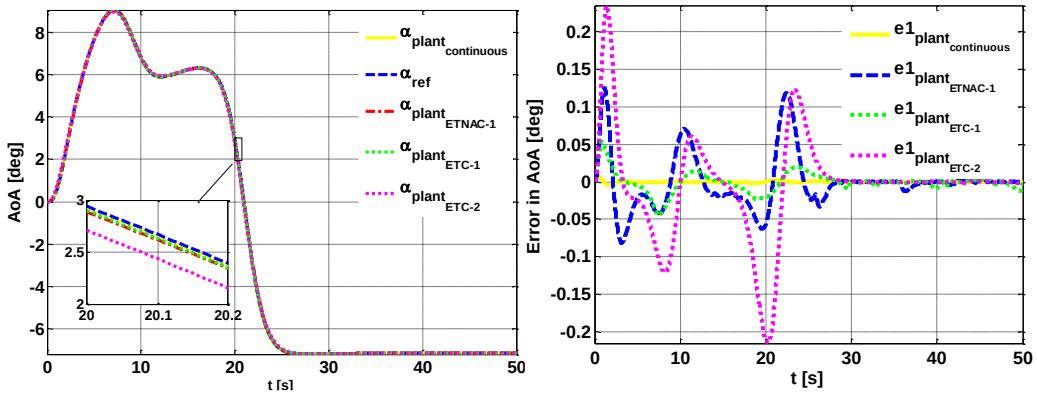

(a) (b)

Figure 4. Case 1: (a) AoA α histories and (b) Tracking error in α.

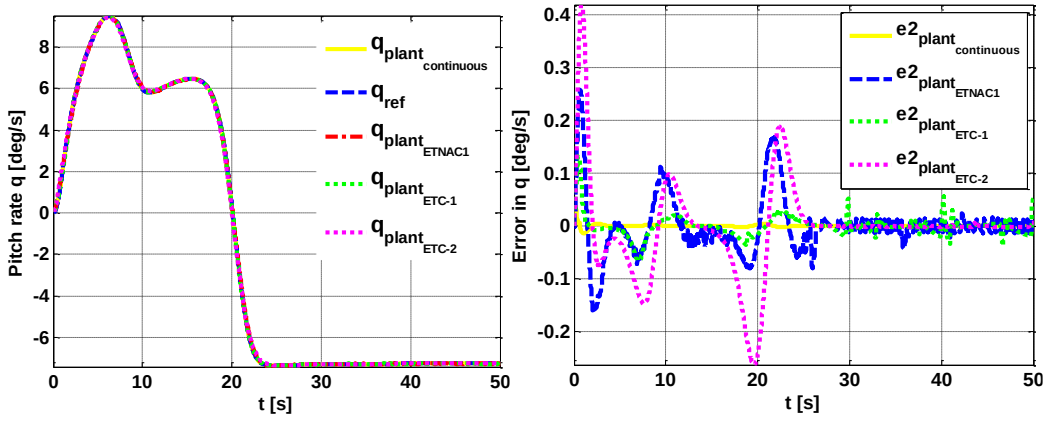

(a) (b)

Figure 5. Case 1: (a) Pitch rate q histories and (b) Tracking error in q.

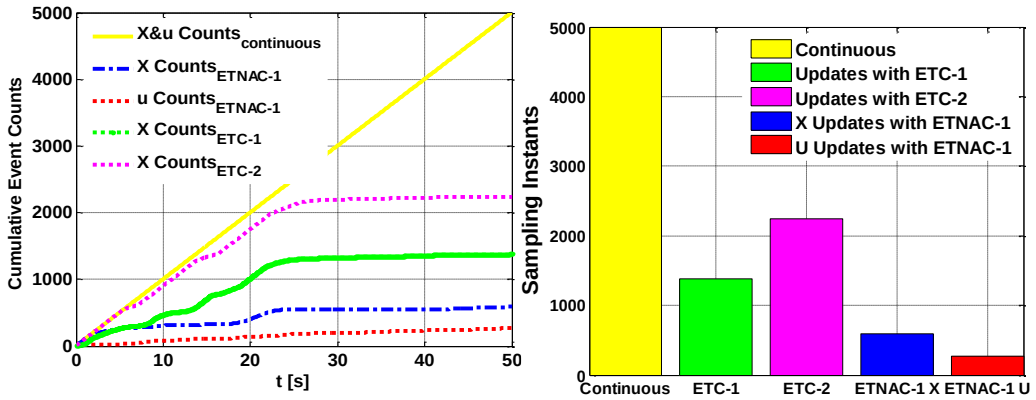

(a) (b)

Figure 6. Case 1: (a) History of sampling events for state and control and (b) Cumulative sampling events.

Although all the schemes except the continuous update scheme show a flat trend of cumulative event counts after 30 seconds in Figure 8a, it should be noted that the use of the MSO and an estimation error-based triggering condition helps ETNAC-1 to have fewer triggers compared to the ETC-1, which accounts for uncertainties, but does not have an

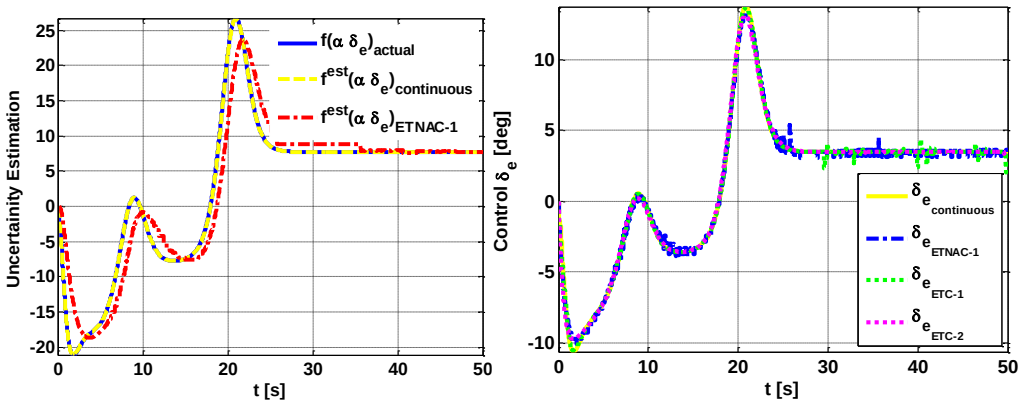

(a) (b)

Figure 7. Case 1: (a) Uncertainty approximation with ETNAC 1 and (b) Control δ_e histories

observer in the loop. Furthermore, it can be observed from Figure 8b that once the error in AoA is close to zero, the MSO-based ETNAC-1 shows much smoother behaviour compared to ETC-1, which shows oscillations in its error history. Figures 9a and 9b show the control trends and uncertainty estimation history, respectively, for case 2.

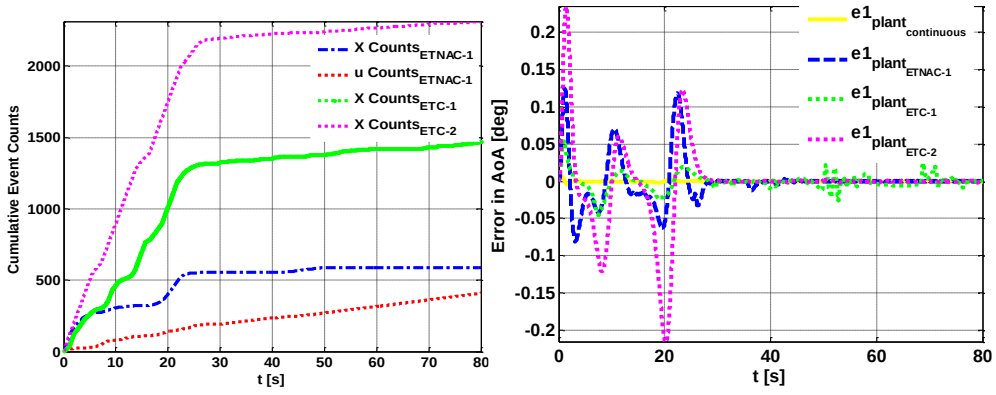

(a) (b)

Figure 8. Case 2 (Two Way Dynamically Triggered ETNAC 1): (a) Histories of sampling events for state and control and (b) Error in α.

Overall, excellent performance in terms of tracking, state estimation, and uncertainty estimation is achieved with ETNAC-1, while data communication and computational costs are reduced significantly.

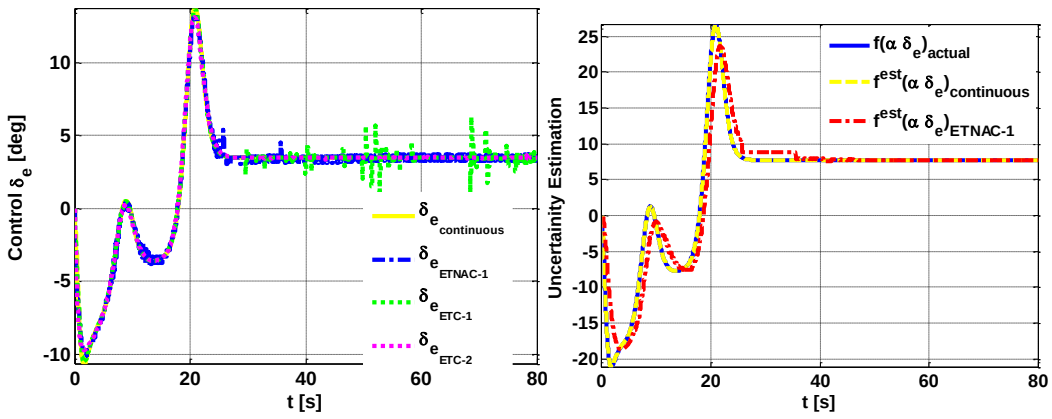

(a) (b)

Figure 9. Case 2 (Two Way Dynamically Triggered ETNAC 1): (a) Control δ_e and (b) Uncertainty approximation with ETNAC-1.

4.1.2.2. ETNAC-2. This section contains the results from static event-triggering, as described in subsection 3.1.2. The threshold values are set at 0.5×10^{-2}, 1×10^{-4}, and 5×10^{-2} for Trg_{2a}^{s} , Trg_{2a}^{u}, and Trg_{2b}^{u}, respectively. As in the previous simulation, a 3rd order polynomial regression is used to interpolate the state values during inter-event times. The overall trends are similar to the ETNAC-1 response. Excellent performance was achieved in terms of tracking and estimation, but the total number of sampling instants is comparatively less. The number of sampling instants for state and control are 555 and 229 respectively, thus reducing the communication frequency by more than 95.42%. To avoid repetition, we have provided only the plots for cumulative sampling instants (Figure 10a) and uncertainty approximation (Figure 10b) for ETNAC-2. As observed with ETNAC-1,

ETNAC-2 also shows hardly any event-triggering once the MSO converges. In the statically triggered case (ETNAC-2), if the user-defined thresholds are very high, then less sampling events occur, but this can also cause high jumps in the system response. One of the examples is given in Figure 11a, where the threshold is set to 0.1 and only 120 sampling events are observed, but it caused high jumps. However, these jumps can be avoided. For example, in this case, control triggering thresholds can be lowered or K_2 and γ can further be tuned. When K_2 was changed to $-9I$ and γ to $35I$, it resulted in a much smoother response, as can be seen in Figure 11b.

4.1.3. Results with One-Way ETNAC with MSO in the Controller Module.

4.1.3.1. ETNAC-4. Now, results with ETNAC-4 are given where the observer is located in the control system module. Note that now the state and the control are both transmitted and updated with one tracking error-based event-triggering condition.

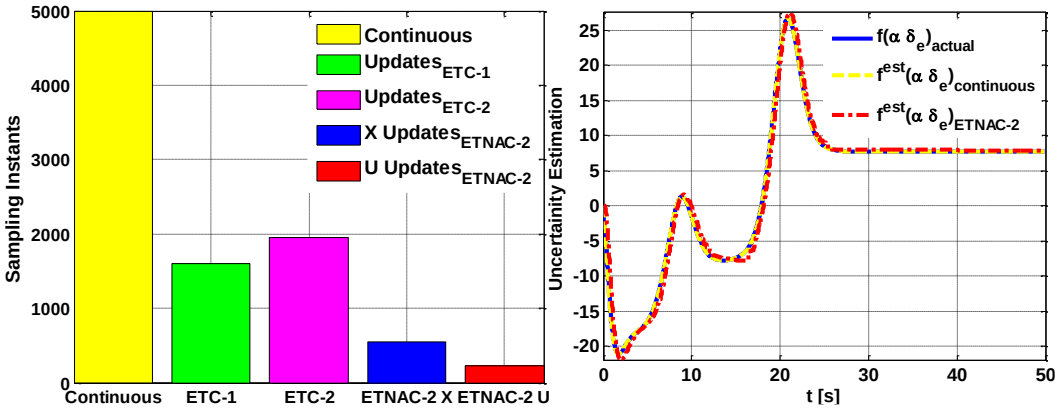

(a) (b)

Figure 10. Case 3 (Statically Triggered Two Way ETNAC): (a) Cumulative sampling events and (b) Uncertainty approximation.

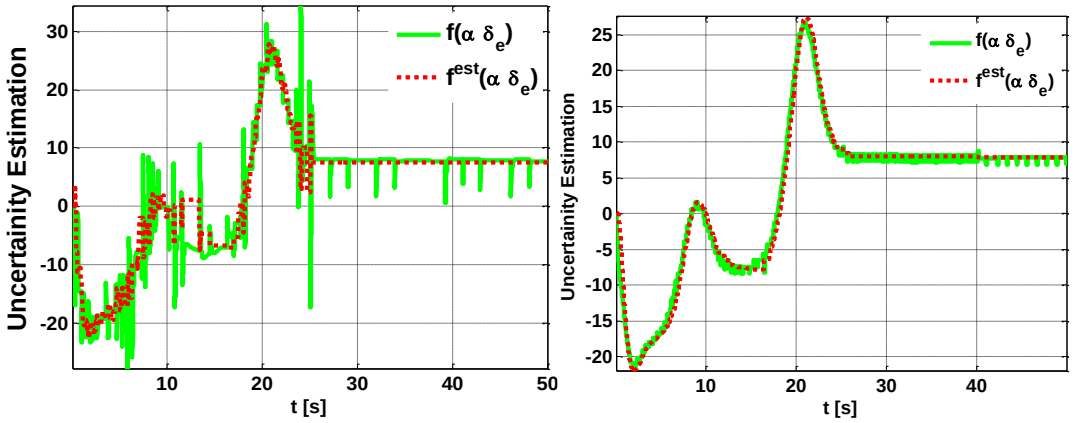

(a) (b)

Figure 11. Case 4: (a) ETNAC-2 response with high threshold and (b) ETNAC-2 response after smoothing.

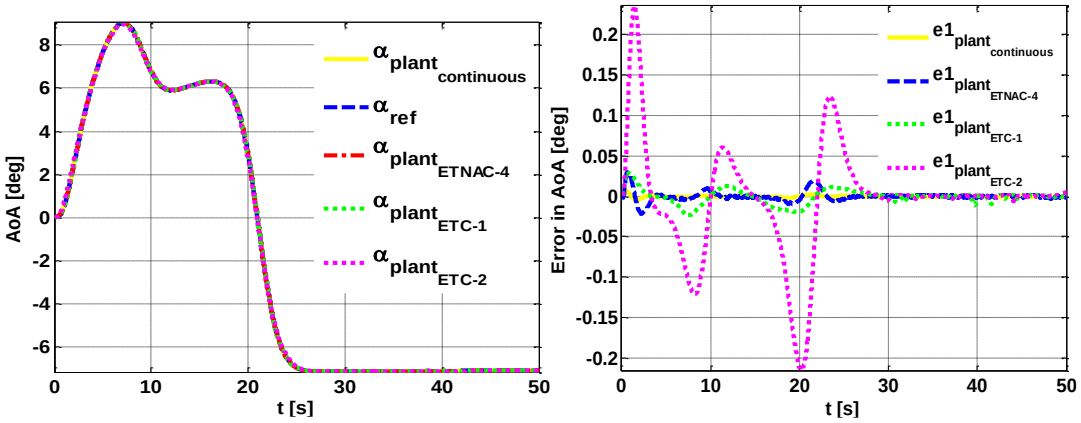

(a) (b)

Figure 12. Case 5 (Statically Triggered One-Way ETNAC-4): (a) AoA α and (b) Tracking error in α.

First, consider the case of static event-triggering condition, as given in (34). Again, the results are compared with statically triggered ETC-1 and ETC-2. State tracking and estimation performance are found to be excellent, as can be seen in Figures 12-14. The uncertainty approximation plot given in 14a is quite accurate. This time, the number of sampling instants reduces to 653, which results in a 86.94% reduction in data

communication and computations over a period of 50 seconds. On the other hand, 1608 updates for each (state and control) are seen with ETC-1 and 1839 for each with ETC-2. The steady state response is found to be like that of ETNAC-1 and ETNAC-2.

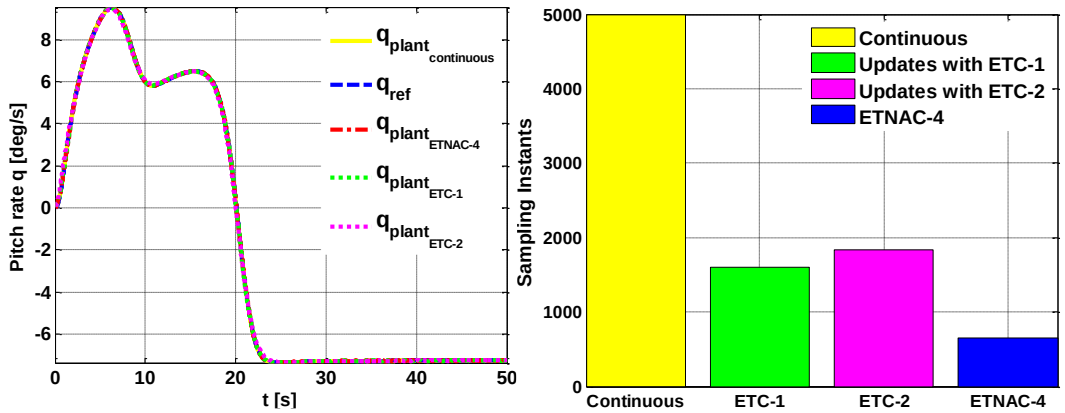

(a) (b)

Figure 13. Case 5 (Statically Triggered One-Way ETNAC-4): (a) Pitch Rate q and (b) Cumulative sampling events.

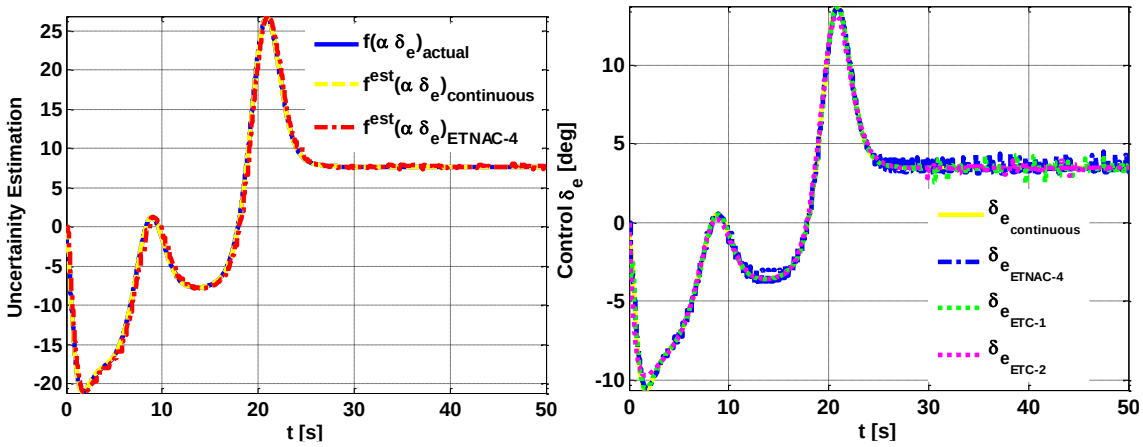

(a) (b)

Figure 14. Case 5 (Statically Triggered One-Way ETNAC): (a) Uncertainty approximation with ETNAC-4 and (b) Control δ_e History.

4.1.3.2. ETNAC-3. Results from the ETNAC-3 scheme, which is described in subsection 3.2.1, are provided in this section. Again, excellent tracking and uncertainty

approximation are achieved with ETNAC-3, while sampling instants are reduced to only 789 (as compared to ETC-1, where it is 1381 and ETC-2, where it is 1217). This implies that the same performance is almost achieved, with 84.22% less communication and less computations. Overall, the trends in results are similar to the static case except for the slight increase in the number of sampling instants. In the steady state, after 25 seconds small oscillations are observed at an almost periodic interval of 5 seconds as shown in Figure 15b.

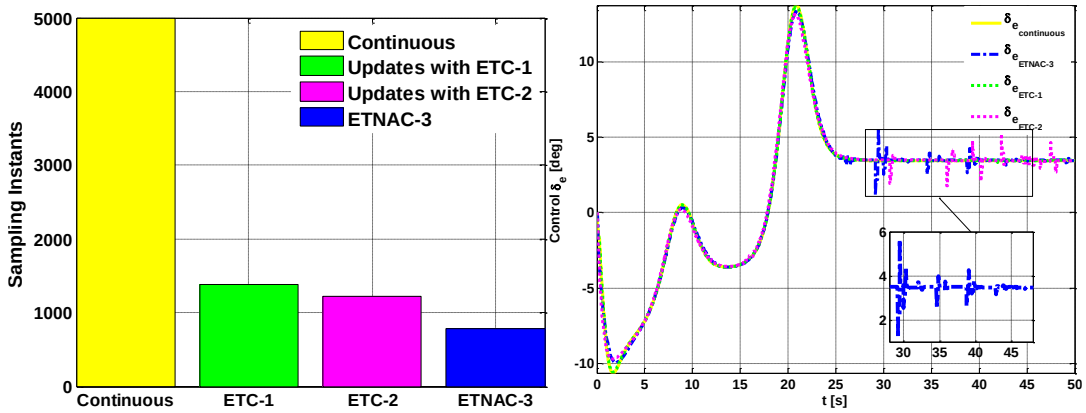

(a) (b)

Figure 15. Case 6 (Dynamically Triggered One-Way ETNAC-3): (a) Cumulative Sampling events and (b) Control δ_e History.

These oscillations diminished over the time for ETNAC-3, which is in contrast to the ETC methods like ETC-1. This is because the trigger condition is directly related to the tracking error and when the states become constant (after 30 seconds as can be seen in Figure 15b, a magnifier is added for ETNAC-3 plot only), and after the each update it goes off track to touch one side of threshold and then back to the other end of the threshold. It diminishes over time because it learns and adapts accordingly. But in other ETC methods, it continued to happen.

4.1.4. Results with One-Way ETNAC with MSO in the Sensor Subsystem.

4.1.4.1. ETNAC-5. In this subsection, results are given for ETNAC-5, where the observer is placed on top in the sensor subsystem and the triggering condition is dynamic, based on (40). In this case, the MSO converges, and the estimation error goes to zero even faster, as state values are available to the MSO all the time. Excellent tracking is observed

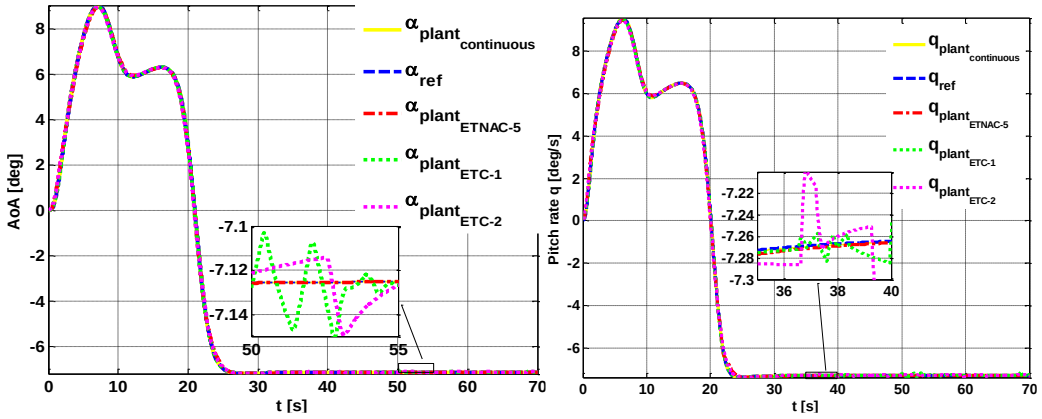

(a) (b)

Figure 16. Case 8 (One-Way Dynamically Triggered ETNAC-5): (a) AoA α and (b) Pitch Rate q.

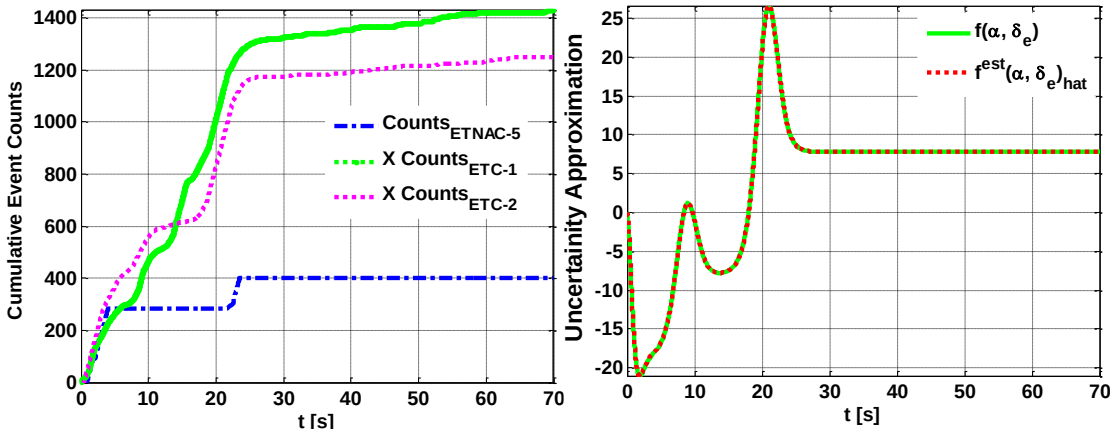

(a) (b)

Figure 17. Case 8 (One-Way Dynamically Triggered ETNAC-5): (a) Cumulative events history and (b) Uncertainty approximation.

with little oscillations. It saves more on communication, as the number of sampling instants reduces to only 136. Plots for this case are given in Figures 16 and 17.

Similar results are obtained by using ETNAC-6 (static event-triggering). Since the trends are similar, no plots are given.

4.2. UNCERTAIN LINEAR SYSTEM: RESULTS, DISCUSSION, AND ANALYSIS

This example is used in this paper since it has been used in many ETC papers such as in [2], [3], [25],[40], and [41]. In this study, we have furthermore added an uncertainty term to its dynamics in order to test the robustness of the proposed method.

$$\begin{bmatrix}\dot{x}_1\\ \dot{x}_2\end{bmatrix} = \begin{bmatrix}0 & 1\\ -2 & 3\end{bmatrix}\begin{bmatrix}x_1\\ x_2\end{bmatrix} + \begin{bmatrix}0\\ 1\end{bmatrix}(u + f(x)) \tag{49}$$

where the unknown uncertainty is expressed as $f(x) = 0.2x_1 + 0.2x_2$. A second order reference system is chosen with a natural frequency of 0.5 and a damping ratio of 0.707. A time-varying square wave is used as the reference input. We evaluated only ETNAC-1 in this study as proof of concept. Parameter values used are $L = 1$, $\gamma = 20$, $\sigma = 3$, $Q = 1I$, and $K_2 = -3I$, and β_{a} is calculated as per (23). Values for K_1 and K_3 are calculated as per (12) and (13). The sampling time is set at $\Delta t = 0.01$ sec for the continuous simulation and it is run for 100 seconds. In Figures 18a and 18b, the time histories for states are shown: the reference states, actual states, and the estimated states. Overall, the estimation and tracking performance are found to be good, the states stay bounded. Note that now only 663 state and 541 control sampling instants are observed as compared to 10,000 sampling instants in the continuous case. The control evolution given in Figure 19a is stable. The uncertainty estimation plot in Figure 19b is quite good except for minor oscillations.

Though initially it has small jumps at peaks, they diminish over time as NNWs adapt and converge. These jumps appear at the peaks since the reference state has constant values for that duration and the states hover around that value under the given thresholds. That is the reason the sampling rate is even lower at peaks, as can be observed in Figure 20a. State sampling is reduced by 93.37% and control sampling by 94.59%, which are significant reductions.

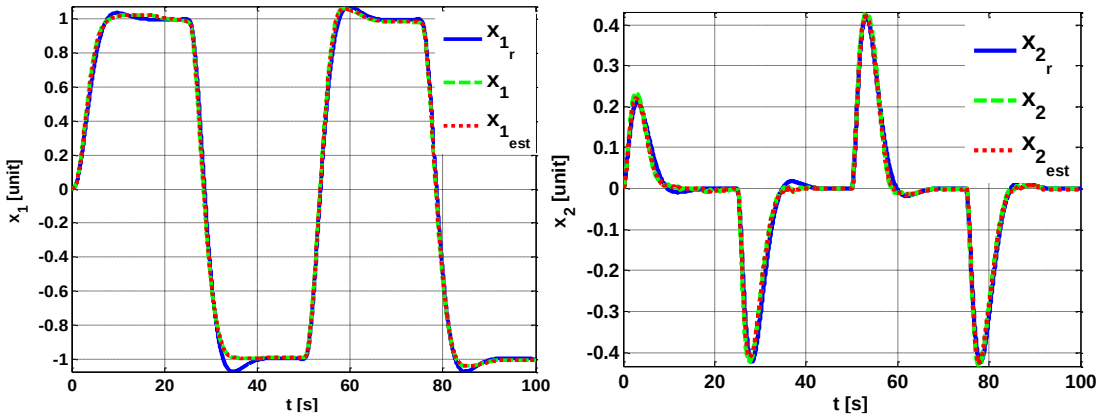

(a) (b)

Figure 18. Two Way Dynamically Triggered ETNAC-1: (a) State-1 $x_1, x_{1_r} \& \hat{x}_1$ histories and (b) State-2 $x_2, x_{2_r} \& \hat{x}_2$ histories.

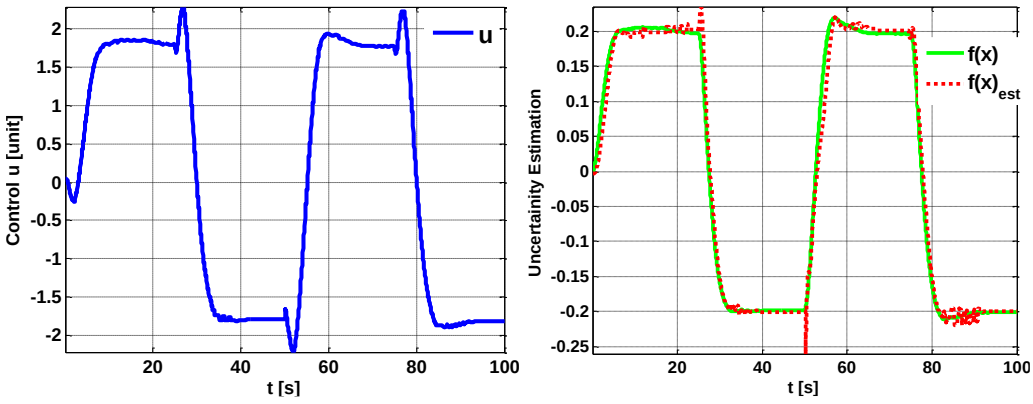

(a) (b)

Figure 19. Two Way Dynamically Triggered ETNAC: (a) Control (u) history and (b) Uncertainty approximation.

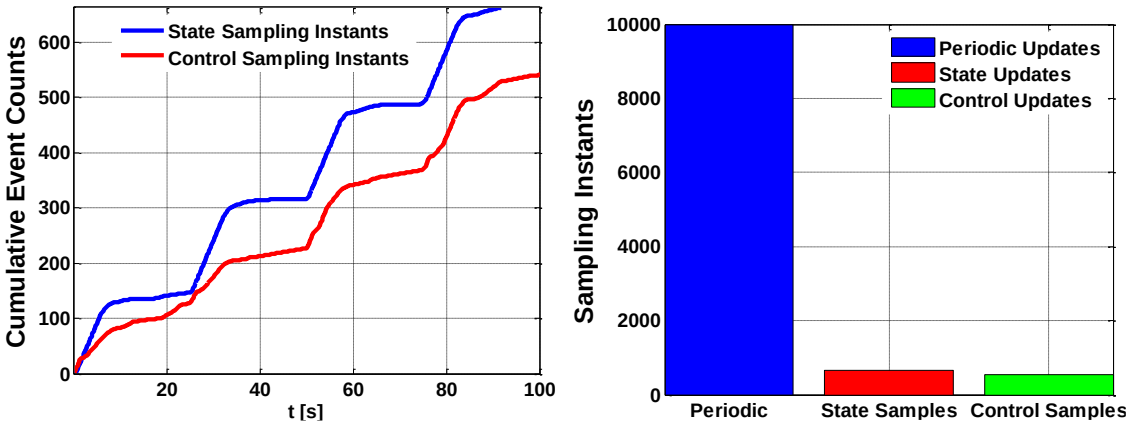

(a) (b)

Figure 20. Two Way Dynamically Triggered ETNAC: (a) History of sampling events for state and control and (b) Cumulative event.

4.3. BRIEF SUMMARY OF THE OBSERVATIONS/RECOMMENDATION

A brief summary of observations on the proposed ETNAC designs and numerical results is given below:

I-Proposed ETNAC architectures are given with the observer at the top level, at the bottom, or at both levels. Similarly, different dynamic and static triggering conditions are developed for each architecture. Such combinations of design and conditions offer flexibility to a control system designer.

II- It is suggested that if the output is constantly varies, then dynamic triggering is more suitable as it provides comparatively smoother results.

III-The two-way ETNAC gives flexibility for the problems where the state and control transmission frequencies need to be separated. As seen in the first example, where the uncertainty was a direct function of control, a higher frequency of control execution could yield smoother results.

IV-For a constant output system, the one-way ETNAC with the observer in the controller module yielded the best results. There was hardly any data exchange once the observer tracked the plant accurately and the uncertainty estimation converged.

V-Another thing to note is that although all ETNAC techniques are useful in both data communication reduction and computational savings, it is recommended to place the observer in the sensor subsystem if the communication cost is more important, and to place the observer in the controller module if the computational resources are restricted.

VI-In general, a 3^{rd} order polynomial regression is good enough for the state interpolation during the inter-event time, although any order can be used. Note that at a very small cost of transmitting a few coefficients could result in much savings in communication and computational cost.

VII-Relating triggering conditions to estimation and tracking errors allows them to be performance-centric, or in other words more realistic.

VIII-It should be noted that the ETNAC designs are more complex since they have an observer as a part of the controller-sensor systems and possess dynamic triggering conditions. They need more storage than simpler ETC designs and have to communicate more quantities relatively through their subsystems. In addition, their advantages which can be seen from the performance comparisons provided in this section, far outweigh the disadvantages.

5. CONCLUSIONS

Six MSO-based ETNAC schemes were derived; the performance of all versions were evaluated and compared with existing ETC schemes for their transient and steady state performance and efficiency. A summary has been provided on the features of the proposed schemes. Each of the proposed schemes can estimate, compute the model uncertainties, save communication and computational cost by utilizing its event-triggered mechanism, and guarantee stability and good close loop performance. From the representative simulated examples, which showed 95% less sampling instants and maintained good tracking, it appears that the proposed schemes have much practical potential to be used in embedded networked systems.

ACKNOWLEDGEMENT

This research was partially supported by NASA under grants NNX15AM51A and NNX15AN04A.

REFERENCES

[1] S. Gupta," Increasing the Sampling Efficiency for Control System," *IEEE Transactions on Automatic Control*, vol. 8, no. 3, pp. 263-264, 1963.

[2] P. Tabuada, "Event-triggered Real Time Scheduling of Stabilizing Control Tasks", *IEEE Transactions on Automatic Control*, vol. 52, no. 9, pp.1680 –1685, Sept 2007. doi: 10.1109/TAC.2007.904277

[3] W.P.M.H. Heemels, K.H. Johansson, P. Tabuada," An Introduction To Event - Triggered And Self-Triggered Control" *51st IEEE Conference on Decision and Control*, Maui, USA , pp. 3270-3285, 2012. doi: 10.1109/CDC.2012.6425820

[4] McCulloch, "A Logical Calculus of the Ideas Immanent in Nervous Activity," *The Bull. Math. Biophys*, vol. 5, no. 4, pp.115-133, 1943. doi: 10.1007/BF02478259

[5] K.S. Narendra and K. Parthasarathy," Identification and Control of Systems Using Neural Network," *IEEE Trans. on Neural Net*, vol. 1, no. 1, pp. 4-27, 1990. doi: 10.1109/72.80202

[6] R.M. Sanner and J.-J.E. Slotine, "Gaussian Networks for Direct Adaptive Control," *IEEE Trans. on Neural Network*, vol. 3, no. 6, pp. 837-863, 1992. doi: 10.1109/72.165588

[7] F. L. Lewis, A. Yesildirek and Kai Liu "Multilayer Neural-Net Robot Controller with Guaranteed Tracking Performance," *IEEE Trans. on Neural Network*, vol. 7, no. 2, pp. 388-399, 1996. doi: 10.1109/72.485674

[8] G. Zhang and X. Zhang, "Practical Robust Neural Path Following Control for Underactuated Marine Vessels with Actuators Uncertainties," *Asian Journal of Control*, 19, pp. 173– 187. doi: org/10.1002/asjc.1345

[9] G. Zhang, C. Huang, Zhang, and W. Zhang, "Practical Constrained Dynamic Positioning Control for Uncertain Ship Through The Minimal Learning Parameter Technique", *IET Control Theory & Applications*, vol. 12, no. 18, pp.2526-2533, 2018. doi: 10.1049/iet-cta.2018.5036

[10] G. Zhang, Y. Deng, W. Zhang, and C. Huang, "Novel DVS Guidance and Path-Following Control for Underactuated Ships in Presence of Multiple Static and Moving Obstacles", *Ocean Engineering170*, pp. 100-110, 2018. doi: 10.1016/j.oceaneng.2018.10.009

[11] D. Ali and S. Frimpong, "Artificial Intelligence Models for Predicting the Performance of Hydro-Pneumatic Suspension Struts in Large Capacity Dump Trucks," *International Journal of Industrial Ergonomics, Elsevier*, vol. 67, pp. 283-295, Sep 2018. doi: 10.1016/j.ergon.2018.06.005

[12] D. Ali, M. Hayat, L. Alagha, and O. Molatlhegi, "An Evaluation of Machine Learning and Artificial Intelligence Models for Predicting the Flotation Behavior of Fine High-Ash Coal," *Advanced Powder Technology, Elsevier*, vol. 29, no. 12, pp. 3493-3506, Dec 2018. doi: 10.1016/j.apt.2018.09.032

[13] A.U. Rehman and K. Awuah-Offei, "Investigating the Information Diffusion Potential of Social Media Networks," *Mining Engineering*, vol. 70, no. 4, pp. 28-32, Society for Mining, Metallurgy and Exploration, Apr 2018.

[14] J. Lunze and D. Lehmann, "A State-Feedback Approach to Event Based Control", *IEEE Transaction on Automatic*, vol. 46, no. 1, pp. 211-215, 2010. doi: 10.1016/j.automatica.2009.10.035

[15] T. Liu and Z.P. Jiang," A Small-Gain Approach to Event-Triggered Control of Nonlinear Systems," *In Proc. of the 33rd Chinese Control Conference*, pp. 5857-5862, 2014. doi: 10.1109/ChiCC.2014.6895942

[16] R. Postoyan, P. Tabuada, D. Nesic and A. Anta, "A Framework for The Event-Triggered Stabilization of Nonlinear Systems" *IEEE transactions on Automatic Control*, vol. 60, no. 4, pp.982-996, 2015. doi: 10.1109/TAC.2014.2363603

[17] E. Garcia and P.J. Antsaklis," Model-Based Event-Triggered Control for System with Quantization and Time Varying Network Delays," *IEEE Tans. on Autom. Control*., vol. 58, no.2, pp. 422-434, 2013. doi: 10.1109/TAC.2012.2211411

[18] D. Wang, C. Mu, H. He and D. Liu, "Event-Driven Adaptive Robust Control of Nonlinear Systems with Uncertainties Through NDP Strategy," in *IEEE Transactions on Systems, Man, and Cybernetics: Systems*, vol. 47, no. 7, pp. 1358-1370, July 2017. doi: 10.1109/TSMC.2016.2592682

[19] A. Sahoo, H. Xu and S. Jagannathan, "Neural Network-Based Event-Triggered State Feedback Control of Nonlinear Continuous-Time Systems," in *IEEE Transactions on Neural Networks and Learning Systems*, vol. 27, no. 3, pp. 497-509, March 2016. doi: 10.1109/TNNLS.2015.2416259

[20] A. Sahoo, H. Xu and S. Jagannathan, "Near Optimal Event-Triggered Control of Nonlinear Discrete-Time Systems Using Neurodynamic Programming," *IEEE Trans. on Neural Net. and Learning Sys*, vol. 27, no. 99, pp.1801-1815, Sep 2016. doi: 10.1109/TNNLS.2015.2453320

[21] X. Wang and N. Hovakimyan, "L1 Adaptive Control of Event-Triggered Networked Systems," *Proc. of IEEE American Control Conference (ACC),*Baltimore, MD, pp. 2458–2463, 2010. doi: 10.1109/ACC.2010.5530583

[22] X. Wang, E. Kharisov and N. Hovakimyan, "Real-Time L1 Adaptive Control for Uncertain Networked Control Systems," in *IEEE Transactions on Automatic Control*, vol. 60, no. 9, pp. 2500-2505, Sept. 2015. doi: 10.1109/TAC.2014.2380653

[23] K.J. Åström and B. Bernhardsson, “Comparison of Periodic and Event Based Sampling for First Order Stochastic Systems,” *Proc. of IFAC World Conf.*, vol. 32, no. 2, pp. 5006–35011, 1999. doi: 10.1016/S1474-6670(17)56852-4

[24] A. Albattat, B.C. Gruenwald and T. Yucelen, “On Event-Triggered Adaptive Architectures for Decentralized and Distributed Control of Large-Scale Modular Systems”, *Sensors*, vol. 16, no. 8, pp. 1-31, 2016. doi: 10.3390/s16081297

[25] A. Albatat, B.C. Gruenwald, T. Yucelen, “Design and Analysis of Adaptive Control System Over Wireless Network,” *ASME J. Dynamic System, Measurements and Control*, vol. 139, no. 7, pp. 1-8, 2017. doi: 10.1115/1.4035094

[26] R. Padhi, N. Unnikrishnan and S. N. Balakrishnan, "Model-Following Neuro-Adaptive Control Design for Non-Square, Non-Affine Nonlinear Systems," *IET Control Theory & Applications*, vol. 1, no. 6, pp. 1650-1661, 2007. doi: 10.1049/iet-cta:20060364

[27] K. Rajagopal, S. N. Balakrishnan, N. Nguyen, K. Krishnakumar and A. Mannava, “Neuroadaptive Model Following Controller Design for Non-Affine and Non-Square Aircraft Systems”, *AIAA Guidance, Navigation, and Control Conference*, pp. 1-21, 2009. doi: 10.2514/6.2009-5737

[28] A. Ghafoor, S.N. Balakrishnan and T. Yucelen, "Modified State Observer Based Decentralized Neuro-Adaptive Controller for Large Scale Interconnected Uncertain Systems," *2018 Annual American Control Conference (ACC)*, Milwaukee, WI, 2018, pp. 1701-1706. doi: 10.23919/ACC.2018.8431513

[29] A. Ghafoor, J. Yao, S.N. Balakrishnan, J. Sarangapani and T. Yucelen, “Event Triggered Neuroadaptive Controller (ETNAC) Design for Uncertain Affine Nonlinear Systems” *ASME DSCC 2018*-9103, USA, 2018. doi: 10.1115/DSCC2018-9103

[30] A. Ghafoor, S.N. Balakrishnan, S. Jagannathan and T. Yucelen, "Event-Triggered Neuro-Adaptive Controller (ETNAC) Design for Uncertain Linear Systems," *2018 IEEE Conference on Decision and Control (CDC)*, FL, USA, 2018, pp. 2217-2222. doi: 10.1109/CDC.2018.8618962

[31] A. Ghafoor and S.N. Balakrishnan, "Modified State Observer based Two-Way ETNAC for Uncertain Linear Systems", *International Joint Conference on Neural Network (IJCNN) 2019*, Budapest, Hungary, #20379 2019.

[32] A. Ghafoor, P. Galchenko, S. N. Balakrishnan, H. Pernicka and T. Yucelen, "ETNAC Design Enabling Formation Flight at Liberation Points," *IEEE American Control Conference (ACC) 2019*, Philadelphia, PA, USA, 2019, pp. 3689-3694.

[33] D. Yue, E. Tian and Q. Han, "A Delay System Method for Designing Event-Triggered Controllers of Networked Control Systems," in *IEEE Transactions on Automatic Control*, vol. 58, no. 2, pp. 475-481, Feb. 2013. doi: 10.1109/TAC.2012.2206694

[34] E. Tian, Z. Wang, L. Zou, and Dong Yue, "Chance-constrained H∞ control for a class of time-varying systems with stochastic nonlinearities: The finite-horizon case," in *Automatica*, vol. 107, pp. 296-305, ISSN 0005-1098, 2019. doi.org/10.1016/j.automatica.2019.05.039

[35] Q. Zhao and J. Sun, "Event-Triggered Control for Uncertain Linear Systems," *2018 Annual American Control Conference (ACC)*, Milwaukee, WI, 2018, pp. 6248-6252. doi: 10.23919/ACC.2018.8431207

[36] Y. Qi, Y. Liu and P. Zeng, "Event-triggered guaranteed cost control for uncertain switched linear systems," *2017 36th Chinese Control Conference (CCC)*, Dalian, 2017, pp. 2415-2420. doi: 10.23919/ChiCC.2017.8027720

[37] N. S. Tripathy, I. N. Kar and K. Paul, "Stabilization of Uncertain Discrete-Time Linear System With Limited Communication," in *IEEE Transactions on Automatic Control*, vol. 62, no. 9, pp. 4727-4733, Sept. 2017. doi: 10.1109/TAC.2016.2626967

[38] D.P. Borgers, V.S. Dolk and W.P.M.H. Heemels, "Riccati-Based Design of Event-Triggered Controllers for Linear Systems With Delays," in *IEEE Transactions on Automatic Control*, vol. 63, no. 1, pp. 174-188, Jan. 2018. doi: 10.1109/TAC.2017.2713047

[39] A. Margun, I. Furtat, K. Zimenko and A. Kremlev, "Event-triggered output robust controller," *2017 25th Mediterranean Conference on Control and Automation (MED)*, Valletta, 2017, pp. 625-630. doi: 10.1109/MED.2017.7984187

[40] H. Chen, Y. Fan and J. Chen, "Optimized Event-Triggered and Self-Triggered Control for Linear Systems," *2019 34rd Youth Academic Annual Conference of Chinese Association of Automation (YAC)*, Jinzhou, China, 2019, pp. 579-584. doi: 10.1109/YAC.2019.8787709

[41] M. Kishida, M. Kögel and R. Findeisen, "Event-triggered actuator signal update using self-triggered sampled data for uncertain linear systems," *2017 American Control Conference (ACC)*, Seattle, WA, 2017, pp. 3035-3041. doi: 10.23919/ACC.2017.7963413

[42] K. Li, B. Zheng and J.H. Park, "Event Based Robust Consensus for Multi-Agent Systems via Sliding-Mode Control," *2018 Chinese Control and Decision Conference (CCDC)*, Shenyang, 2018, pp. 4483-4488. doi: 10.1109/CCDC.2018.8407906

[43] A. Young, C. Cao, V. Patel, N. Hovakimyan and E. Lavretsky, "Adaptive Control Design Methodology For Nonlinear-in-Control Aircraft Applications", *Journal of Guidance, Control and Dynamics*, vol. 30, no. 6, pp. 1770-1783, 2007. doi: 10.2514/1.27969

[44] E. Lavretsky and K. Wise, "Robust and Adaptive Control: With Aerospace Applications," *Springer*, New York, 2012, Chap. 11.

[45] D.S. Bernstein, "Matrix Mathematics: Theory, Facts, and Formulas," *Princeton University Press*, Princeton, NJ, 2009.

[46] H. K. Khalil, "Nonlinear Systems," *Prentice Hall*, Upper Saddle River, NJ, 1996.

[47] B. Stevens and F. Lewis, "Aircraft Control and Simulation," Wiley, New YorK, 1992.

II. EVENT-TRIGGERED NEURO-ADAPTIVE CONTROL FOR FORMATION CONTROL WITH REDUCED JITTER IN A DEEP SPACE ENVIRONMENT

A. Ghafoor*, P. Galchenko, S.N. Balakrishnan, and H. Pernicka

Department of Mechanical and Aerospace Engineering, Missouri University of Science and Technology, Rolla, MO 65401

T. Yucelen

Department of Mechanical Engineering, University of South Florida, Tampa, FL 33620

ABSTRACT

This study considers the feasibility of an event-triggered neuro-adaptive controller providing formation control while reducing jitter for microsatellites used in deep space missions. A single microsatellite at the Sun-Earth/Moon L_1 libration point is considered as a follower spacecraft in formation with a single leader spacecraft. A halo orbit is generated as a reference trajectory for the leader spacecraft and modeled as a virtual node defined along the reference trajectory about which the follower spacecraft maintains its relative position. For such microsatellites, limited capabilities of the platform, including restricted controls and actuation, and sensitive responses to uncertainties and jitter make the controller design challenging. To address such challenges, an event-triggered neuro-adaptive controller (ETNAC) is proposed in this paper. ETNAC is based on the use of an observer, known as the Modified State Observer (MSO) that is used for online approximation of the uncertainties in the dynamics. In addition to uncertainty approximation, the MSO also offers filtering effects; its formulation has two tunable gains

that allow for fast estimation without inducing high frequency oscillations in the system. At the same time, for the event-triggering mechanism (ETM), the system state is sensed continuously but fed back only when required in an aperiodic fashion, and control is recomputed only with updated information. In this way, inter-event time increases compared to that of continuous updates, resulting in reduced jittering. Two new ETNAC schemes are considered in this study. The system's theoretical derivations and the numerical implementation of each scheme are presented. Lyapunov analysis is used to prove stability and derive the event-triggering conditions. Simulation and performance results show that ETNAC can be an excellent solution for such highly nonlinear, sensitive, and resource-constrained problems.

1. INTRODUCTION

Advances in hardware capabilities of the microsatellite platform have begun to enable deep space missions with microsatellites [1]. They can play an increasing role in advanced mission concepts with savings in cost, size, weight, and power as compared to traditional large monolithic spacecraft. To achieve the objectives of these missions, often a number of microsatellites is needed that maintain a tight flight formation, requiring precision control. With the maturity of the microsatellite platform and the recent development of micropropulsion systems designed for such architectures, the required tight formation tolerances can now be achieved. This study addresses the design of robust and precise control solutions to enable the use of these technologies in precision formation flight (PFF).

A number of advanced mission concepts has been studied that require precision formation flight in a deep space environment. Planet finding missions such as the Terrestrial Planet Finder [2] and Darwin [3] seek to "create" infrared interferometers using multiple spacecraft in PFF to emulate powerful telescopes to search for distant planets. The Micro-Arcsecond X-Ray Interferometry Mission (MAXIM) [4] mission seeks to observe and study black hole phenomena, while the Laser Interferometer Space Antenna [5] mission seeks to study gravitational waves. Other missions such as the NASA Stellar Imager [6] seek to use small spacecraft in PFF to create a virtual telescope for observation of stellar surfaces. Each of these unique missions seek to utilize swarms of spacecraft in PFF to enable advanced missions that would otherwise be unfeasible for large monolithic spacecraft due to size, weight, and power requirements.

Three-body dynamics, often described by the circular restricted three-body problem (CR3BP) equations, give rise to libration points, which are locations relative to two primary bodies where dynamic forces/accelerations acting on a spacecraft are in equilibrium. These points offer unique advantages to deep space missions as they allow for spacecraft to enter and remain in orbits at these locations with only modest station keeping effort, facilitating long duration scientific missions such as MAXIM and Stellar Imager. However, missions like MAXIM require millimeter/submillimeter [7] position control, while the Stellar Imager requires position control in the micrometer range [8]. To achieve these tolerances, micropropulsion systems must be capable of producing thrust values in the nano- to micronewton range. Marchand and Howell studied a variety of control strategies including linear quadratic regulator (LQR) and feedback linearization methods to quantify propulsion requirements for advanced missions such as MAXIM and the Terrestrial Planet Finder [9].

Using the CR3BP model as well as an ephemeris model, it was found that thrust levels ranged from nano- to millinewtons for large monolithic spacecraft, as well as requiring nearly continuous control when trying to achieve submillimeter position control. While studies by Howell and Marchand have found the potential existence of natural formations at libration points [10], further study is needed before continuous or impulsive control strategies are implemented.

Previous studies have explored continuous and impulsive controllers for PFF through linear, nonlinear, and adaptive control techniques. An optimal nonlinear controller technique, θ-D, was used by Xin et al. to bring relative position error into the submillimeter range [11] [12] , while Li used a combination of LQR control with neural network learning to accommodate the nonlinearities in the basic dynamics and achieve range error levels in the order of tens of millimeters [13]. By using nonlinear control and robust adaptive methods, Xu was able to keep formation errors in the sub-kilometer range while estimating the spacecraft mass and bounds of the disturbances experienced [14]. Similar adaptive techniques used by Queiroz were able to estimate the mass and disturbances while reducing relative errors to the submeter range [15]. Work by Gurfil with nonlinear control techniques along with neural networks reduced relative errors to the submillimeter range [16].

While utilizing continuous controllers provides acceptable relative position performance, jitter and propellant budgets onboard the spacecraft are increased compared to impulsive methods. Work by Qi used an impulsive control strategy, which was able to maintain the spacecraft in a bounded relative position error corridor as small as 100 centimeters [17]. However, this case was limited to CR3BP dynamics without consideration of other disturbances outside of thruster errors.

Another important concern is that continuously updated control and actuation can cause jitter in the spacecrafts position and pointing, which can lead to diminished scientific return. Some papers, which study jitter independently, include [18]-[25], showing that jitter induced vibration can lead to diminished controller performance, or even instability in navigation and control algorithms. High frequency jitter can also be critical to the integrity of microsatellite hardware, which typically does not undergo the extended vibration testing conducted on larger monolithic spacecraft. Some effort has been made to measure jitter in microsatellites, such as [27], [21], [22] and [23], and employ techniques to reduce jitter. Two such techniques reduce jitter through controller development and actuation leading to vibration isolation such as managing angular momentum using a magnetic torquer [27] or by adaptive moment distribution control logic [20]. Along with the other contributions of this paper, we have proposed a unique and direct way to reduced jitter through the controller algorithm itself. Jitter is induced each time the control is updated and the actuators are activated, inducing a sudden step input into the dynamics of the system. This is where event-triggering mechanism (ETM) is useful, as an update in control is only applied when needed, leading to longer periods of smooth motion as compared to traditional periodic and continuous controllers. This period of smooth motion, during which there are no additional internal/external inputs into the system, is termed as periods of silence. The reduced occurrence of actuator updates increases the period of silence and thereby directly reduces the amount of jitter induced, without compromising the performance of the controller metrics. To enable the application of microsatellites to PFF at libration points, methods to improve relative position error precision under disturbances

must be considered while keeping control updates, jitter, and propellant budgets reasonable to facilitate onboard implementation. These important factors are considered in this study.

This effort proposes an event-triggered neuro-adaptive controller (ETNAC) providing PFF control for deep space mission applications using microsatellites. This method is able to reduce jitter by increasing the periods of silence, estimate and address uncertainties and perturbations, while maintaining a tight relative position error tolerance. Gupta described a number of techniques to sample state information efficiently in [33] leading to the development of the event-triggered strategy. Heemels [35] proposed the event-triggered condition design process for linear systems in which a control Lyapunov function was adopted to guarantee input-to-state stability. Tabuada ensured asymptotic stability with an event-triggered controller [34] and gave a proof for the existence of the lower bound of inter-event times. As uncertainty and perturbations are inevitable parts of the system dynamics, adaptive control methods can be used to learn these uncertainties and adjust the control accordingly [36]. Some other notable contributions in adaptive event-triggered control are given in [28]-[43].

In this study, ETNAC is developed and applied to a notional deep space mission. The case study defined here considers formation flight at the Sun-Earth/Moon L_1 libration point, with a halo orbit as the reference trajectory. A reference virtual node, defined as the leader of a formation of an arbitrary number of spacecraft, is placed along the reference trajectory about which the follower spacecraft will maintain some defined relative position. (Note that this leader node need not necessarily have an actual spacecraft stationed there.) This formation can be easily expanded to any number of spacecraft, each with their own relative position from the reference node, such that a virtual structure is formed. The virtual

structure has a central node, defined as the reference node (i.e. the leader), and a number of nodes defined by fixed locations from the reference node. The shape of the virtual structure can be defined as desired; for example, the Stellar Imager mission proposes a parabolic virtual structure to emulate a parabolic mirror [7]. This structure remains fixed over time and its reference node follows the natural motion of the desired halo trajectory. Each spacecraft can then be assigned to a relative node about which they maintain their position. By maintaining their position, formation flight is enabled. Using a single follower spacecraft to demonstrate this relative position control to the reference node is sufficient to show the concept feasibility and is a key objective of this study enabled by the ETNAC control approach. The virtual structure concept is shown in Figure 1, where n_{ref} is the reference node and where n_1, n_2, ... are relative nodes at fixed locations, given by $\vec{r}_1, \vec{r}_2$, ..., respectively, from the reference node. In this study, a relative node was arbitrarily placed

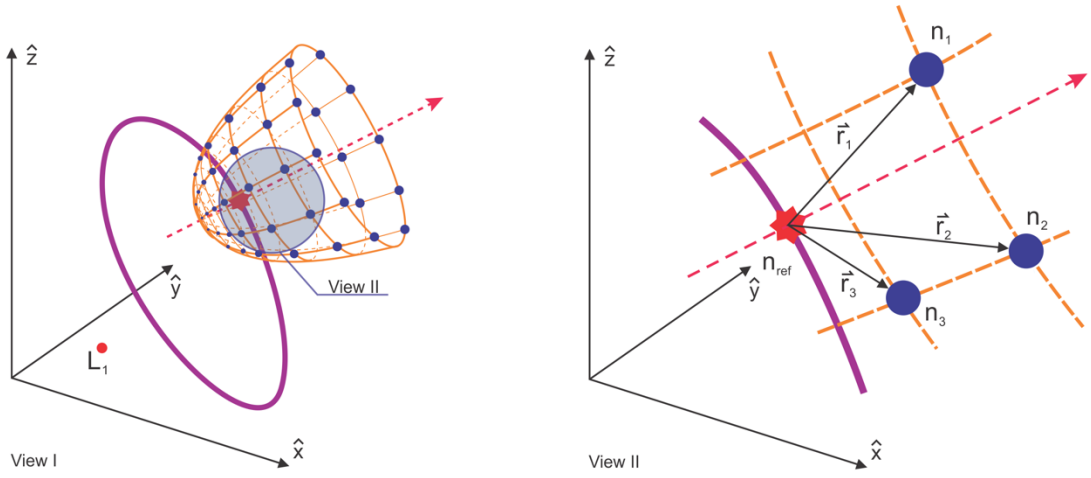

Figure 1. The fixed virtual structure (View I) is defined with the reference node on the halo trajectory, with relative nodes (View II) placed at fixed locations from the reference node. By placing and maintaining spacecraft at these relative nodes, formation flight is enabled.

at a fixed 100 m separation (with equal components along the three rotating axes) from the reference node and the spacecraft was required to maintain this relative position to the reference node throughout the simulation.

In event-triggered control, the state of the system is sensed continuously but sent to the controller only when required. Typically, this communication cycle is aperiodic. A condition, called the "event-triggered condition," is derived to determine when to transmit such information. The control is then applied to maintain the PFF of the spacecraft, while perturbations are applied to the system to assess the robustness of the control method. Numerical studies are further used to determine/conclude if ETNAC is capable of maintaining the reference trajectory, while robust to system perturbations and noise.

Two new techniques proposed in this paper are based on where the observer is placed within the control system architecture. The first one is referred to as ETNAC-1 in which the observer operates in parallel with the controller and is only updated at the event condition. In this method, only state and four curve fitting parameters are transmitted at the event condition. The controller and observer are updated at the sampling instant and transmitted to the plant. Though the plant receives only data for the sampling instant, the observer is continuously simulated between the current and last sampling instant times. In this inter-event simulation, neural network (NN) learning and different curve fitting algorithms can be used to manage computation bandwidth. As such, the observer and controller are only updated aperiodically at the event condition, extending the inter-event time. The second proposed method is referred to as ETNAC-2 in which the observer executes outside of the event driven conditions. The observer is thus continuously updated in a periodic fashion while having access to state measurements at all times. When an event

trigger condition is met, the system state, observer state, and NN weights are transmitted to the controller, which is thus updated in an aperiodic fashion. This flexibility enables an appropriate methodology to be chosen depending upon the spacecraft platform capabilities and performance requirements.

The remainder of the paper is organized as follows: Section II presents the systems dynamics/state model and Section III contains the problem formulation. Section IV provides the proposed solution (ETNAC) summary. Section V contains discussions of the numerical implementation, results, and analysis. Section VI summarizes the conclusions from this study followed by proofs and references.

2. SYSTEM DYNAMICS

2.1. CIRCULAR RESTRICTED THREE-BODY PROBLEM (CR3BP)

The well-known nondimensional CR3BP equations of motion [18] used in this study are given as

$$\begin{aligned} \ddot{x} &= 2\dot{y} + x - (1-\mu)\frac{x+\mu}{{R_1}^3} - \mu\frac{x-(1-\mu)}{{R_2}^3} \\ \ddot{y} &= -2\dot{x} + y - (1-\mu)\frac{y}{{R_1}^3} - \mu\frac{y}{{R_2}^3} \\ \ddot{z} &= -(1-\mu)\frac{z}{{R_1}^3} - \mu\frac{z}{{R_2}^3} \end{aligned} \tag{1}$$

where μ is the mass ratio parameter of the two primary bodies $\left(\frac{m_2}{m_1+m_2}\right)$ and R_1 and R_2 represent the distances of the third body (the spacecraft with components *x*, *y*, and *z* in terms of the rotating frame defined by the primaries' motion) from the respective primary bodies. These equations of motion describe the natural (unperturbed and uncontrolled)

motion of this third body of negligible mass, whose motion is determined by the gravitational forces of the two primary bodies.

2.2. SOLAR RADIATION PRESSURE

Deep space trajectories can be significantly perturbed by solar radiation pressure (SRP), which is modeled in this study with magnitude

$$P_{sun} = \frac{\psi_{sun}}{c\, r_s} \tag{2}$$

where ψ_{sun} is the solar constant at one astronomical unit (AU), ranging between 1,361 W/m^2 and 1,363 W/m^2 based on the solar cycle, c is the speed of light, and r_s is the distance between the spacecraft and the Sun in astronomical units. The spacecraft is modeled as having uniform sides and the force generated by SRP is expressed in vector form [18] as

$$F_{srp} = -P_{sun} c_r A_{\odot} \frac{r_{sat\odot}}{|r_{sat\odot}|} \tag{3}$$

where $A_{\odot}$ is the exposed area of the spacecraft to the Sun, c_r is the coefficient of reflectivity, and $r_{sat\odot}$ is the spacecraft-to-Sun position vector.

2.3. SPACECRAFT AND THRUSTER MODEL

Marchand and Howell have shown that for tight precision control, thrusters need to be capable of producing thrust in the nano- to millinewtons range [9]. While there are thruster systems in development, such as Plasmonic Force Propulsion (PFP) [29]- [32], that can produce thrust in the nano- to micronewton range, this study considers the millinewton range as such technology is readily available. The spacecraft in this study is modeled as a 1U (10 x 10 x 10 cm^3) CubeSat with a single thruster capable of producing between 1 to

50 millinewtons of thrust, where the control effort becomes saturated if it exceeds the thruster capability. It is assumed that attitude control is available (such as momentum wheels) to point the thruster, thus providing three axis translational control.

2.4. FULL STATE MODEL

If the third body in the CR3BP is defined as a spacecraft, with its state vector defined by $Z \triangleq [x\ y\ z\ \dot{x}\ \dot{y}\ \dot{z}]^T$, the addition of a control vector u and the perturbation $d(Z)$ due to solar radiation pressure, the CR3BP system (1) then can be described by

$$\dot{Z}(t) = f(Z) + B\,(u + d(Z))$$

$$\text{where} \quad f(Z) = \begin{bmatrix} \dot{x} \\ \dot{y} \\ \dot{z} \\ 2\dot{y}+x-(1-\mu)\frac{x+\mu}{{r_1}^3}-\mu\frac{x-(1-\mu)}{{r_2}^3} \\ -2\dot{x}+y-(1-\mu)\frac{y}{{r_1}^3}-\mu\frac{y}{{r_2}^3} \\ -(1-\mu)\frac{z}{{r_1}^3}-\mu\frac{z}{{r_2}^3} \end{bmatrix}, \quad B = \begin{bmatrix} 0 & 0 & 0 \\ 0 & 0 & 0 \\ 0 & 0 & 0 \\ 1 & 0 & 0 \\ 0 & 1 & 0 \\ 0 & 0 & 1 \end{bmatrix}, \quad u = \tag{4}$$

$[u(1)\ \ u(2)\ \ u(3)]^T$ and $d(Z) = \left[F_{srp,x}\ \ F_{srp,y}\ \ F_{srp,z}\right]^T$.

3. PROBLEM FORMULATION

In this section, the spacecraft dynamics are written in a more general form and then the ETNAC design for this general problem is developed in the next section. The dynamics of an uncertain nonlinear system as in (1), with perturbations and control can be expressed as

$$\dot{X}(t) = f\big(X(t)\big) + B\,(u(t_i) + d\big(X(t)\big)) \qquad t_i \le t < t_{i+1}, \quad \forall\, i = 1,2,\ldots \tag{5}$$

where $X \in \mathbb{R}^n$ is the state of the actual system, $d\big(X(t)\big): \overline{\mathbb{R}}_+ \times \mathbb{R}^n \to \mathbb{R}^m$ is the unknown perturbation in the system, $f\big(X(t)\big) \in \mathbb{R}^n$is a known function and $B \in \mathbb{R}^{n\times m}$ is a known matrix, and $u(t_i) \in \mathbb{R}^m$ is the control input. The dynamics of the desired nonlinear system defining the reference trajectory for (1), is represented using

$$\dot{X_d}(t) = f^*(X_d(t)) \tag{6}$$

where $X_d \in \mathbb{R}^n$ is the desired state of the system and $f^* \in \mathbb{R}^n$ is a known function.

The control objective is to design an event-sampled state-based adaptive controller $u(t_i)$ for the system (1) that follows the desired response $X_d(t)$ while keeping sampling events minimum. Note that the desired trajectory for this study is defined by a vector with magnitude 100 m (with equal components along all three axes) relative to the leader on the halo orbit located at the Sun-Earth/Moon L_1 point.

4. ETNAC DESIGN

In order to accomplish the objective stated in the last section, two ETNAC schemes are developed for the controller/observer design. The first scheme is shown in Figure 2, where the observer runs in parallel with the controller module shown at the bottom. In the second scheme, shown in Figure 3, the observer stays with the top module where plant-related calculations are made. For both schemes, the stability and performance analyses are provided.

4.1. EVENT- SAMPLED STATE BACKGROUND

In the ETNAC framework, the system state is measured continuously but transmitted to the control system only at the specific instants when an event occurs. This event is determined by a condition called as "event-triggering condition." These time instants are denoted as $\{t_i\}_{i=1}^{\infty}$ where $t_{i+1} > t_i, \forall\, i = 1,2,\ldots$ and $t_0 = 0$ is the initial sampling instant. Note that these times are typically aperiodic. For later use, the event-sampling error is defined as

$$e_{evt} \triangleq X(t) - X(t_i)\,, \quad t_i \le t < t_{i+1}, \quad \forall\, i = 1,2,\ldots \tag{7}$$

where $X(t_i)$ is the sampled state at t_i. At each state sampling instant $t = t_i$, current sampled state $X(t_i)$ is sent to the controller, overwriting the previous sampled state $X\,(t_{i-1}\,)$ and

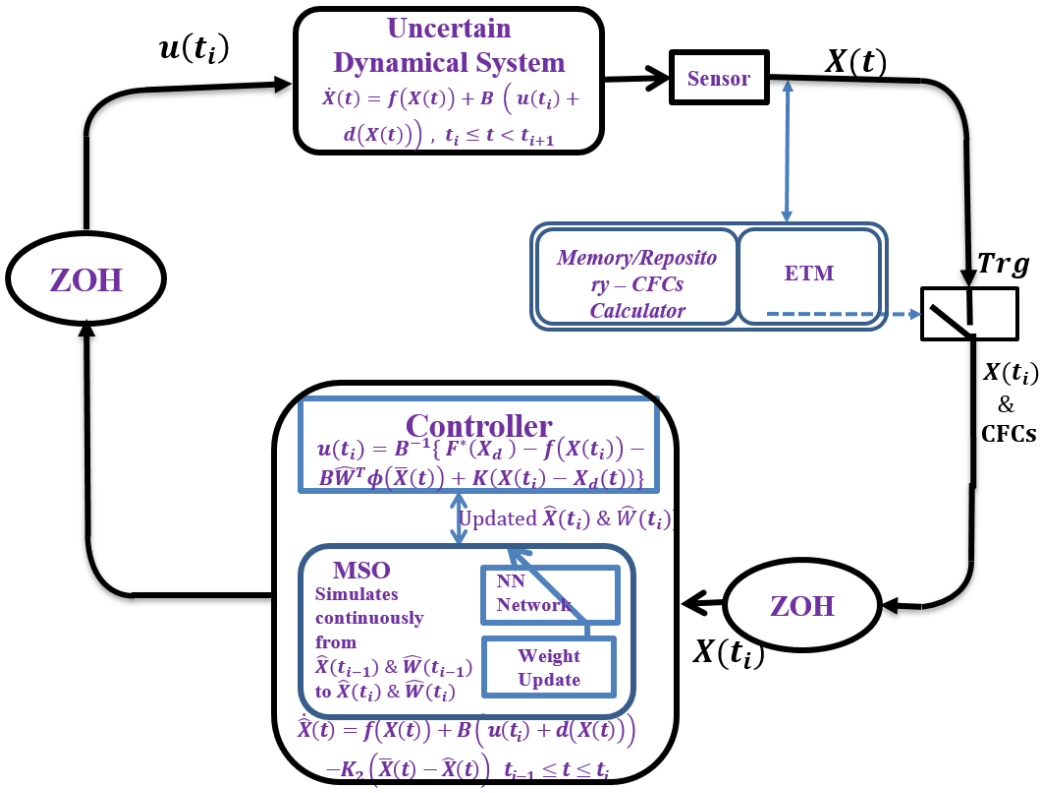

Figure 2. ETNAC-1 Block Diagram

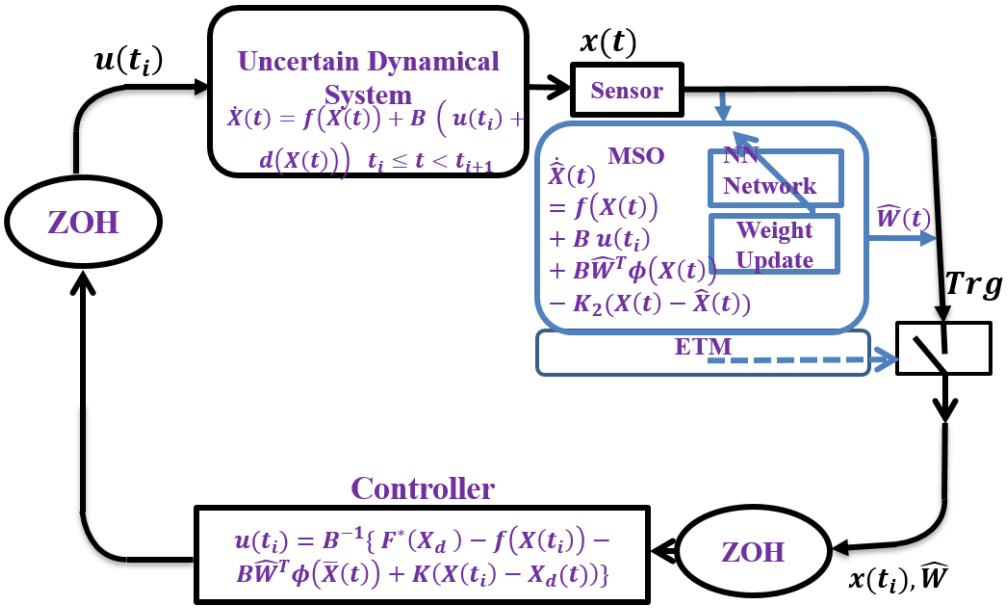

Figure 3. ETNAC-2 Block Diagram

held by using a Zero-Order-Hold (ZOH) until the next state is received. In this way event-sampling error is reset to zero as $e_{evt} = 0$, when $t = t_i$. Due to this event-triggered update, control signal become piecewise continuous.

Some standard assumptions were made during this work, with similar assumptions seen in the control literature ([51], [42], [52], and [53] etc.).

Assumption 1: The uncertainty can be linearly parametrized. From the universal function approximation property of NN, a real valued function $d(X(t))$ in a compact set $A \subseteq \mathbb{R}^n$ can be approximated with some residual error ϵ such that (s.t.),

$$d(X(t)) = W^T\phi(X(t)) + \epsilon(X,t) \tag{8}$$

where $W \in \mathbb{R}^{s\times m}$ is the unknown but ideal weight matrix ($s \in \mathbb{N}_+$) that belongs to a compact set Ω, and $X \in D_x$ for a sufficiently large compact set D_x. Note that user chosen basis functions $\phi(X)\colon \mathbb{R}^n \to \mathbb{R}^s$ are bounded as $\|\phi(X)\| \le \phi^*$ and $\epsilon(t,X)$ is the residual

error satisfying $|\epsilon(t,X)| \leq \epsilon^*$. Also, it is assumed that all states are available for measurement.

Assumption 2: The basis functions $\phi(.)$ and system function $f(.)$ are locally Lipschitz continuous s.t.,

$$\begin{aligned} \|\phi(X) - \phi(Y)\| &\leq L_\phi \, \|X - Y\| \\ \|f(X) - f(Y)\| &\leq L_f \, \|X - Y\| \end{aligned} \tag{9}$$

where $X, Y \in D_x$ and $L_\phi, L_f \in \mathbb{R}_+$. Note that the norm notation used in this paper is valid for the 2-norm or Frobenius norm.

Now both ETNAC schemes are given in detail.

4.2. ETNAC-1: STATICALLY TRIGGERED ETNAC WITH MSO PERFORMED AT CONTROL SYSTEM

In ETNAC an intermediate step is to design an appropriate Modified State Observer (MSO) [26]. Even though all states are assumed measurable, the MSO notion is used here because it approximates uncertainty online using NNs, and moreover, it also offers a filtering effect for high frequency oscillations. It has been shown to avoid large oscillations in its transient performance that is usually observed with a typical model reference adaptive controller [26]-[50]. Note that the development and design of the MSO here is quite different from [26], in order to accommodate the asymmetric data transfer to the controller. The equations defining the MSO are given by

$$\begin{aligned} \dot{\hat{X}}(t) &= f\big(\bar{X}(t)\big) + B\left(u(t_i) + \hat{d}\big(\bar{X}(t)\big)\right) - K_2(\bar{X}(t) - \hat{X}(t)) \\ &= f\big(\bar{X}(t)\big) + B\,u(t_i) + B\widehat{W}^T\phi\big(\bar{X}(t)\big) - K_2(\bar{X}(t) - \hat{X}(t)) \end{aligned} \tag{10}$$

where $\hat{d}(\bar{X}(t)) \triangleq \widehat{W}^T\phi(\bar{X}(t))$ represents the estimate of $d(X(t))$, K_2 is a user defined Hurwitz gain matrix and

$$\bar{X}(t) \triangleq \begin{cases} X(t_i) & t = t_i \\ C_1 t^n + C_2 t^{n-1} \ldots + C_n t + C_{n+1} & t_i < t < t_{i+1} \end{cases} \quad \forall i = 1,2 \ldots$$

where $C_i \;\; i = 1,2, \ldots n$ are polynomial regression-based curve-fitting coefficients (CFCs). These coefficients are determined in the system, using state data points. Different numbers of data points can be used depending on the used order of regression. After the coefficients are determined, they are transmitted along with the state information whenever the state sampling condition becomes true.

Note that in this design, though the observer is updated only at sampling instants, it is essentially simulated continuously. Using some selected time instants where the state is measured, it is curve fit at discrete aperiodic sampling times, with the CFCs transmitted on the feedback network. The true state (measurement) is interpolated using the CFCs between the past and the current trigger time instants for the weight estimate. The controller is updated at the sampling time t_{i+1} with the values of $\hat{X}(t_{i+1})$ and $\widehat{W}(t_{i+1})$.

By adding and subtracting $W^T\phi(\bar{X}(t))$ in (8)

$$d(X(t)) = W^T\phi(X(t)) + W^T\phi(\bar{X}(t)) - W^T\phi(\bar{X}(t)) + \epsilon(X,t)$$

$$= W^T\phi(\bar{X}(t)) + \check{\epsilon} \qquad t_i \le t < t_{i+1}, \quad \forall\, i = 1,2, \ldots \tag{11}$$

where $\check{\epsilon} \triangleq W^T\phi(X(t)) - W^T\phi(\bar{X}(t)) + \epsilon = W^T[\phi(X(t)) - \phi(\bar{X}(t))] + \epsilon$ is the residual error. Substituting (11) into (5) gives

$$\dot{X}(t) = f(X(t)) + Bu(t_i) + BW^T\phi(X(t)) + \epsilon$$

$$= f(X(t)) + Bu(t_i) + BW^T\phi(\bar{X}(t)) + \check{\epsilon}. \tag{12}$$

To design a control which guarantee desire objectives of $X(t) \rightarrow X_d$, the tracking error is designed to follow the stable dynamics

$$\left(\dot{X}(t) - \dot{X}_d(t)\right) - K(X(t) - X_d(t)) = 0 \tag{13}$$

where the user-defined Hurwitz diagonal matrix K is given by

$$K = diag\left(\frac{1}{\tau_1}, \ldots\ldots, \frac{1}{\tau_n}\right). \tag{14}$$

where $\tau_1 \ldots \tau_n$ can be interpreted as desired time constants. Using the desired and actual systems dynamics equations in (13)

$$Bu(t_i) = F^*(X_d) - f\big(X(t)\big) - Bd\big(X(t)\big) + K\big(X(t) - X_d(t)\big). \tag{15}$$

In [26], a slack variable technique is used to make B invertible. Two slack variables introduced as $u_s \in \mathbb{R}^{(n-m)\times 1}$ and $B_s \in \mathbb{R}^{n\times(n-m)}$. B_s is chosen such that augmented $\bar{B} \triangleq [B\ B_s]$ becomes square and invertible. Augmented control will be then $\overline{U} \triangleq [u(t_i), u_s]^T$. Adding $B_s u_s$ on both sides of equation (15) gives

$$\begin{aligned} Bu(t_i) + B_s u_s &= F^*(X_d) - f\big(X(t)\big) - Bd(X(t)) + K(X(t) - X_d(t)) + B_s u_s \\ \bar{B}\overline{U} &= [B\ \ B_s][u(t_i)\ \ u_s]^T \\ &= F^*(X_d) - f\big(X(t)\big) - Bd(X(t)) + B_s u_s \\ &\quad + K(X(t) - X_d(t)) \end{aligned} \tag{16}$$

So, if the approximation $\hat{d}(\bar{X}(t) \cong d(X(t))$ is available, then the augmented control at a sampling instant can be written as

$$\begin{aligned} \overline{U} \triangleq \begin{bmatrix} u(t_i) \\ u_s \end{bmatrix} &= \bar{B}^{-1}\{F^*(X_d) - f\big(X(t_i)\big) \\ &\quad - B\hat{d}\big(\bar{X}(t) + B_s u_s + K\big(\bar{X}(t) - X_d(t)\big)\ \big\}. \end{aligned} \tag{17}$$

From (17) we can easily extract $u(t_i)$ or slack variables can be added/subtracted in (5) and the augmented control $\bar{U}$ can be applied directly. Note that slack variables have no active role but essentially act as a catalyst to simplify computations.

Defining the tracking error as

$$e_r(t) \triangleq X(t) - X_d(t) \tag{18}$$

the dynamics after some algebra is

$$\dot{e}_r(t) = Ke_r(t) - Ke_{evt} + f\big(X(t)\big) - f\big(X(t_i)\big) + B(\widetilde{W}^T\phi\big(X(t_i)\big) + \check{\epsilon}) \tag{19}$$

where $\widetilde{W} \triangleq W - \widehat{W}$. The estimation error is defined as

$$e_a(t) \triangleq X(t) - \hat{X}(t) \tag{20}$$

and the dynamics can then be reduced to

$$\begin{aligned}\dot{e}_a(t) = K_2e_a(t) - K_2e_{ext} + B\widetilde{W}^T\phi\big(\bar{X}(t)\big) + B\check{\epsilon} + f\big(X(t)\big) \\ - f\big(\bar{X}(t)\big) \qquad t_i \le t < t_{i+1}, \quad \forall\, i = 1,2,\end{aligned} \tag{21}$$

where $e_{int} \triangleq X(t) - \bar{X}(t)$ is the interpolation error. The event sampling error and interpolation error need to be bounded for the actual tracking error to be bounded.

The weight update rule for $\widehat{W}$ is assumed as

$$\dot{\widehat{W}} = \gamma\, Proj_m(\widehat{W}, \phi\big(\bar{X}(t)\big)\, \bar{e}_a{}^T PB) \tag{22}$$

where

$$\bar{e}_a = \begin{cases} X(t_i) - \hat{X}(t_i) & t = t_i \\ \bar{X}(t) - \hat{X}(t) & t_i < t < t_{i+1} \end{cases}$$

and $\gamma \in \mathbb{D}_+^{s\times s}$ is the adaptation rate used in the weight update rule, and $Proj_m\,(.,.)$ denotes the smooth projection operator [44]. Note that the projection operator guarantees that $\widehat{W} \in \Omega$, and that there exists a $W^* \in \Omega$ s.t. $\|\widehat{W}\| \le W^*$ and P is the solution of the linear Lyapunov equation

$$0 = {K_2}^T P + P K_2 + Q$$
$$0 = K^T P_r + P_r K + Q_r \tag{23}$$

where $Q, P, Q_r, P_r > 0$. The event-triggering condition is true when (24) is violated

$$\|e_r\| \leq \propto \tag{24}$$

where $\propto$ is a user defined threshold error for event-triggering.

4.2.1. Stability Analysis.

Theorem 1: Consider the system in (1) with the observer in (10) and the desired system described by (6). Let Assumptions (1-2) hold. Consider the NN approximation, with the control generated by (17), and the weight update law in (22). Let the control be updated only at the event sampling instants when (24)is violated. Then the state estimation error and the tracking error are locally uniformly ultimately bounded (UUB).

Proof: Proof is given in the appendix.

I.Corollary 1: Ultimate Upper Bound on Tracking Error:

Consider the system in (1) with the observer in (10) and the desired system described by (6). Let Assumptions (1-2) hold. Consider the NN approximation, with control generated by (17), and the weight update law in (22). Let the control be updated only at the event sampling instant when (24) is violated, then the ultimate bound on e_r can be given by e_{r_0} s.t.

$$\|e_r(t)\| = \|X(t) - X_d(t)\| \leq e_{r_0} \tag{25}$$

where $e_{r_0}$is defined as $e_{r_0} \triangleq \sqrt{\vartheta_1 / \lambda_{min}(P_r)}$ and $\vartheta_1 \triangleq \lambda_{max}(P_r)\psi_1 + \lambda_{max}(P_r)\varepsilon$.

Proof: Proof is given in the appendix.

4.3. ETNAC-2: STATICALLY TRIGGERED ETNAC WITH MSO PERFORMED AT SYSTEM

The block diagram of this scheme is given in Figure 3, in which the observer is in parallel with the actual system. The standard MSO expressions for observer are used as

$$\begin{aligned}\dot{\hat{X}}(t) &= f\big(X(t)\big) + B\,u(t_i) + B\hat{d}\big(X(t)\big) - K_2(X(t) - \hat{X}(t)) \\ &= f\big(X(t)\big) + B\,u(t_i) + B\widehat{W}^T\phi\big(X(t)\big) - K_2(X(t) - \hat{X}(t))\end{aligned} \tag{26}$$

with the approximation $\hat{d}\big(X(t)\big) \triangleq \widehat{W}^T\phi\big(X(t)\big)$. Note that now the state is available to the observer continuously. Only sampled control, which include X and $\widehat{W}$, at each sampling instant is transmitted to the control system. A control that guarantees $X(t) \rightarrow X_d$, can be achieved using

$$\big(\dot{X}(t) - \dot{X}_d(t)\big) - K(X(t) - X_d(t)) = 0 \tag{27}$$

where the user-defined Hurwitz diagonal matrix K is similar to (13). Control is synthesized following similar steps as with the ETNAC-1 algorithm, beginning with

$$\begin{aligned}\overline{U} = \begin{bmatrix} u(t_i) \\ u_s \end{bmatrix} = \bar{B}^{-1}\{\, &F^*\big(X_d\,, u_n(t_i)\big) - f\big(X(t_i)\big) + B_s u_s - B\hat{d}(X(t)) \\ &+ K(X(t_i) - X_d(t))\}\end{aligned} \tag{28}$$

Now dynamics for the tracking error $e_r(t)$ can be simplified as

$$\dot{e}_r(t) = Ke_r(t) - Ke_{evt} + \; + f\big(X(t)\big) - f\big(X(t_i)\big) + B\widetilde{W}^T\phi\big(X(t_i)\big) + \check{\epsilon} \tag{29}$$

and the dynamics of state estimation error e_a are reduced to

$$\dot{e}_a(t) = K_2 e_a(t) + B\widetilde{W}^T\phi\big(X(t)\big) \tag{30}$$

The weight update rule for $\widehat{W}$ is given as

$$\dot{\widehat{W}} = \gamma\, Proj_m(\widehat{W}, \phi\big(X(t)\big)\, e_a(t)^T PB) \tag{31}$$

where $\gamma \in \mathbb{R}_+$ is the adaptation rate for update rule of $\widehat{W}$, $Proj_m(.,.)$ denotes the smooth projection operator [44] (note that the projection operator ensures that $\widehat{W} \in \Omega$, and that there exists $W^* \in \Omega$ s.t. $\left\|\widehat{W}\right\| \leq W^*$), and P is the solution to linear Lyapunov equation

$$\begin{aligned} 0 &= {K_2}^T P + P K_2 + Q \\ 0 &= K^T P_r + P_r K + Q_r \end{aligned} \tag{32}$$

where $Q, P, Q_r, P_r > 0$. Event triggering condition is true when (33) is violated

$$\|e_r\| \leq \propto \tag{33}$$

where $\propto$ is a user-defined threshold error for event triggering.

4.3.1. Stability Analysis.

Theorem 2: Consider the system in (1) with the observer in (26) and the desired system described by (6). Let Assumptions (1-2) hold. Consider the NN approximation, with control generated by (28), and the weight update law in (31). Let the control be updated at the event sampling instants when (33) is violated, then the state estimation error is locally asymptotically stable and the tracking error is locally uniformly ultimately bounded (UUB).

Proof: Proof is given in the appendix.

5. RESULTS

System (1) with its state model as in (4) is simulated in this study using MATLAB. Simulation is carried out in non-dimensional units. The results, however, are presented in SI units. Different gains and parameter values used are $K_2 = diag(10^5, 10^5, 10^5, 10^4, 10^3, 10^4)$, $\gamma = diag(10^6, 10^6, 10^6)$, and $B_s = \begin{bmatrix} I_{3\times3} \\ -I_{3\times3} \end{bmatrix}$, $u_s =$

$[1\ 1\ 1\ 1\ 1\ 1]^T$. To generate a baseline, results are first given with continuous updates and then the ETNAC schemes are applied for different values of $\propto$ to determine the performance of ETNAC.

5.1. RESULTS WITH CONTINUOUS INPUT

The reference (virtual leader) and spacecraft (follower) trajectories for the duration of one complete halo orbit, approximately 180 days, are shown in Figure 4, respectively, indicating that the follower spacecraft, subjected to SRP perturbations, should maintain its desired location of 100 meters to the reference leader node on the halo orbit. Plots throughout the remainder of the paper are given for a duration of five days, by which time the follower spacecraft reaches steady state behavior; this allows the system behavior to be observed and analyzed more closely. Figure 5a shows the time histories of the followers relative tracking (to its node located 100 meters from the virtual leader reference node), while Figure 5b represent control components histories. There is no constraint on control and the update interval is approximately 5 seconds in this case. It can be seen that the performance is excellent with the steady state error in the sub micrometer range. Initial tracking errors are in the 1-5 millimeter range while the neural network takes some time to learn and converge, after which the error quickly approaches the steady state value. No major oscillations are observed, even during the transient phase. Control along the $\hat{x}$-axis is significantly higher because the SRP perturbation acts primarily along the $\hat{x}$-axis. It shows that if the actuator hardware technology is available (no constraint on control is assumed), then with the proposed control architecture excellent performance can be achieved in the sub micrometer range, which is not seen in literature so far. On the other

hand, Figures 6a and 6b show the follower relative tracking error and control histories in the case where a 1 millinewton (mN) minimum control constraint is applied to meet the practical design requirements, along with a maximum update interval of approximately 25 seconds (higher update intervals lead to instability in the response). This shows that even with current existing hardware, a submillimeter accuracy is obtained with continuous control. In this case the response has significant jitter, but this is due to constraints coming in from physical hardware limitations, not from the proposed design. It is clearly evident from Figure 5, where response without constraints is smooth. Figure 7a shows the state estimation errors, which converge to the micrometer range soon after the NN converges. Figures 7b, 8a, and 8b show the histories of the original and the approximated uncertainties

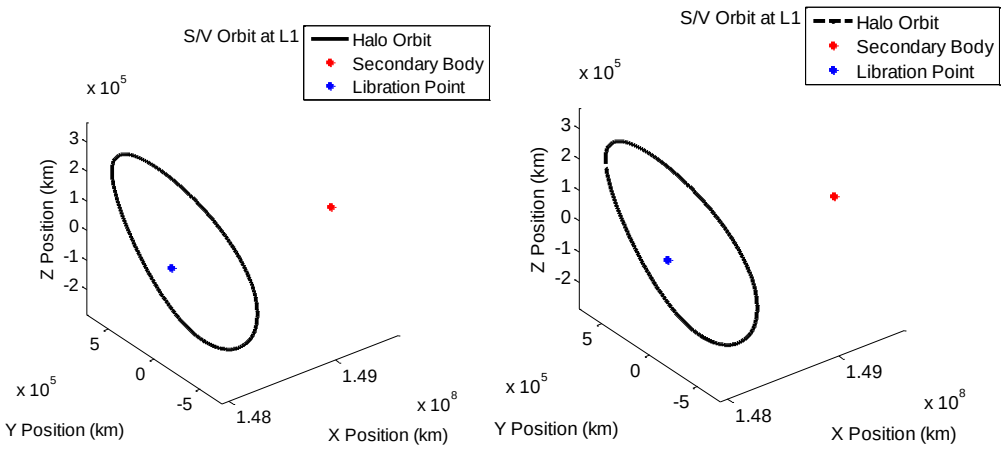

(a) (b)

Figure 4. Desired (a) and actual spacecraft (b) trajectories for one complete orbit with continuous updates.

along the $\hat{x}$, $\hat{y}$ and $\hat{z}$ axis directions, respectively, where the estimated values converge quickly to the true perturbations, which are in the range of 10^{-9} nondimensional units (approximately 0.015 nN). Note that the original perturbation is from the truth model given

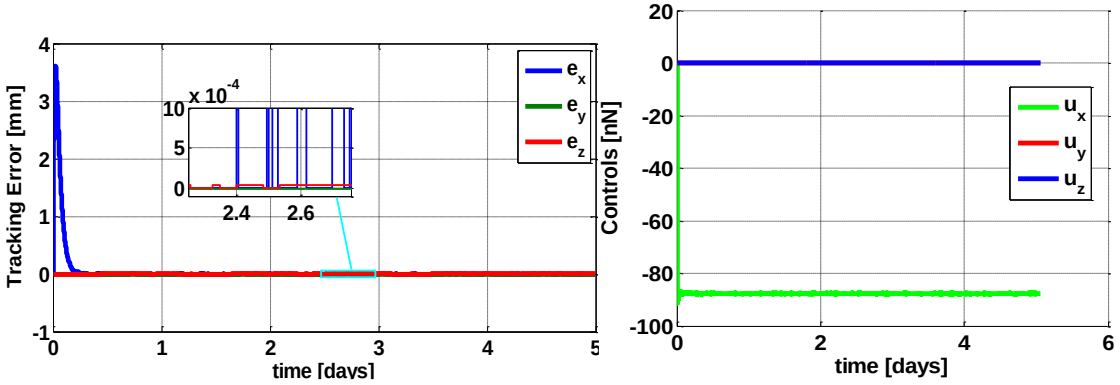

(a) (b)

Figure 5. Continuous Update Case: Tracking error (a), and control components(b), without any control constraints and at higher update rate.

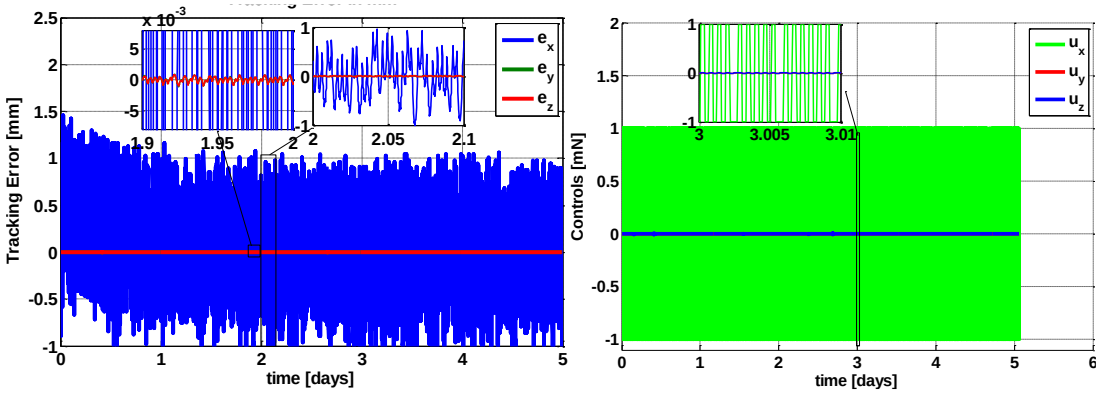

(a) (b)

Figure 6. Continuous Update Case: Tracking error (a), and control components(b), with control constraints and at lower update rate.

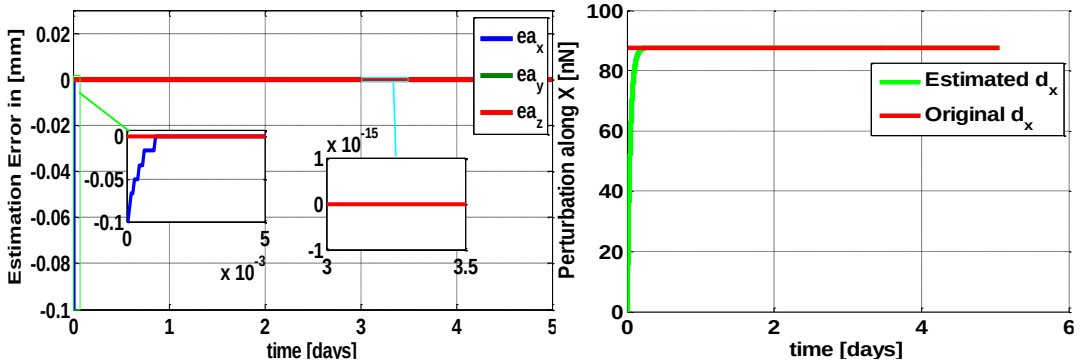

(a) (b)

Figure 7. Continuous Update Case: State Estimation error (a) Uncertainty approximation along $\hat{x}$ (b).

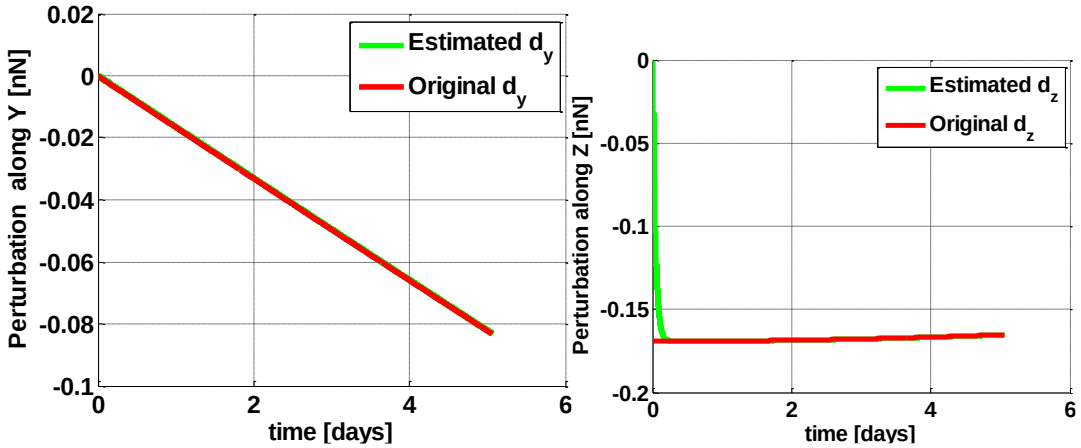

(a) (b)

Figure 8. Continuous Update Case: Uncertainty approximation along $\hat{y}$ (a) and along $\hat{z}$ direction (b).

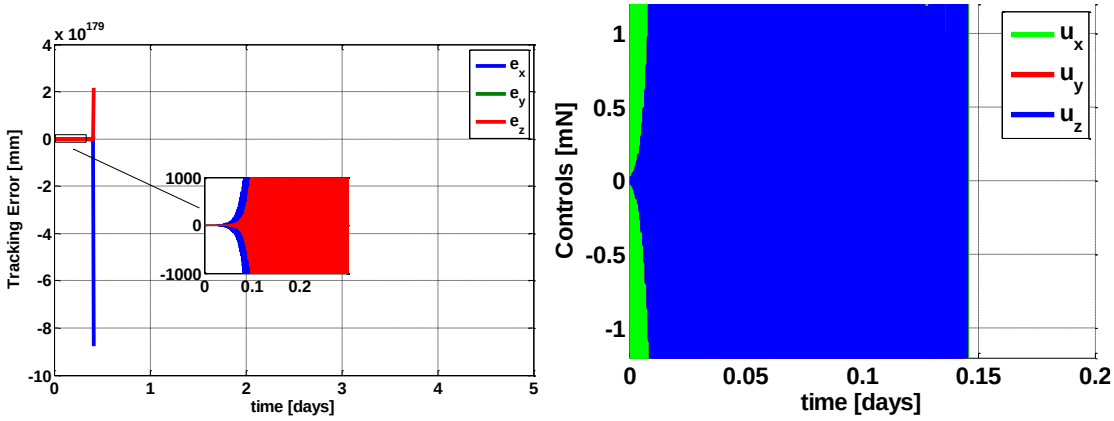

(a) (b)

Figure 9. Continuous update with 26 seconds timing interval, Tracking Error (a) and Control (b).

in equation (2)-(3) and the estimated values are from the NN based MSO. Note also that the maximum time interval for continuous updates was found to be approximately 25 seconds (Figure 6), as higher values resulted in system divergence. The plots in the Figures 9a and 9b shows that whenever control is updated at a continuous/periodic rate of 0.0385Hz (~26 seconds period), it could not stabilize, and the system diverged. After setting up this baseline, now results are given with event-triggering.

5.2. RESULTS WITH ETNAC-1

In this method, the controller and the observer have access to sampled state information only at the event condition. Table 1 provides a summary of the number of updates needed for different cases, where the values of $\propto$ are varied, in order to demonstrate the overall performance of the ETNAC-1 scheme. Detailed results for Case 3 with a threshold error $\propto = 1$ mm are presented. Note this proposed method is unique for reducing jitter in microsatellites. During the inter-event time (called the period of silence), there are no step inputs in the microsatellite operations, leading to steady dynamics and reducing jitter.

i. ETNAC-1, Case 3: Error Threshold 1 mm, duration 5 days

The number of sampling updates using ETNAC-1 was 9235, as compared to 17,202 sampling instants using continuous control, resulting in a reduction of sampling instants by 46.3144%.

Figures 10 shows the tracking and estimation error histories. Once the threshold error of 1 mm is reached, the event-triggered system is activated, and it updates the observer system and the controller acts to bring the tracking error into the desired range. This control is held constant by a ZOH until the error threshold is reached again. This inter-event period of silence helps to reduce jitter and to smooth operations in the microsatellite. The overall performance is found to be satisfactory as the tracking error remains within the desired threshold throughout. The estimation error is in the sub-millimeter range in this case even when observer only has access to the last sampled state and is updated only a few times with a polynomial regression model of the states.

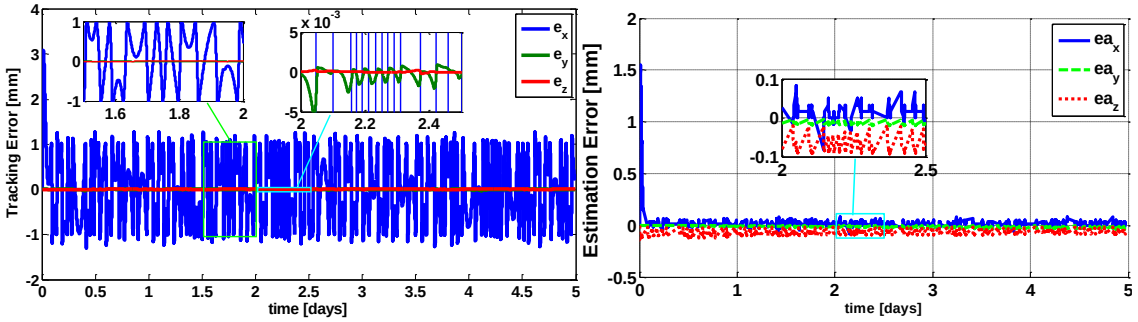

(a) (b)

Figure 10. Case 3: Tracking error (a) and state estimation error (b) with ETNAC-1.

Figure 11a shows control components histories while Figure 11b shows overall magnitude (norm) over the given time. Control is not updated continuously and is always lower and upper bounded by 1 mN and 50 mN, respectively. It can be seen that excellent performance is achieved even with these restrictions. Control value remained between 1 mN to 3mN. Figure 12a shows the cumulative control update counts. *Control updates are reduced by 46.3144 % over a period of five days while maintaining a 1 mm error bound.* This indicates that the period of silence is almost doubled that of the maximum possible with continuous control (approximately 25 seconds). The difference between cumulative control updates for both continuous control and ETNAC is clear. This longer period of silence leads to smoother operations and reduces jitter in microsatellite control. No events are observed until the error threshold is reached and after that it keeps updating information in a nonlinear fashion depending upon the tracking error threshold. Although initially the event rate is high, over time it becomes more aperiodic as steady state behavior is achieved. This is because it takes time for the NN weights to converge, which can also be seen from the uncertainty approximation plots. Histogram in Figure 12b shows the duration of inter-event time and the number of times it occurred. The horizontal axis shows the duration of

inter-event time in terms of 25 seconds (maximum possible with continuous updates) and the vertical axis represent that how many times that inter-event time was obtained. Minimum inter-event time was equal to the 1 continuous time step which is skipped in diagram. Maximum was approximately 150 seconds (6x increase) which happened two time only and 50 seconds (2x increase) happened most frequently around 1400 times.

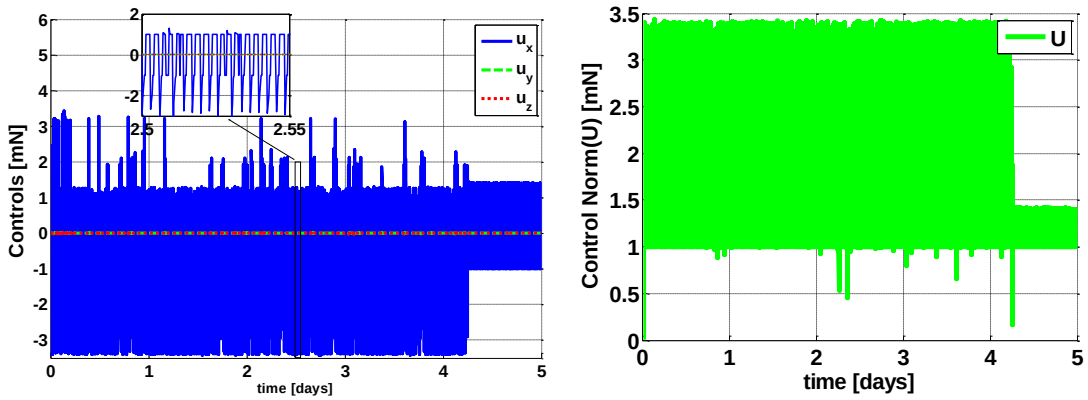

(a) (b)

Figure 11. Case 3: Control components histories (a) and its magnitude histories (b) with ETNAC-1.

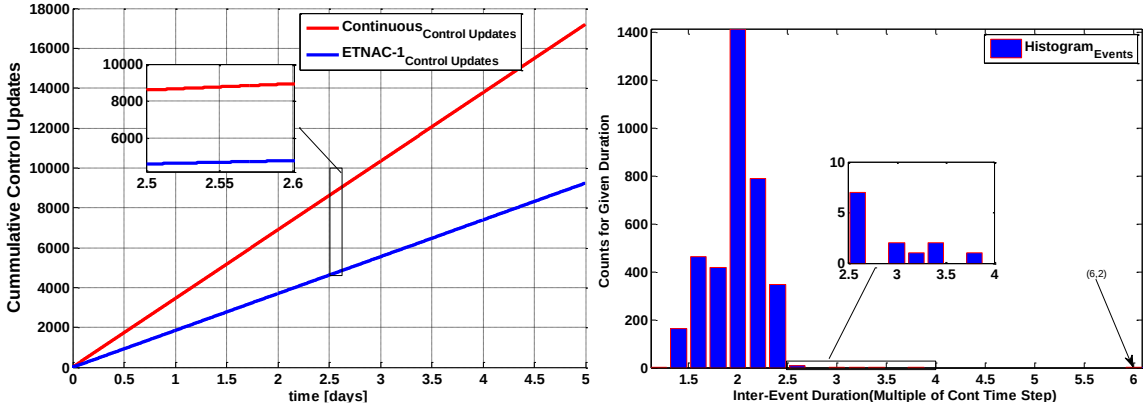

(a) (b)

Figure 12. Case 3: cumulative event counts (a), and histogram of control update events (b), with ETNAC-1.

Note that this period of silence is even higher in the case of higher thresholds ($\propto$). Plots are omitted for those cases but Table 1 summarizes the results for them.

Disturbance estimation plots along $\hat{x}$, $\hat{y}$ and $\hat{z}$ directions are given in Figures 13a, 13b and 13c, respectively. Note that the initial NN weights are set at zero and no update happens until the tracking error crosses the threshold level. Once the event-triggered condition occurs, the NN begins receiving updated information and the perturbations are learned. The true state (measurement) is interpolated using CFCs between the past and the current trigger time instants for use in the weight estimates. The order of the regression can be chosen after analyzing the output behavior. In this study, different regression orders were tested from first order to fifth order. It was found that the third order polynomial regression yielded the best results since the system trajectory between two points along the system trajectory at two different event sampling instants is of a parabolic shape. Four state measurements points were used, the current and last sampling instance and two in between measurements at uniform separation in order to find the CFCs needed to curve fit the data. Once acquired, these CFCs were later transmitted to the feedback network at the sampling instant. Note that regression is done at the plant level and that only the CFCs are sent to the feedback network at the event condition. If higher order regression is desired, this can be easily implemented by utilizing additional measurements in the data selected to fit. The only consideration for higher order cases is sending a few extra coefficients, which are still worth extending period of silence as compared to continuous updates. It can be seen from the figures that the estimates are close to the true values, though some oscillations exist.

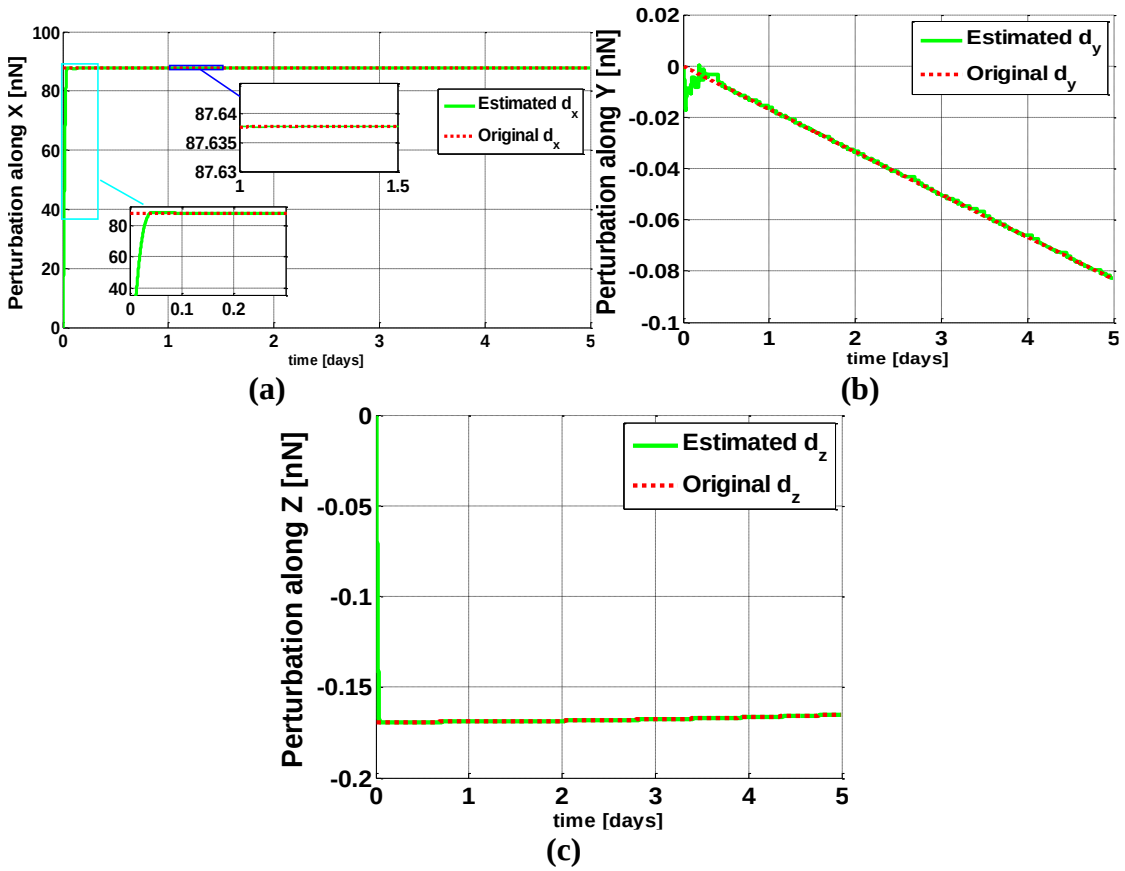

Figure 13. Case 3: Perturbation estimation along $\hat{x}$ (a), along $\hat{y}$ (b), and along $\hat{z}$ (c) with ETNAC-1.

It is of interest to examine estimation behavior during inter-event times for different order polynomial fitting. Four cases are presented in Figure 14, ranging from1st order regression to 4th order regression, respectively. Figure 14(a) is for a 1st order polynomial regression fit, which is essentially just linear interpolation between two sampling instants. As the actual trajectory is curved, the estimation error is in the 100s of kilometers range. As expected, the error in interpolation changes depending upon inter-event time, where the error increases as the inter-event time increases. In Figure 14(b), interpolation error during inter-event time is based on a 2nd order polynomial regression, in which case the error is

reduced to around 500 millimeters (but is still too high). Using a 3rd order polynomial regression, as shown in Figure 14(c), produced the best results by reducing error to just

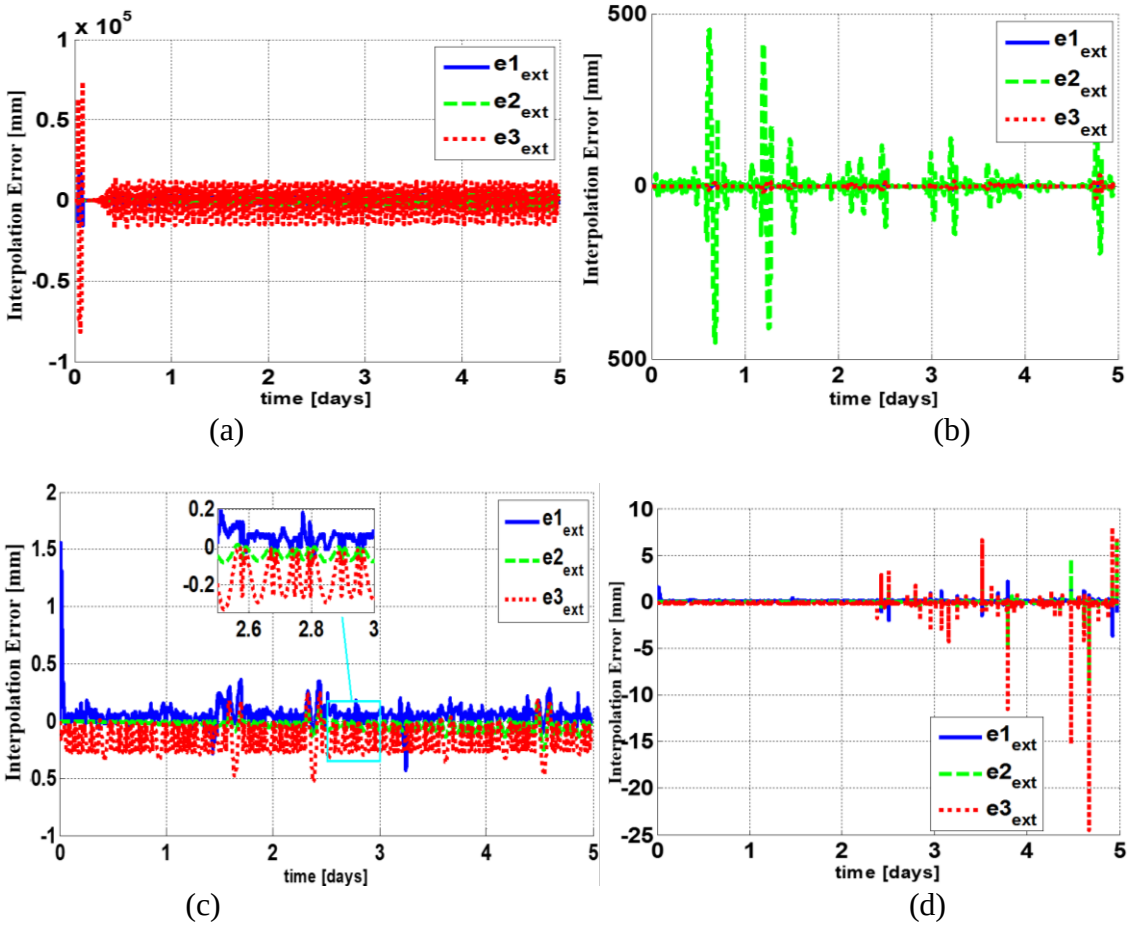

Figure 14. Interpolation error during inter-event time for different order of polynomial regression with ETNAC-1: 1st order (a), 2nd order (b), 3rd order (c) and 4th order (d).

around 0.2 millimeters. The final case shown in Figure 14(d) is for a 4th order approximation, in which error again started growing due to over fitting. Thus, depending upon the system and its output behavior, any order of polynomial regression can be used without increasing data communication cost, making this method robust and flexible.

A summary of the overall performance of the ETNAC-1 controller is given in Table 1 for different values of threshold error ($\propto$) for a period of 365 days. A baseline ΔV is

established from the known SRP perturbation, where if perfect knowledge of the perturbation is known, then the minimal ΔV required to maintain a spacecraft at the reference node subjected to the SRP is given as $\Delta d(X)$. Because the follower spacecraft is maintained at a node located at a fixed position from the reference node, it's ΔV will never achieve this minimum (because it is not tracking the true nominal halo orbit). However, this is a useful metric with which to compare the additional ΔV required to maintain the spacecraft at the relative node, as this gives a common reference for each additional spacecraft that can be placed in the virtual structure. More specifically, the fifth column of the table shows the "extra" ΔV required to "force" the follower to track a slightly "non-natural" halo orbit.

Table 1. ETNAC-1 Comparison and ΔV analysis for different values of $\propto$ for a duration of 365 days, continuous control updates are 12,55,781.

Case No	**Error Threshold Level (mm)**	ΔV **m/s per year**	$\Delta d(X)$ **m/s per year**	$\Delta V - \Delta d(X)$ **m/s per year**	**Sampling Instants with ETNAC-1**	**% Reduction**
1	1	7.8789	2.7714	5.1075	660,818	47.3379
2	5	10.3085	2.7714	7.5371	450,355	64.1374
3	10	14.3707	2.7714	11.5993	166,416	86.7480
4	100	16.8641	2.7714	14.0927	28,287	97.7457
5	1000	17.8887	2.7714	15.1173	20,093	98.5874

For these cases only inter-event time histograms are represented in Figure 15 a-e. These figures show the durations of the periods of silence observed and number of times they occurred for each case.

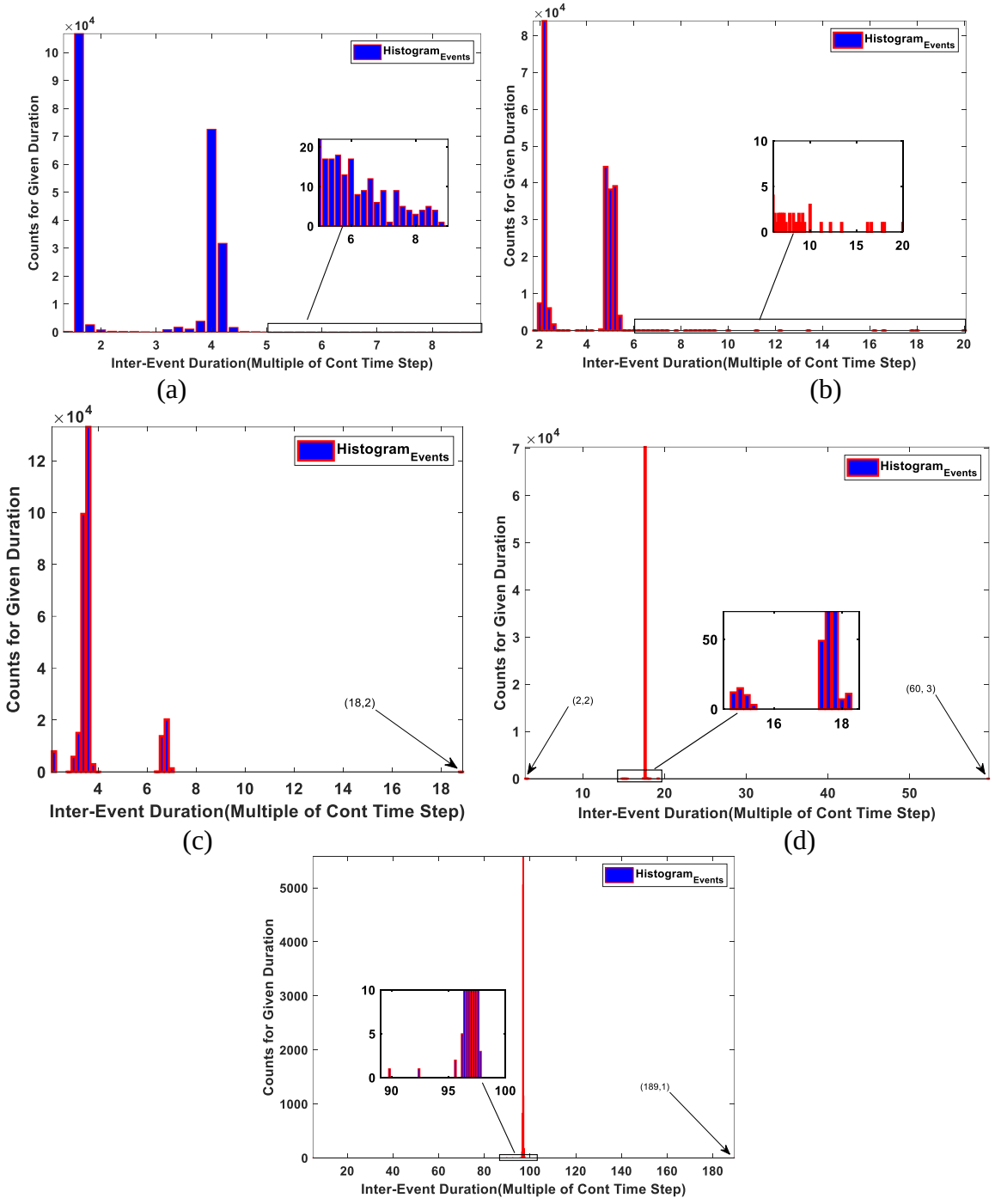

Figure 15. Histogram of inter-event times for different values of $\propto$ for a duration of 365 days with ETNAC-1: 1st case where $\propto = 1$mm (a), 2nd case where $\propto = 5$mm (b), 3rd case where $\propto = 10$mm (c), 4th case where $\propto = 100$mm (d) and 5th case where $\propto = 1000$mm (e).

The advantage of using the ETNAC-1 based controller is clear from the reductions in control updates achieved while maintaining reasonable additional ΔV values. Actually, these additional ΔV values are in the range of 0.00001-0.001 m/s per year. They are little higher in these cases due to practical design restrictions on controller. As can be seen ETNC-1 is able to reduce control updates up to 98.4% as compared to continuous updates. This proves the ETNAC-1 capabilities for the obtaining longer periods of silence resulting in reduced jitter, which is critical for microsatellite operations and scientific observations. Another interesting point observed from the results in Table 1 is that for the simulation where the event-triggering threshold is at 1 mm, the ability to maintain an error threshold in the sub-millimeter range using ETNAC is achieved. *Most existing literature shows error reduction only to the millimeter range using continuous control, while using the aperiodic ETNAC design has allowed error to be reduced to below the millimeter range while still reducing control updates significantly.* Another point to note is the ΔV values. As the threshold level decreases, the difference in ΔV as compared to the perturbation remains small, which shows the efficiency, efficacy and robustness of the controller performance. As the threshold level increases, the amount of ΔV required begins to increase as expected, while the number of events decreases. This becomes a design parameter, where a tradeoff between ΔV and control updates reduction can be selected based on the platform and the mission requirement.

5.3. RESULTS WITH ETNAC-2

The results using ETNAC-2 are presented next. Case 3, with threshold error $\propto =$ 1 mm, is again given in detail while Table 2 gives a summary for different values of threshold error ($\propto$) to illustrate the overall performance.

ii. ETNAC-2, Case 3: Error Threshold 1 mm, duration 5 days

The number of sampling instants using ETNAC-2 was 9,290, as compared to 17,202 sampling instants using continuous control, resulting in a reduction of sampling instants by 46.43%.

The response of the system with ETNAC-2 is given for a 1 mm threshold, as shown in Figure 16, for tracking and estimation error histories. Once the tracking error reaches the user defined threshold level, the event-triggering mechanism (ETM) is activated and the control is updated, lowering the error below the threshold. This control remains at hold by ZOH until the error reaches the threshold again. In this way, tracking error remains under an allowable range at all time, as can be seen from Figure 16a, while at the same time providing much longer period of silence in turn to smooth operations. Estimation error also converges quickly and remains at a small steady state error level, as expected because the state information is available to the MSO at all times. As can be seen from the results, the overall performance is very satisfactory in terms of tracking, estimation, and longer smoother durations for science operations.

The original and the estimated perturbation in $\hat{x}$, $\hat{y}$ and $\hat{z}$ directions are presented in Figure 17a, 17b, and 17c, respectively. The NN weights were initialized with a zero vector but over time converge and all three perturbation estimations converge smoothly to

accurate values. Though the perturbation is mostly dominate along the $\hat{x}$ direction, the NN still captures the perturbations along the $\hat{y}$ and $\hat{z}$, despite the fact that the perturbation along

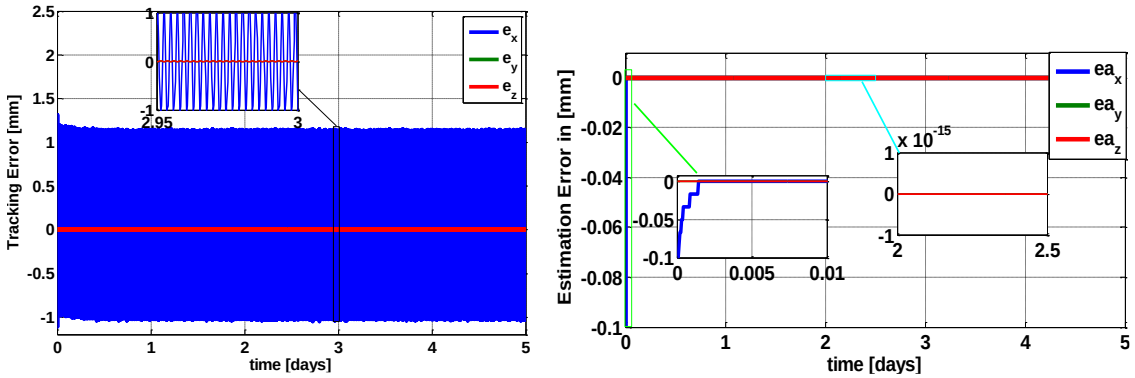

(a) (b)

Figure 16. Case 3: Tracking error (a) and state estimation error (b) with ETNAC-2.

these axes is small. In this case, ETM does not affect the estimation process as the MSO is outside the event condition and has continuous access to state information.

In Figures 18a and 18b, respectively the time history of the control components and its magnitude are presented. The control magnitude remains constant using ZOH between events and is bounded between 1 mN and 50 mN due to system design restrictions. It can be seen that each control component depends upon the magnitude of the tracking error, as expected. Despite the restrictions on magnitude and only being aperiodically updated when event-triggered, the controller is still able to achieve desired goals. Magnifier on plot provides a closer look that how much period of silence is extended with ETM as compare to continuous control.

The cumulative event counts are presented in Figure 19a. Initially there are no updates until the error first reaches the threshold level, after which the events are triggering in a comparatively smoother way. It also shows that the number of control updates is now reduced to only 9290 instead of 17,202 over the period of five days, which is a 46.43%

reduction. Figure 19b shows the histogram for inter-event duration in terms of multiples of 25 seconds. The overall performance is summarized in Table 2 for different values of threshold error $\propto$.

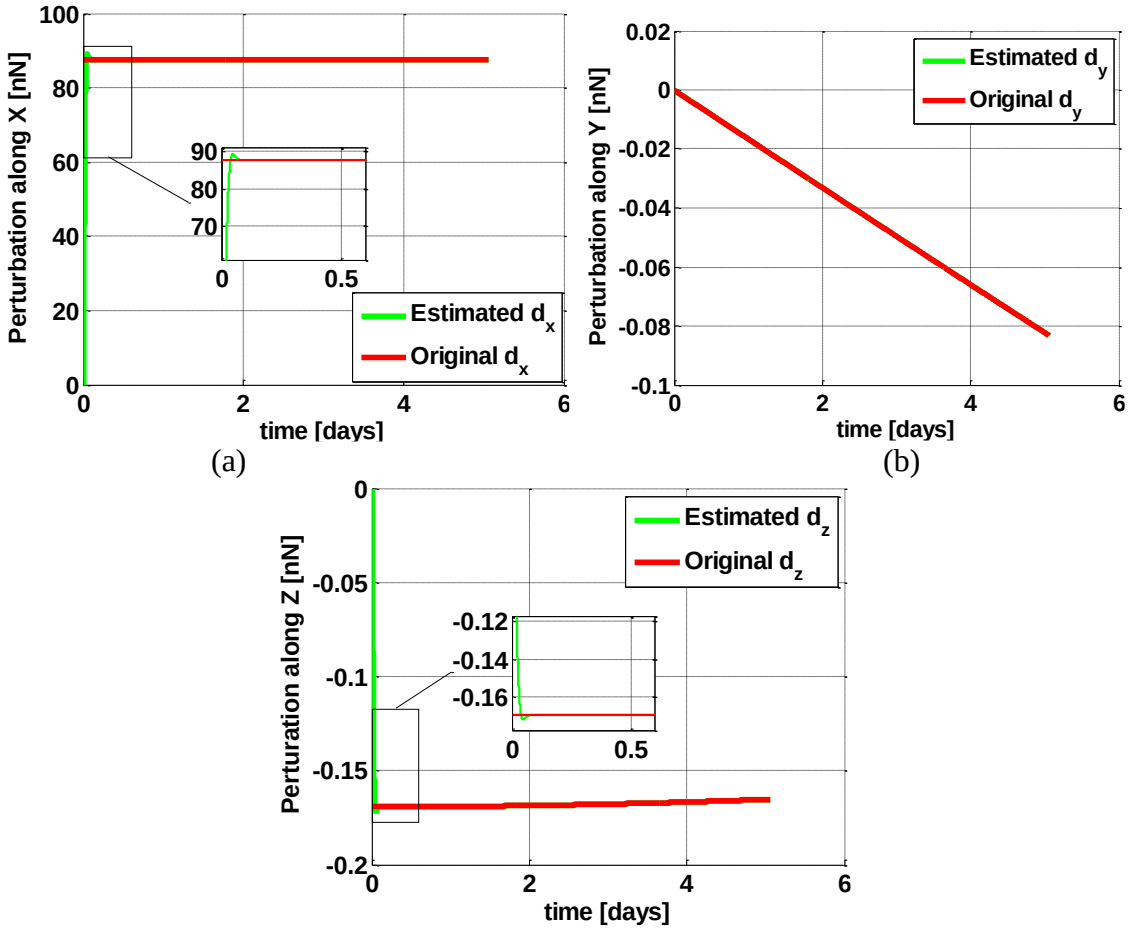

Figure 17. Case 3: Perturbation estimation along $\hat{x}$ (a), along $\hat{y}$ (b), and along $\hat{z}$ (c), with ETNAC-2.

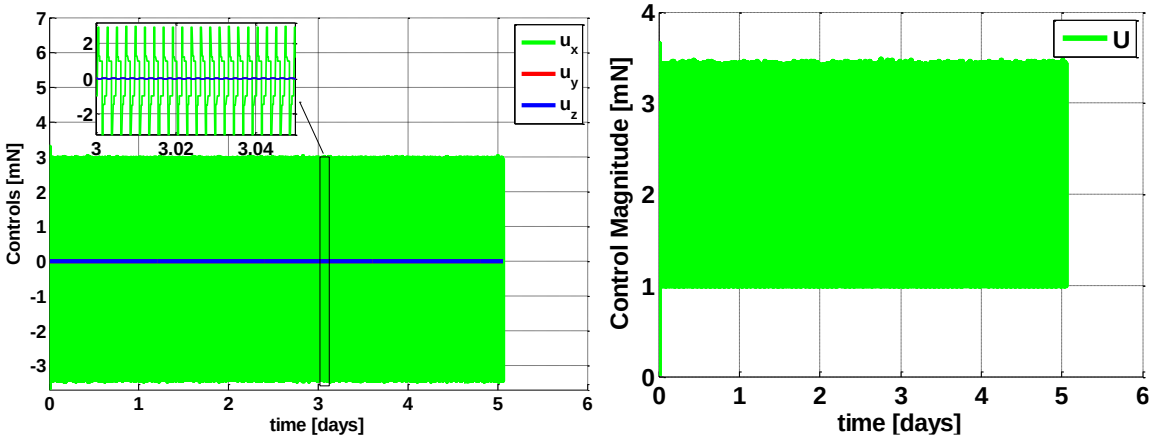

(a) (b)

Figure 18. Case 3: Control components histories (a) and its magnitude histories (b) with ETNAC-2.

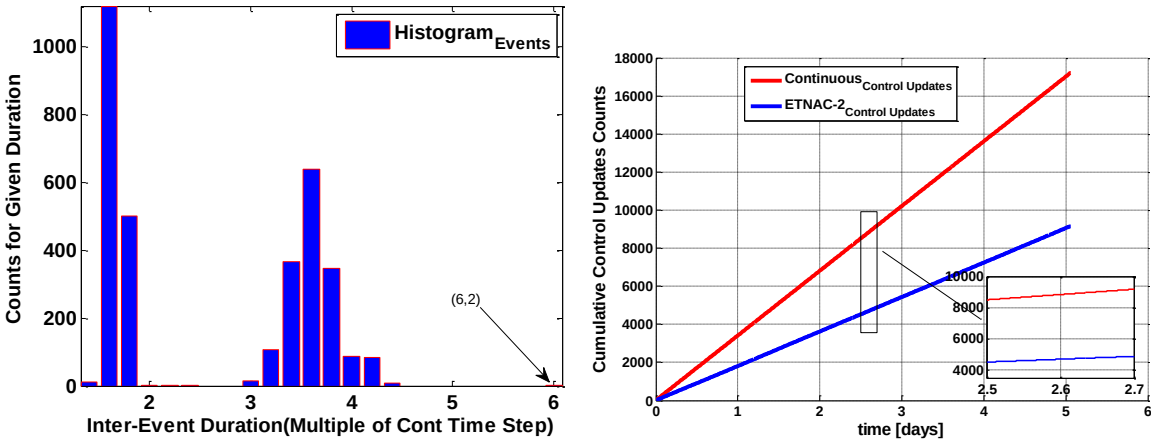

(a) (b)

Figure 19. Case 3: cumulative event counts (a), and histogram of control update events (b), with ETNAC-2.

As Table 2 shows, ETNAC-2 proved to be very effective in achieving the error-level objectives while providing a reduction in control updates and much longer periods of silence, which is very useful in microsatellite operations in deep space missions. Similar trends as shown in Table 1 are also observed. For smaller thresholds, ΔV is comparatively lower but sampling instants are slightly higher, and vice versa for higher thresholds.

Table 2 ETNAC-2 comparison and ΔV analysis for different values of $\propto$ for a duration of 365 days, continuous sampling instants 12,55,781.

Case No	**Error Threshold Level (mm)**	ΔV **m/s per year**	$\Delta \boldsymbol{d}(\boldsymbol{X})$ **m/s per year**	$\Delta V - \Delta \boldsymbol{d}(\boldsymbol{X})$ **m/s per year**	**Sampling Instants with ETNAC-2**	**% Reduction**
1	1	7.6254	2.7714	4.8540	669,568	46.6820
2	5	10.1178	2.7714	7.3465	558,691	55.5170
3	10	14.3708	2.7714	7.2814	225,849	82.0152
4	100	16.7935	2.7714	14.0221	85,016	93.2300
5	1000	17.5861	2.7714	14.8147	63,323	94.9575

Note that it is not just about the reduction in number of updates. There is also the possibility of additional environmental, dynamic, or even structural changes (the spacecraft mass will decrease as ΔV is used). As such, the system can face a range of different uncertainties over time. In such cases, ETNAC will be able to respond quickly. The entire purpose of ETNAC is that it can respond quickly, learn, and adapt when needed. If the sampling rate is set too slow (for reducing number of updates with continuous), it will take longer to adapt and there is an increased risk of divergence. As such, even though it is possible to have an initial high continuous sampling rate and later reduce to a slower continuous sampling rate, there is no guarantee that the high sampling rate won't be needed again. ETNAC allows for the sampling rate to effectively change over time, allowing the sampling rate to be, in effect, autonomously chosen.

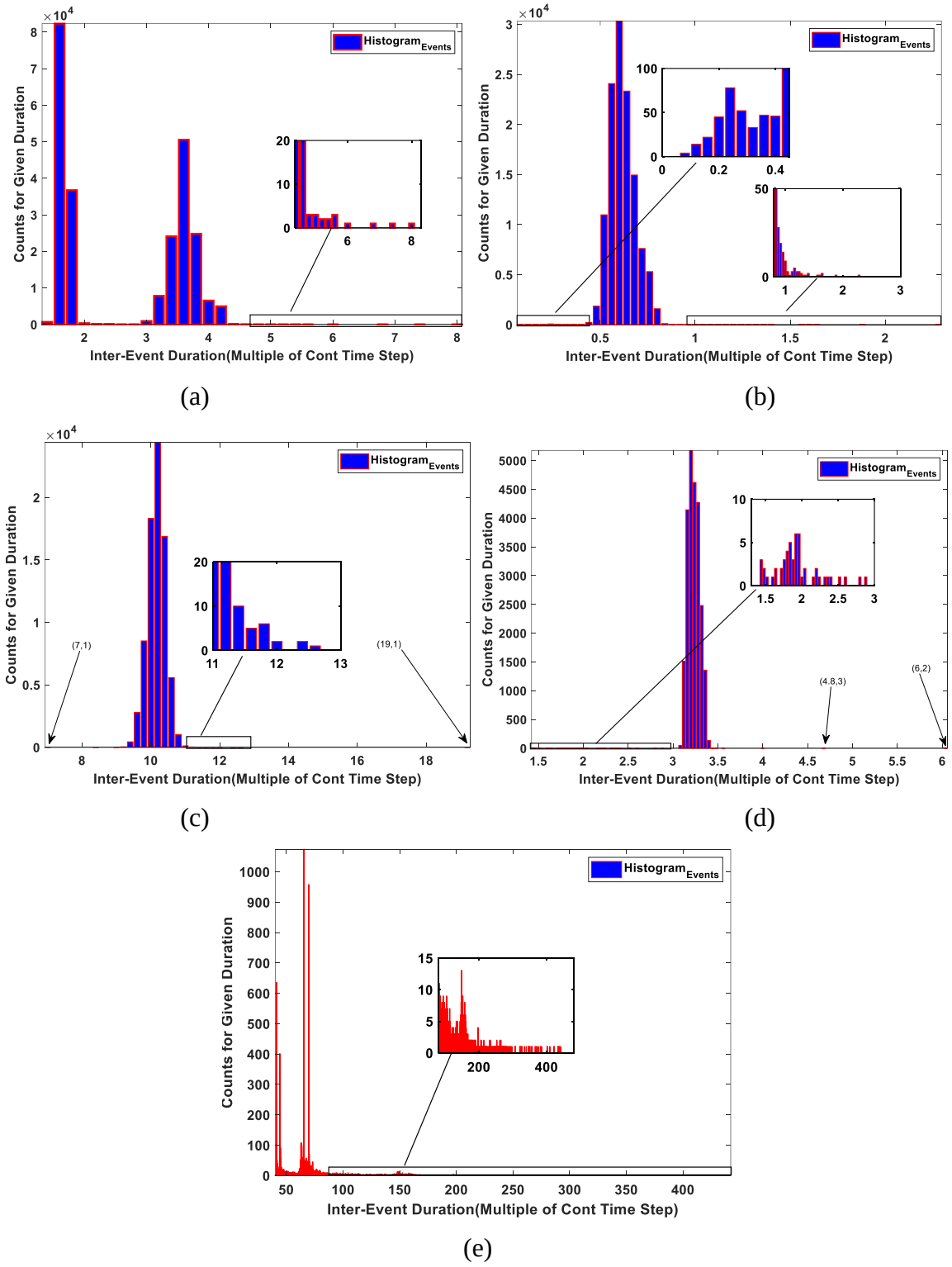

Figure 20. Histogram of inter-event times for different values of $\propto$ for a duration of 365 days with ETNAC-2: 1st case where $\propto$= 1mm (a), 2nd case where $\propto$= 5mm (b), 3rd case where $\propto$= 10mm (c), 4th case where $\propto$= 100mm (d) and 5th case where $\propto$= 1000mm (e).

These comparisons again show the potential of the proposed ETNAC methods for the given application to achieve the desired goal of tracking and robustness, by efficiently countering the uncertainty of perturbations, while at the same time improving periods of silence which in turn reduces jitters.

6. CONCLUSIONS

A modified state observer-based neuro-adaptive event-triggered control (ETNAC) was derived and implemented with the circular restricted three-body problem for a pair of spacecrafts flying in formation along a halo orbit at the Sun-Earth/Moon L_1 point. The goal was to maintain the tracking error in the millimeter/submillimeter range in the presence of uncertainties while reducing jitter by increasing periods of silence for spacecraft through the notion of event-triggering. Simulation results showed that this goal was achieved successfully using the proposed ETNAC schemes. From the numerical results it is shown that control updates can be reduced as much as 98% without inducing any oscillations while maintaining the tracking error under the desired range. For smooth operation and better functioning of the microsatellite science, these reduced control updates and longer periods of silence can be considered significant. These results indicate the potential of the proposed technique for application to the microsatellite platform and deep space missions while reducing control updates and increasing period of silence time in the the microsatellites.

7. FUNDING SOURCES

This research was supported in part by the National Aeronautics and Space Administration under Grants NNX15AM51A and NNX15AN04A.

REFERENCES

[1] "CubeSats Overview." *NASA*, URL: https://www.nasa.gov/mission_pages/cubesats/overview [retrieved 12 April 2019].

[2] "Proposed Missions - Terrestrial Planet Finder." *NASA*, URL: www2.jpl.nasa.gov/missions/proposed/tpf.html [retrieved 14 November 2018].

[3] "Darwin Overview." *European Space Agency*, 2009, URL: www.esa.int/Our_Activities/Space_Science/Darwin_overview [retrieved 14 November 2018].

[4] "The MAXIM Mission." *NASA*, URL: bhi.gsfc.nasa.gov/docs/mission/mission.html [retrieved 14 November 2018].

[5] "Laser Interferometer Space Antenna." *NASA*, URL: lisa.nasa.gov [retrieved 14 November 2018].

[6] "The Stellar Imager (SI) Vision Mission." *NASA*, 30 June 2014, URL: hires.gsfc.nasa.gov/si/ [retrieved 14 November 2018].

[7] "MAXIM Pathfinder." *NASA*, URL: bhi.gsfc.nasa.gov/docs/pathfinder/pathfinder.html [retrieved 14 November 2018].

[8] K. G. Carpenter, C. J. Schrijver, and M. Karovska, "SI - The Stellar Imager," *AIAA* Summary Paper, URL: https://hires.gsfc.nasa.gov/si/documents.html [retrieved 14 November 2018].

[9] B. G. Marchand and K. C. Howell, "Control Strategies for Formation Flight in the Vicinity of the Libration Points," *Journal of Guidance, Control, and Dynamics*, Vol. 28, No. 6, pp. 1210–1219, 2005. doi: 10.2514/1.11016

[10] K. C. Howell and B. G. Marchand, "Natural and Non-Natural Spacecraft Formations Near the L1 and L2 Libration Points in the Sun-Earth/Moon Ephemeris System," *Journal of Dynamical Systems*, Vol. 20, No. 1, pp. 149–173, 2005. doi: 10.1080/1468936042000298224

[11] M. Xin, S. N. Balakrishnan, and H. J. Pernicka," Multiple Spacecraft Formation Control With U–D Method," *IET Control Theory & Applications*, Vol. 1, No. 2, pp. 485–493, 2007. doi: 10.1049/iet-cta:20050410

[12] M. Xin, S. N. Balakrishnan, and H. J. Pernicka, "Position and Attitude Control of Deep-Space Spacecraft Formation Flying Via Virtual Structure And Θ-D Technique," *Journal of Dynamic Systems, Measurement, and Control*, Vol. 129, No. 5, pp. 689-698, 2007. doi: 10.1115/1.2764509

[13] P. Li, P. Cui, and H. Cui, "An Improved Nonlinear Control Strategy for Deep Space Formation Flying Spacecraft," *Acta Mechanica Sinica/Lixue Xuebao*, Vol. *25, No.* 6, pp. 847–856, 2009. doi: 10.1007/s10409-009-0274-2

[14] M. Xu, N. Zhou, and J. Wang, "Robust Adaptive Strategy for Station Keeping of Halo Orbit," *Proceedings of the 24th Chinese Control and Decision Conference, CCDC 2012*, pp.3086–3091, 2012. doi: 10.1109/CCDC.2012.6244486

[15] M. S. De Queiroz, V. Kapila, and Q. Yan, "Adaptive Nonlinear Control of Multiple Spacecraft Formation Flying," *Journal of Guidance, Control, and Dynamics*, Vol. *23, No.* 3, pp. 385–390, 2000. doi: 10.2514/2.4549

[16] P. Gurfil, M. Idan, and N. J. Kasdin, "Neuro Control of Spacecraft Formation Flying in The Elliptic Restricted Three-Body Problem," *AIAA Guidance, Navigation, and Control Conference and Exhibit*, (August), pp. 1–11, Aug 2002. doi:10.2514/6.2002-4962

[17] R. Qi, S. Xu, and M. Xu, " Impulsive Control for Formation Flight about Libration Points," *Journal of Guidance, Control, and Dynamics*, Vol. *35*, *No.* 2, pp.484–496, 2012. doi: 10.2514/1.54383

[18] N. Yoshida, O. Takahara, K. Kodeki,, "Spacecraft with Very High Pointing Stability: Experiences and Lessons Learned," IFAC Proceedings Volumes, vol. 46, no. 19, pp. 547-552, ISSN 1474-6670, 2013.

[19] M. Levine, S. Shaklan, and J. Kasting, "Terrestrial Planet Finder Coronagraph", *Science and Technology Definition Team (STDT), JPL Document D-34923*, NASA Report, June 2016.

[20] H. Wang, L. Chen, Z. Jin, and J. L. Crassidis, "Adaptive Momentum Distribution Jitter Control for Microsatellite," *Journal of Guidance, Control, and Dynamics*, vol. 42, no.3, pp.632-641, 2019. doi:10.2514/1.G003909

[21] NASA report, "https://www.elisascience.org/files/publications/LISA_L3_20170120.pdf"

[22] S.B. Chen, M. Xuan, L. Zhang, S. Gu, X. Gong, H. Y. Sun, "Simulating and Testing Microvibrations on an Optical Satellite Using Acceleration Sensor-Based Jitter Measurements," *Sensors* 2019, vol.*19*, no. 8, 1797.

[23] J. pan, C. Che,Y. Zhan, M. Wang, "Satellite Jitter Estimation and Validation Using Parallax Images," Sensors, vol. 17, no. 1, 2017. doi: 10.3390/s17010083.

[24] L. Arena, F. Piergentili, and F. Santoni, "Design, Manufacturing, and Ground Testing of a Control-Moment Gyro for Agile Microsatellites," *Journal of Aerospace Engineering*, vol. 30, no. 5, pp. 04017039, 2017. doi:10.1061/(ASCE)AS.1943-5525.0000754

[25] A. Khalid Al-Saif, A. F. Mosaad, and K. Aldakkan, "Suppression of Microvibrations of Low-Earth-Orbit Satellites with Flexible Solar Panels", *Journal of Aerospace Engineering*, vol. 25, no. 1, pp. 117-124, 2012. doi:10.1061/(ASCE)AS.1943-5525.0000132

[26] A. Iwasaki, "Detection and Estimation of Satellite Attitude Jitter Using Remote Sensing Imagery, ch#13 from 'Advances in Space Technology by Jason Hall'" , *Publisher InTech*, ISBN 978-953-307-551-8, Feb 2011.

[27] Inamori, T., Wang, J. H., Saisutjarit, P., and Nakasuka, S., "Jitter Reduction of a Reaction Wheel by Management of Angular Momentum Using Magnetic Torquers in Nano- and Micro-Satellites," Advances in Space Research, Vol. 52, No. 1, 2013, pp. 222–231, 2013. doi.org/10.1016/j.asr.2013.02.014

[28] D. A. Vallado, "Fundamentals of Astrodynamics and Applications," 4th ed., *Microcosm Press*, 2013, Chaps. 1, 7-10.

[29] J. L. Rovey, X. Yang, P. D. Friz, C. Hu, and M. S. Glascock, "Plasmonic Force Propulsion Revolutionizes Nano/Picosatellite Capability," *NASA Innovative Advanced Concepts Phase I Final Report*, May 2014.

[30] J. L. Rovey, P. D. Friz, C. Hu, M. S. Glascock, and X. Yang, "Plasmonic Force Space Propulsion," *Journal of Spacecraft and Rockets*, Vol. 52, No. 4, pp. 1163–1168, 2015. doi: 10.2514/1.A33155

[31] P. Galchenko and H. J. Pernicka, “Precision Formation Flying and Spacecraft Pointing Using Plasmonic Force Propulsion,” *Proceedings of the 2017 AAS/AIAA Astrodynamics Specialist Conference* AAS 17-831, Stevenson, WA, Aug 2017, Vol. 162, pp. 2958-2997.

[32] P. Galchenko and H. J. Pernicka, “Precision Control of Microsatellite Swarms using Plasmonic Force Propulsion,” AAS 18-472, Presented at the 2018 *AAS/AIAA Astrodynamics Specialist Conference*, Snowbird, UT, August 2018.

[33] S. Gupta, “Increasing the Sampling Efficiency for f Control System,” *Automatic Control, IEEE Transactions*, Vol. 8, No. 3, pp. 263-264, 1963.

[34] P. Tabuada, “Event Triggered Real Time Scheduling Of Stabilizing Control Tasks,” *IEEE Transaction .Automatic*, Vol. 52, No. 9, pp.1680-1685, 2007. doi: 10.1109/TAC.2007.904277

[35] W.P.M.H. Heemels, K.H. Johansson, and P. Tabuada,”An Introduction To Event - Triggered And Self-Triggered Control,” *51st IEEE Conference on Decision and Control, Maui, USA* , pp. 3270-3285, 2012. doi:10.1109/CDC.2012.6425820

[36] K. S. Narendra and K. Parthasarathy,”Identification and Control of Systems Using Neural Network,” *IEEE Trans. On Neural Net*, Vol. 1, No. 1, pp. 4-27, 1990. doi: 10.1109/72.80202

[37] A. Ghafoor, S.N. Balakrishnan, T. Yucelen, “Modified State Observer Based Decentralized Neuroadaptive Controller for Large Scale Interconnected Uncertain Systems,” *ACC 2018* Milwaukee USA, pp.1701-1706. doi: 10.23919/ACC.2018.8431513

[38] X. Wang, E. Kharisov, and N. Hovakimyan, “Real-Time Adaptive Control for Uncertain Networked Control Systems,” *IEEE Trans. Autom. Control*, vol. 60, no. 9, pp. 2500–2505, 2015. doi: 10.1109/TAC.2014.2380653

[39] X. Wang, N. Hovakimyan, “ L1 Adaptive Control of Event Triggered Network System,*” Proc of American Control Conference,* Baltimore, *MD, USA*, pp. 2458-2463, Jun 2010. doi: 10.1109/ACC.2010.5530583

[40] V. Narayanan and S. Jagannathan, "Event-Triggered Distributed Approximate Optimal State and Output Control of Affine Nonlinear Interconnected Systems," in *IEEE Transactions on Neural Networks and Learning Systems*, vol. 29, no. 7, pp. 2846-2856, July 2018. doi: 10.1109/TNNLS.2017.2693205

[41] V. Narayanan and S. Jagannathan, "Event-sampled adaptive neural network control of robot manipulators," *International Joint Conference on Neural Networks (IJCNN)*, Vancouver, BC, 2016, pp.4941-4946, 2016. doi: 10.1109/IJCNN.2016.7727850

[42] A. Albattat, B. Gruenwald, and T. Yucelen, "Design and Analysis of Adaptive Control Systems Over Wireless Networks," *ASME. J. Dyn. Sys., Meas., Control*, Vol. 139, No. 7, pp. 1-8, 2017. doi: 10.1115/1.4035094

[43] A. Ghafoor, J. Yao, S.N. Balakrishnan, J. Sarangapani and T. Yucelen, "Event Triggered Neuroadaptive Controller Design For Uncertain Affine Nonlinear Systems," *Proc. of ASME conf. on DSCC 2018* USA, pp. V001T03A003. doi: 10.1115/DSCC2018-9103

[44] S.N. Balakrishnan and H. Zhang, "Robust Adaptive Critic Based Neuro Controllers For Helicopter with Unmdled Uncertainties," *Proc. Of AIAA Conf. on Guidance, Navigation and Control*, 2001. doi: 10.1109/IJCNN.2000.861282

[45] R. Padhi, N. Unnikrishnan, and S. N. Balakrishnan, "Model-Following Neuro-Adaptive Control Design for Non-Square, Non-Affine Nonlinear Systems," *IET Control Theory & Applications*, Vol. 1, No. 6, pp. 1650-1661, 2007. doi: 10.1049/iet-cta:20060364

[46] K. Rajagopal, S.N. Balakrishnan, N. Nguyen, K. Krishnakumar and A. Mannava, "Neuroadaptive Model Following Controller Design for Non-Affine and Non-Square Aircraft Systems", *AIAA Guidance, Navigation, and Control Conference*, pp. 1-21, 2009. doi: 10.2514/6.2009-5737

[47] V.S.S. Pappu, J. E. Steck, K. Rajagopal, and S. N. Balakrishnan, "Modified State Observer Based Adaptation for a General Aviation Aircraft - Simulation and Flight Test", *AIAA Guidance, Navigation, and Control Conference*, AIAA 2014-1297. doi: 10.2514/6.2014-1297

[48] K. Rajagopal, S.N. Balakrishnan, J.E. Steck, and D. Kimbal, "Robust Adaptive Control of a General Aviation Aircraft", *AIAA Atmospheric Flight Mechanics Conference*, Canada, AIAA2010-7942. doi: 10.2514/6.2010-7942

[49] K. Rajagopal, S. N. Balakrishnan, N. Nguyen, and K. Krishnakumar, "Time Delay Margin Analysis of Modified State Observer Based Adaptive Control," *AIAA Guidance, Navigation, and Control Conference*, AIAA-2013-4755. doi: 10.2514/6.2013-4755

[50] V. S. S. Pappu, J. E. Steck, B. S. Steele, K. Rajagopal and S. N. Balakrishnan, "Hardware-In-Loop and Flight Testing of Modified State Observer Based Adaptation for a General Aviation Aircraft," *AIAA Guidance, Navigation, and Control Conference,* AIAA 2015-1997. doi: 10.2514/6.2015-1997

[51] V. Stepanyan and K. Krishnakumar, "Adaptive Control with Reference Model Modification," *Journal of Guidance, Control, and Dynamics*, vol. 35, no. 4, pp. 1370-1374, 2012. doi: 10.2514/1.55756

[52] H. Wong and V. Kapila, "Spacecraft Formation Flying near Sun-Earth L2 Lagrange Point: Trajectory Generation and Adaptive Full-State Feedback Control," *NASA Formation Flying Symposiuam*, Washington DC, 2004.

[53] N. Szanto, V. Narayanan and S. Jagannathan, "Event-sampled direct adaptive NN output- state-feedback control of uncertain strict-feedback system," *IEEE Tran. On NN&learning Systems*, vol. 29, no. 5, pp. 1850-1863, 2018. doi: 10.1109/TNNLS.2017.2678922

[54] K. Shahid and K. D. Kumar. "Formation Control at the Sun-Earth L2 Libration Point Using Solar Radiation Pressure", *Journal of Spacecraft and Rockets*, Vol. 47, No. 4, pp. 614-626, 2010. doi: 10.2514/1.47342

[55] X. Ming, L. Yuying, F. Xiaoyu, "Formation flying on quasi-halo orbits in restricted Sun–Earth/Moon system," *Science Direct Aerospace Science and Technology*, vol. 67, pp. 118-125, August 2017. doi: 10.1016/j.ast.2017.03.038

[56] E. Lavretsky and K. Wise, "Robust and Adaptive Control: With Aerospace Applications," Springer, New York, 2012, Chap. 11.

[57] D. S. Bernstein, "Matrix Mathematics: Theory, Facts, and Formulas," 2nd ed., *Princeton University Press*, Princeton, NJ, 2009, Chaps. 8, 9.

[58] H. K. Khalil, "Nonlinear Systems," 3rd ed., *Prentice Hall*, Upper Saddle River, NJ, 1996, Chap. 5.

III. SEGREGATED PRESCRIBED PERFORMANCE GUARANTEEING NEURO-ADAPTIVE CONTROLLER (SPPGNAC) FOR CONSTRAINED UNCERTAIN NONLINEAR SYSTEMS

Abdul Ghafoor and S. N. Balakrishnan

Department of Mechanical and Aerospace Engineering, Missouri University of Science and Technology, Rolla, MO 65409

ABSTRACT

In this paper, a neuro-adaptive controller design is proposed that guarantees strict performance for the constrained uncertain nonlinear system. This performance can be independently prescribed for each individual/segregated state and/or error signal of the given system. Most practical applications are nonlinear in nature, involve different physical limitations that put different symmetric/asymmetric constraints on the state signals, and have uncertainties and disturbances from inaccurate models, environmental changes, structural changes, and some performance requirements need to be insured throughout. To address these problems simultaneously, a control architecture is proposed for uncertain constrained nonlinear systems. Main features of the proposed design are (i) guaranteed priori user-defined tracking performance for all times (transient and steady state) that can satisfy constraints on the state signals, (ii) flexibility to have different constraints on separate state and error signal, and not just on the norm of errors or states, (iii) flexibility to have symmetric/asymmetric constraints/bounds, (iv) change in control can be regulated in proportion to proximity of threshold which helps to avoid excessive input force, which is generally observed in barrier-Lyapunov-function (BLF)-based controls, (v) it can

estimate and address uncertainties and can identify unmodeled dynamics by using artificial-neural-network (ANN)-based modified state observer (MSO). Benchmark numerical examples are used to show the effectiveness of the proposed technique.

1. INTRODUCTION

Many real-world applications involve hardware limitations that put constraints on system states. Most of the practical systems are inherently nonlinear and cannot be controlled or stabilized in an efficient manner by using linearized models. At the same time, the presence of disturbances and uncertainties cannot be avoided. All these problems need to be addressed simultaneously. In addition, some performance is needed to be ensured all the time to avoid undesired operations. To address these problems, a BLF-based control architecture called the segregated prescribed performance guaranteeing neuro-adaptive control (SPPGNAC) is proposed in this paper.

A robotic end effector cannot exceed some velocity if it is handling a soft object on a packaging plant, or it cannot employ force beyond some specified limit if it is handling a fragile object like eggs. These types of limitations can be observed in many fields, from chemical industry to space technology, and all of them have different limitations on their systems. These limitations show up as symmetric/asymmetric constraints in problem formulations. Note that these constraints will not be the same for each state signal. Therefore, separate constraints and performance metrics on each separate state signal is more practical than having one universal constraint on the norm of all states or errors. Furthermore, with all these limitations, some specific performance of the system may need

to be guaranteed all the time. For instance, it is required that a robotic end effector should not transgress a given workspace, or a satellite cannot violate a bound around its trajectory, otherwise it will diverge from its orbit. The presence of uncertainties or external disturbances are unavoidable in any system dynamics. These can originate from structural changes, environmental changes, or inaccurate/approximate modeling. Therefore, it is important for the controller to be adaptive and robust to take care of such abnormalities.

Some efforts have been made to address these issues. Regarding adaptive controls to address uncertainties and disturbances, after McCulloch [1], a pioneer in the field of calculus of ANN, more and more researchers have been attracted by the power of neural networks (NN) as effective function approximators. Narendra [2] considered the application of the ANN in the control of nonlinear systems. Amongst other developments, Sanner et al. in [3] and Lewis in [4] used different radial basis and multilayer ANN in control schemes to approximate uncertainties and disturbances. Other relevant contributions for function approximation are [5] and [6] from Farrell et al. and Lewis et al. respectively. Padhi et al. presented the MSO in [7] to estimate uncertain dynamics to use in the control. Different control schemes are presented in [8], [9], and [10] where MSO is used.

For constrained systems, the notion of set invariance was applied in [11] and [12] by Liu and by Lin et al., respectively. Model predictive control (MPC) was utilized by Allgöwer et al. in [13] and by Mayne et al. in [14] to insure constraints, while in [15] and [16], reference governors are utilized by Bemporad and Gilbert et al. to satisfy constraints. Additionally, Ngo, Mahony, and Jiang employed BLF in [17] to handle constraints for systems in the Brunovsky form. This motivated Tee, Ge, and Tay, who presented an

asymmetric BLF for the control of the electrostatic parallel plate in press [18]. Later, they extended it to the nonlinear system in [19] and were able to guarantee strict performance on partial states. Krstic et al. in [20] and Marino and Tomei in [21] extended backstepping in adaptive control for parametric-uncertain systems with non-matching conditions. Despite the availability of such literature, only a few efforts such as the research from Krstic and Bement [22] have been made in adaptive-backstepping-based constrained control to achieve a non-overshooting tracking response for strict feedback systems. Li and Krstic in [23], proposed a modified backstepping design based on positively invariant feasibility regions for nonlinear systems with control singularities. Other papers with BLF-based control for uncertain systems include Bechlioulis and Rovithakis [24], [25]-[26], Ren et al. [27], Muse [28], Kostarigka et al. [29], and Ehsan and Yucelen et al. [30]-[31]. In [24], constrained system is converted to an equivalent unconstrained system that still satisfies given performance requirements, but it was assumed that all states are accessible to control. In [25], this condition was relaxed with further assumptions on desired states. On the other hand, [26] extended this approach to general dynamical systems, but only to measurable outputs. In [28], a BLF-based model reference adaptive controller (MRAC) was developed. In [30], the authors proposed a BLF-based MRAC for linear systems assuming time invariant uncertainties. Later, the same authors extended the idea of BLF-based MRAC to time varying parameters in [31].

Still the constraint formulation used in these papers do not adequately address the practical requirements of real-life systems. Either only one universal constraint is considered on the norm of the state vector or the error vector or constraints can be insured only on the partial state vector. In some work, BLF-based MRAC is focused only on error

performance. The assumptions made are not very practical. There is a gap in actual physical system's limitations and the way the constraints have been modeled in the literature.

This is where the proposed SPPGNAC is expected to be useful, as it can handle the discussed problems simultaneously. It can be directly applied to a nonlinear model, ensures separate independent symmetric/asymmetric constraints on state signals at the same time, guarantees prescribed performance, can estimate and address uncertainties and disturbances online independent of BLF, can model the unknown dynamics, and it also offers a way to regulate the excessive control effort near the boundary as it is observed in the BLF-based controls.

The rest of this paper is organized as follows: Section II presents the mathematical background, and Section III contains the problem formulation. Section IV provides the formulations of the proposed SPPGNAC. Section V describes the stability analysis, while Section VI covers the discussions on the numerical implementation, results and analysis. Finally, Section VII summarize the conclusions from this study followed by acknowledgement and the references.

2. MATHEMATICAL BACKGROUND

For a variable $s \in \mathbb{R}$, a BLF on its absolute value, $f_{bl}(|s|)$, $f_{bl}: \mathbb{R} \to \mathbb{R}$ is defined [31] as

$$f_{bl}(|s|) \triangleq \alpha_s \frac{s^2}{(\epsilon_s - |s|)} \tag{1}$$

where $\epsilon_s \in \mathbb{R}_+$ is a user-defined bound/constraint on $|s|$, $\alpha_s > 0$, and $|s| \in \mathsf{C}_{\epsilon_s}$ for $\mathsf{C}_{\epsilon_s} \triangleq \{ s: |s| \in [0, \epsilon_s) \}$. The derivative of f_{bl} with respect to s^2 is given as

$$Df_{bl_{|s|}} = \frac{d\, f_{bl}(|s|)}{d\, s^2} = \alpha_s \frac{(\epsilon_s - \frac{1}{2}|s|)}{(\epsilon_s - |s|)^2}. \tag{2}$$

One modification made here in the definition of BLF in (1) as compare to [31] is the multiplication by a parameter α_s, which helps to regulate the excessive change in $f_{bl}$and $Df_{bl_{|s|}}$. Note that because BLF is applied on the absolute value of s and a symmetric trend is seen on both the negative and positive sides of the plot of f_{bl}, as can be seen from Figure 1a and 1b, it is therefore called a symmetric BLF. It will enforce only symmetric constraints/bounds on the variable. The effect of α_s is shown in Figure 1b where now the value of f_{bl} goes high only when $|s|$ reaches close to ϵ_s. From definitions in (1) and (2), followings hold [31],

i) $f_{bl}(|s|)$ is continuously differentiable on C_{ϵ_s}

ii) If $|s| = 0$, then $f_{bl}(|s|) = 0$

iii) If $|s| \to \epsilon_s$, then $f_{bl}(|s|) \to \infty$

iv) As long as $|s| \in \mathsf{C}_{\epsilon_s}$ then $0 \leq f_{bl}(|s|) \leq \gamma_s$. Since $|s| < \epsilon_s$, from (1) it is clear that $f_{bl}(|s|)$ is bounded by some $\gamma_s \in \mathbb{R}_+$

v) As long as $|s| \in \mathsf{C}_{\epsilon_s}$,then $0 < Df_{bl_{|s|}} \leq \beta_{|s|}$. Since $|s| < \epsilon_s$, from (2) it is clear that $Df_{bl_{|s|}}$ is bounded by some $\beta_{|s|} \in \mathbb{R}_+$.

Symmetric BLF can be extended to an asymmetric case, where we can have different upper and lower constraints on the given variable. One example is shown in

Figure 1c, where PCs on the positive and negative sides are different now. For an asymmetrically constrained s, its BLF can be given as

$$f_{bl}(|s|) \triangleq f_{asym}(s)\, \bar{f}_{bl}(|s|) + \left(1 - f_{asym}(s)\right) \underline{f}_{bl}(|s|) \tag{3}$$

where $\bar{f}_{bl}(|s|) \triangleq \frac{s^2}{(\bar{\epsilon}_s - |s|)}$, $\underline{f}_{bl}(|s|) \triangleq \frac{s^2}{(\underline{\epsilon}_s - |s|)}$, $\bar{\epsilon}_s$ is upper priori PC on s, $\underline{\epsilon}_s$ is lower priori

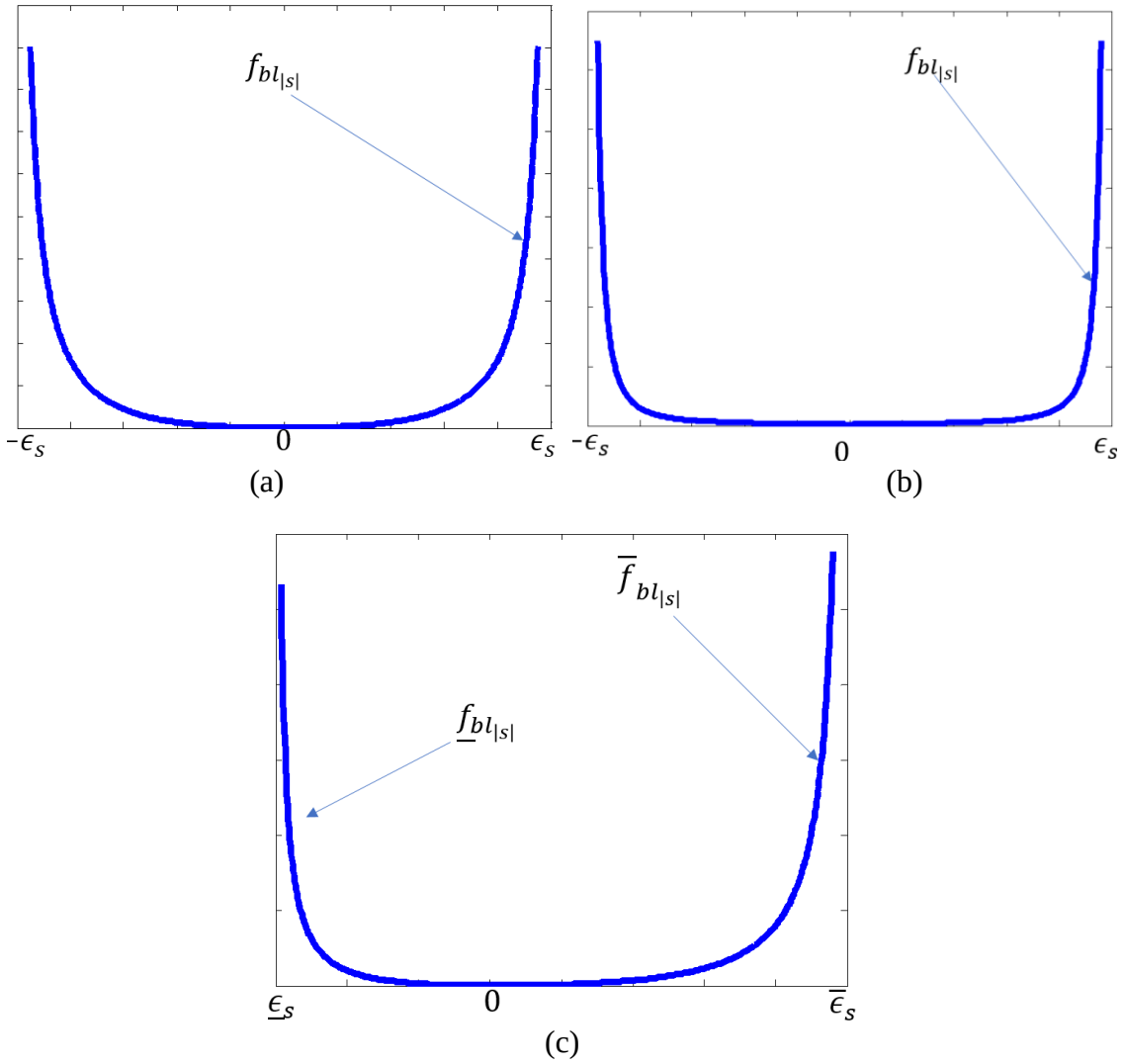

Figure 1. (a) Symmetric BLF with $\alpha_s = 1$, (b) Symmetric BLF with $\alpha_s < 1$, and (c) Asymmetric BLF

PC on s, and $f_{asym}(s)$ is defined as

$$f_{asym}(s) = \begin{cases} 1 & if \quad s \geq 0 \\ 0 & if \quad s < 0 \end{cases}. \tag{4}$$

Note that in these plots, the lower and upper bounds/constraints are shown on the negative and positive sides of the plots. However, it can be applied to any type of plot, considering the reference point as zero and the lower and upper sides as negative and positive, respectively.

Now BLF concept is extended to a vector. For a matrix $P \in \mathbb{R}^{q \times q}$, the weighted Euclidian norm of a vector $T \in \mathbb{R}^q$ is defined as $\|T\|_P = \sqrt{T^T P T}$. A BLF on it can be given as

$$f_{bl}(\|T\|_P) \triangleq \alpha_T \frac{{\|T\|_P}^2}{(\epsilon_T - \|T\|_P)} \tag{5}$$

where $\epsilon_T \in \mathbb{R}_+$ is a user-defined priori PC on $\|T\|_P$, $\alpha_T > 0$, and $\|T\|_P \in \mathsf{C}_{\epsilon_T}$ for $\mathsf{C}_{\epsilon_T} \triangleq \{ \|T\|_P : \|T\|_P \in [0, \epsilon_T) \}$. The derivative of $f_{bl}(\|T\|_P)$ with respect to (w.r.t) $\|T\|_P^2$ is given as

$$Df_{bl_{\|T\|_P}} = \frac{d\, f_{bl}(\|T\|_P)}{d\, \|T\|_P^2} = \alpha_T \, \frac{(\epsilon_T - \frac{1}{2}\|T\|_P)}{(\epsilon_T - \|T\|_P)^2}. \tag{6}$$

From (6) and (7), a bound can be set on the norm of a vector of the signals as well.

3. PROBLEM FORMULATION

The general dynamics of an uncertain nonlinear affine system can be expressed as

$$\dot{X}(t) = f\big(X(t)\big) + g\,(\,u(t) + d\big(X(t)\big)\,) \tag{7}$$

where $X = [x_1 \quad ... \quad x_i \quad \cdots x_n]^T \in \mathbb{R}^n$ is the full state vector of the system, $f\big(X(t)\big) \in \mathbb{R}^{n\times 1}$ and $g \in \mathbb{R}^{n\times m}$ are known system matrices, $d\big(X(t)\big): \bar{\mathbb{R}}_+ \times \mathbb{R}^n \to \mathbb{R}^m$ is the unknown uncertainty in the system, and $u(t) \in \mathbb{R}^m$ is the control input.

The desired dynamics of the nonlinear system defining the reference trajectory is represented using

$$\dot{X_d}(t) = f^*(X_d(t)) \tag{8}$$

where $X_d \in \mathbb{R}^n$ is the desired state of the system and $f^* \in \mathbb{R}^n$ is a known function. System functions $f(X)$ and $f^*(X_d)$ are pointwise bounded for any bounded X and X_d, respectively.

The control objective is to design an adaptive controller $u(t)$ for the system in (7) that forces it to follow the desired response $(X_d(t))$, subject to constraints on the state $\underline{\epsilon}_{x_i} < x_i < \bar{\epsilon}_{x_i}$ and on error $\underline{\epsilon}_{e_j} < e_j < \bar{\epsilon}_{e_j}$ for $i = 1,2,3 \ldots q,\ \ j = 1,2,3 \ldots l$ where $q, l \in \mathbb{N}_+$ and $q, l \leq n$. Note that each state signal x_i can have its own separate different upper and lower constraint $\bar{\epsilon}_{x_i}, \underline{\epsilon}_{x_i} \in \mathbb{R}$ and also, for each error signal e_j certain separate upper and lower bounds $\bar{\epsilon}_{e_j}, \underline{\epsilon}_{e_j} \in \mathbb{R}$ need to be guaranteed all the time.

Assumption 1: The uncertainty can be linearly parametrized. Using the universal function approximation property of neural networks (NN), we know that a real valued smooth function $d\big(X(t)\big): \mathbb{R}^n \to \mathbb{R}$ in a compact set $A \subseteq \mathbb{R}^n$ can be approximated with some residual error ϵ such that

$$d\big(X(t)\big) = W^T \phi(X(t)) + \epsilon(X(t)) \tag{9}$$

where $W \in \mathbb{R}^{z\times m}$ is the unknown but ideal weight matrix ($z \in \mathbb{N}_+$) that belongs to a compact set Ω, and $X \in D_x$ for a sufficiently large compact set D_x, and $\phi: \mathbb{R}^n \to \mathbb{R}^z$ is a vector of known basis functions. Note that $\phi(X)$ is bounded such that $\|\phi(X)\| \leq \phi^*$, ϵ is

the residual error satisfying $|\epsilon| \leq \epsilon^*$, and also it is considered that all states are available for measurements.

Substituting (9) in (7) results in

$$\dot{X}(t) = f\big(X(t)\big) + g\left(u(t) + W^T\phi\big(X(t)\big) + \epsilon\big(X(t)\big)\right). \tag{10}$$

4. PROPOSED SEGREGATED PRESCRIBED PERFORMANCE GUARANTEEING NEURO-ADAPTIVE CONTROLLER (SPPGNAC)

In this section, the SPPGNAC is developed for the system in (7) to guarantee priori prescribed performance while at the same time satisfying given symmetric/asymmetric constraints. An intermediate step in control development is to design an appropriate MSO. The proposed MSO equation can be written as

$$\begin{aligned}\dot{\hat{X}}(t) =\ & f\big(X(t)\big) + g\,u(t) + g\,\hat{d}\big(X(t)\big) - K_2\left(X(t) - \hat{X}(t)\right)\\ =\ & f\big(X(t)\big) + g\,u(t) + g\,\widehat{W}^T\phi\big(X(t)\big) - K_2(X(t) - \hat{X}(t))\end{aligned} \tag{11}$$

where $\hat{d}(\bar{X}(t)) \triangleq \widehat{W}^T\phi\big(X(t)\big)$ represents the estimate of $d(X(t))$, ϕ: $\mathbb{R}^n \to \mathbb{R}^n$ is a vector of known basis functions used in the uncertainty approximation, and K_2 is a user defined Hurwitz gain matrix. Even though all states are assumed measurable here, the MSO notion is used because it helps with the estimation of the uncertainties/disturbances and to avoid large oscillations during the system's transient state.

Assumption 2: Functions $f(.)$, $f^*(.)$, and $\phi(.)$ are locally Lipschitz continuous (LLC)

$$\|f(X) - f(Y)\| = L_f\|X - Y\|$$

$$\|f^*(X) - f^*(Y)\| = L_{f^*}\|X - Y\| \tag{12}$$

$$\|\phi(X) - \phi(Y)\| = L_{\phi}\|X - Y\|$$

where $X, Y \in D_x$ and $L_{f^*}, L_{\phi}, L_f \in \mathbb{R}_+$.

The feedback controller can be generated as

$$u(t) = u_n(t) + u_a(t) + u_{blf}(t) \tag{13}$$

where $u_n \in \mathbb{R}^m$ is the nominal feedback control input that forces the nominal/known system to reach the desired state in the absence of uncertainties and constraints, u_a is the adaptive controller which is used to cancel the uncertainties, and u_{blf} is the BLF-based control input that is used to bound the states and error to ensure that the constraints are met and guarantees the prescribed performance. Nominal control is found from the stable dynamics of the tracking error from the nominal system (known system without uncertainty, $\dot{X}_n(t) = f\big(X(t)\big) + g\ u_n(t))$) to the desired system as

$$\dot{X}_n(t) - \dot{X}_d(t) = K(X(t) - X_d(t)) \tag{14}$$

where K is the user-defined Hurwitz gain matrix. Using the system dynamics, it can be written as

$$f\big(X(t)\big) + g\ u_n(t)) - f^*(X_d) = K\big(X(t) - X_d(t)\big). \tag{15}$$

From (15),

$$gu_n(t) = f^*(X_d) - f\big(X(t)\big) + K(X(t) - X_d(t))$$

$$gu_n(t) = e_f + Ke_r \tag{16}$$

where $e_r \triangleq X(t) - X_d(t)$ is the tracking error and e_f is defined as $e_f \triangleq f^*(X_d) - f\big(X(t)\big)$. If g is invertible, then the nominal control can be given as

$$u_n(t) = g^{-1}(Ke_r + e_f) \tag{17}$$

and $u_a \in \mathbb{R}^m$, the adaptive control input, is given as

$$u_a = -\hat{f}\big(X(t)\big) = -\widehat{W}^T \phi\big(X(t)\big) \tag{18}$$

where $\widehat{W}$ is the estimate of W. BLF-based control u_{blf} is expressed as

$$\begin{aligned} u_{blf} = -\sum_{j=1}^{l} \{ & f_{asym}\left(e_{r_j}\right) \alpha_{e_{r_j}} D\bar{f}_{bl}\big|_{e_{r_j}|} g^T K_{e_{r_j}} e_r \\ & + \left(1 - f_{asym}\left(e_{r_j}\right)\right) \alpha_{e_{r_j}} D\underline{f}_{bl}\big|_{e_{r_j}|} g^T K_{e_{r_j}} e_r \} \\ & - \sum_{i=1}^{q} \{ f_{asym}(x_i)\, \alpha_{x_i} D\bar{f}_{bl|x_i|} g^T K_{x_i} X \\ & + \left(1 - f_{asym}(x_i)\right) \alpha_{x_i} D\underline{f}_{bl|x_i|} g^T K_{x_i} X \} \end{aligned} \tag{19}$$

where e_{r_j} is the j^{th} tracking error signal, $\overline{\epsilon}_{e_{r_j}}$ is the upper bound/constraint on the e_{r_j}, $\bar{f}_{bl}(e_{r_j})$ is the upper bound-based BLF for e_{r_j}, and $D\bar{f}_{bl}\big|_{e_{r_j}|}$ is the derivative of $\bar{f}_{bl}$ w.r.t to ${e_{r_j}}^2$. Similarly, $\underline{f}_{bl}(e_{r_j})$ is the lower bound ($\underline{\epsilon}_{e_{r_j}}$) based BLF for e_{r_j}, and $D\underline{f}_{bl}\big|_{e_{r_j}|}$ is its derivative w.r.t to ${e_{r_j}}^2$, where $l \in \mathbb{N}_+$ for $1 \leq l \leq n$ (meaning that the separate upper and lower bounds can be imposed/disabled on any of the error signal from 1 to n independently). Matrix $K_{e_{r_j}}$ is used to select the j^{th} error signal (e_{r_j}) from the error vector e_r. The $K_{e_{r_j}}$ is(are) square matrix(matrices) with only j^{th}diagonal element as 1 and rest of the entities as zeros. Similar to $K_{e_{r_j}}$, matrix K_{x_i} also has only i^{th} diagonal elements as 1 and is used to select the i^{th} state signal (x_i) from the X. In similar fashion, $D\bar{f}_{bl|x_i|}$ is derivative of $\overline{f}_{bl}(|x_i|)$ w.r.t to ${x_i}^2$ when $\overline{\epsilon}_{x_i}$ is upper constraint on state signal x_i where $q \in \mathbb{N}_+$ and $1 \leq q \leq n$ (meaning any of the state signals from 1 to n can have their own

separate upper and lower constraints). Likewise, $\underline{\epsilon}_{x_i}$, $\underline{f}_{bl}(|x_i|)$, and $D\underline{f}_{bl}{}_{|x_i|}$ are respectively, the lower constraint on x_i, the lower-constraint-based BLF for x_i, and the derivative of $\underline{f}_{bl}(|x_i|)$ w.r.t. ${x_i}^2$. These constraints on x_i and e_{r_j} can be represented as $\underline{\epsilon}_{x_i} < x_i < \overline{\epsilon}_{x_i}$ and $\underline{\epsilon}_{e_{r_j}} < e_{r_j} < \overline{\epsilon}_{e_{r_j}}$. Scalars $\alpha_{(.)} > 0$ are used to regulate the u_{blf} to avoid excessive control u_{blf}. If g is invertible, then overall feedback control can be given as

$$u(t) = u_n(t) + u_a(t) + u_{blf}(t)$$

$$= g^{-1}\Bigg[Ke_r + e_f - g\widehat{W}^T\phi\big(X(t)\big) - g\sum_{j=1}^{l}\{f_{asym}\left(e_{r_j}\right)\ \alpha_{e_{r_j}}\ D\bar{f}_{bl}\big|_{e_{r_j}}\ g^T K_{e_{r_j}} e_r$$

$$+ \left(1 - f_{asym}\left(e_{r_j}\right)\right)\alpha_{e_{r_j}}\ D\underline{f}_{bl}\big|_{e_{r_j}}\ g^T K_{e_{r_j}} e_r\}$$

$$- g\sum_{i=1}^{q}\{f_{asym}(x_i)\ \alpha_{x_i}\ D\bar{f}_{bl|x_i|}\ g^T K_{x_i} X$$

$$+ \left(1 - f_{asym}(x_i)\right)\alpha_{x_i}\ D\underline{f}_{bl}{}_{|x_i|}\ g^T K_{x_i} X\}\Bigg]$$

$$
\begin{aligned}
&= g^{-1}\Bigg[Ke_r + e_f - g\widehat{W}^T\phi\big(X(t)\big) \\
&- \sum_{j=1}^{l}\{f_{asym}\left(e_{r_j}\right)\ \alpha_{e_{r_j}}\ D\bar{f}_{bl}\big|_{e_{r_j}|}\ gg^T K_{e_{r_j}} e_r \\
&+ \left(1 - f_{asym}\left(e_{r_j}\right)\right)\alpha_{e_{r_j}}\ D\underline{f}_{bl}\big|_{e_{r_j}|} gg^T K_{e_{r_j}} e_r\} \\
&- \sum_{i=1}^{q}\{f_{asym}(x_i)\ \alpha_{x_i}\ D\bar{f}_{bl|x_i|} gg^T K_{x_i} X \\
&+ \left(1 - f_{asym}(x_i)\right)\alpha_{x_i}\ D\underline{f}_{bl|x_i|} gg^T K_{x_i} X\}\Bigg].
\end{aligned}
\tag{20}
$$

In the case where g is not invertible, a slack variables-based technique can be used. Two slack variables are introduced as $u_s \in \mathbb{R}^{(n-m)\times 1}$ and $g_s \in \mathbb{R}^{n\times(n-m)}$. The g_s is chosen such that the augmented $\bar{G} \triangleq [g, g_s]$ becomes a square and invertible matrix [7]. The augmented control then can be given as $\bar{U} \triangleq [u(t), u_s]^T$. Adding $g_s u_s$ on both sides of equation (20),

$$
\begin{aligned}
gu(t) + g_s u_s = {} & Ke_r + e_f - g\widehat{W}^T\phi\big(X(t)\big) - \sum_{j=1}^{l}\{f_{asym}\left(e_{r_j}\right)\ \alpha_{e_{r_j}}\ D\bar{f}_{bl}\big|_{e_{r_j}|}\ gg^T K_{e_{r_j}} e_r \\
&+ \left(1 - f_{asym}\left(e_{r_j}\right)\right)\alpha_{e_{r_j}}\ D\underline{f}_{bl}\big|_{e_{r_j}|} gg^T K_{e_{r_j}} e_r\} \\
&- \sum_{i=1}^{q}\{f_{asym}(x_i)\ \alpha_{x_i}\ D\bar{f}_{bl|x_i|} gg^T K_{x_i} X \\
&+ \left(1 - f_{asym}(x_i)\right)\alpha_{x_i}\ D\underline{f}_{bl|x_i|} gg^T K_{x_i} X\}\ + g_s u_s
\end{aligned}
$$

$$\bar{G}\bar{U} = [g \;\; g_s][u \;\; u_s]^T$$

$$= Ke_r + e_f - g\widehat{W}^T\phi\big(X(t)\big) - \sum_{j=1}^{l}\{f_{asym}\left(e_{r_j}\right)\,\alpha_{e_{r_j}}\,D\bar{f}_{bl}\big|_{e_{r_j}}\,gg^TK_{e_{r_j}}e_r$$

$$+\left(1 - f_{asym}\left(e_{r_j}\right)\right)\alpha_{e_{r_j}}\,D\underline{f}_{bl}\big|_{e_{r_j}}gg^TK_{e_{r_j}}e_r\}$$

$$-\sum_{i=1}^{q}\{f_{asym}(x_i)\,\alpha_{x_i}\,D\bar{f}_{bl_{|x_i|}}gg^TK_{x_i}X$$

$$+\left(1 - f_{asym}(x_i)\right)\alpha_{x_i}\,D\underline{f}_{bl_{|x_i|}}gg^TK_{x_i}X\}\; + g_su_s$$

$$\bar{U} = \begin{bmatrix} u \\ u_s \end{bmatrix} = \bar{G}^{-1}[Ke_r + e_f - g\widehat{W}^T\phi\big(X(t)\big)$$

$$-\sum_{j=1}^{l}\{f_{asym}\left(e_{r_j}\right)\,\alpha_{e_{r_j}}\,D\bar{f}_{bl}\big|_{e_{r_j}}\,gg^TK_{e_{r_j}}e_r$$

$$+\left(1 - f_{asym}\left(e_{r_j}\right)\right)\alpha_{e_{r_j}}\,D\underline{f}_{bl}\big|_{e_{r_j}}gg^TK_{e_{r_j}}e_r\} \qquad (21)$$

$$-\sum_{i=1}^{q}\{f_{asym}(x_i)\,\alpha_{x_i}\,D\bar{f}_{bl_{|x_i|}}gg^TK_{x_i}X$$

$$+\left(1 - f_{asym}(x_i)\right)\alpha_{x_i}\,D\underline{f}_{bl_{|x_i|}}gg^TK_{x_i}X\}\; + g_su_s\;].$$

where $\bar{G} \triangleq [g \;\; g_s]$. Note that the control u can be easily extracted from (21) or $\bar{U}$ can be used directly by adding and subtracting g_su_s into (10). This control will bring $X(t) \to X_d$ while satisfying the constraints/ bounds on the state and error signals, provided we have a close approximation of the uncertainty, which is obtained through the MSO. The MSO brings $\hat{X}(t) \to X(t)$, where a NN is used to approximate the uncertainty.

Tracking error dynamics are given by

$$\dot{e}_r(t) \triangleq \dot{X}(t) - \dot{X}_d(t)$$

$$= f\big(X(t)\big) + g\left(u(t) + W^T\phi\big(X(t)\big) + \epsilon\big(X(t)\big)\right) - f^*\big(X_d(t)\big). \tag{22}$$

After some algebra, it can be shown as

$$\begin{aligned}\dot{e}_r(t) = {} & e_f + Ke_r(t) + g\big(\widetilde{W}^T\phi\big(X(t)\big) + \epsilon\big) \\ & - \sum_{j=1}^{l}\{f_{asym}\left(e_{r_j}\right)\alpha_{e_{r_j}} D\bar{f}_{bl}\big|_{e_{r_j}}\big| gg^T K_{e_{r_j}} e_r \\ & + \left(1 - f_{asym}\left(e_{r_j}\right)\right)\alpha_{e_{r_j}} D\underline{f}_{bl}\big|_{e_{r_j}}\big| gg^T K_{e_{r_j}} e_r\} \\ & - \sum_{i=1}^{q}\{f_{asym}(x_i)\,\alpha_{x_i} D\bar{f}_{bl|x_i|} gg^T K_{x_i} X \\ & + \left(1 - f_{asym}(x_i)\right)\alpha_{x_i} D\underline{f}_{bl}{}_{|x_i|} gg^T K_{x_i} X\}\end{aligned} \tag{23}$$

where $\widetilde{W} \triangleq W - \widehat{W}$. The estimation error is defined as

$$e_a(t) \triangleq X(t) - \hat{X}(t) \tag{24}$$

and its dynamics are written as

$$\begin{aligned}\dot{e}_a(t) &\triangleq \dot{X}(t) - \dot{\hat{X}}(t) \\ &= K_2 e_a(t) + g\widetilde{W}^T\phi\big(X(t)\big) + g\epsilon.\end{aligned} \tag{25}$$

The weight update rule for $\widehat{W}$ is used as

$$\dot{\widehat{W}} = \gamma_w\, Proj_m(\widehat{W}, \phi\big(X(t)\big)\, e_a{}^T P_a g) \tag{26}$$

where $\gamma_w \in \mathbb{D}_+^{v\times v}$ is the adaptation rate used in the weight update rule, $v \in \mathbb{N}_+$, and $Proj_m\,(.,.)$ denotes the smooth projection operator [32] . Note that the projection operator

guarantees that $\widehat{W} \in \Omega$, and that there exists a $W^* \in \Omega$ s.t. $\left\|\widehat{W}\right\| \leq W^*$. Matrix P_a is obtained from the linear Lyapunov equation

$$0 = {K_2}^T P_a + P_a K_2 + Q_a \tag{27}$$

where $Q_a > 0 \; and \; K_2 < 0$.

5. STABILTY ANALYSIS

Theorem 1: Consider the system in (7) with the observer in (11) and the desired system described by (8). Let assumptions 1 and 2 hold. Consider the NN approximation with the control generated by (20/21) and the weight update law in (26). If initial tracking error signals and state signals are in their corresponding performance sets such that $e_{r_j}(0) \in \mathsf{C}_{\epsilon_{e_{r_j}}}$ *for any* j^{th} *tracking error signal and* $x_i(0) \in \mathsf{C}_{\epsilon_{x_i}}$ *for any* i^{th} *state signal where* $\epsilon_{e_{r_j}} \triangleq \{ e_{r_j} \colon \; e_{r_j} \in (\underline{\epsilon}_{e_{r_j}}, \overline{\epsilon}_{e_{r_j}}) \}$ *and* $\epsilon_{x_i} \triangleq \left\{ x_i \colon \; x_i \in \left(\underline{\epsilon}_{x_i}, \overline{\epsilon}_{x_i}\right)\right\}$*, then the following holds:*

a. The time derivative of the barrier Lyapunov function candidate defined in (C.1) is negative definite.

b. Any i^{th} *state signal*(x_i) *will always stay in its given constraints set* $\mathsf{C}_{\epsilon_{x_i}} \left(x_i(t) \in \mathsf{C}_{\epsilon_{x_i}}\right)$.

c. Any j^{th} *tracking error signal* $\left(e_{r_j}\right)$ *will always stay in its given constraint set* $\mathsf{C}_{\epsilon_{e_{r_j}}}, \left(e_{r_j}(t) \in \mathsf{C}_{\epsilon_{e_{r_j}}}\right)$.

d. All the close loop signals are bounded.

e. Control $u(t)$ *is bounded by* u_{max} *where*

$$u_{max} \triangleq \|g^{-1}\| \Big(\|\overline{f^*}(X_d)\| + \|\overline{f}(X(t))\| + \|K\|\epsilon_{e_r} +$$

$$\|g\|\widehat{W}^*\phi^* + \sum_{j=1}^{l}\{\left|\alpha_{e_{r_j}}\right| \overline{\beta}_{|e_{r_j}|}\|g\|^2\,\overline{\epsilon}_{e_r} + \left|\alpha_{e_{r_j}}\right| \underline{\beta}_{|e_{r_j}|}\|g\|^2\underline{\epsilon}_{e_r}\Big\} + \tag{28}$$

$$\sum_{i=1}^{q}\{\left|\alpha_{x_i}\right|\bar{\beta}_{|x_i|}\|g\|^2\,\overline{\epsilon}_{x_i} + \left|\alpha_{x_i}\right| \underline{\beta}_{|x_i|}\|g\|^2\,\underline{\epsilon}_{x_i}\}\Big).$$

Proof: Stability is proved by Lyapunov analysis and is given in Appendix C.

5.1. SPPGNAC FOR CONSTRAINTS ON VECTORS

To apply bounds on the norm of the state vector X and/or on the norm of the error vector e_r, the controller formulation changes to (29):

$$\begin{aligned} u(t) &= u_n(t) + u_a(t) + u_{blf}(t) \\ &= g^{-1}[\, f^*(X_d) - f\big(X(t)\big) + Ke_r - \\ & g\widehat{W}^T\phi\big(X(t)\big) - \alpha_e\, Df_{bl_{\|e_r\|_{P_r}}} g g^T P^T e_r - -\alpha_X\, Df_{bl_{\|X\|_{P_X}}} g g^T P^T X\,] \end{aligned} \tag{29}$$

or to (30), in the case where g is not invertible,

$$\begin{aligned} \overline{U} = \begin{bmatrix} u \\ u_s \end{bmatrix} = \bar{G}^{-1}[\, & f^*(X_d) - f\big(X(t)\big) + Ke_r - g\widehat{W}^T\phi\big(X(t)\big) \\ & - \alpha_e Df_{bl_{\|e_r\|_{P_r}}} g g^T P^T e_r - \alpha_X\, Df_{bl_{\|X\|_{P_X}}} g g^T P^T X \\ & + g_s u_s]] \end{aligned} \tag{30}$$

where P is obtained from $0 = K^T P + PK + Q$, for $Q > 0 \;\; and \; K < 0$.

In some studies such as [30]-[31], BLF-based symmetric PCs are applied on the norm of the error vector, but the method is coupled with the NN-based adaptation. However, the proposed method is advantageous since it not only satisfies constraints by applying BLF-based control directly, but its MSO-based adaptation mechanism runs

independently. In this way, it offers adaptability and can estimate uncertainties without being impacted by BLF, which is not the case in [30]-[31].

Tracking error dynamics for this case are found by using system dynamics from (10) and (8) with controller (29/30) as

$$\begin{aligned}\dot{e}_r(t) = {} & Ke_r(t) + g\left(\widetilde{W}^T\phi\left(X(t)\right) + \epsilon\right) - \alpha_e D f_{bl_{\|e_r\|_{P_r}}} g g^T P^T e_r \\ & - \alpha_X D f_{bl_{\|X\|_{P_X}}} g g^T P^T X.\end{aligned} \tag{31}$$

Dynamics of the estimation error and NN weights update rule remain the same as given in (24) and (26), respectively.

Corollary 1: Consider the system in (7) with the observer in (11) and the desired system described by (8). Let assumptions 1 and 2 hold. Consider the NN approximation with the control generated by (29/30) and the weight update law in (26). If $\|e_r(0)\|_P \in \mathsf{C}_{\epsilon_{e_r}}$ *(initial error norm is under the bound* $\|e_r(0)\|_P < \epsilon_{e_r}$*) and/or if* $\|X(0)\|_P \in \mathsf{C}_{\epsilon_X}$ *(initial state norm is under the constraint* $\|X(0)\|_{P_r} < \epsilon_X$*) where* $\mathsf{C}_{\epsilon_{e_r}} \triangleq \{ e_r\colon \|e_r\|_P \in [0, \epsilon_{e_r}) \}$ *and* $\mathsf{C}_{\epsilon_X} \triangleq \{ X\colon \|X\|_P \in [0, \epsilon_X)\}$*, then the following holds:*

a. *The time derivative of the barrier Lyapunov candidate function defined later in (C.1) is negative definite.*

b. *The tracking error vector* (e_r) *and state vector* (X) *will always be bounded, and stay in their corresponding constrained sets* $e_r \in \mathsf{C}_{\epsilon_{e_r}}$ *and* $X \in \mathsf{C}_{\epsilon_X}$ *.*

c. *All the close loop signals are bounded.*

Proof: Corollary 1 can be easily proved by choosing a BLF candidate as

$$L_2(e_r, e_a, \widetilde{W}, X) = f_{bl}(\|e_r\|_P) + f_{bl}(\|X\|_P) + tr\left(\widetilde{W}^T \gamma_w{}^{-1} \widetilde{W}\right) + e_a{}^T P_a e_a. \quad (32)$$

Its time derivative is

$$\dot{L_2}(e_r, e_a, \widetilde{W}, X) = 2Df_{bl_{\|e_r\|_P}} e_r^T P \dot{e}_r + 2Df_{bl_{\|X\|_P}} X^T P \dot{X} + 2\, tr\left(\widetilde{W}^T \gamma_w{}^{-1} \dot{\widetilde{W}}\right) + 2e_a{}^T P \dot{e}_a. \quad (33)$$

Following the same approach that is taken for the proof of the theorem 1, it is found that

$$\dot{L_2}(.) \leq -\xi a_6 \|e_r\|_P{}^2 - \xi a_7 \|X\|_P{}^2 - \xi \lambda_{min}(Q_a)\|e_a\|^2. \quad (34)$$

This is true as long as $\|e_r\|_P \geq \frac{b_6}{a_6}$, $\|X\|_P \geq \frac{b_7}{a_7}$, and $\|e_a\| \geq \frac{b_8}{a_8}$ where $a_6 \triangleq (1-\xi)Df_{bl_{\|e_r\|_P}} \lambda_{min}(Q) - \left(2\alpha_{e_r} Df_{bl_{\|e_r\|_P}} \|gg^T\| \|P\|\right)^2$, $b_6 \triangleq 2Df_{bl_{\|e_r\|_P}} \|P_r g\| \{\widetilde{W}^* \phi^* + \epsilon^*) \|P_r K\| \|e_f\|\}$, $a_7 \triangleq (1-\xi)Df_{bl_{\|X\|_P}} \lambda_{min}(Q) - \left(2\alpha_X Df_{bl_{\|e_r\|_P}} \|gg^T\| \|P\|\right)^2$, $b_7 \triangleq 2Df_{bl_{\|X\|_P}} \{\|f^*(X_d)\| + \|KX_d\| (\widetilde{W}^* \phi^* + \epsilon^*) \|g\|\}$, $a_8 \triangleq (1-\xi)\lambda_{min}(Q_a)$, and $b_8 \triangleq 2\epsilon^* \|P_a g\|$. These coefficients are clearly positive. Rest can be proven by following the same arguments made during the proof of theorem 1, given in Appendix C.

6. NUMERICAL SIMULATION AND ANALYSIS

In this section, SPPGNAC is used for different problems, and its performance is analyzed. Two benchmark examples from [31] and [4] are considered for this purpose.

First, some general guidelines are given on how to choose different controller gains and related parameters.

6.1. PARAMETERS SELECTION

In this subsection, some general directions are given on how to choose different parameters and gains for the controller. Note that this selection is arbitrary as long as the selected parameters/gains follow previously discussed conditions/assumptions.

Selection of the slack variables g_s and u_s should be such that $\overline{G}$ becomes invertible. For any matrix $g = \begin{bmatrix} 0_{n2\times m} \\ R_{n/2\times m} \end{bmatrix}$ where $R_{n/2\times m}$ is any arbitrary matrix/vector, one way to choose the slack variables is to select $g_s = [-R_{n/2\times m}, R_{n/2\times m}]^T$ and $u_s = [1_{m\times 1}]$. In this way, it will result in $\overline{G} = \begin{bmatrix} 0_{n/2\times m} & -R_{n/2\times m} \\ R_{n/2\times m} & R_{n/2\times m} \end{bmatrix}$. For example, if $g = [0,1]^T$, choosing $g_s = [-1,1]^T$ and $u_s = \begin{bmatrix} 1 \\ 1 \end{bmatrix}$ will make $\overline{G} = \begin{bmatrix} 0 & -1 \\ 1 & 1 \end{bmatrix}$ invertible where its inverse is $\overline{G}^{-1} = \begin{bmatrix} 1 & 1 \\ -1 & 1 \end{bmatrix}$. When this is multiplied as $\bar{U} = \begin{bmatrix} u \\ u_s \end{bmatrix} = \overline{G}^{-1} \begin{bmatrix} k_1 e_1 + \cdots \\ k_2 e_2 + \cdots \end{bmatrix} = \begin{bmatrix} 1 & 1 \\ -1 & 1 \end{bmatrix} \begin{bmatrix} k_1 e_1 + \cdots \\ k_2 e_2 + \cdots \end{bmatrix} = \begin{bmatrix} (k_1 e_1 + \cdots) + (k_2 e_2 + \cdots) \\ (\dots) \end{bmatrix}$, from here u can be extracted as $u = (k_1 e_1 + \cdots) + (k_2 e_2 + \cdots)$ or $\bar{U}$ can be directly applied by adding and subtracting $g_s u_s$ in system dynamics. Note that in the latter case, the positive and negative of $g_s u_s$ will cancel its effect in the final expression after inversion. Another method of slack variables selection is to use the lower nonzero part of g as upper g_s and choose u_s with all elements as one. For example, if $g = [0,1]^T$, choosing $g_s = [1,0]^T$ and $u_s = \begin{bmatrix} 1 \\ 1 \end{bmatrix}$ will make $\overline{G} = \begin{bmatrix} 0 & 1 \\ 1 & 0 \end{bmatrix}$. In this case, selection of K should be $K = \begin{bmatrix} 0 & 0 \\ k_1 & k_2 \end{bmatrix}$. Now the inverse of $\overline{G}$ will be as $\overline{G}^{-1} = \begin{bmatrix} 0 & 1 \\ 1 & 0 \end{bmatrix}$. When this

is multiplied as $\bar{U} = \begin{bmatrix} u \\ u_s \end{bmatrix} = \bar{G}^{-1} \begin{bmatrix} (.) \\ (k_1 e_1 + \cdots) + (k_2 e_2 + \cdots) \end{bmatrix} = \begin{bmatrix} 0 & 1 \\ 1 & 0 \end{bmatrix} \begin{bmatrix} (.) \\ (k_1 e_1 + \cdots) + (k_2 e_2 + \cdots) \end{bmatrix} = \begin{bmatrix} (k_1 e_1 + \cdots) + (k_2 e_2 + \cdots) \\ (.) \end{bmatrix}$, from here u can be extracted as $u = (k_1 e_1 + \cdots) + (k_2 e_2 + \cdots)$ or $\bar{U}$ can be directly applied by adding and subtracting $g_s u_s$. After inversion, the positive and negative of $g_s u_s$ will cancel its effect in the final expression.

Selection of the K requires the same process as any general feedback controller. It is recommended to choose it as a diagonal matrix in the case where g is invertible like $K = \begin{bmatrix} k_1 & 0 & \dots \\ 0 & k_2 & \cdots \\ \vdots & \vdots & \vdots \end{bmatrix}$ or to include all entities of error like $K = \begin{bmatrix} k_1 & k_2 & \dots \\ 0 & 0 & \cdots \\ \vdots & \vdots & \vdots \end{bmatrix}$ or $K = \begin{bmatrix} \vdots & \vdots & \dots \\ 0 & 0 & \cdots \\ k_1 & k_2 & \cdots \end{bmatrix}$, depending upon the given g and the selection of slack variables.

Similarly, K_2 should be Hurwitz, and it is recommended to choose it as a diagonal matrix.

The matrix $K_{(.)_i}$ is used to include only the i^{th} signal from a vector. Therefore, $K_{(.)_i}$ should be a square matrix with only i^{th} diagonal element as 1 and all the rest of the entities as zeros. For example, for the state signals, $K_{x_1} = \begin{bmatrix} 1 & 0 & \dots \\ 0 & 0 & \cdots \\ \vdots & \vdots & \vdots \end{bmatrix}$ for the first state signal (x_1), $K_{x_2} = \begin{bmatrix} 0 & 0 & 0 & 0 & \dots \\ 0 & 1 & 0 & 0 & \cdots \\ 0 & 0 & 0 & 0 & \vdots \\ \vdots & & \vdots & & \end{bmatrix}$ for x_2, and so on.

Selection of the scalars $\alpha_{(.)}$ should be such that $0 < \alpha_{(.)} < 1$ if the BLF-based control is needed to avoid excessive input and $\alpha_{(.)} > 1$ for the other way around. These selections are elaborated upon in the next subsection where simulation and results are discussed.

6.2. EXAMPLE 1: SCALAR EXAMPLE

First a scalar example is considered. The dynamics of the scalar system are given as

$$\dot{x} = x + u + d(x) \tag{34}$$

where the uncertainty is $d(x) = x^3$. The reference system and the MSO developed for this system are given in (35) and (36), respectively:

$$\dot{x}_d = -x_d + r(t) \tag{35}$$

$$\dot{\hat{x}} = x + u + \hat{d}(x) + K_2\, e_a \tag{36}$$

where $r(t)$ is the reference input and x_d is the desired state and output of the refence system. Other gains/parameters used are $K = -2$, $K_2 = -3$, $K_{x_1} = 1$, $K_{e_1} = 1$, $L_\phi = 1$, and $L_f = 1$. There is no need for slack variables for this problem as g is 1 (invertible). At first a general case (case 1) is considered where symmetric constraints are imposed on the state and on the tracking error:

$$-1.5 < x < 1.5, \qquad -0.08 < e_r < 0.08. \tag{37}$$

State and error are initialized as $x(0) = 0.01$, $e_r(0) = 0.01$, $x_d(0) = 0$ and $e_a(0) = 0.01$. Note that these values need to be under the bound. For case 1, both the α_x and α_e are taken as 1.

Figures 2a and 2b show the time histories of the state and the tracking error, respectively. Excellent performance is achieved in term of tracking and estimation. Neither the state or tracking error violates the bounds at any time. The control history is shown in Figure 3a, where an overall control (red line plot) is shown along with its different components including nominal control, adaptive control, and BLF-based controls. It can be seen that the BLF-based controls (Cayan and black plots) rise high whenever state or

error signals get closer to their respective bounds, such as during the periods when the reference square wave is at its peaks. For this reason, once constrained variables (in this case, state and error signals) are initialized under their bounds, then the control will never let them transgress their bounds/constraints. Figure 3b represents uncertainty in dynamics and its approximation. As can be seen, uncertainty is closely approximated. This is another advantage of SPPGNAC, as compared to [30]-[31] where the NN weight update and uncertainty approximation is coupled with BLF-based control and cannot be separately estimated. However, proposed SPPGNAC still provides a way to estimate uncertainties and to identify unknown/uncertain dynamics. On the other hand, an evolution of the NN weight is given in Figure 4a. The approximated NN weight converged to the actual value, which is 1. This is because the basis function used was x^3. Different basis function were tested, and all resulted in close approximation of uncertainty. Some small jumps are observed in estimated NN weight when the state signal switches from one peak to the other. This is expected as the NN weight update depends upon the estimation error and it changes when the state signal switches.

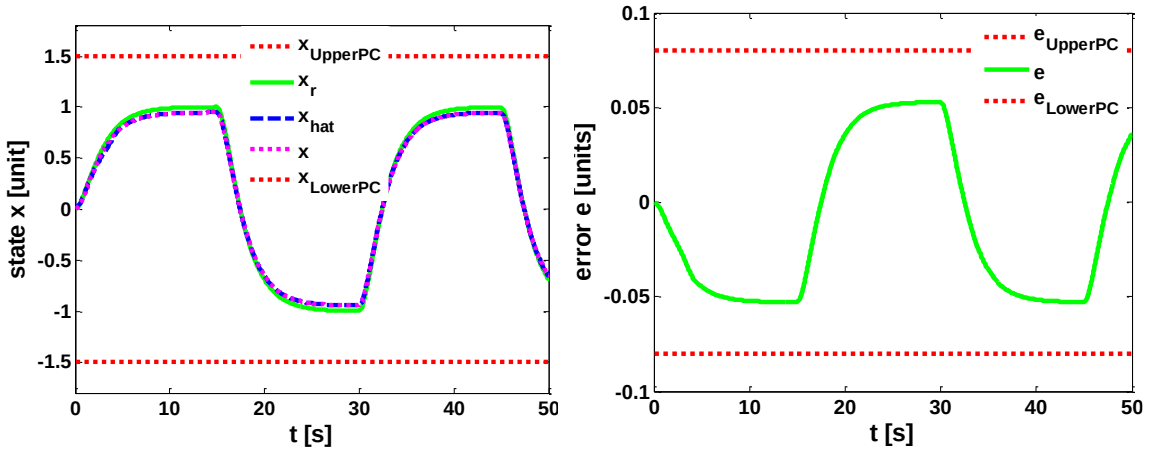

(a) (b)

Figure 2. Case 1 (Symmetric case): (a) State histories (b) Tracking error.

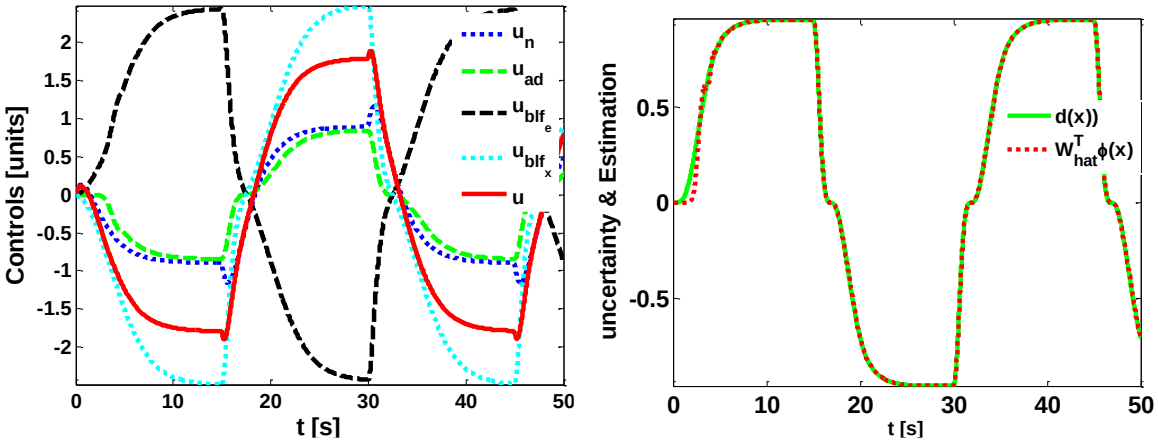

(a) (b)

Figure 3. Case 1 (Symmetric case): (a) Control histories (b) Uncertainty and its approximation.

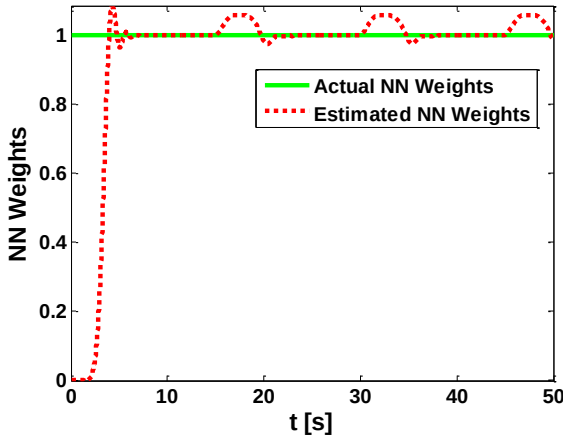

Figure 4. Case 1 (Symmetric case): Actual and estimated NN weights.

A general observation in BLF-based control is that it exerts a premature excessive control input, even when the constrained variable is not very close to its bound. This is where the proposed method offers another advantage: by tuning the $\alpha_{(.)}$, this undesired behavior can be avoided. By choosing $\alpha_{(.)} > 1$, the controller will react faster and excessively. On the other hand, selecting $0 < \alpha_{(.)} < 1$ will make the BLF-based control smaller in magnitude until the constrained variable gets very close to its bound, yet it will insure constraints. For further elaboration, two instances are shown in Figures 5a and 5b,

where the case 1 example is simulated again with the same controller gains and the symmetric constraint is set to 0.1. As shown in Figure 5a, when α_e is set to 0.01, still the error value increases up to 0.09, which is comparatively close to the set bound of 0.1. Note that it is still ensuring that the constraints will not be violated. Although, it caused some small oscillations at some of the peak regions, for example during the period between 25-30 seconds. However, this can be avoided by choosing slightly higher α_e, as is shown in Figures 6b. On the other hand, Figure 5b shows that when α_e is set to 2, the control becomes excessive decreasing the maximum error to even less than half of the set bound. This proves that the additional flexibility offered by SPPGNAC can be very useful for control applications.

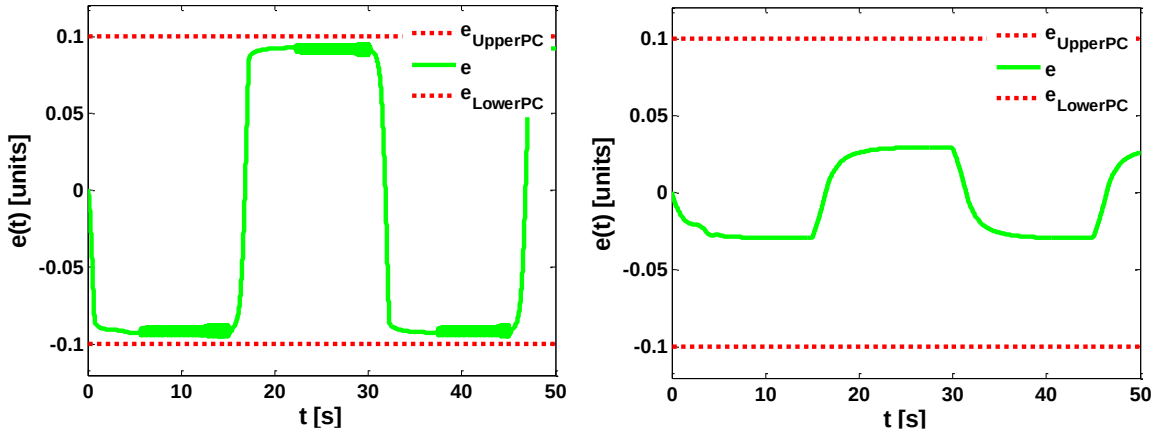

(a) (b)

Figure 5. Case 2: (a) Error response when $\alpha_e = 0.01$, (b) Error response when $\alpha_e = 2$.

In the third case, the simulation of example 1 is carried out again with asymmetric constraints/bounds on the state and error. The asymmetric constraints that are imposed are:

$$-0.6 < x < 1.6\ , \qquad -0.07 < e_r < 0.1. \tag{38}$$

The controller gains and basis functions for NN approximation are kept the same. Scalars α_e and α_x are set to 0.1 and 0.01, respectively. Figures 6a and 6b show the time histories of the state and tracking error. Though this time lower PC on state is -0.6 and the

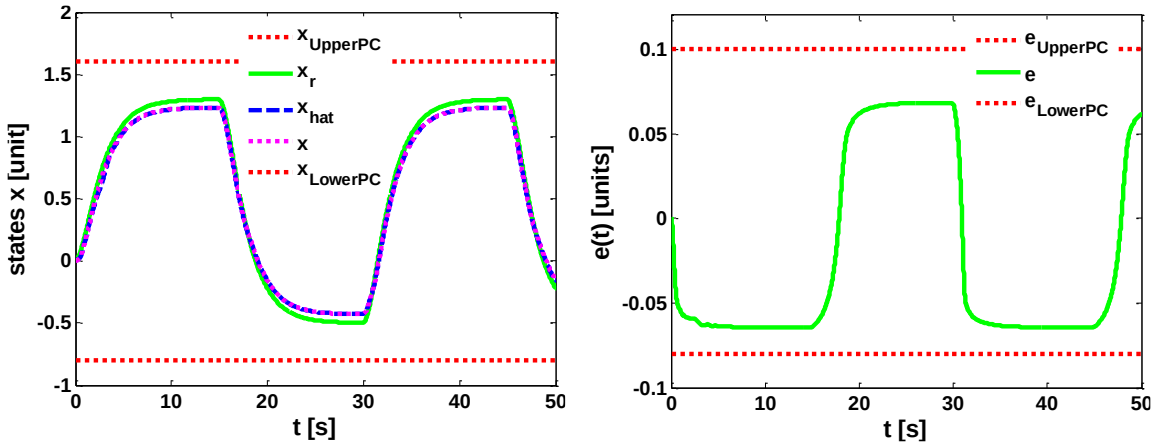

(a) (b)

Figure 6. Case 3 (Asymmetric case): (a) State histories (b) Tracking error.

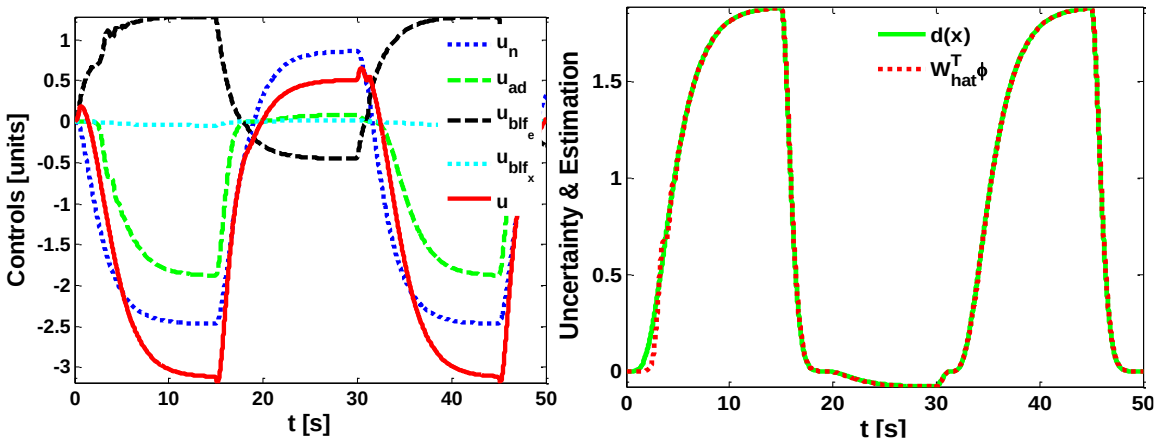

(a) (b)

Figure 7. Case 3 (Asymmetric case): (a) Controls histories (b) Uncertainty and its approximation.

upper PC is 1.6, it was the effectiveness of SPPGNAC that the state and error signals could not transgress the PCs at any time. Similarly, asymmetric PCs on error were

also ensured, as can be seen in Figure 6b. Overall, an excellent tracking and estimation performance is achieved. The controls history is shown in Figure 7a, where all different control components, including nominal, adaptive, BLF-based controls, and overall control as the sum (red line) are shown. The control remained stable as state and error were initialized under their PCs. Figure 7b indicates that the uncertainty is accurately approximated. The NN weight converged to 1 in this case as well, but the plot is omitted to avoid repetition.

6.3. EXAMPLE 2: UNCERTAIN NONLINEAR ROBOTIC MANIPULATOR DYNAMICS

Another example of nonlinear dynamics of an uncertain two-link robotic manipulator is considered for numerical implementation. Dynamics of an n link robotic manipulator can be given as

$$M(q)\,\ddot{q} + V_m(q,\dot{q})\,\dot{q} + G(q) + F(\dot{q}) + \tau_d(t) = \tau(t) \tag{39}$$

where $q \in \mathbb{R}^n$, $M(q)$ is the inertia matrix, $V_m(q,\dot{q})$ is the Coriolis/centripetal matrix, $G(q)$ is the gravity vector, $F(\dot{q})$ is the friction matrix, $\tau_d(t)$ is an unknown disturbance, and $\tau(t)$ is the control torque. For a robotic manipulator, certain properties are assumed such as the mass matrix $M(q)$ is always a positive definite matrix and satisfies $B_{m1}I \leq M(q) \leq B_{m2}I$ where B_{m1} and B_{m2} are known positive constants. Coriolis/centripetal matrix $V_m(q,\dot{q})$ is bounded by $V_b\|\dot{q}\|$ such that V_b is constant. Gravity and friction matrices are bounded in the way that $G_B > 0$ and $B_F\|\dot{q}\| + B_f$ such that B_F and B_f are positive constants. The matrix $\dot{M} - 2V_m$ is skew symmetric. Disturbance τ_d is bounded such that

$\|\tau_d\| \leq \tau_{dM}$ with τ_{dM} is positive constant. The nonlinear state space representation of (67) can be given as

$$\begin{bmatrix} \dot{q} \\ \ddot{q} \end{bmatrix} = \begin{bmatrix} \dot{q} \\ -M^{-1}(q)(V_m(q,\dot{q})\,\dot{q} + G(q)) \end{bmatrix} + d(q,\,\dot{q}) + \begin{bmatrix} 0 \\ M^{-1}(q) \end{bmatrix} \tau(t). \tag{40}$$

The desired trajectory of the robotic manipulator $q_d(t) \in \mathbb{R}^n$ satisfies $\|Q_d\| \leq q_B$, where $Q_d(t) = [q_d(t)\ \dot{q}_d(t)\ \ddot{q}_d(t)]^T$ and $d(q,\,\dot{q}) = \begin{bmatrix} 0 \\ -M^{-1}(q)(\tau_d(t) + F(\,\dot{q})) \end{bmatrix}$ is the unknown uncertainty/disturbance in the dynamics. The following parameters are used in the simulation: $m_1 = 1kg, m_2 = 2.3kg, l_1 = 1m, l_2 = 1m, g = 9.8, L = 1, L_\phi = 1, L_f = 1$, $Q = I, B_F = 0.3, B_f = 0.2, \tau_d = 0.01\,q,\ \gamma_w = 20I,$ gains are $K = -diag(3,3,2,2)$, $K_2 = -diag(10,10,5,5)$, the slack variables used are $B_s = [I_{2\times2}, 0_{2\times2}]^T$ and $u_s = [1,1]^T, K_{x_1} = diag(1,0,0,0),\ K_{x_2} = diag(0,1,0,0),\ K_{e_1} = diag(1,0,0,0), K_{e_2} = diag(0,1,0,0)$, $\alpha_{e_1} = 0.04,\ \alpha_{e_2} = 0.04, \alpha_{x_1} = 0.1,$ and $\alpha_{x_2} = 0.1$. the desired responses are $\sin(\omega t)$ for the first joint and $cos\,(\omega t)$ for the second joint of the robotic manipulator. First, different bounds are imposed on each state signal and on each tracking error signal instead of putting one universal bound on the norm of them:

$$\begin{aligned} -1 < q_1 < 1.5 \qquad & -0.02 < e_{r_1} < 0.05 \\ -1.2 < q_2 < 0.8 \qquad & -0.03 < e_{r_2} < 0.01 \end{aligned} \tag{41}$$

States and errors are initialized under the given bounds as $q_1(0) = 0.025,\ q_2(0) = 0.52, e_{r_1}(0) = 0.025$, and $e_{r_2}(0) = 0.002$. Figure 8a presents the time history of the first state where $q1, q1_d$, and $q1_a$ represent the actual, desired, and approximated angle for the first link of the robotic manipulator. Similarly, Figure 8 b presents the time history of

second state where $q2, q2_d$, and $q2_a$ represent the actual, desired, and approximated angle for the second link. As can be observed, each separate state respected its corresponding constrains at all times during both transient and steady states. No oscillations were observed and the actual and estimated states converged to the desired state. Error plots and their bounds are given in Figures 9a and 9b. Errors were also kept under their respective bunds. This again proves that with the SPPGNAC, each variable can have a different constraint/bound and it can be activated or disabled as per need, which is not possible if bound is applied on the norm of the variables vector. Figure 10a shows that uncertain dynamics were closely estimated and addressed using the NN-based MSO. Figure 10b presents the history of overall control showing stable trends. Some small jumps are observed at around 3 sec and at around 6 second. This happened because of switching between upper and lower constraints. It can be observed that controls rise a little high whenever some variable (control or state) starts rising or getting close to its respective

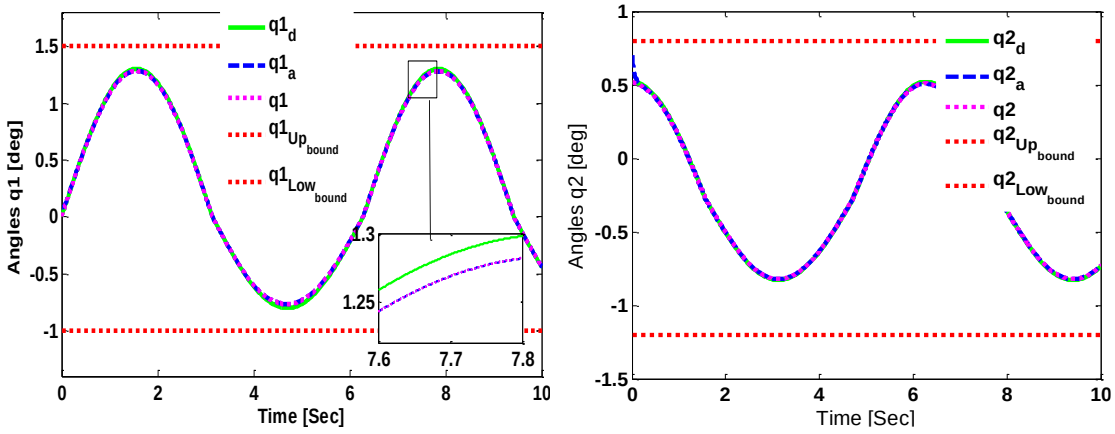

(a) (b)

Figure 8. Case 4 (Asymmetric case): (a) Time histories of state q_1 and its bound (b) Time histories of state q_2 and its bound.

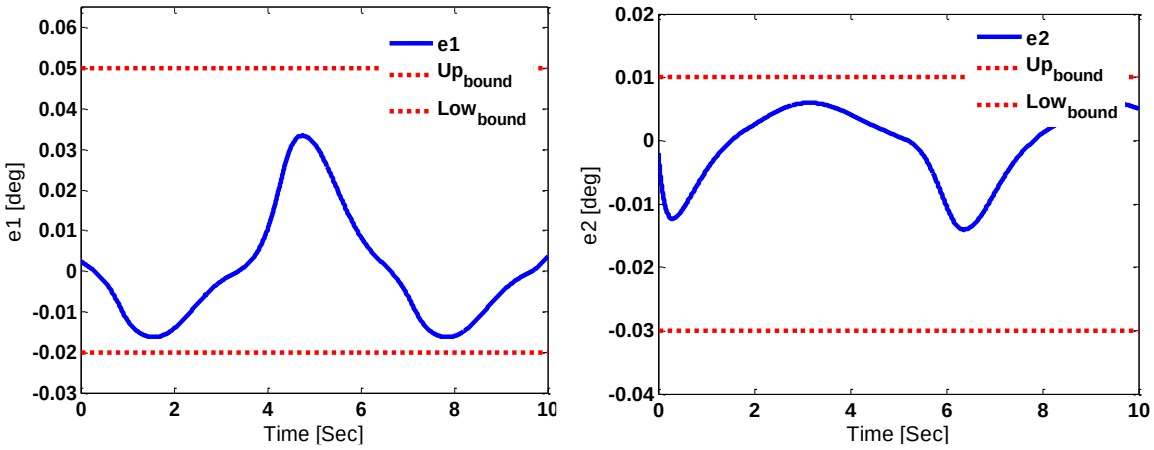

(a) (b)

Figure 9. Case 4 (Asymmetric case): (a) Tacking error e_1 and its bound (b) Tacking error e_2 and its bound.

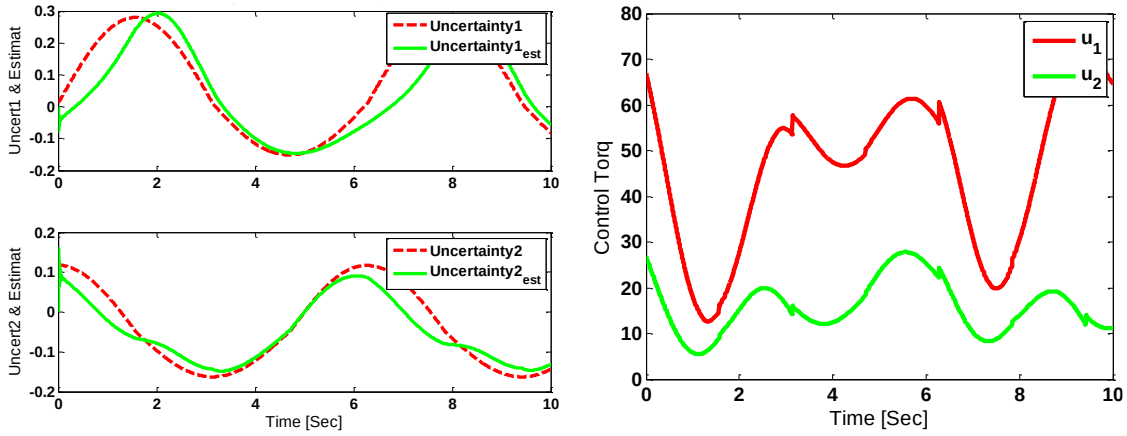

(a) (b)

Figure 10. Case 4 (Asymmetric case): (a) Uncertainties and their approximation (b) Time histories of control.

bounds. That is the reason that once the variable is constrained (in this case the state and error are initialized under given bounds), the control will never let them transgress their constraint.

A simulation for nonlinear robotic manipulator dynamics from the case 3 is carried out again for a different set of asymmetric constraints which are given in (42). The controller gains and other related parameters are kept the same other than that the scalars

α_{e_1}, $\alpha_{e_2}, \alpha_{x_1}$, and α_{x_2} are changed to 1×10^{-3}, 1×10^{-3}, 1×10^{-2}, and 1×10^{-2}, respectively:

$$\begin{aligned} -2 < q_1 < 3 \qquad & \qquad -0.1 < e_{r_1} < 0.2 \\ -2.5 < q_2 < 1.0 \qquad & \qquad -0.1 < e_{r_2} < 0.05. \end{aligned} \tag{42}$$

Results are given in Figures 11-13 for states histories, tracking errors, uncertainty approximation, and control trends. Again, excellent performance is attained in terms of tracking and estimation, and constraints are satisfied throughout. Uncertainty is approximated reasonably, and control trends are observed to be stable. Different set of constraints and the controller gains K and K_2 were tested, and it was found that the errors and states could never transgress their PCs if initialized under their respective bounds, but those plots are omitted due to limited space. These results proved that SPPGNAC can address the aforementioned problems simultaneously and have immense potential for control applications.

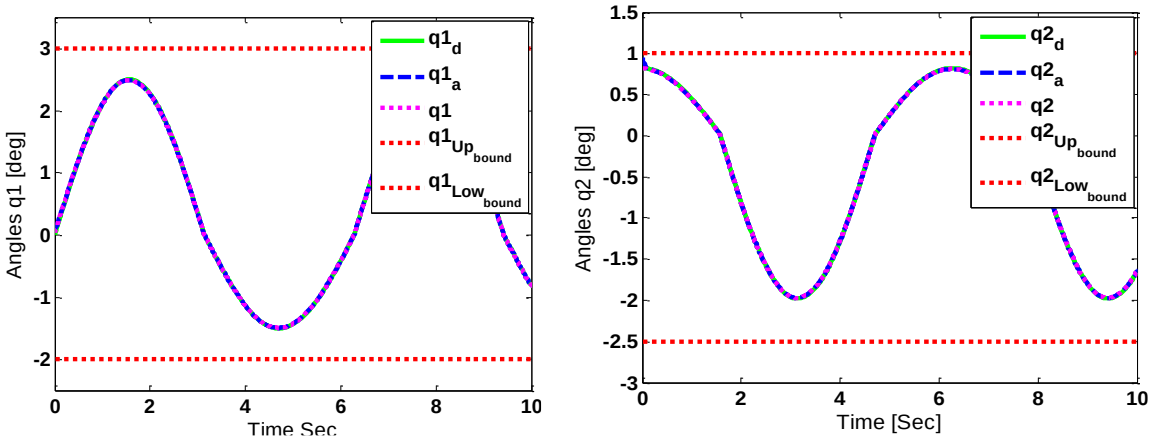

(a) (b)

Figure 11. Case 4 (Asymmetric case): (a) Time histories of state q_1 and its bounds (b) Time histories of state q_2 and its bounds.

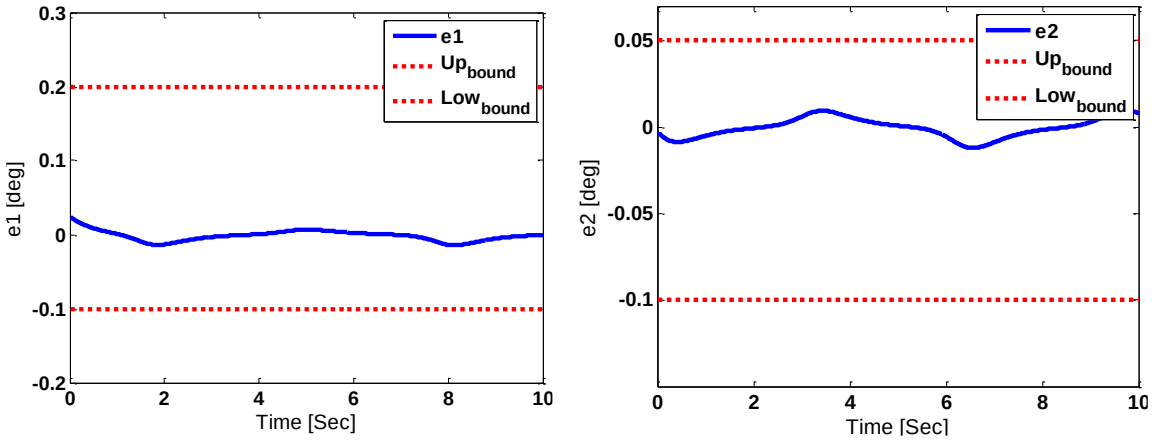

(a) (b)

Figure 12. Case 4 (Asymmetric case): (a) Tacking error e_1 and its bounds, (b) Tacking error e_2 and its bounds.

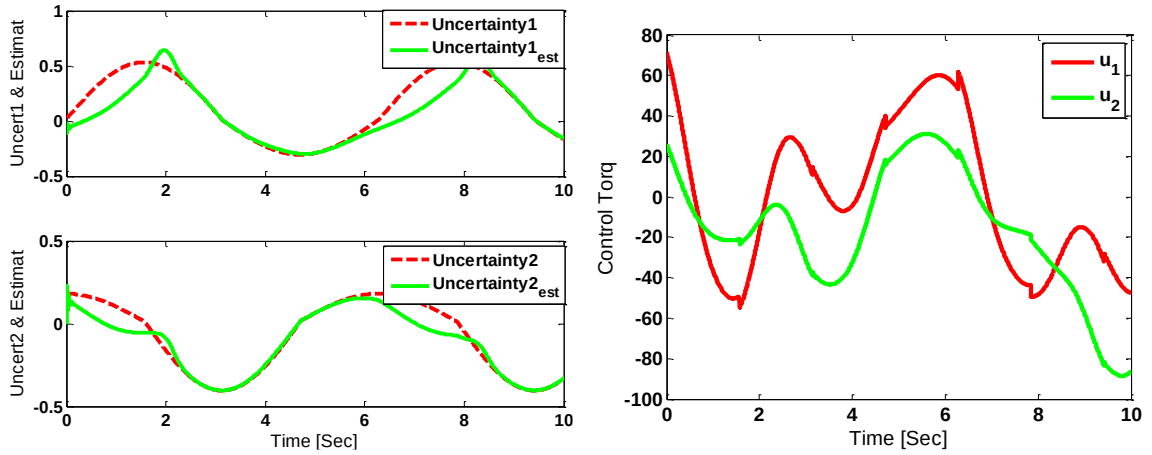

(a) (b)

Figure 13. Case 4 (Asymmetric case): (a) Uncertainties and their approximation (b) Time histories of control.

7. CONCLUSIONS

SPPGNAC, a BLF-based neuro-adaptive controller, is derived and tested for constrained uncertain nonlinear systems. The goal was to keep the tracking error in the given bound while ensuring state constraints. Simulations were carried out for two standard

systems from the control literature, one was an uncertain scalar example, and the other was an uncertain nonlinear 2-link robotic manipulator system. The results showed that the given goal was achieved successfully using the proposed scheme. It did not only satisfy different constraints on each separate state signal and on each separate error signal, but also provided a way to adjust the controller response in proportion to the bounds' closeness. Uncertainty in dynamics was closely approximated, which helps to not only identify unmodeled dynamics, but also to address any other kind of external disturbances from structural or environmental changes. This discussion indicates the potential of the proposed control architecture for the constrained uncertain nonlinear systems.

ACKNOWLEDGMENT

This research was supported in part by the National Aeronautics and Space Administration under Grant NNX15AM51A and NNX15AN04A.

REFERENCES

[1] W. S. Mcculloch and W. Pitts, "A logical calculus nervous activity," *Bull. Math. Biol.*, 1990.

[2] K. S. Narendra and K. Parthasarathy, "Identification and Control of Dynamical Systems Using Neural Networks," *IEEE Trans. Neural Networks*, 1990.

[3] R. M. Sanner and J.-J. E. Slotine, "Direct Adaptive Control Using Gaussian Networks," *IEEE Trans. Neural Networks*, 1992.

[4] F. L. Lewis, S. Jagannathan, and A. Yeşildirek, "Neural Network Control of Robot Arms and Nonlinear Systems," in *Neural Systems for Control*, 1997.

[5] J. A. Farrell and M. M. Polycarpou, *Adaptive Approximation Based Control: Unifying Neural, Fuzzy and Traditional Adaptive Approximation Approaches*. 2006.

[6] S. S. Ge, C. C. Hang, T. H. Lee, and T. Zhang, *Stable Adaptive Neural Network Control*. 2002.

[7] R. Padhi, N. Unnikrishnan, and S. N. Balakrishnan, "Model-following neuro-adaptive control design for non-square, non-affine nonlinear systems," *IET Control Theory Appl.*, 2007.

[8] A. Ghafoor, S. N. Balakrishnan, and T. Yucelen, "Modified State Observer Based Decentralized Neuroadaptive Controller for Large Scale Interconnected Uncertain Systems," in *Proceedings of the American Control Conference*, 2018.

[9] A. Ghafoor, S. N. Balakrishnan, S. Jagannathan, and T. Yucelen, "Event Triggered Neuro-Adaptive Controller (ETNAC) Design for Uncertain Linear Systems," in *Proceedings of the IEEE Conference on Decision and Control*, 2019.

[10] A. Ghafoor, J. Yao, S. N. Balakrishnan, J. Sarangapani, and T. Yucelen, "Event triggered neuroadaptive controller (ETNAC) design for uncertain affine nonlinear systems," in *ASME 2018 Dynamic Systems and Control Conference, DSCC 2018*, 2018.

[11] D. Liu and A. N. Michel, "Asymptotic stability of systems with partial state saturation nonlinearities," in *Proceedings of the IEEE Conference on Decision and Control*, 1994.

[12] D. Liu, "Control Systems With Actuator Saturation: Analysis And Design by T. Hu and Z. Lin; Birkhäuser, Boston, 2001, xvi+ 392pp., ISBN 0-8176-4219-6," *Int. J. Robust Nonlinear Control*, 2004.

[13] R. Findeisen, L. Imsland, F. Allgower, and B. A. Foss, "Output-feedback nonlinear model predictive control using high-gain observers in original coordinates," in *European Control Conference, ECC 2003*, 2003.

[14] D. Q. Mayne, J. B. Rawlings, C. V. Rao, and P. O. M. Scokaert, "Constrained model predictive control: Stability and optimality," *Automatica*, 2000.

[15] A. Bemporad, "Reference governor for constrained nonlinear systems," *Autom. Control. IEEE Trans.*, 1998.

[16] E. Gilbert and I. Kolmanovsky, "Nonlinear tracking control in the presence of state and control constraints: A generalized reference governor," *Automatica*, 2002.

[17] K. B. Ngo, R. Mahony, and Z. P. Jiang, “Integrator backstepping using barrier functions for systems with multiple state constraints,” in *Proceedings of the 44th IEEE Conference on Decision and Control, and the European Control Conference, CDC-ECC ’05*, 2005.

[18] K. P. Tee, S. S. Ge, and E. H. Tay, “Adaptive control of a class of uncertain electrostatic microactuators,” in *Proceedings of the American Control Conference*, 2007.

[19] K. P. Tee, S. S. Ge, and E. H. Tay, “Automatica Barrier Lyapunov Functions for the control of output-constrained,” *Automatica*, 2009.

[20] M. Krstić and P. V. Kokotović, “Control Lyapunov functions for adaptive nonlinear stabilization,” *Syst. Control Lett.*, 1995.

[21] D. S. Naidu, “Book review: Nonlinear Control Design: Geometric, Adaptive and Robust, R. Marino and P. Tomei, Prentice Hall International (UK) Limited, London, 1995, xiii+396 pp., ISBN 0-13-342635-1,” *Int. J. Robust Nonlinear Control*, 1998.

[22] M. Krstic and M. Bernent, “Non-overshooting control of strict-feedback nonlinear systems,” in *Proceedings of the American Control Conference*, 2007.

[23] Z. H. Li and M. Krstić, “Maximizing regions of attraction via backstepping and CLFs with singularities,” *Syst. Control Lett.*, 1997.

[24] C. P. Bechlioulis and G. A. Rovithakis, “Robust adaptive control of feedback linearizable MIMO nonlinear systems with prescribed performance,” *IEEE Trans. Automat. Contr.*, 2008.

[25] C. P. Bechlioulis and G. A. Rovithakis, “Adaptive control with guaranteed transient and steady state tracking error bounds for strict feedback systems,” *Automatica*, 2009.

[26] C. P. Bechlioulis and G. A. Rovithakis, “Prescribed performance adaptive control for multi-input multi-output affine in the control nonlinear systems,” *IEEE Trans. Automat. Contr.*, 2010.

[27] B. Ren, S. S. Ge, K. P. Tee, and T. H. Lee, “Adaptive neural control for output feedback nonlinear systems using a barrier Lyapunov function,” *IEEE Trans. Neural Networks*, 2010.

[28] “AIAA Guidance, Navigation, and Control Conference 2011,” *AIAA Guidance, Navigation, and Control Conference 2011*. 2011.

[29] A. K. Kostarigka and G. A. Rovithakis, “Adaptive dynamic output feedback neural network control of uncertain MIMO nonlinear systems with prescribed performance,” *IEEE Trans. Neural Networks Learn. Syst.*, 2012.

[30] T. Yucelen, G. De La Torre, and E. N. Johnson, “Improving transient performance of adaptive control architectures using frequency-limited system error dynamics,” *Int. J. Control*, 2014.

[31] E. Arabi, B. C. Gruenwald, T. Yucelen, and N. T. Nguyen, “A set-theoretic model reference adaptive control architecture for disturbance rejection and uncertainty suppression with strict performance guarantees,” *Int. J. Control*, 2018.

[32] E. Lavretsky and K. Wise, *Robust and Adaptive Control With Aerospace Applications*. 2013.

[33] D. S. Bernstein, *Matrix Mathematics*. 2014.

.

SECTION

2. OVERALL CONCLUSIONS

In this dissertation different event-triggered and set-theoretic-based neuroadaptive control, schemes were developed and tested.

In the first paper, six MSO-based ETNAC schemes were derived; performance of all versions was evaluated and compared with existing ETC schemes for their transient and steady-state performance and efficiency. From benchmark examples, it is showed that sampling instants can be reduced up to 95% without compromising on performance. Each scheme was able to address uncertainties, estimate unknown model even at significantly reduced in communication and computation, yet providing good tracking. It appears that the proposed schemes have much practical potential to be used in embedded networked systems.

In the second paper, ETNAC was derived and implemented for the CR3PB where a pair of spacecrafts in formation at halo orbit at the sun-Earth/Moon L_1 orbit is considered. Simulation results showed that ETNAC was able to maintain tracking errors in millimetre/submillimeter range while reducing control updates by 65% even with restricted control while estimating and cancelling solar perturbations. These reduced updates lead to longer periods of silence which are very useful for smooth operations in microsatellites. These results prove the potential of the proposed technique for application to the microsatellite platform and deep space missions.

In the third paper, a BLF-based neuro-adaptive controller is derived and tested for constrained uncertain nonlinear systems. Simulations were carried out for two standard systems from the control literature, one was an uncertain scalar example, and the other was an uncertain nonlinear 2-link robotic manipulator system. The results showed that excellent tracking was achieved while satisfying different symmetric/asymmetric constraints for each state and error signal. It also provided a way to regulate the control input, in proportion to the bounds' closeness. Uncertainty in dynamics was closely approximated, which helps to not only identify unmodeled dynamics but also to address any other kind of external disturbances from structural or environmental changes. The results indicate the potential of the proposed control architecture for the constrained uncertain nonlinear systems.

This discussion also concludes that the proposed advance control designs have enormous potential for control applications.

APPENDIX A.

PROOFS OF THE THEOREMS OF THE PAPER I

The proofs for the theorems of the Paper I are done using Lyapunov analysis and are given below. Note that all the references for Appendix A are from the Paper I.

A.1. PROOF OF THEOREM 1

The estimation and tracking errors are taken separately.

A.1.1. Estimation Error. This proof is divided into three cases: case (i) relates to the state sampling instants ($t = t_i^s,\ i = 1,2, ...$) when the Trg_{1a}^s is active and actual sampled state is available. Since during this time, $\bar{x}(t) = x(t_i^s) = x(t)$, so $e_a = \bar{e}_a$, $e_{evt} = 0$, and $e_{int} = 0$. Case (ii) relates to the time when the MSO model 2 is used for the inter-event time simulation. Note that during this time $\bar{x}(t) = C_1 t^n + C_2 t^{n-1} \ldots + C_n t + C_{n+1}$ so $e_{evt} \neq 0$ and $e_{int} \neq 0$, and case (iii) relates to the time period during the inter-event time when the MSO model 1 is used for the observer propagation. During this period $e_{evt} \neq 0$, $e_{int} \neq 0$, and $\dot{\widehat{W}} = 0$.

Case (i): Lyapunov analysis is used to prove the theorem. Choosing a Lyapunov candidate function as

$$L(e_a, \widetilde{W}) = {e_a}^T P e_a + tr(\widetilde{W}^T \gamma^{-1} \widetilde{W}) \tag{A.1}$$

its time derivative is

$$\dot{L}(e_a, \widetilde{W}) = 2{e_a}^T P \dot{e}_a + 2\, tr(\widetilde{W}^T \gamma^{-1} \dot{\widetilde{W}}) \tag{A.2}$$

$$= 2{e_a}^T P\left(K_2 e_a(t) + B u_{evt} + B\widetilde{W}^T \phi(\bar{x}(t_i^s)) + B\check{\epsilon} + (A - K_2) e_{int}\right) + 2tr\left(\widetilde{W}^T \gamma^{-1} \dot{\widetilde{W}}\right).$$

Since at the sampling instant $\widetilde{W} \triangleq W - \widehat{W}$, so $\dot{\widetilde{W}} = -\dot{\widehat{W}}$, $u_{evt} = 0$, $e_{int} = 0$, $e_a = \bar{e}_a$, $\check{\epsilon} = \epsilon$ since $\bar{x}(t) = x(t)$. Also, by using $\dot{\widehat{W}} = \gamma\, Proj_m(\widehat{W},\ \phi\big(\bar{x}(t)\big)\, {e_a}^T PB)$ and ${K_2}^T P + PK_2 = -Q$ leads to

$$\dot{L}(.) = -{e_a}^T Q e_a + 2{\bar{e}_a}^T PB\widetilde{W}^T\phi\big(\bar{x}(t)\big) + 2{e_a}^T PB\epsilon - 2tr\left(\widetilde{W}^T\gamma^{-1}\gamma\, Proj_m\big(\widehat{W},\ \phi\big(\bar{x}(t)\big)\, {e_a}^T PB\big)\right). \tag{A.3}$$

By adding and subtracting $\widetilde{W}^T\phi\big(\bar{x}(t)\big)\,{\bar{e}_a}^T PB$ and using the trace property $tr(AB) = tr(BA)\ if\ A \in \mathbb{R}^{n\times m}$ and $B \in \mathbb{R}^{m\times n}$ for any $n, m \in \mathbb{N}_+$

$$\dot{L}(.) = -{e_a}^T Q e_a + 2{\bar{e}_a}^T PB\widetilde{W}^T\phi\big(\bar{x}(t)\big) + 2{e_a}^T PB\epsilon + 2tr\{\big(-\widetilde{W}^T Proj_m\big(\widehat{W}, \phi\big(\bar{x}(t)\big)\,{\bar{e}_a}^T PB\big) - \phi\big(\bar{x}(t)\big)\,{\bar{e}_a}^T PB\}\big) - 2tr\big\{\widetilde{W}^T\phi\big(\bar{x}(t)\big)\,{\bar{e}_a}^T PB\big\}. \tag{A.4}$$

By lemma 11.3 of [44] (from Paper I),

$$2tr[\,\big(\widehat{W} - W\big)^T\{Proj_m\big(\widehat{W},\ \phi\big(\bar{x}(t)\big)\,{\bar{e}_a}^T PB\big) - \phi\big(\bar{x}(t)\big)\,{\bar{e}_a}^T PB\}] \le 0. \tag{A.5}$$

After some simplifications, (A.5) becomes

$$\dot{L}(.) \le -{e_a}^T Q e_a + 2{\bar{e}_a}^T PB\widetilde{W}^T\phi\big(\bar{x}(t)\big) + 2{e_a}^T PB\epsilon - 2{\bar{e}_a}^T PB\widetilde{W}^T\phi\big(\bar{x}(t)\big)$$

$$= -{e_a}^T Q e_a + 2{e_a}^T PB\epsilon. \tag{A.6}$$

Applying norm properties [45] (from Paper I) to the terms on the right-hand side of (A.6) leads to

$$\dot{L} \le -\lambda_{min}(Q)\|e_a\|^2 + 2\|PB\|\|e_a\|\|\epsilon\| = -\{\lambda_{min}(Q)\|e_a\|^2 - 2\|PB\|\epsilon^*\|e_a\|\} \tag{A.7}$$

$$= -\left(\sqrt{\lambda_{min}\,(Q)}\|e_a\| - \frac{\|PB\|\epsilon^*}{\sqrt{\lambda_{min}\,(Q)}}\right)^2 + \frac{(\|PB\|\epsilon^*)^2}{\lambda_{min}\,(Q)}$$

since $\|\epsilon\| \leq \epsilon^*$. By defining $b_b \triangleq \frac{\|PB\|\epsilon^*}{\sqrt{\lambda_{min}\,(Q)}}$

$$\dot{L}(.) \leq -\left(\sqrt{\lambda_{min}\,(Q)}\|e_a\| - b_b\right)^2 + {b_b}^2$$

$$= -(1-\xi)\left(\sqrt{\lambda_{min}\,(Q)}\|e_a\| - b_b\right)^2 - \xi\left(\sqrt{\lambda_{min}\,(Q)}\|e_a\| - b_b\right)^2 + {b_b}^2. \quad 0 < \xi < 1 \tag{A.8}$$

This equation can be rewritten as

$$\dot{L}(.) \leq -(1-\xi)\left(\sqrt{\lambda_{min}\,(Q)}\,\|e_a\| - b_b\right)^2 \tag{A.9}$$

when $\|e_a\| \geq \left(\sqrt{\frac{{b_b}^2}{\xi}} + b_b\right)/\sqrt{\lambda_{min}\,(Q)}$. It can thus be concluded the estimation error is UUB at the sampling instants $t = t_i^s$.

Case (ii): By using the Lyapunov function as in (1) and following similar steps as in case (i) with simplifications $\bar{e}_a = \bar{x} - \hat{x} = \bar{x} - x + x - \hat{x} = e_{int} + e_a$, $\left\|\phi\left(x(t)\right) - \phi(x(t_i^s))\right\| \leq L\,\|x(t) - x(t_i^s)\| = L\|e_{evt}\|$, $\|\epsilon\| \leq \epsilon^*$, $\left\|\phi\left(x(t_i^s)\right)\right\| \leq \phi^*$, $\|e_{ext}\| \leq \varsigma \in \mathbb{R}_+$, $\partial \triangleq \|P(A - K_2)\|$, $\varepsilon \triangleq \partial * \varsigma$ $\|W\| \leq W^*$ and $\left\|\widetilde{W}\right\| \leq \widetilde{W}^*$ and using $\|u_{evt}\|^2 \leq \beta_u$ & $\|e_{evt}\|^2 \leq \propto_a \beta_a \|e_a\|^2$ results in its time derivative as

$$\dot{L}(e_a, \widetilde{W}) \leq -(1-\xi)\left(\sqrt{a_2}\,\|e_a\| - \frac{b_2}{\sqrt{a_2}}\right)^2$$

$$\text{if} \quad \|e_a\| \geq \left(\sqrt{\frac{b_2}{\sqrt{a_2}\xi}} + \frac{b_2}{\sqrt{a_2}}\right)/\sqrt{a_2} \tag{A.10}$$

where $a_2 \triangleq \lambda_{min}\,(Q)$ and $b_2 \triangleq 2\{\|PB\|(\widetilde{W}^*\varsigma\phi^* + W^*L\,\varsigma + \epsilon^*) + \varepsilon)\}$. From (10), $\dot{L}(.)$ is negative definite and upper bounded by a function of e_a for $\|e_a\| \geq (\sqrt{\frac{b_2}{\sqrt{a_2}\xi}} + \frac{b_2}{\sqrt{a_2}})/\sqrt{a_2}$, which proves that e_a is also UUB during the inter-event simulation time.

Case (iii): Again using the same Lyapunov function as in (1), and following similar steps as in case (i) with the estimation error dynamics from (17a (from Paper I)), the time derivative of Lyapunov function is found as:

$$\begin{aligned}\dot{L}\big(e_a, \widetilde{W}\big) = 2{e_a}^T P \Big(&A_m e_a(t) + B_m\big(r(t) - r(t_i^s)\big)\\ &+ BK_1\big(x(t) - \hat{x}(t_i^s)\big) + BW^T\phi\big(x(t)\big)\\ &- B\widehat{W}^T\phi\big(\hat{x}(t_i^s)\big)\Big) + 2tr\Big(\widetilde{W}^T\gamma^{-1}\dot{\widetilde{W}}\Big).\end{aligned} \tag{A.11}$$

After some algebra (A.11) can be rewritten

$$\begin{aligned}\dot{L}(.) = &-{e_a}^T Q_m e_a + 2{e_a}^T PB_m\Delta r(t) + 2{e_a}^T PBK_1 e_a + 2{e_a}^T PBK_1 e_{evt}\\ &+ 2{e_a}^T PBW^T\phi\big(x(t)\big) - 2{e_a}^T PB\widehat{W}^T\phi\big(\hat{x}(t)\big)\\ &+ 2{e_a}^T PB\widehat{W}^T\big[\phi\big(\hat{x}(t)\big) - \phi\big(\hat{x}(t_i^s)\big)\big].\end{aligned} \tag{A.12}$$

By applying norm properties [45] (from Paper I) to the terms on the right-hand side of (A.12) results in

$$\begin{aligned}\dot{L} \leq &-\lambda_{min}\,(Q_m)\|e_a\|^2 + 2\|PB_m\|\|\Delta r\|\|e_a\| + 2\|PBK_1\|\|e_a\|^2\\ &+ 2\|PBK_1\|\|e_a\|\|e_{evt}\| + 2\|PB\|\|W\|\big\|\phi\big(x(t)\big)\big\|\|e_a\|\\ &+ 2\|PB\|\big\|\widehat{W}\big\|\big\|\phi\big(\hat{x}(t)\big)\big\|\|e_a\|\\ &+ 2\|PB\|\|e_a\|\big\|\widehat{W}\big\|\big\|\phi\big(x(t)\big) - \phi\big(x(t_i^s)\big)\big\|.\end{aligned} \tag{A.13}$$

Equation (A.13) can be simplified by using the inequalities $\big\|\phi\big(x(t)\big) - \phi\big(x(t_i^s)\big)\big\| \leq L\,\|x(t) - x(t_i^s)\| = L\|e_{evt}\|$, $\|\phi(.)\| \leq \phi^*$, $\|W\| \leq W^*$, and $\big\|\widehat{W}\big\| \leq \widehat{W}^*$. Furthermore,

during the inter-event period, $\dot{\hat{x}}(t) = A\,\hat{x}(t) + B\left(u(t) + \hat{f}\left(x(t_i^s)\right)\right) = A_m\hat{x}(t) + B_m r(t)$, so $B\|PB_m\|\|\Delta r\| \le c_1$, $B_m\Delta r(t) \le c_2$. Also applying Young's inequality [45] (from Paper I) for $\|e_{evt}\|$ and its multiplicative terms, yields

$$\begin{aligned}\dot{L}(.) &\le -\lambda_{min}(Q_m)\|e_a\|^2 + c_1\|e_a\| + 2\|PBK_1\|\|e_a\|^2 + \left(\frac{1}{\sigma}\right)\|PBK_1\|^2\|e_{evt}\|^2 \\ &\quad + \sigma\|e_a\|^2 + 2\|PB\|W^*\phi^*\|e_a\| + 2\|PB\|\|\widehat{W}\|\phi^*\|e_a\| + \left(\frac{1}{\sigma}\right)L^2\|e_{evt}\|^2 \\ &\quad + \sigma\left(\|PB\|\widehat{W}^*\right)^2\|e_a\|^2 \\ &\le \left(-\lambda_{min}(Q_m) + 2\|PBK_1\| + \sigma\left(1 + \|PB\|\widehat{W}^*\right)^2\right)\|e_a\|^2 \\ &\quad + \left(c_1 + 2\|PB\|\phi^*\left(W^* + \widehat{W}^*\right)\right)\|e_a\| \\ &\quad + \left(\frac{1}{\sigma}\right)(\|PBK_1\|^2 + L^2)\|e_{evt}\|^2.\end{aligned} \tag{A.14}$$

If $\|e_{evt}\|^2 \le \beta_a\|e_a\|^2$ and $\beta_a = \frac{(\|PBK_1\|^2 + L^2)}{\sigma}$ then

$$\begin{aligned}\dot{L}(.) &\le \left(-\lambda_{min}(Q_m) + 2\|PBK_1\| + \sigma\left(1 + \|PB\|\widehat{W}^*\right)^2 + 1\right)\|e_a\|^2 \\ &\quad + \left(c_1 + 2\|PB\|\phi^*\left(W^* + \widehat{W}^*\right)\right)\|e_a\| \\ &= \left(-\lambda_{min}(Q_m) + 2\|PBK_1\| + \sigma\left(1 + \|PB\|\widehat{W}^*\right)^2 + 1\right)\|e_a\|^2 \\ &\quad + \left(c_1 + 2\|PB\|\phi^*\left(W^* + \widehat{W}^*\right)\right)\|e_a\|.\end{aligned} \tag{A.15}$$

By defining $a_3 = \lambda_{min}(Q_m) - 2\|PBK_1\| - \sigma\left(1 + \|PB\|\widehat{W}^*\right)^2 - 1$ and $b_3 \triangleq \{c_1 + 2\|PB\|\phi^*\left(W^* + \widehat{W}^*\right)\}$, (64) is reduced to,

$$\dot{L}(.) \le -(1-\xi)\left(\sqrt{a_3}\,\|e_a\| - \frac{b_3}{\sqrt{a_3}}\right)^2 \quad if \;\; \|e_a\| \ge \frac{\sqrt{\frac{b_3}{\sqrt{a_3}\xi}} + \frac{b_3}{\sqrt{a_3}}}{\sqrt{a_3}} \tag{A.16}$$

Since $\dot{L}(.)$ is negative definite if $\|e_a\| \geq \frac{\sqrt{\frac{b_3}{\sqrt{a_3}\xi}}+\frac{b_3}{\sqrt{a_3}}}{\sqrt{a_3}}$, so e_a is UUB during the inter-event time period as well.

A.1.2. Tracking Error. Tracking error part is divided into two cases where case (i) relates to the sampling instant when $Trg^{u}_{1\,a/b}$ is active. Note that at this time $u_{evt} = 0$ and $e_{evt} \neq 0$. Case (ii) relates to the period during inter-event times; Note that during this period, $u_{evt} \neq 0$, $e_{evt} \neq 0$, and $\dot{\widehat{W}} = 0$.

Case (i): Choosing a Lyapunov candidate function as

$$L\left(e_r, \widetilde{W}\right) = {e_r}^T P e_r + tr\left(\widetilde{W}^T \gamma^{-1} \widetilde{W}\right) \tag{A.17}$$

its time derivative can be obtained as

$$\dot{L}\left(e_r, \widetilde{W}\right) = 2{e_r}^T P \dot{e}_r + 2\, tr(\widetilde{W}^T \gamma^{-1} \dot{\widetilde{W}}) \tag{A.18}$$

$$= 2{e_r}^T P\left(A_m e_r + B\widetilde{W}^T \phi\left(x(t_i^s)\right) + B\check{\epsilon} + BK_1 e_{evt}\right) + 2tr\left(\widetilde{W}^T \gamma^{-1} \dot{\widetilde{W}}\right).$$

By noting that $\dot{\widetilde{W}} = -\dot{\widehat{W}}$, $\bar{x}(t) = x(t_i)$, $\check{\epsilon} = \epsilon$, ${A_m}^T P + P A_m = -Q_m$, and $e_{evt} = 0$, and after some algebra, it is found that

$$\begin{aligned} \dot{L}(.) = &-{e_r}^T Q_m e_r + 2{e_r}^T PB\widetilde{W}^T \phi\left(x(t_i)\right) + 2{e_r}^T PB\epsilon \\ &- 2tr\left(\widetilde{W}^T Proj_m\left(\widehat{W}, \phi\left(x(t_i^s)\right) {e_a}^T PB\right)\right). \end{aligned} \tag{A.19}$$

Now applying norm properties [45] (from Paper I) to the terms on the right-hand side of (A.19) leads to

$$\begin{aligned} \dot{L}(.) \leq &-\lambda_{min}\,(Q_m)\|e_r\|^2 + 2\|PB\|\|e_r\|\left\|\widetilde{W}^T\right\|\left\|\phi\left(x(t_i^s)\right)\right\| \\ &+ 2\|PB\|\|e_r\|\|\epsilon\| + 2\left\|\widetilde{W}^T\right\|\left\|\phi\left(x(t_i^s)\right)\right\|\|e_a\|\|PB\|. \end{aligned} \tag{A.20}$$

Since $\|\epsilon\| \leq \epsilon^*$, $\left\|\widetilde{W}^T\right\| \leq \widetilde{W}^*$, $\|e_a\| \leq \mathsf{C}$ (from the boundedness of e_a for some $\mathsf{C} \in \mathbb{R}_+$) and $\left\|\phi\left(x(t_i^s)\right)\right\| \leq \phi^*$ so

$$\dot{L}(.) \leq -\lambda_{min}\,(Q_m)\|e_r\|^2 + 2\|PB\|\widetilde{W}^*\phi^*\|e_r\| + 2\|PB\|\epsilon^*\|e_r\| + 2\widetilde{W}^*\phi^*\complement\,\|PB\|.$$

Defining $\|PB\|(\widetilde{W}^*\phi^* + \epsilon^*) \triangleq \alpha_r$ and $\mathfrak{c} \triangleq 2\widetilde{W}^*\phi^*\complement\|PB\|$, results in

$$\dot{L}(.) = -\left(\sqrt{\lambda_{min}\,(Q_m)}\|e_r\| - \frac{\alpha_r}{\sqrt{\lambda_{min}\,(Q_m)}}\right)^2 + \frac{(\alpha_r)^2}{\lambda_{min}\,(Q_m)} + \mathfrak{c}.$$

When $\|e_r\| \geq (\sqrt{((\frac{\alpha_r}{\sqrt{\lambda_{min}\,(Q_m)}})^2 + \mathfrak{c})/\xi} + \frac{\alpha_r}{\sqrt{\lambda_{min}\,(Q_m)}})/\sqrt{\lambda_{min}\,(Q_m)}$, then

$$\dot{L}(.) \leq -(1-\xi)\left(\sqrt{\lambda_{min}\,(Q_m)}\|e_r\| - \frac{\alpha_r}{\sqrt{\lambda_{min}\,(Q_m)}}\right)^2. \tag{A.21}$$

Equation (A.21) leads to an UUB for $e_r\ as$ $\|e_r\| \geq (\sqrt{((\frac{\alpha_r}{\sqrt{\lambda_{min}\,(Q_m)}})^2 + \mathfrak{c})/\xi} + \frac{\alpha_r}{\sqrt{\lambda_{min}\,(Q_m)}})/\sqrt{\lambda_{min}\,(Q_m)}$.

Case (ii): Choosing the same Lyapunov function candidate as in (A.17), its time derivative is given by

$$\dot{L}\left(e_r, \widetilde{W}\right) = 2{e_r}^T P\dot{e}_r + 2\,tr\left(\widetilde{W}^T\gamma^{-1}\dot{\widetilde{W}}\right). \tag{A.22}$$

Using error dynamics $\dot{e}_r$ and after some algebra, $\dot{L}\left(e_r, \widetilde{W}\right)$ is found as

$$\begin{aligned}\dot{L}(.) \leq\ & -\lambda_{min}\,(Q_m)\|e_r\|^2 + 2\|PB\|\left\|\widetilde{W}\right\|\left\|\phi\left(x(t_i^s)\right)\right\|\|e_r\| \\ & + 2\|PB\|\|e_r\|\|W\|\left\|\phi\left(x(t)\right) - \phi\left(x(t_i^s)\right)\right\| \\ & + 2\|PB\|\|e_r\|\|\epsilon\| + 2\|PBK_1\|\|e_r\|\|e_{evt}\|.\end{aligned} \tag{A.23}$$

Noting that $\left\|\phi\left(x(t)\right) - \phi(x(t_i^s))\right\| \leq L\,\|x(t) - x(t_i^s)\| = L\|e_{evt}\|$, $\|\epsilon\| \leq \epsilon^*$, $\left\|\phi\left(x(t_i^s)\right)\right\| \leq \phi^*$, $\|W\| \leq W^*$, and $\left\|\widetilde{W}\right\| \leq \widetilde{W}^*$ in (A.23) leads to

$$\dot{L}(.) \leq -\lambda_{min}\,(Q_m)\|e_r\|^2 + 2\|PK\|\|e_r\|\|e_{evt}\| + 2\|PB\|\,W^*L\|e_{evt}\|\|e_r\| + 2\{\|PB\|\left(\widetilde{W}^*\phi^* + \epsilon^*\right)\|e_r\|. \tag{A.24}$$

Using Young's inequality [45] (from Paper I) for $\|e_r\|$ and its multiplicative terms,

$$\begin{aligned}\dot{L}(.) &\leq -\lambda_{min}\,(Q_m)\|e_r\|^2 + \left(\frac{1}{\sigma}\right)\|PK\|^2\|e_{evt}\|^2 + \sigma\|e_r\|^2 + \left(\frac{1}{\sigma}\right)L^2\|e_{evt}\|^2 \\ &\quad + \sigma(\|PB\|\,W^*)^2\|e_r\|^2 + 2\{\|PB\|(\widetilde{W}^*\phi^* + \epsilon^*)\|e_r\| \\ &= \left(-\lambda_{min}\,(Q_m) + \sigma(1 + (\|PB\|\,W^*)^2)\right)\|e_r\|^2 + (\|PK\|^2 \\ &\quad + L^2)/\sigma\,\|e_{evt}\|^2 + 2\{\|PB\|\left(\widetilde{W}^*\phi^* + \epsilon^*\right)\|e_r\|.\end{aligned} \tag{A.25}$$

If $\|e_{evt}\|^2 \leq \beta_a\,\|e_a\|^2 \leq \beta_{evt}\mathrm{C} \leq \mathrm{C}_{evt} \in \mathbb{R}_+$ where $\beta_{evt} = \frac{(\|PK\|^2 + L^2)}{\|PBK_1\|^2 + L^2}$, then

$$\begin{aligned}\dot{L}(.) &\leq \left(-\lambda_{min}\,(Q_m) + 1 + \sigma(1 + (\|PB\|\,W^*)^2)\right)\|e_r\|^2 \\ &\quad + 2\|PB\|\left(\widetilde{W}^*\phi^* + \epsilon^*\right)\|e_r\| + \mathrm{C}_{evt}.\end{aligned} \tag{A.26}$$

By defining $a_4 \triangleq \lambda_{min}\,(Q_m) - 1 - \sigma(1 + (\|PB\|\,W^*)^2)$, $b_4 \triangleq \|PB\|(\widetilde{W}^*\phi^* + \epsilon^*)$, and under the condition $\|e_r\| \geq (\sqrt{\frac{b_4 + \mathrm{C}_{evt}\sqrt{a_4}}{\sqrt{a_4}\xi}} + \frac{b_4}{\sqrt{a_4}})/\sqrt{a_4}$, (A.26) yields

$$\dot{L} \leq -(1-\xi)\left(\sqrt{a_4}\,\|e_r\| - \frac{b_4}{\sqrt{a_4}}\right)^2. \tag{A.27}$$

Because the Lyapunov time-derivative is negative definite and bounded by a function of e_r as long as $\|e_r\| \geq (\sqrt{\frac{b_4 + \mathrm{C}_{evt}\sqrt{a_4}}{\sqrt{a_4}\xi}} + \frac{b_4}{\sqrt{a_4}})/\sqrt{a_4}$, so e_r is UUB during the inter-event time as well.

A.2. PROOF OF THEOREM 3

The estimation and tracking errors are taken separately.

A.2.1. Estimation Error. This proof is divided into two cases. Case (i) relates the sampling time instants, when $t = t_i,\ i = 1,2$ ... and the actual sampled state is available. Note at these instants $\bar{x}(t) = x(t_i),\ e_a = \bar{e}_a\ ,\ e_{evt} = 0$ and $e_{int} = 0$ and case (ii) is associated with the inter-event time. During this period $\bar{x}\ (t) = C_1 t^n + C_2 t^{n-1} \ldots + C_n t + C_{n+1}$ so $e_{evt} \neq 0$ and $e_{int} \neq 0$.

Case (i): By choosing a Lyapunov candidate function as

$$L\left(e_a, \widetilde{W}\right) = {e_a}^T P e_a + tr\left(\widetilde{W}^T \gamma^{-1} \widetilde{W}\right) \tag{A.28}$$

its time derivative is found as

$$\dot{L}(.) \leq -(1-\xi)\left(\sqrt{\lambda_{min}\,(Q)}\,\|e_a\| - b_b\right)^2 \qquad \text{if} \qquad \|e_a\| \geq \left(\sqrt{\frac{{b_b}^2}{\xi}} + b_b\right)/\sqrt{\lambda_{min}\,(Q)} \tag{A.29}$$

From equation (A.29), it can be concluded that as long as $\|e_a\| \geq \left(\sqrt{\frac{{b_b}^2}{\xi}} + b_b\right)/\sqrt{\lambda_{min}\,(Q)}$, then $\dot{L}(.)$ is negative and in the process it can be concluded that e_a is UUB at the sampling instants $t = t_i$.

Case (ii): During inter-event time using Lyapunov function as in (A.28), its time derivative is given as

$$\dot{L}\left(e_a, \widetilde{W}\right) = 2{e_a}^T P \dot{e}_a + 2\ tr(\widetilde{W}^T \gamma^{-1} \dot{\widetilde{W}}) \tag{A.30}$$

$$= 2{e_a}^T P(K_2 e_a + B\widetilde{W}^T \phi\left(\bar{x}(t)\right) + B\check{\epsilon} + (A - K_2)e_{ext}) + 2tr(\widetilde{W}^T \gamma^{-1} \dot{\widetilde{W}})$$

$$= {e_a}^T\left({K_2}^T P + P K_2\right)e_a + 2{e_a}^T PB\widetilde{W}^T \phi\left(\bar{x}(t)\right) + 2{e_a}^T PB\check{\epsilon} + 2{e_a}^T P(A - K_2)e_{ext} - 2tr\left(\widetilde{W}^T \gamma^{-1} \dot{\widetilde{W}}\right). \tag{A.31}$$

By using the projection operator [44] (from Paper I) for the weight updates $\dot{\widehat{W}} = \gamma\, Proj_m(\widehat{W}, \phi(\bar{x}(t))\, \bar{e}_a{}^T PB)$, the Lyapunov equation $K_2{}^T P + PK_2 = -Q$, also $\bar{e}_a = \bar{x} - \hat{x} = \bar{x} - x + x - \hat{x} = e_{int} + e_a$, by adding and subtracting $\widetilde{W}^T \phi(\bar{x}(t))\, \bar{e}_a{}^T PB$ and following similar steps as in proof of theorem 1, (A.31) can be written as

$$\begin{aligned}\dot{L}(.) = -e_a{}^T Q e_a + 2(\bar{e}_a - e_{int})^T PB\widetilde{W}^T \phi(\bar{x}(t)) + 2e_a{}^T PB\check{\epsilon} + 2e_a{}^T P(A \\ - K_2)e_{int} + 2tr(-\widetilde{W}^T\{Proj_m(\widehat{W}, \phi(\bar{x}(t))\, \bar{e}_a{}^T PB) \\ + \widetilde{W}^T \phi(\bar{x}(t))\, \bar{e}_a{}^T PB - \widetilde{W}^T \phi(\bar{x}(t))\, \bar{e}_a{}^T PB\}) \\ = -e_a{}^T Q e_a + 2\bar{e}_a{}^T PB\widetilde{W}^T \phi(\bar{x}(t)) - 2e_{int}{}^T PB\widetilde{W}^T \phi(\bar{x}(t)) \\ + 2e_a{}^T PB\check{\epsilon} + 2e_a{}^T P(A - K_2)e_{int} \\ + \quad 2tr\{(-\widetilde{W}^T Proj_m(\widehat{W}, \phi(\bar{x}(t))\, \bar{e}_a{}^T PB) \\ - \phi(\bar{X}(t))\, \bar{e}_a{}^T PB\}) - 2tr\{\widetilde{W}^T \phi(\bar{x}(t))\, \bar{e}_a{}^T PB\}.\end{aligned} \tag{A.32}$$

By lemma 11.3 of [44] (projection operator properties as given in (A.5)),

$$\begin{aligned}\dot{L}(.) \le -e_a{}^T Q e_a + 2\bar{e}_a{}^T PB\widetilde{W}^T \phi(\bar{x}(t)) - 2e_{int}{}^T PB\widetilde{W}^T \phi(\bar{x}(t)) \\ + 2e_a{}^T PB\check{\epsilon} + 2e_a{}^T P(A - K_2)e_{int} \\ - 2tr\{\widetilde{W}^T \phi(\bar{x}(t))\, \bar{e}_a{}^T PB\}.\end{aligned} \tag{A.33}$$

Since $tr\{\widetilde{W}^T \phi(\bar{x}(t))\, \bar{e}_a{}^T PB\} = tr\{\, \bar{e}_a{}^T PB\widetilde{W}^T \phi(\bar{x}(t))\} = \bar{e}_a{}^T PB\widetilde{W}^T \phi(\bar{x}(t))$ as it is a salar, also $\check{\epsilon} = W^T[\phi(x(t)) - \phi(\bar{x}(t))] + \epsilon$, so

$$\begin{aligned}= -e_a{}^T Q e_a - 2e_{int}{}^T PB\widetilde{W}^T \phi(\bar{x}(t)) \\ + 2e_a{}^T PBW^T[\phi(x(t)) - \phi(\bar{x}(t))] + 2e_a{}^T PB\epsilon \\ + 2e_a{}^T P(A - K_2)e_{int}.\end{aligned} \tag{A.34}$$

Now applying norm properties [45] (from Paper I) to the terms on the right-hand side of (A.34),

$$\begin{aligned}\dot{L} \leq -\lambda_{min}(Q)\|e_a\|^2 + 2\|PB\|\left\|\widetilde{W}\right\|\|e_{int}\|\left\|\phi\left(\bar{x}(t)\right)\right\| \\ + 2\|PB\|\|e_a\|\|W\|\left\|\phi\left(x(t)\right) - \phi\left(\bar{x}(t)\right)\right\| \\ + 2\|PB\|\|e_a\|\|\epsilon\| + 2\|P(A-K_2)\|\|e_a\|\|e_{int}\|.\end{aligned} \tag{A.35}$$

By using the inequalities $\left\|\phi\left(x(t)\right) - \phi(\bar{x}(t))\right\| \leq L\,\|x(t) - \bar{x}(t)\| = L\|e_{int}\|$, $\|\epsilon\| \leq \epsilon^*$, $\left\|\phi\left(\bar{x}(t)\right)\right\| \leq \phi^*$, $\|W\| \leq W^*$, $\left\|\widetilde{W}\right\| \leq \widetilde{W}^*$, $\|e_{int}\| \leq \varsigma$, $\partial \triangleq \|P(A-K_2)\|$, and $\varepsilon \triangleq \partial * \varsigma$ and after some simplification leads to

$$\begin{aligned}\dot{L}(.) \leq -\lambda_{min}(Q)\|e_a\|^2 + 2\{\|PB\|(W^*L\,\varsigma + \epsilon^*) + \varepsilon)\}\,\|e_a\| \\ + 2\|PB\|\widetilde{W}^*\phi^*\varsigma.\end{aligned} \tag{A.36}$$

By defining $a_5 \triangleq \lambda_{min}(Q)$, $b_5 \triangleq 2\{\|PB\|(\widetilde{W}^*\varsigma\phi^* + W^*L\,\varsigma + \epsilon^*) + \varepsilon)\}$, and $c_5 \triangleq 2\|PB\|\widetilde{W}^*\phi^*\varsigma$, (A.36) yields

$$\begin{aligned}\dot{L} \leq -(1-\xi)\left(\sqrt{a_5}\,\|e_a\| - \frac{b_5}{\sqrt{a_5}}\right)^2 \quad if \quad \|e_a\| \\ \geq \left(\sqrt{\frac{b_5 + c_{5\sqrt{a_5}}}{\sqrt{a_5}\xi}} + \frac{b_5}{\sqrt{a_5}}\right)/\sqrt{a_5}\end{aligned} \tag{A.37}$$

So, from (A.37) $\dot{L}$ is negative definite if $\|e_a\| \geq \left(\sqrt{\frac{b_5 + c_{5\sqrt{a_5}}}{\sqrt{a_5}\xi}} + \frac{b_5}{\sqrt{a_5}}\right)/\sqrt{a_5}$. It shows that e_a is UUB during the inter-event time as well.

A.2.2. Tracking Error. Like the estimation error, the tracking error proof is also divided into two cases: case (i) relates the sampling instants and case (ii) is associated with the inter-event period.

Case (i): At sampling instant: Choosing the Lyapunov function candidate as

$$L(e_r, \widetilde{W}) = {e_r}^T P e_r + tr(\widetilde{W}^T \gamma^{-1} \widetilde{W}) \tag{A.38}$$

by noting that $-Q_m = {A_m}^T P + P A_m$ and $\|e_a\| \leq \mathcal{E}$ for $\mathcal{E} \in \mathbb{R}_+$, its time derivative is found as

$$\begin{aligned} \dot{L}(.) \leq -\lambda_{min}(Q_m)\|e_r\|^2 + 2\|PB\|\widetilde{W}^*\phi^*\|e_r\| + 2\|PB\|\epsilon^*\|e_r\| \\ + 2\widetilde{W}^*\phi^*\mathcal{E}\|PB\|. \end{aligned} \tag{A.50}$$

By defining $a_6 \triangleq \lambda_{\min}(Q_m)$, $b_6 \triangleq \|PB\|(\widetilde{W}^*\phi^* + \epsilon^*)$, $c_6 \triangleq 2\widetilde{W}^*\phi^*\mathcal{E}\|PB\|$ and under the condition $\|e_r\| \geq (\sqrt{\frac{b_6 + c_6\sqrt{a_6}}{\sqrt{a_6}\xi}} + \frac{b_6}{\sqrt{a_6}})/\sqrt{a_6}$, (A.39) is reduced to

$$\dot{L} \leq -(1-\xi)\left(\sqrt{\lambda_{min}(Q_m)}\|e_r\| - \frac{\alpha_r}{\sqrt{\lambda_{min}(Q_m)}}\right)^2. \tag{A.40}$$

From (A.40), it clear that $\dot{L}$ is negative definite as long as $\|e_r\| \geq (\sqrt{\frac{b_6 + c_6\sqrt{a_6}}{\sqrt{a_6}\xi}} + \frac{b_6}{\sqrt{a_6}})/\sqrt{a_6}$, which proves that e_r is UUB for the case (i).

Case (ii): Choosing the same Lyapunov candidate function as in (A.38), its time derivative is obtained as

$$\begin{aligned} \dot{L}(e_r, \widetilde{W}) &= 2{e_r}^T P_r \dot{e}_r + 2\, tr(\widetilde{W}^T \gamma^{-1} \dot{\widetilde{W}}) \\ &= 2{e_r}^T P_r\left(A_m e_r(t) + B\widetilde{W}^T\phi(x(t_i)) + B\check{\epsilon} + BK_1 e_{evt}\right) \end{aligned} \tag{A.41}$$

After some algebra and by choosing $\beta = \sigma/(1 + (L\|PB\|)^2)$ for $\|e_{evt}\|^2 \leq \propto_r \beta_r\|e_r\|^2$, it can be reduced to

$$\dot{L} \leq -(1-\xi)\left(\sqrt{a_7}\,\|e_r\| - \frac{b_7}{\sqrt{a_7}}\right)^2 \quad \text{if} \quad \|e_r\| \geq \left(\sqrt{\frac{{b_7}^2}{\xi}} + b_7\right)/\sqrt{a_7}\,. \tag{A.42}$$

where $a_7 \triangleq \lambda_{min}(Q_m)$-$\sigma\|PBK_1\|^2$-$\sigma W^{*2}$-1 and $b_7 \triangleq \|PB\|(\widetilde{W}^*\phi^* + \epsilon^*)$. Since $\dot{L}$ is negative definite from (A.42), so as long as $\|e_r\| \geq \left(\sqrt{\frac{b_7^2}{\xi}} + b_7\right)/\sqrt{a_7}$ is true, which shows that e_r is UUB during the inter-event time as well. So, from case (i) and (ii), it can be concluded that e_r is UUB all the time.

A.3. PROOF OF THEOREM 4

A.3.1. Estimation Error. In this case the estimation error analysis follows the same approach as used for the proof of the theorem 1.

A.3.2. Tracking Error. Proof for the UUB of the tracking error is similar to the one for scheme 1 since the tracking error expression is same in both cases.

APPENDIX B.

PROOFS OF THE THEOREMS OF THE PAPER II

The proofs for the theorems of the Paper II are done using Lyapunov analysis. Similar approaches are taken for the stability proof in adaptive event-triggered control literature such as those in [34], [38], [42], and [40] etc (from Paper II). Note that all references for Appendix B are from Paper II.

B.1. PROOF OF THE THEOREM 1

This proof is divided into two cases: case (i) At sampling instant, when $t = t_i,\ i =$ 1,2, ... when the actual sampled state is available $\bar{X}(t) = X(t_i)$, $e_a = \bar{e}_a$ and $e_{evt} = e_{ext} =$ 0 and case (ii) during inter-event time when $\bar{X}(t) = C_1 t^n + C_2 t^{n-1} \ldots + C_n t + C_{n+1}$, $e_a = \bar{e}_a,\ e_{evt} \neq 0$ and $e_{ext} \neq 0$.

Case (i): Choosing a suitable Lyapunov function candidate as:

$$L\left(e_r, e_a, \widetilde{W}\right) = {e_r}^T P e_r + tr\left(\widetilde{W}^T \gamma^{-1} \widetilde{W}\right) + {e_a}^T P e_a \tag{B.1}$$

its time derivative is given by

$$\dot{L}\left(e_r, e_a, \widetilde{W}\right) = 2{e_r}^T P_r \dot{e}_r + 2{e_a}^T P \dot{e}_a + 2\ tr\left(\widetilde{W}^T \gamma^{-1} \dot{\widetilde{W}}\right).$$

Using error dynamics from (19) and (21) (from Paper II), (B.1) can be given as

$$\begin{aligned} \dot{L}\left(e_r, e_a, \widetilde{W}\right) = 2{e_r}^T P_r \big(& K e_r(t) - K e_{evt} + f\left(X(t)\right) - f\left(X(t_i)\right) \\ & + B\widetilde{W}^T \phi\left(X(t_i)\right) + \check{\epsilon}\big) + 2{e_a}^T P (K_2 e_a(t) - K_2 e_{ext} \\ & + B\widetilde{W}^T \phi\left(\bar{X}(t)\right) + B\check{\epsilon} + f\left(X(t)\right) - f\left(\bar{X}(t)\right)) \\ & + 2tr(\widetilde{W}^T \gamma^{-1} \dot{\widetilde{W}}) \end{aligned} \tag{B.2}$$

Because at sampling instant $\widetilde{W} = W - \widehat{W}$ *so* $\dot{\widetilde{W}} = -\dot{\widehat{W}},\ e_{ext} = 0\ , \check{\epsilon} = W^T\left[\phi\left(X(t)\right) - \phi\left(X(t_i)\right)\right] + \epsilon = \epsilon,\ f\left(X(t)\right) - f\left(\bar{X}(t)\right) = 0, e_{evt} = e_{ext} = 0$and $e_a = \bar{e}_a$, so (B.2) can be rewritten as

$$\begin{aligned}\dot{L}(.) = {e_r}^T(K^T P_r + P_r K)e_r + 2{e_r}^T P_r B\widetilde{W}^T\phi\big(X(t_i)\big) + 2{e_r}^T P_r B\epsilon \\ + {e_a}^T\big({K_2}^T P + PK_2\big)e_a + 2{e_a}^T PB\widetilde{W}^T\phi\big(\bar{X}(t)\big) \\ + 2{e_a}^T PB\epsilon - 2tr(\widetilde{W}^T\gamma^{-1}\dot{\widehat{W}})\end{aligned} \tag{B.3}$$

By using the projection operator for weight updates, $\dot{\widehat{W}} = \gamma\, Proj_m(\widehat{W}, \phi\big(\bar{X}(t)\big)\,{\bar{e}_a}^T PB)$, Lyapunov equations ${K_2}^T P + PK_2 = -Q, K^T P_r + P_r K = -Q_r$, $e_a = \bar{e}_a$ and by adding and subtracting $\widetilde{W}^T\phi\big(\bar{X}(t)\big)\,{\bar{e}_a}^T PB$, (B.3) can be rewritten as

$$\begin{aligned}\dot{L}(.) = -{e_r}^T Q_r e_r + 2{e_r}^T P_r B\widetilde{W}^T\phi\big(X(t_i)\big) + 2{e_r}^T P_r B\epsilon - {e_a}^T Qe_a \\ + 2{\bar{e}_a}^T PB\widetilde{W}^T\phi\big(\bar{X}(t)\big) + 2{e_a}^T PB\epsilon \\ + 2tr(-\widetilde{W}^T\{Proj_m\big(\widehat{W}, \phi\big(\bar{X}(t)\big)\,{\bar{e}_a}^T PB\big) \\ + \widetilde{W}^T\phi\big(\bar{X}(t)\big)\,{\bar{e}_a}^T PB - \widetilde{W}^T\phi\big(\bar{X}(t)\big)\,{\bar{e}_a}^T PB\})\end{aligned} \tag{B.4}$$

By using the trace properties $tr(A+B) = tr(A) + tr(B)$, $tr(A) = tr(A^T)$ and $tr(AB) = tr(BA)\ if\ A \in \mathbb{R}^{n\times m}$ and $B \in \mathbb{R}^{m\times n}$ for any $n, m \in \mathbb{N}_+$, (B.4) can be rewritten as

$$\begin{aligned}\dot{L}(.) = -{e_r}^T Q_r e_r + 2{e_r}^T P_r B\widetilde{W}^T\phi\big(\bar{X}(t_i)\big) + 2{e_r}^T P_r B\epsilon - {e_a}^T Qe_a \\ + 2{\bar{e}_a}^T PB\widetilde{W}^T\phi\big(\bar{X}(t)\big) + 2{e_a}^T PB\epsilon \\ + 2tr\{\big(-\widetilde{W}^T Proj_m\big(\widehat{W}, \phi\big(\bar{X}(t)\big)\,{\bar{e}_a}^T PB\big) \\ - \phi\big(\bar{X}(t)\big)\,{\bar{e}_a}^T PB\}\big) - 2tr\{\widetilde{W}^T\phi\big(\bar{X}(t)\big)\,{\bar{e}_a}^T PB\}\end{aligned} \tag{B.5}$$

By Lemma 11.3 of [56] (from Paper II), $tr[\,\big(\widehat{W} - W\big)^T\{Proj_m\big(\widehat{W}, \phi\big(\bar{X}(t)\big)\,{\bar{e}_a}^T PB\big) - \phi\big(\bar{X}(t)\big)\,{\bar{e}_a}^T PB\}] \leq 0$. After some simplifications, (B.5) becomes

$$\begin{aligned}\dot{L}(.) &\leq -{e_r}^T Q_r e_r + 2{e_r}^T P_r B\widetilde{W}^T \phi\big(X(t_i)\big) + 2{e_r}^T P_r B\epsilon - {e_a}^T Q e_a \\ &\quad + 2{\bar{e}_a}^T PB\widetilde{W}^T \phi\big(\bar{X}(t)\big) + 2{e_a}^T PB\epsilon - 2{\bar{e}_a}^T PB\widetilde{W}^T \phi\big(\bar{X}(t)\big) \\ &= -{e_r}^T Q_r e_r + 2{e_r}^T P_r B\widetilde{W}^T \phi\big(X(t_i)\big) + 2{e_r}^T P_r B\epsilon - {e_a}^T Q e_a \\ &\quad + 2{e_a}^T PB\epsilon\end{aligned} \tag{B.6}$$

Applying norm properties on (B.6) leads to

$$\begin{aligned}\dot{L}(.) \leq &-\lambda_{min}(Q_r)\|e_r\|^2 + 2\|P_r B\|\big\|\widetilde{W}\big\|\big\|\phi\big(X(t_i)\big)\big\|\|e_r\| \\ &+ 2\|\epsilon\|\|P_r B\|\|e_r\| - \lambda_{min}(Q)\|e_a\|^2 \\ &+ 2\|PB\|\|e_a\|\|\epsilon\|.\end{aligned} \tag{B.7}$$

This equation can further be modified by noting that $\|\epsilon\| \leq \epsilon^*$, $\big\|\phi\big(X(t_i)\big)\big\| \leq \phi^*$, and $\big\|\widetilde{W}\big\| \leq \widetilde{W}^*$.

$$\begin{aligned}\dot{L}(.) \leq &-\lambda_{min}(Q_r)\|e_r\|^2 + 2\|P_r B\|\widetilde{W}^*\phi^*\|e_r\| + 2\epsilon^*\|P_r B\|\|e_r\| - \lambda_{min}(Q)\|e_a\|^2 \\ &+ 2\epsilon^*\|PB\|\|e_a\|.\end{aligned}$$

By defining $a_1 \triangleq \lambda_{min}(Q_r)$, $b_1 \triangleq (\|P_r B\|\widetilde{W}^*\phi^* + \epsilon^*\|P_r B\|)$, $a_2 \triangleq \lambda_{min}(Q)$, and $b_2 \triangleq \epsilon^*\|PB\|$

$$\begin{aligned}\dot{L}(.) &\leq -a_1\|e_r\|^2 + 2b_1\|e_r\| - a_2\|e_a\|^2 + 2b_2\|e_a\| \\ &= -(a_1\|e_r\|^2 - 2b_1\|e_r\|) - (a_2\|e_a\|^2 - 2b_2\|e_a\|)\end{aligned} \tag{B.8}$$

So, $\dot{L}(.) \leq 0$ is negative for $\|e_r\| \geq \frac{2b_1}{a_1}$ and $\|e_a\| \geq \frac{2b_2}{a_2}$.

Because the Lyapunov time-derivative has a UUB as seen in (B.8) and the $\widetilde{W}$ is bounded because the projection operator is used in its derivation, the UUB of tracking error and estimation error are now proved at the sampling time.

Case (ii): During inter-event time, using the same Lyapunov function candidate as in (B.1), its time derivative is given as

$$\dot{L}\left(e_r, e_a, \widetilde{W}\right) = 2{e_r}^T P_r \dot{e}_r + 2{e_a}^T P \dot{e}_a + 2\, tr(\widetilde{W}^T \gamma^{-1} \dot{\widetilde{W}}) \tag{B.9}$$

$$= 2{e_r}^T P_r \left(K e_r(t) - K e_{evt} + f\left(X(t)\right) - f\left(X(t_i)\right) + B\widetilde{W}^T \phi\left(X(t_i)\right) + \check{\epsilon}\right)$$

$$+ 2{e_a}^T P(K_2 e_a(t) - K_2 e_{ext} + B\widetilde{W}^T \phi\left(\bar{X}(t)\right) + B\check{\epsilon} + f\left(X(t)\right)$$

$$- f\left(\bar{X}(t)\right)) + 2tr(\widetilde{W}^T \gamma^{-1} \dot{\widetilde{W}})$$

Because $\widetilde{W} = W - \widehat{W}$ so, $\dot{\widetilde{W}} = -\dot{\widehat{W}}$,

$$\dot{L}(.) = {e_r}^T (K^T P_r + P_r K) e_r - 2{e_r}^T P_r K e_{evt} + 2{e_r}^T P_r (f\left(X(t)\right)$$

$$- f\left(X(t_i)\right)) + 2{e_r}^T P_r B\widetilde{W}^T \phi\left(X(t_i)\right) + 2{e_r}^T P_r B\check{\epsilon}$$

$$+ {e_a}^T \left({K_2}^T P + P K_2\right) e_a - 2{e_a}^T P K_2 e_{ext} \tag{B.10}$$

$$+ 2{e_a}^T PB\widetilde{W}^T \phi\left(\bar{X}(t)\right) + 2{e_a}^T PB\check{\epsilon} + 2{e_a}^T P(f(X(t))$$

$$- f(\bar{X}(t))) - 2tr(\widetilde{W}^T \gamma^{-1} \dot{\widehat{W}})$$

By using the projection operator for weight updates, $\dot{\widehat{W}} = \gamma\, Proj_m(\widehat{W}, \phi\left(\bar{X}(t)\right) {\bar{e}_a}^T PB)$, Lyapunov equations ${K_2}^T P + P K_2 = -Q, K^T P_r + P_r K = -Q_r$, $e_a = X(t) - \hat{X}(t) = X(t) - \bar{X}(t) + \bar{X}(t) - \hat{X}(t) = e_{ext} + \bar{e}_a$ and by adding and subtracting $\widetilde{W}^T \phi\left(\bar{X}(t)\right) {\bar{e}_a}^T PB$, (B.10) can be rewritten as

$$\begin{aligned}\dot{L}(.) = &-{e_r}^T Q_r e_r - 2{e_r}^T P_r K e_{evt} + 2{e_r}^T P_r \left(f\big(X(t)\big) - f\big(X(t_i)\big)\right) \\ &+ 2{e_r}^T P_r B \widetilde{W}^T \phi\big(X(t_i)\big) \\ &+ 2{e_r}^T P_r B W^T \left(\left[\phi\big(X(t)\big) - \phi\big(X(t_i)\big)\right] + B\epsilon\right) \\ &- {e_a}^T Q e_a - 2{e_a}^T P K_2 e_{ext} + 2{e_{ext}}^T P B \widetilde{W}^T \phi\big(\bar{X}(t)\big) \\ &+ 2{\bar{e}_a}^T P B \widetilde{W}^T \phi\big(\bar{X}(t)\big) + 2{e_a}^T P B \epsilon \\ &+ 2{e_a}^T P B W^T (\phi(X(t)) - \phi(\bar{X}(t))) \\ &+ 2{e_a}^T P \left(f\big(X(t)\big) - f\big(\bar{X}(t)\big)\right) \\ &+ 2tr(-\widetilde{W}^T \{Proj_m\big(\widehat{W}, \phi\big(\bar{X}(t)\big)\, {\bar{e}_a}^T P B\big) \\ &+ \widetilde{W}^T \phi\big(\bar{X}(t)\big)\, {\bar{e}_a}^T P B - \widetilde{W}^T \phi\big(\bar{X}(t)\big)\, {\bar{e}_a}^T P B\})\end{aligned} \tag{B.11}$$

By using the trace properties $tr(A+B) = tr(A) + tr(B)$, $tr(A) = tr(A^T)$ and $tr(AB) = tr(BA)\ if\ A \in \mathbb{R}^{n\times m}$ and $B \in \mathbb{R}^{m\times n}$ for any $n, m \in \mathbb{N}_+$, (B.11) can be rewritten as

$$\dot{L}(.) = -e_r{}^T Q_r e_r - 2e_r{}^T P_r K e_{evt} + 2e_r{}^T P_r (f(X(t)) - f(X(t_i)))$$
$$+ 2e_r{}^T P_r B\widetilde{W}^T \phi(X(t_i))$$
$$+ 2e_r{}^T P_r B W^T [\phi(X(t)) - \phi(X(t_i))] + 2e_r{}^T P_r B\epsilon$$
$$- e_a{}^T Q e_a - 2e_a{}^T P K_2 e_{ext} + 2e_{ext}{}^T P B\widetilde{W}^T \phi(\bar{X}(t))$$
$$+ 2\bar{e}_a{}^T P B\widetilde{W}^T \phi(\bar{X}(t)) + 2e_a{}^T P B\epsilon \quad \text{(B.12)}$$
$$+ 2e_a{}^T P B W^T (\phi(X(t)) - \phi(\bar{X}(t)))$$
$$+ 2e_a{}^T P \left(f(X(t)) - f(\bar{X}(t))\right)$$
$$+ 2tr\{(-\widetilde{W}^T Proj_m(\widehat{W}, \phi(\bar{X}(t))\, \bar{e}_a{}^T P B)$$
$$- \phi(\bar{X}(t))\, \bar{e}_a{}^T P B\}) - 2tr\{\widetilde{W}^T \phi(\bar{X}(t))\, \bar{e}_a{}^T P B\}$$

By Lemma 11.3 of [56] (from Paper II) $tr[\,(\widehat{W} - W)^T \{Proj_m(\widehat{W}, \phi(\bar{X}(t))\, \bar{e}_a{}^T P B) - \phi(\bar{X}(t))\, \bar{e}_a{}^T P B\}] \leq 0$. After some simplification (B.12) becomes

$$\dot{L}(.) \leq -e_r{}^T Q_r e_r - 2e_r{}^T P_r K e_{evt} + 2e_r{}^T P_r (f(X(t)) - f(X(t_i)))$$
$$+ 2e_r{}^T P_r B\widetilde{W}^T \phi(X(t_i)) + 2e_r{}^T P_r B W^T [\phi(X(t)) - \phi(X(t_i))]$$
$$+ 2e_r{}^T P_r B\epsilon - e_a{}^T Q e_a - 2e_a{}^T P K_2 e_{ext} + 2e_{ext}{}^T P B\widetilde{W}^T \phi(\bar{X}(t))$$
$$+ 2\bar{e}_a{}^T P B\widetilde{W}^T \phi(\bar{X}(t)) + 2e_a{}^T P B\epsilon + 2e_a{}^T P B W^T (\phi(X(t)) - \phi(\bar{X}(t)))$$
$$+ 2e_a{}^T P \left(f(X(t)) - f(\bar{X}(t))\right) - 2\bar{e}_a{}^T P B\widetilde{W}^T \phi(\bar{X}(t))$$

$$
\begin{aligned}
= -{e_r}^T Q_r e_r - 2{e_r}^T P_r K e_{evt} + 2{e_r}^T P_r \left(f\big(X(t)\big) - f\big(X(t_i)\big)\right) \\
+ 2{e_r}^T P_r B \widetilde{W}^T \phi\big(X(t_i)\big) \\
+ 2{e_r}^T P_r B W^T \left[\phi\big(X(t)\big) - \phi\big(X(t_i)\big)\right] + 2{e_r}^T P_r B \epsilon \\
- {e_a}^T Q e_a - 2{e_a}^T P K_2 e_{ext} + 2{e_{ext}}^T P B \widetilde{W}^T \phi\big(\bar{X}(t)\big) \\
+ 2{e_a}^T P B \epsilon + 2{e_a}^T P B W^T \left(\phi\big(X(t)\big) - \phi\big(\bar{X}(t)\big)\right) \\
+ 2{e_a}^T P \left(f\big(X(t)\big) - f\big(\bar{X}(t)\big)\right).
\end{aligned}
\tag{B.13}
$$

Applying norm properties on th right-hand-side of (B.13) leads to

$$
\begin{aligned}
\dot{L}(.) \leq -\lambda_{min}\,(Q_r)\|e_r\|^2 + 2\|P_r K\|\|e_r\|\|e_{evt}\| \\
+ 2\|P_r\|\|e_r\|\left\|f\big(X(t)\big) - f\big(X(t_i)\big)\right\| \\
+ 2\|P_r B\|\left\|\widetilde{W}\right\|\left\|\phi\big(X(t_i)\big)\right\|\|e_r\| \\
+ 2\|P_r B\|\|e_r\|\|W\|\left\|\phi\big(X(t)\big) - \phi\big(X(t_i)\big)\right\| \\
+ 2\|\epsilon\|\|P_r B\|\|e_r\| - \lambda_{min}\,(Q)\|e_a\|^2 \\
+ 2\|P K_2\|\|e_{ext}\|\|e_a\| \\
+ 2\|P B\|\left\|\widetilde{W}\right\|\left\|\phi\big(\bar{X}(t)\big)\right\|\|e_a\| \\
+ 2\|P B\|\|e_a\|\|W\|\left\|\phi\big(X(t)\big) - \phi\big(\bar{X}(t)\big)\right\| \\
+ 2\|P B\|\|e_a\|\|\epsilon\| \\
+ 2\|P\|\|e_a\|\|f(X(t)) - f(\bar{X}(t))\|
\end{aligned}
\tag{B.14}
$$

This equation can further be modified by noting that $\left\|\phi\big(X(t)\big) - \phi(X(t_i))\right\| \leq L_\phi \|X(t) - X(t_i)\| = L_\phi \|e_{evt}\|$, $\|f(X(t)) - f(X(t_i))\| \leq L_f \|X(t) - X(t_i)\| = L_f \|e_{evt}\|$, $\left\|\phi\big(X(t)\big) - \phi(\bar{X}(t))\right\| \leq L_\phi \|X(t) - \bar{X}(t)\| = L_\phi \|e_{ext}\|$, $\|f(X(t)) -$

$f(\bar{X}(t))\| \leq L_f \|X(t) - \bar{X}(t)\| = L_f\|e_{ext}\|, \|\epsilon\| \leq \epsilon^*, \quad \left\|\phi\left(X(t_i)\right)\right\| \leq \phi^*, \quad \|W\| \leq W^*$ and $\left\|\widetilde{W}\right\| \leq \widetilde{W}^*$.

$$\begin{aligned}\dot{L}(.) \leq & -\lambda_{min}\,(Q_r)\|e_r\|^2 + 2\|P_rK\|\|e_r\|\|e_{evt}\| + 2\|P_r\|L_f\|e_{evt}\|\|e_r\| \\ & + 2\|P_rB\|\widetilde{W}^*\phi^*\|e_r\| + 2L_\phi\|P_rB\|W^*\|e_r\|\|e_{evt}\| \\ & + 2\epsilon^*\|P_rB\|\|e_r\| - \lambda_{min}\,(Q)\|e_a\|^2 + 2\|PK_2\|\|e_{ext}\|\|e_a\| \\ & + 2\|PB\|\widetilde{W}^*\phi^*\|e_a\| + 2L_\phi\|PB\|W^*\|e_a\|\|e_{ext}\| + 2\epsilon^*\|PB\|\|e_a\| \\ & + 2L_f\|P\|\|e_{ext}\|\|e_a\|\end{aligned}$$

Also note that $\|e_{evt}\| = \|X(t) - X(t_i)\| = \|X(t) - \bar{X}(t) + \bar{X}(t) - X(t_i)\| \leq \|X(t) - \bar{X}(t)\| + \|\bar{X}(t) - X(t_i)\| = \|e_{ext}\| + \|\bar{X}(t) - X(t_i)\| = \|e_{ext}\| + \|\bar{X}(t) - X_d + X_d - X(t_i)\| \leq \|e_{ext}\| + \|X_d - X(t_i)\| + \|\bar{X}(t) - X_d\| = C_{evt}$. Because X_d and $X(t_i)$ are known and bounded, $\bar{X}(t)$ is also extrapolated state between two known points so it is also known and bounded between two sampled points, so $\bar{X}(t) = \|C_1t^n + C_2t^{n-1} \ldots + C_nt + C_{n+1}\| \leq \tau$ and $\|e_{ext}\| \leq \bar{\mathrm{C}} \in \mathbb{R}_+$, $\|X_d - X(t_i)\| \leq \mathrm{C}_{\bar{e}_{evt}} \in \mathbb{R}_+$ and $\|\check{e}_r\| \leq \mathrm{C}_{\check{e}_r}$ results in $\|e_{evt}\| = \|e_{ext}\| + \|X_d - X(t_i)\| + \|\bar{X}(t) - X_d\| \leq C_{evt}$ where $C_{evt} \triangleq \bar{\mathrm{C}} + \mathrm{C}_{\bar{e}_{evt}} + \mathrm{C}_{\check{e}_r}$. This leads to,

$$\begin{aligned}\dot{L}(.) \leq & -\lambda_{min}\,(Q_r)\|e_r\|^2 + 2\|P_rK\|C_{evt}\|e_r\| + 2\|P_r\|L_fC_{evt}\|e_r\| + 2\|P_rB\|\widetilde{W}^*\phi^*\|e_r\| \\ & + 2L_\phi\|P_rB\|W^*C_{evt}\|e_r\| + 2\epsilon^*\|P_rB\|\|e_r\|) - \lambda_{min}\,(Q)\|e_a\|^2 \\ & + 2\|PK_2\|\bar{\mathrm{C}}\,\|e_a\| + 2\|PB\|\widetilde{W}^*\phi^*\|e_a\| + 2L_\phi\|PB\|W^*\bar{\mathrm{C}}\,\|e_a\| \\ & + 2\epsilon^*\|PB\|\|e_a\| + 2L_f\|P\|\bar{\mathrm{C}}\,\|e_a\|\end{aligned}$$

$$= -\lambda_{min}(Q_r)\|e_r\|^2$$
$$+ 2\big(\|P_rK\|C_{evt} + \|P_r\|L_fC_{evt} + \|P_rB\|\widetilde{W}^*\phi^* + L_\phi\|P_rB\|W^*C_{evt}\|e_r\|$$
$$+ \epsilon^*\|P_rB\|\big)\|e_r\| - \lambda_{min}(Q)\|e_a\|^2 + 2(\|PK_2\|\bar{\mathbb{C}} + \|PB\|\widetilde{W}^*\phi^*$$
$$+ L_\phi\|PB\|W^*\bar{\mathbb{C}} + \epsilon^*\|PB\| + L_f\|P\|\bar{\mathbb{C}})\|e_a\|$$

By defining $a_3 \triangleq \lambda_{min}(Q_r)$, $b_3 \triangleq (\|P_rK\|C_{evt} + \|P_r\|L_fC_{evt} + \|P_rB\|\widetilde{W}^*\phi^* + L_\phi\|P_rB\|W^*C_{evt} + \epsilon^*\|P_rB\|)$, $a_4 \triangleq \lambda_{min}(Q)$, $b_4 \triangleq (\|PK_2\|\bar{\mathbb{C}} + \|PB\|\widetilde{W}^*\phi^* + L_\phi\|PB\|W^*\bar{\mathbb{C}} + \epsilon^*\|PB\| + L_f\|P\|\bar{\mathbb{C}})$

$$\dot{L}(.) \le -a_3\|e_r\|^2 + 2b_3\|e_r\| - a_4\|e_a\|^2 + 2b_4\|e_a\|$$
$$= -(a_3\|e_r\|^2 - 2b_3\|e_r\|) - (a_4\|e_a\|^2 - 2b_4\|e_a\|) \quad \text{(B.15)}$$

So, for $\dot{L}(.) \le 0$, $\|e_r\| \ge \frac{2b_3}{a_3}$ and $\|e_a\| \ge \frac{2b_4}{a_4}$.

Because the Lyapunov time derivative has a UUB as seen in (B.15) and the $\widetilde{W}$ is bounded because the projection operator is used in its derivation, the UUB of tracking error and estimation error are now proved for all time.

B.1.1. Comment (ISS Stability). An interesting point to note is that this formulation, with Theorem 1, exhibits input to state stable (ISS) characteristics. ISS is taken as an assumption in some literature, such as in [34] (from Paper II) etc., but *not* in this formulation. Instead it naturally appears. From (B.1), $L(e_r)$ is continuously differentiable and because $\lambda_{min}(P_r)\|e_r\|^2 + \|\gamma^{-1}\|\|\widetilde{W}\| \le \|L(e_r)\| \le \lambda_{max}(P_r)\|e_r\|^2 + \|\gamma^{-1}\|\|\widetilde{W}\|$, so $\|L(e_r)\|$ is upper and lower bounded by K_∞ functions. Also it shows that e_r will stay bounded and $\dot{L}$ is less than or equal to a negative definite function (B.8) and (B.15), then, by definition [46] (from Paper II), system $\dot{e_r} = f(e_r(t), e_{evt})$ is ISS.

B.2. COROLLARY 1.1: ULTIMATE UPPER BOUND ON TRACKING ERROR

Proof: From (B.8) and (B.15) it follows that $\dot{L} \leq 0$ outside the compact set D_s

$$D_s \triangleq \{e_a, \hat{e}_r : \|e_a\| \leq \psi_1\} \cap \{e_a, \hat{e}_r : \|\hat{e}_r\| \leq \varepsilon\}.$$

Because L cannot grow outside D_s, so it is lower and upper bounded as

$$\lambda_{min}(P_r)\| e_r\|^2 \leq \|L\| \leq \lambda_{max}(P_r)\| e_r\|^2. \tag{B.16}$$

As is known $\|e_r\| = \|e_a\| + \|\hat{e}_r\| \leq \psi_1 + \varepsilon$ so

$$\lambda_{min}(P_r)\| e_r\|^2 \leq \|L\| \leq \lambda_{max}(P_r)\psi_1 + \lambda_{max}(P_r)\varepsilon$$

$$\lambda_{min}(P_r)\| e_r\|^2 \leq \|L\| \leq \lambda_{max}(P_r)\psi_1 + \lambda_{max}(P_r)\varepsilon$$

$$\lambda_{min}(P)\| e_r\|^2 \leq \vartheta_1$$

where $\vartheta_1 \triangleq \lambda_{max}(P_r)\psi_1 + \lambda_{max}(P_r)\varepsilon$. It leads to,

$$\|e_r\| \leq \sqrt{\vartheta_1/\lambda_{min}(P_r)} \tag{B.17}$$

B.3. PROOF OF THEOREM 2

Proof for the Theorem 2 of the Paper II is similar to the one for Scheme 1, because the tracking error expression is the same in both cases and expression for estimation error is just like case (i) of the scheme 1. It can be proved by choosing Lyapunov function candidate as in (1). ISS properties and upper bound on the tracking error for this ETNAC-2 can also be found by following the similar approach as used for Scheme 1.

APPENDIX C.

PROOF OF THE THEOREM OF THE PAPER III

The proof of the theorem 1 from the Paper III is also done using Lyapunov analysis. Choosing a barrier Lyapunov function candidate as

$$
\begin{aligned}
& L\left(e_r, e_a, \widetilde{W}, X\right) \\
&= \sum_{j=1}^{l} \{ f_{asym}\left(e_{r_j}\right) \bar{f}_{bl}\left(\left\| K_{e_{r_j}} e_r \right\|_I\right) \\
&+ \left(1 - f_{asym}\left(e_{r_j}\right)\right) \underline{f}_{bl}\left(\left\| K_{e_{r_j}} e_r \right\|_I\right)\} \\
&+ \sum_{i=1}^{q} \{ f_{asym}(x_i)\, \bar{f}_{bl}\left(\left\| K_{x_i} X \right\|_I\right) \\
&+ \left(1 - f_{asym}(x_i)\right) \underline{f}_{bl}\left(\left\| K_{x_i} X \right\|_I\right)\} \quad + tr\left(\widetilde{W}^T {\gamma_w}^{-1} \widetilde{W}\right) \\
&+ {e_a}^T P_a e_a \\
&= \overline{L}_1 + \underline{L}_1 + \overline{L}_2 + \underline{L}_2 + L_3
\end{aligned}
\tag{C.1}
$$

where $\overline{L}_1 \triangleq \sum_{j=1}^{l} \left\{ f_{asym}\left(e_{r_j}\right) \bar{f}_{bl}\left(\left\| K_{e_{r_j}} e_r \right\|_I\right)\right\}$, $\underline{L}_1 \triangleq \sum_{j=1}^{l} \left\{ \left(1 - f_{asym}\left(e_{r_j}\right)\right) \underline{f}_{bl}\left(\left\| K_{e_{r_j}} e_r \right\|_I\right)\right\}$, $\overline{L}_2 \triangleq \sum_{i=1}^{q} \{ f_{asym}(x_i)\, \bar{f}_{bl}\left(\left\| K_{x_i} X \right\|_I\right)\}$, $\underline{L}_2 \triangleq \sum_{i=1}^{q} \left\{ \left(1 - f_{asym}(x_i)\right) \underline{f}_{bl}\left(\left\| K_{x_i} X \right\|_I\right)\right\}$, and $L_3 \triangleq tr\left(\widetilde{W}^T {\gamma_w}^{-1} \widetilde{W}\right) + {e_a}^T P_a e_a$.

Time derivative of L can be given as

$$
\dot{L}\left(e_r, e_a, \widetilde{W}, X\right) = \dot{\overline{L}}_1 + \dot{\underline{L}}_1 + \dot{\overline{L}}_2 + \dot{\underline{L}}_2 + \dot{L}_3. \tag{C.2}
$$

(i) Now taking each component of L separately. First consider $\overline{L}_1$

$$\dot{\bar{L}}_1\left(e_{r_j}\right) = \sum_{j=1}^{l} \frac{d\, f_{asym}\left(e_{r_j}\right) \bar{f}_{bl}\left(\left\| K_{e_{r_j}} e_r \right\|_I\right)}{d\, \left\| K_{e_{r_j}} e_r \right\|_I^{\,2}} \cdot \frac{d\, \left\| K_{e_{r_j}} e_r \right\|_I^{\,2}}{dt}$$

$$= 2 \sum_{j}^{l} f_{asym}(e_{r_j})\, D\bar{f}_{bl}\big|_{e_{r_j}|}\, {e_r}^T {K_{e_{r_j}}}^T K_{e_{r_j}} \dot{e_r}. \tag{C.3}$$

Using tracking error dynamics from (15), (31) (from the Paper III) becomes

$$\dot{\bar{L}}_1\left(e_{r_j}\right) = 2 \sum_{i}^{l} f_{asym}(e_{r_j})\, D\bar{f}_{bl}\big|_{e_{r_j}|}\, {e_r}^T {K_{e_{r_j}}}^T K_{e_{r_j}} (K e_r + g\left(\widetilde{W}^T \phi\left(X(t)\right) + \epsilon\right)$$

$$- \sum_{j=1}^{l} \{ f_{asym}(e_{r_j})\, \alpha_{e_{r_j}}\, D\bar{f}_{bl}\big|_{e_{r_j}|}\, g g^T K_{e_{r_j}} e_r$$

$$+ \left(1 - f_{asym}\left(e_{r_j}\right)\right) \alpha_{e_{r_j}}\, D\underline{f}_{bl}\big|_{e_{r_j}|} g g^T K_{e_{r_j}} e_r \}$$

$$- \sum_{i=1}^{l} \{ f_{asym}(x_i)\, \alpha_{x_i}\, D\bar{f}_{bl\,|x_i|} g g^T K_{x_i} X$$

$$+ \left(1 - f_{asym}(x_i)\right) \alpha_{x_i}\, D\underline{f}_{bl\,|x_i|} g g^T K_{x_i} X \}).$$

$$= 2\sum_{j}^{l} f_{asym}\left(e_{r_j}\right) D\bar{f}_{bl}\big|_{e_{r_j}|}\, {e_r}^T {K_{e_{r_j}}}^T K_{e_{r_j}} K e_r$$

$$+ 2\sum_{j}^{l} f_{asym}\left(e_{r_j}\right) D\bar{f}_{bl}\big|_{e_{r_j}|}\, {e_r}^T {K_{e_{r_j}}}^T K_{e_{r_j}} \{\, g\left(\widetilde{W}^T \phi\left(X(t)\right) + \epsilon\right)$$

$$- \sum_{i=1}^{q} \{ f_{asym}(x_i)\; \alpha_{x_i}\, D\bar{f}_{bl\,|x_i|} g g^T K_{x_i} X$$

$$+ \left(1 - f_{asym}(x_i)\right) \alpha_{x_i}\, D\underline{f}_{bl\,|x_i|} g g^T K_{x_i} X \}) \qquad \text{(C.4)}$$

$$- 2\sum_{j}^{l} f_{asym}\left(e_{r_j}\right) D\bar{f}_{bl}\big|_{e_{r_j}|}\, {e_r}^T {K_{e_{r_j}}}^T K_{e_{r_j}} \sum_{j=1}^{l} \{ f_{asym}(e_{r_j})\; \alpha_{e_{r_j}}\, D\bar{f}_{bl}\big|_{e_{r_j}|}\, g g^{\prime}$$

$$- 2\sum_{j}^{l} f_{asym}\left(e_{r_j}\right) D\bar{f}_{bl}\big|_{e_{r_j}|}\, {e_r}^T {K_{e_{r_j}}}^T K_{e_{r_j}} \sum_{j=1}^{l} \Big\{ \Big(1$$

$$- f_{asym}\left(e_{r_j}\right)\Big) \alpha_{e_{r_j}}\, D\underline{f}_{bl}\big|_{e_{r_j}|} g g^T K_{e_{r_j}} e_r \Big\}.$$

Equation (C.4) can be simplified by considering the following steps:

A- Note that ${K_{e_{r_j}}}^T K_{e_{r_j}}$ has only one of diagonal entity as 1 corresponding to e_{r_j} and all rest of the elements are 0. So, for a $Y \in \mathbb{R}^n$ and for a Hurwitz matrix K, it leads to ${e_r}^T {K_{e_{r_j}}}^T K_{e_{r_j}} K e_r = e_{r_j} \sum_{i=1}^{n} K(j,i) e_{r_j} = -K(j,j) {e_{r_j}}^2$.

B- Note that $\bar{g} \triangleq g\, g^T \in \mathbb{R}^{n\times n} \geq 0$ (it is a positive semi-definite matrix). Using distributivity of the finite summation/multiplication for $\sum_j^l f_{asym}\left(e_{r_j}\right) D\bar{f}_{bl}\big|_{e_{r_j}|}\, {e_r}^T {K_{e_{r_j}}}^T K_{e_{r_j}} \sum_{j=1}^{l} \{ f_{asym}(e_{r_j})\; \alpha_{e_{r_j}}\, D\bar{f}_{bl}\big|_{e_{r_j}|}\, g g^T K_{e_{r_j}} e_r \} =$

$g g^T \sum_j^l f_{asym}\left(e_{r_j}\right) D\bar{f}_{bl}\big|_{e_{r_j}|}\, e_{r_j} \sum_{j=1}^{l} f_{asym}(e_{r_j})\; \alpha_{e_{r_j}}\, D\bar{f}_{bl}\big|_{e_{r_j}|}\, e_{r_j} =$

$gg^T \sum_j^l D\bar{f}_{bl}\big|_{e_{r_j}}\big|^2 (f_{asym}(e_{r_j}))^2 \alpha_{e_{r_j}} {e_{r_j}}^2$ where for any $e_{r_j} e_{r_k} = \begin{cases} {e_{r_j}}^2 & j = k \\ 0 & j \neq k \end{cases}$ and $(f_{asym}(e_{r_j}))^2 \alpha_{e_{r_j}}$ is a non-negative scalar, so $\sum_j^l f_{asym}\left(e_{r_j}\right) D\bar{f}_{bl}\big|_{e_{r_j}}| {e_r}^T {K_{e_{r_j}}}^T K_{e_{r_j}} \sum_{j=1}^l \{f_{asym}(e_{r_j})\, \alpha_{e_{r_j}} D\bar{f}_{bl}\big|_{e_{r_j}}| gg^T K_{e_{r_j}} e_r\} \geq 0$ and negative of it will be non-positive. By the same principle, $-2\sum_j^l f_{asym}\left(e_{r_j}\right) D\bar{f}_{bl}\big|_{e_{r_j}}| {e_r}^T {K_{e_{r_j}}}^T K_{e_{r_j}} \sum_{j=1}^l \left\{\left(1 - f_{asym}\left(e_{r_j}\right)\right) \alpha_{e_{r_j}} D\underline{f}_{bl}\big|_{e_{r_j}}| gg^T K_{e_{r_j}} e_r\right\} \leq 0$. So, these two terms can be eliminated from (C.4) by using the inequality for higher right-hand side.

C- Consider now the multiplicative terms with e_r

$$\sum_j^l f_{asym}\left(e_{r_j}\right) D\bar{f}_{bl}\big|_{e_{r_j}}| {e_r}^T {K_{e_{r_j}}}^T K_{e_{r_j}} \sum_{i=1}^q \{f_{asym}(x_i)\, \alpha_{x_i} D\bar{f}_{bl|x_i|} gg^T K_{x_i} X$$

$$= \sum_j^l f_{asym}\left(e_{r_j}\right) D\bar{f}_{bl}\big|_{e_{r_j}}| D\bar{f}_{bl|x_i|} f_{asym}(x_j)\, \alpha_{x_j} gg^T(j)\, e_{r_j} x_j$$

Since $e_{r_j} x_j = e_{r_j}\left(x_j - x_{d_j} + x_{d_j}\right) = e_{r_j}\left(e_{r_j} + x_{d_j}\right) = {e_{r_j}}^2 + e_{r_j} x_{d_j}$, so

$$\sum_j^l f_{asym}\left(e_{r_j}\right) D\bar{f}_{bl}\big|_{e_{r_j}}| D\bar{f}_{bl|x_i|} f_{asym}(x_j)\, \alpha_{x_j} gg^T(j)\, e_{r_j} x_j$$

$$= \sum_j^l f_{asym}\left(e_{r_j}\right) D\bar{f}_{bl}\big|_{e_{r_j}}| D\bar{f}_{bl|x_j|} f_{asym}(x_j)\, \alpha_{x_j} gg^T(j)({e_{r_j}}^2 + e_{r_j} x_{d_j})$$

Similarly, $\sum_j^l f_{asym}\left(e_{r_j}\right) D\bar{f}_{bl}\big|_{e_{r_j}|}\, {e_r}^T {K_{e_{r_j}}}^T K_{e_{r_j}} \sum_{i=1}^q \{\big(1 - f_{asym}(x_i)\big)\, \alpha_{x_i}\, D\underline{f}_{bl}{}_{|x_i|} gg^T K_{x_i} X\} = \sum_j^l f_{asym}\left(e_{r_j}\right)\big(1 - f_{asym}(x_j)\big) D\bar{f}_{bl}\big|_{e_{r_j}|}\, D\underline{f}_{bl}{}_{|x_j|}\, \alpha_{x_j} gg^T(j)({e_{r_j}}^2 + e_{r_j} x_{d_j})$.

Considering the results in A-C, (C.4) can be rewritten as

$$\begin{aligned}
\dot{\bar{L}}_1(.) \leq -2 \sum_{j=1}^{l} \{ & f_{asym}\left(e_{r_j}\right) D\bar{f}_{bl}\big|_{e_{r_j}|} (K(j,j) + D\bar{f}_{bl|x_j|} \big| f_{asym}(x_j) \big|\ \left|\alpha_{x_j}\right| (gg^T)_j \\
& + \big(1 - f_{asym}(x_j)\big) D\underline{f}_{bl}{}_{|x_i|}\ \left|\alpha_{x_j}\right| (gg^T)_j \} {e_{r_j}}^2 \\
& + 2 \sum_{i}^{q} f_{asym}\left(e_{r_j}\right) D\bar{f}_{bl}\big|_{e_{r_j}|}\, e_{r_j} \left(\{\left(g\widetilde{W}^T \phi\big(X(t)\big)\right)_i + (g\epsilon)_i \right. \\
& + D\bar{f}_{bl|x_j|} \big| f_{asym}(x_j) \big|\ \left|\alpha_{x_j}\right| (gg^T)_{(i,i)} e_{r_j} x_{d_j} \\
& \left. + D\underline{f}_{bl}{}_{|x_j|} \big(1 - f_{asym}(x_j)\big) \left|\alpha_{x_j}\right| (gg^T)_{(i,i)} e_{r_j} x_{d_j} \right\}
\end{aligned}$$

$$
\begin{aligned}
&= -2\sum_{j}^{q}\{\left|f_{asym}\left(e_{r_j}\right)\right| D\bar{f}_{bl}{}_{\left|e_{r_j}\right|}(\,K(j,j)\\
&+ \left|D\bar{f}_{bl}{}_{|x_j|}\right| \left|f_{asym}(x_j)\right| \left|\alpha_{x_j}\right| (gg^T)_j\\
&+ \left(1 - f_{asym}(x_j)\right) \left|D\underline{f}_{bl}{}_{|x_i|}\right| \left|\alpha_{x_j}\right| (gg^T)_j\}\, e_{r_j}{}^2\\
&+ 2\sum_{i}^{q} f_{asym}\left(e_{r_j}\right) D\bar{f}_{bl}{}_{\left|e_{r_j}\right|}\, e_{r_j}\,(\{\left(g\widetilde{W}^T\phi\left(X(t)\right)\right)_i\\
&+ (g\epsilon)_i + D\bar{f}_{bl}{}_{|x_j|}\left|f_{asym}(x_j)\right| \left|\alpha_{x_j}\right| (gg^T)_{(i,i)} e_{r_j} x_{d_j}\\
&+ D\underline{f}_{bl}{}_{|x_j|}\left(1 - f_{asym}(x_j)\right) \left|\alpha_{x_j}\right| (gg^T)_{(i,i)} e_{r_j} x_{d_j}\}.
\end{aligned}
\tag{C.5}
$$

Applying norm properties [33] (from the Paper III) to the terms on the right-hand side of (C.5),

$$
\begin{aligned}
&\dot{\bar{L}}_1(.) \\
&\leq -2\sum_{j}^{l}\{ (D\bar{f}_{bl}|_{e_{r_j}|} \left|f_{asym}\left(e_{r_j}\right)\right| (\|K(j,j)\| \\
&+ \left|D\bar{f}_{bl|x_j|}\right| |f_{asym}(x_j)| \left|\alpha_{x_j}\right| (gg^T)_j \\
&+ \left(1 - f_{asym}(x_j)\right) \left|D\underline{f}_{bl}{}_{|x_i|}\right| \left|\alpha_{x_j}\right| (gg^T)_j)\ {e_{r_j}}^2\} \\
&+ 2\sum_{i}^{q}\{\left| f_{asym}\left(e_{r_j}\right)\right| \left|D\bar{f}_{bl}|_{e_{r_j}|}\right| \left\{\|g\|\left\|\widetilde{W}^T\phi\left(X(t)\right)\right\|_i \right. \\
&\left. + \|g\|\|\epsilon\|_i\right\} \left|e_{r_j}\right| \\
&+ \left|D\bar{f}_{bl|x_j|}\right| |f_{asym}(x_j)| \left|\alpha_{x_j}\right| \|gg^T\|_{(i,i)} \left|e_{r_j}x_{d_j}\right| \\
&+ \left|D\underline{f}_{bl}{}_{|x_j|}\right| |1 - f_{asym}(x_j)| \left|\alpha_{x_j}\right| \|gg^T\|_{(i,i)} \left|e_{r_j}x_{d_j}\right|\}.
\end{aligned}
\tag{C.6}
$$

Equation (C.6) can be further modified by noting that $\|\epsilon\| \leq \epsilon^*$, $\|\phi(X)\| \leq \phi^*$, $\left\|\widetilde{W}\right\| \leq \widetilde{W}^*$, and $\|W\| \leq W^*$. Also applying Young's inequality [33] (from the Paper III) on $e_{r_j}x_{d_j} = \alpha_y {e_{r_j}}^2 + \frac{1}{\alpha_y}{x_{d_j}}^2$ for a $\alpha_y = 1,$ yields in

$$\dot{\bar{L}}_1(.) \leq -2\sum_{j}^{l}\{\,(D\bar{f}_{bl}|_{e_{r_j}|}\left|f_{asym}\left(e_{r_j}\right)\right|(\|K(j,j)\|$$

$$+\left|D\bar{f}_{bl}|_{x_j|}\right|\left|f_{asym}(x_j)\right|\left|\alpha_{x_j}\right|(gg^T)_j$$

$$+\left(1-f_{asym}(x_j)\right)\left|D\underline{f}_{bl}|_{x_i|}\right|\left|\alpha_{x_j}\right|(gg^T)_j\,{e_{r_j}}^2\}$$

$$+2\sum_{i}^{q}\left\{\left|f_{asym}\left(e_{r_j}\right)\right|\left|D\bar{f}_{bl}|_{e_{r_j}|}\right|\{\|g\|\widetilde{W}^*\phi^*+\|g\|\epsilon^*\}\left|e_{r_j}\right|\right.$$

$$+\left|D\bar{f}_{bl}|_{x_j|}\right|\left|f_{asym}(x_j)\right|\left|\alpha_{x_j}\right|\|gg^T\|_{(i,i)}\,(\alpha_y{e_{r_j}}^2+\frac{1}{\alpha_y}{x_{d_j}}^2)$$

$$\left.+\left|D\underline{f}_{bl}|_{x_j|}\right|\left|1-f_{asym}(x_j)\right|\left|\alpha_{x_j}\right|\|gg^T\|_{(i,i)}(\alpha_y{e_{r_j}}^2+\frac{1}{\alpha_y}{x_{d_j}}^2)\right\}$$

$$\leq -2\sum_{j}^{l}\{\,(D\bar{f}_{bl}|_{e_{r_j}|}\left|f_{asym}\left(e_{r_j}\right)\right|(\|K(j,j)\|)\,{e_{r_j}}^2\}$$

$$+2\sum_{j}^{l}\left\{\left|f_{asym}\left(e_{r_j}\right)\right|\left|D\bar{f}_{bl}|_{e_{r_j}|}\right|\{\|g\|\widetilde{W}^*\phi^*\right.$$

$$\left.+\|g\|\epsilon^*\}\left|e_{r_j}\right|\right. \tag{C.7}$$

$$+\left|D\bar{f}_{bl}|_{x_j|}\right|\left|f_{asym}(x_j)\right|\left|\alpha_{x_j}\right|\|gg^T\|_{(i,i)}\,{x_{d_j}}^2$$

$$\left.+\left|D\underline{f}_{bl}|_{x_j|}\right|\left|1-f_{asym}(x_j)\right|\left|\alpha_{x_j}\right|\|gg^T\|_{(i,i)}{x_{d_j}}^2)\right\}$$

Note that $\left|x_{d_j}\right| \leq \overline{x_{d_j}}$, so by defining $c_{1_j} \triangleq \left|D\bar{f}_{bl}|_{x_j|}\right|\left|f_{asym}(x_j)\right|\left|\alpha_{x_j}\right|\|gg^T\|_{(i,i)}\,\overline{x_{d_j}}^{\,2} + \left|D\underline{f}_{bl}|_{x_j|}\right|\left|1-f_{asym}(x_j)\right|\left|\alpha_{x_j}\right|\|gg^T\|_{(i,i)}\overline{x_{d_j}}^{\,2}$ results in

$$\dot{\bar{L}}_1(.) \leq -\sum_j^l \{ (2D\bar{f}_{bl}|_{e_{r_j}|} \left|f_{asym}\left(e_{r_j}\right)\right| (\|K(j,j)\|)\, {e_{r_j}}^2\}$$

$$+ 2\sum_{j=1}^{l} \{\left| f_{asym}\left(e_{r_j}\right)\right| \left|D\bar{f}_{bl}|_{e_{r_j}|}\right| \{\|g\|\widetilde{W}^*\phi^* \quad \text{(C.8)}$$

$$+ \|g\|\epsilon^*\} \left|e_{r_j}\right| + \sum_{j=1}^{l} c_{1_j}$$

Define $a_{1_j} \triangleq 2D\bar{f}_{bl}|_{e_{r_j}|} \left|f_{asym}\left(e_{r_j}\right)\right| (\|K(j,j)\|$ and $b_{1_j} \triangleq$

$\{\left| f_{asym}\left(e_{r_j}\right)\right| \left|D\bar{f}_{bl}|_{e_{r_j}|}\right| \{\|g\|\widetilde{W}^*\phi^* + \|g\|\epsilon^*\}$. Note that defined coefficients are positive. Now (C.8) can be rewritten as

$$\dot{\bar{L}}_1(.) \leq -\sum_j^l a_{1_j}\, {e_{r_j}}^2 + \sum_j^l 2b_{1_j} \left|e_{r_j}\right| + \sum_j^l c_{1_j} \quad \text{(C.9)}$$

For $\xi \in \mathbb{R}_+$, such that $0 < \xi < 1$.

$$\dot{\bar{L}}_1(.) \leq -\xi \sum_j^l a_{1_j}\, {e_{r_j}}^2 - \sum_i^l \{(1-\xi)a_{1_j}\, {e_{r_j}}^2 - 2b_{1_j} \left|e_{r_j}\right| - c_{1_j}\}$$

$$= -\xi \textstyle\sum_j^l a_{1_j}\, {e_{r_j}}^2 - \sum_i^l \{ \left(\sqrt{(1-\xi)a_{1_j}}\, e_{r_j}\right)^2 - 2\sqrt{(1-\xi)a_{1_j}}.\frac{b_{1_j}}{\sqrt{(1-\xi)a_{1_j}}} \left|e_{r_j}\right| +$$

$$\left(\frac{b_{1_j}}{\sqrt{(1-\xi)a_{1_j}}}\right)^2 - \left(\frac{b_{1_j}}{\sqrt{(1-\xi)a_{1_j}}}\right)^2 - c_{1_j}\}$$

$$= -\xi \sum_j^l a_{1_j}\, {e_{r_j}}^2 - \sum_j^l \{[\sqrt{(1-\xi)a_{1_j}}\, \left|e_{r_j}\right| - \frac{b_{1_j}}{\sqrt{(1-\xi)a_{1_j}}}]^2 - \frac{{b_{1_j}}^2}{(1-\xi)a_{1_j}} - c_{1_j}\}$$

$$\leq -\xi \sum_j^l a_{1_j} {e_{r_j}}^2 \quad , \qquad \text{if } \left|e_{r_j}\right| \geq \frac{\left(\sqrt{{b_{1_j}}^2+(1-\xi)a_{1_j}c_{1_j}}\right)+b_{1_j}}{(1-\xi)a_{1_j}}. \tag{C.10}$$

(ii) Now taking $\underline{\dot{L}}_1\left(e_{r_j}\right)$

$$\underline{\dot{L}}_1\left(e_{r_j}\right) = \sum_{j=1}^{l} \frac{d\,(1-f_{asym}\left(e_{r_j}\right))\underline{f}_{bl}\left(\left\|K_{e_{r_j}}e_r\right\|_I\right)}{d\,\left\|K_{e_{r_j}}e_r\right\|_I^2}.\frac{d\,\left\|K_{e_{r_j}}e_r\right\|_I^2}{dt}$$

$$= 2\sum_j^q \left(1-f_{asym}\left(e_{r_j}\right)\right) D\underline{f}_{bl}\Big|_{e_{r_j}|} {e_r}^T {K_{e_{r_j}}}^T K_{e_{r_j}}\dot{e_r}.$$

Following the same approach as is taken for (i), it can be proved that

$$\underline{\dot{L}}_1\left(e_{r_j}\right) \leq -\xi \sum_j^l a_{2_j} {e_{r_j}}^2 \quad , \text{ if } \left|e_{r_j}\right| \geq \frac{\left(\sqrt{{b_{2_j}}^2+(1-\xi)a_{2_j}c_{2_j}}\right)+b_{2_j}}{(1-\xi)a_{2_j}} \tag{C.11}$$

where $a_{2_j} \triangleq 2D\underline{f}_{bl}\Big|_{e_{r_j}|}(\left|1-f_{asym}\left(e_{r_j}\right)\right|)(\|K(j,j)\|, b_{2_j} \triangleq 2\{\left|1-f_{asym}\left(e_{r_j}\right)\right|\left|D\underline{f}_{bl}\Big|_{e_{r_j}|}\right|\{\|g\|\widetilde{W}^*\phi^* + \|g\|\epsilon^*\}$, and $c_{2_j} \triangleq \left|D\bar{f}_{bl|x_j|}\right|\left|f_{asym}(x_j)\right|\left|\alpha_{x_j}\right|\|gg^T\|_{(i,i)}\,\overline{x_{d_j}}^2 + \left|D\underline{f}_{bl}\Big|_{x_j|}\right|\left|1-f_{asym}(x_j)\right|\left|\alpha_{x_j}\right|\|gg^T\|_{(i,i)}\overline{x_{d_j}}^2$. The defined coefficients a_{2_j}, b_{2_j}, and c_{2_j} are positive scalars.

(iii) Now consider the $\dot{\underline{L}}_2$

$$\dot{\bar{L}}_2(x_i) = \sum_i^q \frac{d\,\bar{f}_{bl}\left(\left\|K_{x_i}X\right\|_I\right)}{d\left\|K_{x_i}X\right\|_I^{\,2}} \cdot \frac{d\left\|K_{x_i}X\right\|_I^{\,2}}{dt} = 2\sum_i^q D\bar{f}_{bl}\left\|_{K_{x_i}X}\right\|_I X^T {K_{x_i}}^T K_{x_i}\dot{X}. \tag{C.12}$$

By using the system dynamics from (10 (from the Paper III)),

$$\begin{aligned}\dot{\bar{L}}_2(x_i) = 2\sum_i^q D\bar{f}_{bl}\left\|_{K_{x_i}X}\right\|_I X^T {K_{x_i}}^T K_{x_i}(f^*(X_d) + KX - KX_d + g\widetilde{W}^T\phi\big(X(t)\big) + g\epsilon \\ - \sum_{j=1}^{l}\{f_{asym}\left(e_{r_j}\right)\,\alpha_{e_{r_j}}\,D\bar{f}_{bl}\big|_{e_{r_j}|}\,gg^T K_{e_{r_j}}e_r \\ + \left(1 - f_{asym}\left(e_{r_j}\right)\right)\alpha_{e_{r_j}}\,D\underline{f}_{bl}\big|_{e_{r_j}|}gg^T K_{e_{r_j}}e_r\} \\ - \sum_{i=1}^{q}\{f_{asym}(x_i)\,\alpha_{x_i}\,D\bar{f}_{bl}\left\|_{K_{x_i}X}\right\|_I gg^T K_{x_i}X \\ + \left(1 - f_{asym}(x_i)\right)\alpha_{x_i}\,D\underline{f}_{bl}\left\|_{K_{x_i}X}\right\|_I gg^T K_{x_i}X\}).\end{aligned}$$

$$\begin{aligned}= 2\sum_i^q D\bar{f}_{bl}\left\|_{K_{x_i}X}\right\|_I X^T {K_{x_i}}^T K_{x_i}(f^*(X_d) + KX - KX_d + g\widetilde{W}^T\phi\big(X(t)\big) + g\epsilon \\ - \sum_{j=1}^{l}\{f_{asym}\left(e_{r_j}\right)\,\alpha_{e_{r_j}}\,D\bar{f}_{bl}\big|_{e_{r_j}|}\,gg^T K_{e_{r_j}}e_r \\ + \left(1 - f_{asym}\left(e_{r_j}\right)\right)\alpha_{e_{r_j}}\,D\underline{f}_{bl}\big|_{e_{r_j}|}gg^T K_{e_{r_j}}e_r\} \\ - \sum_{i=1}^{q}\{f_{asym}(x_i)\,\alpha_{x_i}\,D\bar{f}_{bl}\left\|_{K_{x_i}X}\right\|_I gg^T K_{x_i}X \\ + \left(1 - f_{asym}(x_i)\right)\alpha_{x_i}\,D\underline{f}_{bl}\left\|_{K_{x_i}X}\right\|_I gg^T K_{x_i}X\})\end{aligned}$$

$$= 2\sum_{i}^{q} D\bar{f}_{bl}\left\|_{K_{x_i}X}\right\|_I X^T {K_{x_i}}^T K_{x_i} KX$$

$$+ 2\sum_{i}^{q} D\bar{f}_{bl}\left\|_{K_{x_i}X}\right\|_I X^T {K_{x_i}}^T K_{x_i} \Bigg\{ f^*(X_d) - KX_d + g\widetilde{W}^T \phi\big(X(t)\big) + g\epsilon$$

$$- \sum_{j=1}^{l} \{ f_{asym}\left(e_{r_j}\right)\, \alpha_{e_{r_j}}\, D\bar{f}_{bl}\big|_{e_{r_j}|}\, gg^T K_{e_{r_j}} e_r$$

$$+ \left(1 - f_{asym}\left(e_{r_j}\right)\right) \alpha_{e_{r_j}}\, D\underline{f}_{bl}\big|_{e_{r_j}|} gg^T K_{e_{r_j}} e_r \} \Bigg\} \qquad \text{(C.13)}$$

$$- 2\sum_{i}^{q} D\bar{f}_{bl}\left\|_{K_{x_i}X}\right\|_I X^T {K_{x_i}}^T K_{x_i} \sum_{i=1}^{q} \{ f_{asym}(x_i)\, \alpha_{x_i}\, D\bar{f}_{bl|x_i|} gg^T K_{x_i} X\}$$

$$- 2\sum_{i}^{q} D\bar{f}_{bl}\left\|_{K_{x_i}X}\right\|_I X^T {K_{x_i}}^T K_{x_i} \sum_{i=1}^{q} \Big(1$$

$$- f_{asym}(x_i)\Big) \alpha_{x_i}\, D\underline{f}_{bl}\left\|_{K_{x_i}X}\right\|_I gg^T K_{x_i} X.$$

Equation (C.13) can be simplified by considering the following steps:

D- Note that ${K_{x_i}}^T K_{x_i}$ has only one of diagonal entity as 1 corresponding to x_i and the all other elements are 0, resulting in $X^T {K_{x_i}}^T K_{x_i} KX = x_i \sum_{j=1}^{n} K(i,j)x_j = -K(i,i){x_i}^2$ for a $Y \in \mathbb{R}^n$ and a Hurwitz matrix K.

E- Following the similar steps as taken in notes B-C during the proof of (i), it can be shown that

$$-gg^T \sum_{i=1}^{q}\sum_{i=1}^{q} D\bar{f}_{bl}\left\|_{K_{x_i}X}\right\|_I D\bar{f}_{bl}\left\|_{K_{x_i}X}\right\|_I f_{asym}(x_i)\, \alpha_{x_i}\, {x_i}^2 \le 0 \qquad \text{and}$$

$$-2\sum_{i}^{q} D\bar{f}_{bl}\left\|_{K_{x_i}X}\right\|_I X^T {K_{x_i}}^T K_{x_i} \sum_{i=1}^{q} \left(1 - f_{asym}(x_i)\right) \alpha_{x_i}\, D\underline{f}_{bl}\left\|_{K_{x_i}X}\right\|_I gg^T K_{x_i} X \le 0. \qquad \text{So,}$$

these two terms can be taken out from (C.13) considering inequality. Also,

$\sum_i^q D\bar{f}_{bl}\left\|_{K_{x_i}X}\right\|_I X^T {K_{x_i}}^T K_{x_i} \sum_{j=1}^l \{f_{asym}\left(e_{r_j}\right)\ \alpha_{e_{r_j}} D\bar{f}_{bl}\left|_{e_{r_j}}\right| gg^T K_{e_{r_j}} e_r =$

$\sum_i^q D\bar{f}_{bl}\left\|_{K_{x_i}X}\right\|_I D\bar{f}_{bl}\left\|_{K_{e_{r_i}}e_r}\right\|_I f_{asym}(e_{r_i})\ \alpha_{e_{r_i}}\ gg^T(i)x_i(x_i - x_{d_i})$

Similarly, $\sum_i^q D\bar{f}_{bl}\left\|_{K_{x_i}X}\right\|_I X^T {K_{x_i}}^T K_{x_i} \sum_{j=1}^l \{\left(1 - f_{asym}\left(e_{r_j}\right)\right)\alpha_{e_{r_j}} D\underline{f}_{bl}\left|_{e_{r_j}}\right| gg^T K_{e_{r_j}} e_r\} =$

$\sum_i^q D\bar{f}_{bl}\left\|_{K_{x_i}X}\right\|_I D\underline{f}_{bl}\left\|_{K_{e_{r_i}}e_r}\right\| \left(1 - f_{asym}(e_{r_i})\right)\ \alpha_{e_{r_i}}\ gg^T(i)\{{x_i}^2 - x_i x_{d_i}\}$

Noting D-E, (C.13) can be simplified as

$$\begin{aligned}\dot{\bar{L}}_2(.) \le -2\sum_i^q \{ & D\bar{f}_{bl}\left\|_{K_{x_i}X}\right\|_I K(i,i) + D\bar{f}_{bl}\left\|_{K_{e_{r_i}}e_r}\right\|_I f_{asym}(e_{r_i})\ \left|\alpha_{e_{r_i}}\right| \\ & + \left(1 - f_{asym}(e_{r_i})\right)\left|\alpha_{e_{r_i}}\right|\ D\underline{f}_{bl}\left\|_{K_{e_{r_i}}e_r}\right\|_I \}\ {x_i}^2 \\ & + 2\sum_i^q D\bar{f}_{bl}\left\|_{K_{x_i}X}\right\|_I x_i\ (\{\left(f^*(X_d)\right)_i - (KX_d)_i + \left(g\widetilde{W}^T\phi(X(t))\right)_i \\ & + (g\epsilon)_i + f_{asym}(e_{r_i})\alpha_{e_{r_i}} D\bar{f}_{bl}\left\|_{K_{e_{r_i}}e_r}\right\|_I (gg^T)_{(i,i)} x_i x_{d_i} \\ & + \left(1 - f_{asym}(e_{r_i})\right)\alpha_{e_{r_i}} D\underline{f}_{bl}\left\|_{K_{e_{r_i}}e_r}\right\|_I (gg^T)_{(i,i)} x_i x_{d_i}\}\end{aligned}$$

$$
\begin{aligned}
= -2\sum_{i}^{q}\Bigg\{\Bigg(& D\bar{f}_{bl}\left\|_{K_{x_i}X}\right\|_I 2K(i,i) + D\bar{f}_{bl}\left\|_{K_{e_{r_i}e_r}}\right\|_I f_{asym}(e_{r_i})\ \left|\alpha_{e_{r_i}}\right| \\
& + \left(1 - f_{asym}(e_{r_i})\right)\left|\alpha_{e_{r_i}}\right|\ D\underline{f}_{bl}\left\|_{K_{e_{r_i}e_r}}\right\|_I\Bigg) x_i{}^2\Bigg\} \\
& + 2\sum_{i}^{q}\{D\bar{f}_{bl}\left\|_{K_{x_i}X}\right\|_I x_i\ ((f^*(X_d))_i - (KX_d)_i \\
& + \left(g\widetilde{W}^T\phi(X(t))\right)_i + (g\epsilon)_i \\
& + f_{asym}(e_{r_i})\alpha_{e_{r_i}} D\bar{f}_{bl}\left\|_{K_{e_{r_i}e_r}}\right\|_I (gg^T)_{(i,i)}x_i x_{d_i} \\
& + \left(1 - f_{asym}(e_{r_i})\right)\alpha_{e_{r_i}} D\underline{f}_{bl}\left\|_{K_{e_{r_i}e_r}}\right\|_I (gg^T)_{(i,i)}x_i x_{d_i})\}\,.
\end{aligned}
\tag{C.14}
$$

Applying norm properties [33] (from the Paper III) to the terms on the right-hand side of (C.14) results in

$$
\begin{aligned}
&\dot{\bar{L}}_2(.) \\
&\leq -2\sum_{i}^{q}\{ (Df_{bl}\|_{K_{x_i}X}\|_I K(i,i) \\
&+ D\bar{f}_{bl}\|_{K_{e_{r_i}e_r}}\|_I |f_{asym}(e_{r_i})| \left|\alpha_{e_{r_i}}\right| \\
&+ |1 - f_{asym}(e_{r_i})| \left|\alpha_{e_{r_i}}\right| D\underline{f}_{bl}\|_{K_{e_{r_i}e_r}}\|_I) x_i{}^2\} \\
&+ 2\sum_{i}^{q}\{ (D\bar{f}_{bl}\|_{K_{x_i}X}\|_I \left\{\|f^*(X_d)\|_i + \|KX_d\|_i \right. \\
&\left. + \|g\|\|\widetilde{W}^T\phi(X(t))\|_i + \|g\|\|\epsilon\|_i\right\} |x_i| \\
&+ f_{asym}(e_{r_i}) \left|\alpha_{e_{r_i}}\right| D\bar{f}_{bl}\|_{K_{e_{r_i}e_r}}\|_I \|gg^T\|_{(i,i)} |x_i x_{d_i}| \\
&+ \left(1 - f_{asym}(e_{r_i})\right) \left|\alpha_{e_{r_i}}\right| D\underline{f}_{bl}\|_{K_{e_{r_i}e_r}}\|_I \|gg^T\|_{(i,i)} |x_i x_{d_i}|\}.
\end{aligned}
\tag{C.15}
$$

This equation can be further modified by noting that $\|\epsilon\| \leq \epsilon^*$, $\|\phi(X)\| \leq \phi^*$, $\|\widetilde{W}\| \leq \widetilde{W}^*$, and $\|W\| \leq W^*$. Also applying Young's inequality [33] (from the Paper III) on $x_i x_{d_i} = \alpha_y x_i{}^2 + \frac{1}{\alpha_y} x_{d_i}{}^2$ for $\alpha_y = 1$.

$$\dot{\bar{L}}_2(.) \le -2\sum_i^q \Bigg\{ \Bigg(D\bar{f}_{bl}\left\|_{K_{x_i}X}\right\|_I K(i,i) + D\bar{f}_{bl}\left\|_{K_{e_{r_i}}e_r}\right\|_I \left|f_{asym}(e_{r_i})\right| \left|\alpha_{e_{r_i}}\right| + \left|1 - f_{asym}(e_{r_i})\right| \left|\alpha_{e_{r_i}}\right| D\underline{f}_{bl}\left\|_{K_{e_{r_i}}e_r}\right\|_I \Bigg) {x_i}^2 \Bigg\}$$

$$+ 2\sum_i^q \Bigg\{ D\bar{f}_{bl}\left\|_{K_{x_i}X}\right\|_I \left\{ \|f^*(X_d)\|_i + \|KX_d\|_i + \|g\|\widetilde{W}^*\phi^* + \|g\|\epsilon^* \right\} |x_i|$$

$$+ f_{asym}(e_{r_i}) \left|\alpha_{e_{r_i}}\right| D\bar{f}_{bl}\left\|_{K_{e_{r_i}}e_r}\right\|_I \|gg^T\|_{(i,i)} \left(\alpha_y {x_i}^2 + \frac{1}{\alpha_y}{x_{d_i}}^2\right)$$

$$+ \left(1 - f_{asym}(e_{r_i})\right) \left|\alpha_{e_{r_i}}\right| D\underline{f}_{bl}\left\|_{K_{e_{r_i}}e_r}\right\|_I \|gg^T\|_{(i,i)} \left(\alpha_y {x_i}^2 + \frac{1}{\alpha_y}{x_{d_i}}^2\right) \Bigg\}$$

$$= -\sum_i^q \{ (D\bar{f}_{bl}\left\|_{K_{x_i}X}\right\|_I 2K(i,i)) {x_i}^2 \}$$

$$+ 2\sum_{i=1}^q \{ D\bar{f}_{bl}\left\|_{K_{x_i}X}\right\|_I \left\{ \|f^*(X_d)\|_i + \|KX_d\|_i + \|g\|\widetilde{W}^*\phi^* + \|g\|\epsilon^* \right\} |x_i|$$

$$+ f_{asym}(e_{r_i}) \left|\alpha_{e_{r_i}}\right| D\bar{f}_{bl}\left\|_{K_{e_{r_i}}e_r}\right\|_I \|gg^T\|_{(i,i)} {x_{d_i}}^2$$

$$+ \left(1 - f_{asym}(e_{r_i})\right) \left|\alpha_{e_{r_i}}\right| D\underline{f}_{bl}\left\|_{K_{e_{r_i}}e_r}\right\|_I \|gg^T\|_{(i,i)} {x_{d_i}}^2 \}$$

Note that $\left|x_{d_i}\right| \le \overline{x_{d_i}}$, so by defining $c_{3_i} \triangleq f_{asym}(e_{r_i}) \left|\alpha_{e_{r_i}}\right| D\bar{f}_{bl}\left\|_{K_{e_{r_i}}e_r}\right\|_I \|gg^T\|_{(i,i)} \overline{x_{d_i}}^2 + \left(1 - f_{asym}(e_{r_i})\right) \left|\alpha_{e_{r_i}}\right| D\underline{f}_{bl}\left\|_{K_{e_{r_i}}e_r}\right\|_I \|gg^T\|_{(i,i)} \overline{x_{d_i}}^2$ results in

$$\dot{\bar{L}}_2(.) \leq -\sum_i^q \{2(D\bar{f}_{bl}\left\|_{K_{x_i}X}\right\|_I K(i,i))\ {x_i}^2\}$$

$$+\sum_{i=1}^{q}\{2D\bar{f}_{bl}\left\|_{K_{x_i}X}\right\|_I \{\|f^*(X_d)\|_i + \|KX_d\|_i \quad \text{(C.16)}$$

$$+\|g\|\widetilde{W}^*\phi^* + \|g\|\epsilon^*\}|x_i|\} + \sum_{i=1}^{q} c_{3_i}$$

Define $a_{3_i} \triangleq 2D\bar{f}_{bl_{|x_i|}}K(i,i)$ and $b_{3_i} \triangleq D\bar{f}_{bl_{|x_i|}}\{\|f^*(X_d)\|_i + \|KX_d\|_i + \|g\|\widetilde{W}^*\phi^* + \|g\|\epsilon^*\}$. Note that defined coefficients are positive.

$$\dot{\bar{L}}_2(.) \leq -\sum_i^q a_{3_i}\,{x_i}^2 + \sum_i^q 2b_{3_i}|x_i| + \sum_i^q c_{3_i} \quad \text{(C.17)}$$

For $\xi \in \mathbb{R}_+$, such that $0 < \xi < 1$.

$$\dot{\bar{L}}_2(.) \leq -\xi\sum_i^q a_{3_i}\,{x_i}^2 - \sum_i^q\{(1-\xi)a_{3_i}\,{x_i}^2 - 2b_{3_i}|x_i| - c_{3_i}\}$$

$$= -\xi\sum_i^q a_{3_i}\,{x_i}^2 - \sum_i^q\left(\left\{\sqrt{(1-\xi)a_{3_i}}\,|x_i| - \frac{b_{3_i}}{\sqrt{(1-\xi)a_{3_i}}}\right\}^2 - \frac{{b_{3_i}}^2}{(1-\xi)a_{3_i}} - c_{3_i}\right\}$$

$$\leq -\xi\sum_i^q a_{3_i}\,{x_i}^2 \qquad \text{if} \quad |x_i| \geq \frac{\left(\sqrt{{b_{3_i}}^2 + (1-\xi)a_{3_i}c_{3_i}}\right) + b_{3_i}}{(1-\xi)a_{3_i}} \quad \text{(C.18)}$$

(iv) Now consider the $\underline{\dot{L}}_2(x_i)$

$$\dot{\underline{L}}_2(x_i) = \sum_{i=1}^{q} \frac{d\ \left(1 - f_{asym}(x_i)\right) \underline{f}_{bl}\left(\left\|K_{x_i}X\right\|_I\right)}{d\ \left\|K_{x_i}X\right\|_I^{\ 2}} . \frac{d\ \left\|K_{x_i}X\right\|_I^{\ 2}}{dt}$$

$$= 2\sum_{i}^{q}\left(1 - f_{asym}(x_i)\right)\ D\underline{f}_{bl_{|x_i|}} X^T {K_{x_i}}^T K_{x_i}\dot{X}. \tag{C.19}$$

Following the same approach as is taken for (iii), it can be shown that

$$\dot{\underline{L}}_2(x_i) \le -\xi \sum_{i}^{q} a_{4_i}\ {x_i}^2$$

$$\text{if} \qquad |x_i| \ge \frac{\left(\sqrt{{b_{4_i}}^2 + (1-\xi)a_{4_i}c_{4_i}}\right) + b_{4_i}}{(1-\xi)a_{4_i}} \tag{C.20}$$

where $a_{4_i} \triangleq 2D\underline{f}_{bl_{|x_i|}}\left|1 - f_{asym}(x_i)\right|\{K(i,i),\ b_{4_i} \triangleq D\bar{f}_{bl_{|x_i|_l}}\{\|f^*(X_d)\|_i + \|KX_d\|_i +$

$\|g\|\widetilde{W}^*\phi^* + \|g\|\epsilon^*\}$, and $c_{4_i} \triangleq f_{asym}(e_{r_i})\left|\alpha_{e_{r_i}}\right|\ D\bar{f}_{bl_{|e_{r_i}|}}\|gg^T\|_{(i,i)}\ \overline{x_{d_i}}^2 + \left(1 -\right.$

$\left. f_{asym}(e_{r_i})\right)\left|\alpha_{e_{r_i}}\right|\ D\underline{f}_{bl_{|e_{r_i}|}}\|gg^T\|_{(i,i)}\overline{x_{d_i}}^2$.

(v) Now taking L_3,

$$\dot{L_3}(e_a, \widetilde{W}) = 2{e_a}^T P_a \dot{e}_a + 2\ tr(\widetilde{W}^T {\gamma_w}^{-1}\dot{\widetilde{W}})$$

$$= 2{e_a}^T P_a K_2 e_a(t) + 2{e_a}^T P_a g\widetilde{W}^T\phi\left(X(t)\right) + 2{e_a}^T P_a g\epsilon +$$

$$2tr\left(\widetilde{W}^T {\gamma_w}^{-1}\dot{\widetilde{W}}\right). \tag{C.21}$$

Since $\widetilde{W} = W - \widehat{W}$ so $\dot{\widetilde{W}} = -\dot{\widehat{W}}$. Also by using the projection operator for the weight updates (18 (from the Paper III)), Lyapunov equation (27 (from the Paper III)), and by adding and subtracting $\widetilde{W}^T\phi\left(X(t)\right){e_a}^T Pg$, (C.21) can be rewritten as

$$\dot{L_3}(.) = -{e_a}^T Q_a e_a + 2{e_a}^T P_a g \widetilde{W}^T \phi\big(X(t)\big) + 2{e_a}^T P_a g \epsilon$$
$$+ 2tr\big(-\widetilde{W}^T \{Proj_m\big(\widehat{W}, \phi\big(X(t)\big)\, {e_a}^T P_a g\big) \tag{C.22}$$
$$+ \widetilde{W}^T \phi\big(X(t)\big)\, {e_a}^T P_a g - \widetilde{W}^T \phi\big(X(t)\big)\, {e_a}^T P_a g\big\}.$$

For any matrices $A \in \mathbb{R}^{n\times m}$, $B \in \mathbb{R}^{m\times n}$, and $C \in \mathbb{R}^{n\times n}$, followings are true, $tr(AB) = tr(BA)$, $tr(AB + C) = tr(AB) + tr(C)$, and $tr(C) = tr(C^T)$. Using these trace properties, (C.22) can be rewritten as

$$\dot{L_3}(.) = -{e_a}^T Q_a e_a + 2{e_a}^T P_a g \widetilde{W}^T \phi\big(X(t)\big) + 2{e_a}^T P_a g \epsilon$$
$$+ 2tr\{\big(-\widetilde{W}^T Proj_m\big(\widehat{W}, \phi\big(X(t)\big)\, {e_a}^T P_a g\big) \tag{C.23}$$
$$-\ \phi\big(X(t)\big)\, {e_a}^T P_a g\}\big) - 2tr\big\{\widetilde{W}^T \phi\big(X(t)\big)\, {e_a}^T P_a g\big\}.$$

By Lemma 11.3 of [32] (from the Paper III), $tr\Big[\big(\widehat{W} - W\big)^T \{Proj_m\big(\widehat{W},$ $\phi\big(X(t)\big)\, {e_a}^T PB\big) - \phi\big(X(t)\big)\, {e_a}^T PB\}\Big] \leq 0$ and after some simplifications (C.23) becomes

$$\dot{L_3}(.) \leq -{e_a}^T Q_a e_a + 2{e_a}^T P_a g \widetilde{W}^T \phi\big(X(t)\big) + 2{e_a}^T P_a g \epsilon - 2tr\{\widetilde{W}^T \phi\big(X(t)\big)\, {e_a}^T P_a g\}$$
$$= -{e_a}^T Q_a e_a + 2{e_a}^T P_a g \widetilde{W}^T \phi\big(X(t)\big) + 2{e_a}^T P_a g \epsilon - 2tr\{{e_a}^T P_a g \widetilde{W}^T \phi\big(X(t)\big)\}$$
$$= -{e_a}^T Q_a e_a + 2{e_a}^T P_a g \widetilde{W}^T \phi\big(X(t)\big) + 2{e_a}^T P_a g \epsilon - 2{e_a}^T P_a g \widetilde{W}^T \phi\big(X(t)\big)$$
$$= -{e_a}^T Q_a e_a + 2{e_a}^T P_a g \epsilon \tag{C.24}$$

By applying norm properties [33] (from the Paper III) to the terms on the right-hand side of (C.24),

$$\dot{L_3}(.) \leq -\lambda_{min}\,(Q_a)\|e_a\|^2 + 2\|P_a g\|\|\epsilon\|\|e_a\|.$$
$$\leq -\lambda_{min}\,(Q_a)\|e_a\|^2 + 2\|P_a g\|\epsilon^*\|e_a\|$$
$$= -\xi\lambda_{min}\,(Q_a)\|e_a\|^2 - (1-\xi)\lambda_{min}\,(Q_a)\|e_a\|^2 + 2\|P_a g\|\epsilon^*\|e_a\|$$

Define $a_5 \triangleq (1-\xi)\lambda_{min}\,(Q_a)$ and $b_5 \triangleq \epsilon^* \|P_a g\|$.

$$\dot{L_3}(.) \leq -\xi a_5 \|e_a\|^2 - a_5\|e_a\|^2 + 2b_5\|e_a\|$$

$$= -\xi a_5 \|e_a\|^2 - \left(\sqrt{a_5}\,\|e_a\| - \frac{b_5}{\sqrt{a_5}}\right)^2 + \frac{{b_5}^2}{a_5}$$

$$\leq -\xi a_5 \|e_a\|^2 \quad \text{if } \|e_a\| \geq \tfrac{2b_5}{a_5}. \tag{C.25}$$

By adding (C.10), (C.11), (C.18), (C.20), and (C.25) leads to

$$\dot{L}\left(e_r, e_a, \widetilde{W}, X\right) = \dot{\overline{L}}_1 + \dot{\underline{L}}_1 + \dot{\overline{L}}_2 + \dot{\underline{L}}_2 + \dot{L}_3$$

$$\leq -\xi \sum_{j=1}^{l} a_{1_i}\, {e_r}_j{}^2 - \xi \sum_{j=1}^{l} a_{2_i}\, {e_r}_j{}^2 - \xi \sum_{i=1}^{q} a_{3_i}\, {x_i}^2 - \xi \sum_{i=1}^{q} a_{4_i}\, {x_i}^2 \tag{C.26}$$

$$- \xi \lambda_{min}\,(Q_a)\|e_a\|^2.$$

Now following comments are justified:

a. Since $\dot{L}(.,t)$ is negative from (C.26), thus $L(.,t) \leq L(.,t=0) \leq \overline{L}(.)$ where $\overline{L}(.)$ is the upper bound on L given later in (C.27).

b. Since the time derivative of L is negative definite and a BLF is applied on x_i, if initial $x_i(0) \in \mathsf{C}_{\epsilon_{x_i}}$ then BLF-based control will never let $x_i(t)$ violate its bounds, and it will always stay in its constrained set.

c. Since the time derivative of L is negative definite and a BLF is applied on e_{r_j}, if initial $e_{r_j}(0) \in \mathsf{C}_{\epsilon_{e_{r_j}}}$ then BLF-based control will never let $e_{r_j}(t)$ violate its bounds and it will always stay in its constrained set.

d.

(A) Following (a), (b), and by remarks/definition (iv) from subsection 2 of Paper III, $\overline{f}_{bl}(x_i)$ and $\underline{f}_{bl}(x_i)$ will be bounded by $\overline{\gamma}_{x_i}$ and $\underline{\gamma}_{x_i}$, respectively.

(B) Following (a), (b), and by remarks/definition (iv) from subsection 2 of the Paper III, $\overline{f}_{bl}\left(e_{r_j}\right)$ *and* $\underline{f}_{bl}\left(e_{r_j}\right)$ *will be bounded by* $\overline{\gamma}_{e_{r_j}}$ *and* $\underline{\gamma}_{e_{r_j}}$*, respectively.*

(C) Following (a) , (b), and by remarks/definition (v) from subsection 2 of the Paper III, $D\bar{f}_{bl_{|x_i|}}$ *and* $D\underline{f}_{bl_{|x_i|}}$ *will be bounded by* $\overline{\beta}_{x_i}$ *and* $\underline{\beta}_{x_i}$ *, respectively.*

(D) Following (a),(b), and by remarks/definition (v) from subsection 2 of the PaperI II, $D\bar{f}_{bl}\big|_{e_{r_j}}\big|$ *and* $D\underline{f}_{bl}\big|_{e_{r_j}}\big|$ *will be bounded by* $\overline{\beta}_{e_{r_j}}$ *and* $\underline{\beta}_{e_{r_j}}$*, respectively.*

$(E)\widetilde{W}$ *is bounded because the projection operator is used in its derivation [46]* (from the Paper III).

(F) From (C.25), since $\dot{L}(\, e_a, .) \leq \xi\lambda_{min}\,(Q_a)\|e_a\|^2 + (..)$*, so as long as* $\|e_a\| \geq \frac{2b_5}{a_5}$ *for given* a_5 *and* b_5*, then* $\|e_a(t)\| \leq \bar{e}_a$ *for some* $\bar{e}_a \in \mathbb{R}^+$.

$(G)\, X_a$ *is bounded as* $\|e_a(t)\| \leq \bar{e}_a \rightarrow \|X - X_a\| \leq \|X\| + \|X_a\| \leq \bar{e}_a \rightarrow \|X_a\| \leq \bar{e}_a + \sum_{i=1}^{n} \epsilon_{x_i}$.

After finding A-G, now $\overline{L}(.)$ *can be given as*

$$\overline{L}(.) \triangleq \sum_{j=1}^{l}\{\overline{\gamma}_{e_{r_j}} + \underline{\gamma}_{e_{r_j}}\} + \sum_{i=1}^{q}\left\{\overline{\gamma}_{x_i} + \underline{\gamma}_{x_i}\right\} + |\gamma_w{}^{-1}|\ \widetilde{W}^{*2} + \lambda_{max}\,(P_a)\bar{e}_a{}^2. \tag{C.27}$$

e. Control is bounded by u_{max}*. Using norm on (20, from Paper III),*

$$\|u(t)\| = \left\| g^{-1} \left[Ke_r + e_f - g\widehat{W}^T \phi\big(X(t)\big) - \sum_{j=1}^{l} \{ f_{asym}\left(e_{r_j}\right)\ \alpha_{e_{r_j}}\ D\bar{f}_{bl}\big|_{e_{r_j}|}\ gg^T K_{e_{r_j}} e_r \right.\right.$$

$$+ \left(1 - f_{asym}\left(e_{r_j}\right)\right) \alpha_{e_{r_j}}\ D\underline{f}_{bl}\big|_{e_{r_j}|} gg^T K_{e_{r_j}} e_r \}$$

$$- \sum_{i=1}^{q} \{ f_{asym}(x_i)\ \alpha_{x_i}\ D\bar{f}_{bl\,|x_i|} gg^T K_{x_i} X$$

$$\left.\left. + \left(1 - f_{asym}(x_i)\right) \alpha_{x_i}\ D\underline{f}_{bl}\big|_{x_i|} gg^T K_{x_i} X \} \right] \right\|$$

$$\leq \|g^{-1}\| \left(\|K\| \epsilon_{e_r} + \left\|\overline{f^*}(X_d)\right\| + \left\|\overline{f}\big(X(t)\big)\right\| + \|g\| \widehat{W}^* \phi^* \right.$$

$$+ \sum_{j=1}^{l} \left\{ \left|\alpha_{e_{r_j}}\right| \overline{\beta}_{|e_{r_j}|} \|g\|^2 \overline{\epsilon}_{e_r} + \left|\alpha_{e_{r_j}}\right|\ \underline{\beta}_{|e_{r_j}|} \|g\|^2 \underline{\epsilon}_{e_r} \right\}$$

$$\left. + \sum_{i=1}^{q} \left\{ \left|\alpha_{x_i}\right| \bar{\beta}_{|x_i|} \|g\|^2\ \overline{\epsilon}_{x_i} + \left|\alpha_{x_i}\right|\ \underline{\beta}_{|x_i|} \|g\|^2\ \underline{\epsilon}_{x_i} \right\} \right)$$

$$= u_{max}.$$

BIBLIOGRAPHY

[1] A. Ghafoor, S.N. Balakrishnan, and T. Yucelen, "Modified State Observer Based Decentralized Neuro-Adaptive Controller for Large Scale Interconnected Uncertain Systems," *2018 Annual American Control Conference (ACC)*, Milwaukee, WI, 2018, pp. 1701-1706.
doi: 10.23919/ACC.2018.8431513

[2] A. Ghafoor, J. Yao, S.N. Balakrishnan, J. Sarangapani and T. Yucelen, "Event Triggered Neuroadaptive Controller (ETNAC) Design for Uncertain Affine Nonlinear Systems" *ASME DSCC 2018*-9103, USA, 2018. doi: 10.1115/DSCC2018-9103

[3] A. Ghafoor, S.N. Balakrishnan, S. Jagannathan and T. Yucelen, "Event-Triggered Neuro-Adaptive Controller (ETNAC) Design for Uncertain Linear Systems," *2018 IEEE Conference on Decision and Control (CDC)*, FL, USA, 2018, pp. 2217-2222. doi: 10.1109/CDC.2018.8618962

[4] A. Ghafoor and S.N. Balakrishnan, "Modified State Observer based Two-Way ETNAC for Uncertain Linear Systems", *International Joint Conference on Neural Network (IJCNN) 2019*, Budapest, Hungary, #20379 2019.

[5] A. Ghafoor, P. Galchenko, S. N. Balakrishnan, H. Pernicka, and T. Yucelen, "ETNAC Design Enabling Formation Flight at Liberation Points," *IEEE American Control Conference (ACC) 2019*, Philadelphia, PA, USA, 2019, pp. 3689-3694.

VITA

Abdul Ghafoor was born and raised in Khushab, Pakistan. He received his bachelor degree with honor in Mechatronics Engineering from National University of Sciences and Technology (NUST) in 2010. During his undergraduate, he participated in the National Engineering Robotics Contest (NERC) and also pursued engineering internships at Engro corporation limited and at the PACKAGES private limited.

After working for 2 years as Assistant Manager Technical in NESCOM, He decided to go for his Masters in 2013. He earned his master degree in Electrical and Electronics Engineering (EEE) from Middle East Technical University (METU) Ankara in 2015, with majors in dynamics and Controls. In his master research, he prepared a dynamical model of the Wing-in-Ground (WIG) effect vehicle and designed an autopilot system for it. After getting some professional experience as Design Engineer in Desistek Robotics, Mr. Abdul Ghafoor embarked on a quest to attain his Ph.D. in Mechanical Engineering (Controls and Automation) from Missouri University of Sciences and Technology Rolla, USA, in June 2016.

While pursuing his doctoral degree, He developed and tested 8+ optimal/adaptive/intelligent control algorithms. he also served as Graduate Research Assistant, Graduate Teacher Assistant, taught and managed Control System lab, and mentored undergraduate students. He received his PhD degree in Mechanical Engineering from Missouri University of Sciences and Technology in May 2020. So far, he has 10+ scientific publication in the peer-reviewed journals and international conferences. His research interests are Dynamics & Control, Robotics, Machine Learning, and AI.